

รายงานวิจัยฉบับสมบูรณ์

โครงการ โครงสร้างและพลวัตของไอออนที่ถูกซอลเวต:
ความเข้าใจลึกซึ้งโดยการจำลองบนพื้นฐานกลศาสตร์
ควอนตัม

โดย รองศาสตราจารย์ ดร.อนันต์ ทองระอา

สิงหาคม 2554

รายงานวิจัยฉบับสมบูรณ์

โครงการ โครงสร้างและพลวัตของใอออนที่ถูกซอลเวต: ความเข้าใจลึกซึ้งโดยการจำลองบนพื้นฐานกลศาสตร์ ควอนตัม

ผู้วิจัย

รองศาสตราจารย์ ดร.อนันต์ ทองระอา มหาวิทยาลัยเทคโนโลยีสุรนารี

สังกัด

สนับสนุนโดยสำนักงานกองทุนสนับสนุนการวิจัย

บทคัดย่อ

ผู้วิจัยได้นำเทคนิคการจำลองพลวัตเชิงโมเลกุลขั้นสูงที่ผสมผสานกลศาสตร์ โครงการวิจัยนี้ ควอนตัมและกลศาสตร์โมเลกุล (QM/MM) ทั้งในส่วนที่เป็นเทคนิค QM/MM แบบดั้งเดิม และเทคนิค QMCF (ซึ่งเป็นเทคนิค QM/MM ที่ได้ทำการพัฒนาขึ้นใหม่ เพื่อใช้สำหรับการจำลองพลวัตเชิงโมเลกุล ระบบไอออนในสารละลายโดยไม่จำเป็นต้องสร้างฟังก์ชันศักย์ระหว่างไอออนกับน้ำ) ศึกษาสมบัติเชิงโครงสร้างและเชิงพลวัตของไอออนที่ถูกซอลเวตอยู่ในสารละลายน้ำ ผลการศึกษาที่ได้ ชี้ให้เห็นความสำคัญและความจำเป็นของการคำนวณบนพื้นฐานกลศาสตร์ควอนตัม สำหรับการอธิบาย ลักษณะโครงสร้างและพลวัตของชั้นซอลเวชันของไอออนชนิดต่างๆ โดยข้อมูลที่ได้จากการจำลอง พลวัตเชิงโมเลกุลโดยเทคนิค QM/MM และ QMCF นี้ มีความถูกต้องและน่าเชื่อถือมากกว่าข้อมูลที่ได้ จากการจำลองพลวัตเชิงโมเลกุลที่ดำเนินการโดยใช้กลศาสตร์โมเลกุลเพียงอย่างเดียว นอกจากนี้ ข้อมูลที่ได้จากการจำลองนี้ สามารถนำมาใช้สำหรับการตีความหมายข้อมูลทางสเปกโตรสโกปีได้ด้วย โดยเฉพาะในส่วนของข้อมูลการทดลอง X-ray absorption spectroscopy (XAS) ซึ่งถือเป็นการบูรณา การเทคนิคการจำลองพลวัตเชิงโมเลกุลขั้นสูงร่วมกับเทคนิคการทดลอง XAS ที่มีประสิทธิภาพสำหรับ การศึกษาระบบทางเคมีดังกล่าว

Abstract

A series of molecular dynamics (MD) simulations based on combined quantum mechanics/molecular mechanics (QM/MM) and on quantum mechanical charge field (QMCF) approaches have been performed to investigate solvation structure and dynamics of ions solvated in aqueous electrolyte solution. The results obtained by the QM/MM and QMCF MD simulations clearly demonstrate the importance of QM treatment in obtaining more reliable structural arrangements as well as correct dynamics properties of the solvated ions, *i.e.*, compared to the results derived by means of classical MM simulations. In conjunction with the X-ray absorption spectroscopy (XAS), the QM/MM and QMCF techniques can be seen as the elegant tools in developing refined models for the interpretation of the spectroscopic data.

หน้าสรุปโครงการ

(Executive summary)

1. ชื่อโครงการ

(ภาษาไทย) โครงสร้างและพลวัตของไอออนที่ถูกซอลเวต: ความเข้าใจลึกซึ้งโดยการจำลองบน พื้นฐานกลศาสตร์ควอนตัม

(ภาษาอังกฤษ) Structure and dynamics of solvated ions: More insights through combined QM/MM MD approaches

2. ชื่อหัวหน้าโครงการ หน่วยงานที่สังกัด ที่อยู่ หมายเลขโทรศัพท์ โทรสาร และ e-mail

ดร. อนันต์ ทองระอา ตำแหน่ง รองศาสตราจารย์ สาขาวิชาเคมี สำนักวิชาวิทยาศาสตร์ มหาวิทยาลัยเทคโนโลยีสุรนารี ตำบล สุรนารี อำเภอ เมือง จังหวัด นครราชสีมา 30000 โทร. (044) 224751 Fax. (044) 224750

e-mail: anan_tongraar@yahoo.com, anan@sut.ac.th

- สาขาวิชาที่ทำการวิจัย เคมีเชิงคำนวณ
- 5. ระยะเวลาดำเนินงาน 3 ปี

6. ปัญหาที่ทำการวิจัย และความสำคัญของปัญหา

การศึกษาสมบัติเชิงโครงสร้างและเชิงพลวัตของไอออนที่ถูกซอลเวตอยู่ในสารละลายน้ำได้รับ ความสนใจอย่างกว้างขวาง โดยเฉพาะบรรดานักเคมีและนักชีวเคมี เพื่อสามารถทำความเข้าใจเกี่ยวกับ พฤติกรรมและบทบาทของไอออน (เมื่ออยู่ในสารละลาย) ต่อกระบวนการทางด้านเคมีและชีวเคมีของ สิ่งมีชีวิต การศึกษาสมบัติของไอออนที่อยู่ในสารละลายนั้น สามารถกระทำได้โดยตรงจากการทดลอง โดยใช้อุปกรณ์ที่มีประสิทธิภาพสูง เช่น X-ray NMR IR หรืออื่นๆ อย่างไรก็ตาม พบว่า เทคนิคทางด้าน การทดลองยังมีข้อจำกัดอยู่มาก โดยเฉพาะอย่างยิ่ง ในกรณีที่ต้องการทราบข้อมูลในระดับจุลภาค หรือ ในสภาพที่มีความเข้มขันน้อยๆ ดังนั้น การศึกษาเชิงทฤษฎีโดยใช้เทคนิคซิมูเลชัน ถือเป็นอีกทางเลือก หนึ่ง ข้อได้เปรียบที่สำคัญของการทำซิมูเลชันคือ มีความสะดวกและรวดเร็วกว่าการทำการทดลอง โดยตรงมาก นอกจากนี้ ผลการศึกษาที่ได้จากการทำซิมูเลชันสามารถนำมาใช้เสนอแนะแนวทางการ ทดลองได้ด้วย

ที่ผ่านมา การทำซิมูเลชันมักถูกดำเนินการบนพื้นฐานกลศาสตร์โมเลกุลเป็นส่วนใหญ่ (ข้อจำกัด ของประสิทธิภาพเครื่องช่วยคำนวณ) ซึ่งต้องอาศัยสมมติฐานและการประมาณหลายประการเพื่อช่วยให้ การคำนวณใช้เวลาไม่นานเกินไปนัก ผลการศึกษาที่ได้จึงไม่ค่อยถูกต้องหรือน่าเชื่อถือมากนัก แต่ใน ้ปัจจุบัน ความก้าวหน้าทางด้านเทคโนโลยี (คอมพิวเตอร์ได้รับการพัฒนาทั้งทางด้านประสิทธิภาพและ ความเร็วในการประมวลผล) ช่วยสนับสนุนให้การทำซิมูเลชันสามารถดำเนินการได้รวดเร็วขึ้น รวมทั้ง สามารถกระทำได้ในระดับที่มีความถูกต้องและมีความน่าเชื่อถือมากขึ้นด้วย เทคนิคการทำซิมูเลชันที่ ผู้วิจัยได้นำมาประยุกต์สำหรับการศึกษาระบบของไอออนในสารละลายคือ การจำลองพลวัตเชิงโมเลกุล ที่ผสมผสานกลศาสตร์ควอนตัมและกลศาสตร์โมเลกุล โดยเทคนิคดังกล่าวนี้ ความสำคัญมากที่สุด (ในที่นี้คือ ชั้นซอลเวชันของไอออน) จะถูกอธิบายโดยใช้การคำนวณในระดับ นอน-เอมพิริกัล ได้แก่ การคำนวณ แอบ อินิชิโอ บนพื้นฐานของ บอร์น-ออบเพนไฮเมอร์ ซึ่งมีความ ในขณะที่ส่วนที่เหลือของระบบจะถูกอธิบายโดยใช้การคำนวณในระดับเอมพิริกัล ถูกต้องแม่นยำสูง (อันตรกิริยาระหว่างอนุภาคจะถูกอธิบายโดยฟังก์ชันทางคณิตศาสตร์) ผลการศึกษาที่ได้จากการทำซิมู เลชันโดยวิธีผสมผสานกลศาสตร์ควอนตัมและกลศาสตร์โมเลกุลดังกล่าว สามารถชี้ให้เห็นข้อบกพร่อง และความไม่สมบูรณ์ของการทำซิมูเลชันบนพื้นฐานกลศาสตร์โมเลกุลที่ผ่านๆ มา ประการสำคัญที่ ผู้วิจัยค้นพบคือ การไม่พิจารณาอันตรกิริยาของหลายอนุภาคที่ปรากฏอยู่ในระบบ (การใช้เพียงฟังก์ชัน ศักย์คู่สำหรับอธิบายอันตรกิริยาระหว่างอนุภาคในระบบ โดยอนุมานว่า อันตรกิริยารวมของระบบได้มา จากผลรวมของคู่อันตรกิริยาเท่านั้น โดยอันตรกิริยาของสามอนุภาค สื่อนุภาค และอื่นๆ มีค่าน้อย และ สามารถละทิ้งได้) ส่งผลอย่างมีนัยสำคัญต่อเลขโคออร์ดิเนชัน (จำนวนโมเลกุลของตัวทำละลายที่อยู่ ล้อมรอบไอออน) ที่อาจมีค่าเพิ่มขึ้นหรือลดลงก็ได้ ซึ่งส่งผลโดยตรงต่อลักษณะโครงรูปและขนาดของชั้น ซอลเวชันของไอออนด้วย นอกจากนี้ ยังส่งผลต่อลักษณะเฉพาะของการจัดตัวและการหันเหของ โมเลกุลตัวทำละลายที่อยู่ล้อมรอบไอออนด้วย ผลการศึกษาที่ได้จากการทำซิมูเลชันโดยวิธีผสมผสาน กลศาสตร์ควอนตัมและกลศาสตร์โมเลกุล ได้ให้ข้อมูลในระดับจุลภาคที่สำคัญหลายประการเกี่ยวกับ พฤติกรรมของไอออนที่ถูกซอลเวตอยู่ในสารละลายที่สอดคล้องกับข้อมูลทางด้านการทดลองเป็นอย่างดี

7. วัตถุประสงค์

สืบเนื่องจากการทำซิมูเลชันที่ผสมผสานกลศาสตร์ควอนตัมและกลศาสตร์โมเลกุลที่ประยุกต์กับ ระบบของไอออนในสารละลาย ให้ผลการศึกษาที่น่าสนใจและสอดคล้องกับผลที่ได้จากการทดลองเป็น อย่างดี ผู้วิจัยจึงมีความสนใจที่จะประยุกต์เทคนิคซิมูเลชันขั้นสูงดังกล่าว สำหรับการศึกษาสมบัติเชิง โครงสร้างและเชิงพลวัตของไอออนชนิดอื่นๆ โดยเฉพาะไอออนที่มีความซับซ้อนมากขึ้น เช่น ไอออนที่ ประกอบด้วยอะตอมมากกว่าหนึ่งอะตอม ได้แก่ ไอออนอะซีเตต (CH₃COO) และไอออนคาร์บอเนต (CO₃²) รวมทั้งไอออนบางชนิดที่มีความโพลาไรซ์มาก เช่น ไอออนคลอไรด์ (CI) และไอออนไอโอไดด์ (I) สำหรับระบบของไอออนลบหรือแอนไอออนในสารละลายน้ำนั้น สิ่งที่น่าสนใจก็คือ อันตรกิริยา ระหว่างไอออนลบกับน้ำไม่ค่อยรุนแรงนักเมื่อเปรียบเทียบกับกรณีของไอออนบวกหรือแคทไอออน และ อันตรกิริยาระหว่างไอออนลบกับน้ำมีค่าใกล้เคียงกับอันตรกิริยาระหว่างน้ำด้วยกัน นำมาซึ่งความ

สงสัยว่า เมื่อไอออนลบดังกล่าวละลายอยู่ในน้ำ ไอออนลบจะสามารถเหนี่ยวนำน้ำที่อยู่รอบๆ เกิดเป็น สารเชิงซ้อนที่มีไอออนลบเป็นศูนย์กลาง หรือจะเป็นในลักษณะที่ไอออนลบถูกเหนี่ยวนำโดยโมเลกุลน้ำ (ไอออนลบประพฤติตัวเป็นลิแกนด์โดยมีน้ำเป็นศูนย์กลาง) การศึกษาระบบที่มีอันตรกิริยาอ่อนๆ เช่นนี้ จำเป็นต้องใช้เทคนิคการจำลองพลวัตเชิงโมเลกุลที่มีความถูกต้องสูง โดยคาดหวังว่า ผลการศึกษาที่ได้ ที่จะนำไปสู่ความรู้ความเข้าใจเกี่ยวกับพฤติกรรมของไอออนชนิดนี้ใน จะเป็นข้อมูลพื้นฐานสำคัญ กระบวนการทางเคมีและชีวเคมีที่ซับซ้อนต่อไปได้ ซึ่งผู้วิจัยคาดว่า โดยเทคนิคการจำลองพลวัตเชิง โมเลกุลขั้นสูง ที่ผสมผสานกลศาสตร์ควอนตัมและกลศาสตร์โมเลกุลนี้ จะให้ผลการศึกษาที่สามารถ อธิบายพฤติกรรมของไอออนลบเมื่อละลายอยู่ในน้ำได้ถูกต้องน่าเชื่อถือมากขึ้น (มากกว่าผลการ ศึกษา ที่ผ่านๆ มา ซึ่งดำเนินการในระดับเอมพิริกัลเท่านั้น) นอกเหนือจากสมบัติเชิง โครงสร้างและพลวัต ของชั้นซอลเวชันแล้ว ผู้วิจัยได้สนใจที่จะประยุกต์เทคนิคการซิมูเลชันขั้นสูงดังกล่าว สำหรับการศึกษา การแลกเปลี่ยนลิแกนด์ที่เกิดขึ้น ภายในชั้นซอลเวชันของไอออนด้วย โดยจะศึกษาอัตราเร็วและ กระบวนการของการแลกเปลี่ยนลิแกนด์ สำหรับระบบของไอออนทั้งที่อยู่ในน้ำบริสุทธิ์และใน สารละลายที่มีทั้งน้ำและแอมโมเนียเป็นตัวทำละลาย โดยคาดหวังว่า ผลการศึกษาที่ได้ จะสามารถ ใช้เป็นข้อมูลพื้นฐานสำหรับการอธิบายสมบัติหรือพฤติกรรม ของไอออนที่มีบทบาทต่อกระบวนการ ทางด้านเคมีและชีวเคมีของสิ่งมีชีวิตต่อไป

นอกจากนี้ วัตถุประสงค์ที่สำคัญอีกประการหนึ่งของโครงการนี้คือ การผลิตนักศึกษาระดับ บัณฑิตศึกษาที่มีคุณภาพ เพื่อพัฒนาเป็นนักวิจัยรุ่นใหม่ที่มีความรู้ความสามารถ มีประสบการณ์ในการ ทำวิจัยอย่างดี และพร้อมจะเป็นบุคลากรที่มีคุณภาพในการสร้างความเข้มแข็งทางด้านงานวิจัยพื้นฐาน ของประเทศต่อไป

8. ระเบียบวิธีวิจัย ประกอบด้วย

- 1) การสืบคันข้อมูลที่จำเป็น ได้แก่ วารสารวิชาการต่างประเทศที่เกี่ยวข้องกับหัวข้องานวิจัย โดยทำการสืบคันและรวบรวมข้อมูลให้ได้มากที่สุด เพื่อใช้เป็นข้อมูลเบื้องต้นสำหรับการ วางแนวทางในการทำวิจัยขั้นต่อไป
- 2) การคำนวณทางกลศาสตร์ควอนตัม เพื่อศึกษาผลของสหสัมพันธ์ของอิเล็กตรอน และผล ของส่วนสนับสนุนหลายอนุภาคที่มีต่อระบบที่ทำการศึกษา
- 3) การพัฒนาและปรับแปลงโปรแกรมการจำลองพลวัตเชิงโมเลกุล ได้แก่ การดัดแปลง แก้ไข และการทดสอบการทำงานของโปรแกรมจำลองพลวัตเชิงโมเลกุล ให้สามารถนำมา ประยุกต์กับระบบที่สนใจได้ ขั้นตอนนี้ รวมถึง การสร้างฟังก์ชันศักย์ และการคำนวณหา พารามิเตอร์ต่างๆ ที่จำเป็นสำหรับการจำลองพลวัตเชิงโมเลกุล
- 4) การเก็บรวบรวมและการวิเคราะห์ข้อมูล รวมถึงการนำเสนอผลการศึกษาและการ เปรียบเทียบผลการศึกษาที่ได้จากการจำลองพลวัตเชิงโมเลกุลกับผลการศึกษาที่ได้เคยมี ผู้กระทำมาบ้างแล้ว เพื่อนำไปสู่ข้อสรุป ข้อสังเกต และข้อเสนอแนะต่างๆ ที่จะเป็น

- ประโยชน์ในเชิงลึก เพื่อนำไปสู่ความรู้ความเข้าใจเกี่ยวกับสมบัติเชิงโครงสร้างและเชิง พลวัตของไอออนและซอลเวชันของไอออนที่อยู่ในสารละลายได้มากขึ้น
- 5) จัดเตรียมเอกสารเพื่อส่งตีพิมพ์ในวารสารวิชาการระดับนานาชาติ (จำนวน 6 เรื่อง)

9. เนื้อหางานวิจัย

ในระยะเวลาประมาณ 3 ปี ผู้วิจัยได้ดำเนินการต่างๆ ตามระเบียบวิจัย ดังนี้

- 1) ทำการค้นข้อมูลเอกสารทางวิชาการที่เกี่ยวข้องกับงานวิจัย
- 2) ทำการคำนวณ แอบ อินิชิโอ เพื่อศึกษาผลของการมีอยู่ของหลายอนุภาค (many-body effects) และผลที่เกี่ยวข้องกับสหสัมพันธ์ของอิเล็กตรอน (electron correlation) ที่มีต่อ สมบัติเชิงโครงสร้างและพลังงานของระบบที่ทำการศึกษา
- 3) ทำการสร้างฟังก์ชันศักย์เพื่อใช้อธิบายอันตรกิริยาของอนุภาคในระบบ โดยฟังก์ชันที่สร้าง ขึ้นดังกล่าวนี้ ผ่านการตรวจสอบคุณภาพเป็นอย่างดีเพื่อนำไปใช้ในส่วนของการจำลอง พลวัตเชิงโมเลกุลต่อไป
- 4) ทำการดัดแปลงโปรแกรมจำลองพลวัตเชิงโมเลกุล (QM/MM และ QMCF MD programs) เพื่อใช้สำหรับการจำลองระบบที่ทำการศึกษา
- 5) ทำการจำลองพลวัตเชิงโมเลกุล (QM/MM และ QMCF MD simulations) ของระบบที่ ทำการศึกษา
- 6) ทำการเก็บข้อมูล วิเคราะห์ผลการศึกษา และจัดทำเอกสารผลงานวิจัยตีพิมพ์ใน วารสารวิชาการระดับนานาชาติ จำนวน 6 ฉบับ (ดูภาคผนวก)

10. ผลลัพธ์ที่ได้จากโครงการ

บทความ (articles) ที่ได้รับการตีพิมพ์ในวารสารวิชาการระดับนานาชาติจำนวน 6 เรื่อง ได้แก่

- 1) **Anan Tongraar**, Supot Hannongbua and Bernd M. Rode "QM/MM MD simulations of iodide ion (I) in aqueous solution: A delicate balance between ion-water and water-water H-bond interactions" J. *Phys. Chem. A*, **2010**, 114, 4334-4339.
- 2) **Anan Tongraar**, Jiraroj T-Thienprasert, Saroj Rujirawat and Sukit Limpijumnong "Structure of the hydrated Ca²⁺ and Cl⁻: Combined X-ray absorption measurements and QM/MM MD simulations study" *Phys. Chem. Chem. Phys.* **2010**, 12, 10876-10887.
- 3) Apirak Payaka, **Anan Tongraar** and Bernd M. Rode "QM/MM dynamics of CH₃COO-water hydrogen bonds in aqueous solution" J. *Phys. Chem. A*, **2010**, 114 10443-10453.
- 4) **Anan Tongraar**, Pathumwadee Yotmanee and Apirak Payaka, "Characteristics of CO₃²-water hydrogen bonds in aqueous solution: Insights from HF/MM and B3LYP/MM MD simulations" *Phys. Chem. Chem. Phys.* **2011**, in press, DOI: 10.1039/C1CP21802F.
- 5) Viwat Vchirawongkwin, Chinapong Kritayakornupong and **Anan Tongraar**, "Characterization of the structure and dynamics of an aqueous Hg²⁺ solution by an *ab initio* molecular dynamics study" *J. Mol. Liq.*, **2011**, 163, 147-152.
- 6) Viwat Vchirawongkwin, Chinapong Kritayakornupong, Anan Tongraar and Bernd M. Rode, "Symmetry breaking and hydration structure of carbonate and nitrate in aqueous solution: A study by ab initio quantum mechanical charge field molecular dynamics" J. Phys. Chem. B, 2011, 115, 12527-12536.
- 7) Viwat Vchirawongkwin, Chokchai Pornpiganon, Chinapong Kritayakornupong, Anan Tongraar and Bernd M. Rode, "The stability of bisulfite and sulfonate ions in aqueous solution characterized by hydration structure and dynamics" J. Phys. Chem. B, 2012, 116, 11498-11507.

หมายเหตุ จำนวนบทความตีพิมพ์ที่ระบุในสัญญารับทุนคือ 5 เรื่อง แต่จำนวนบทความที่ได้ จากโครงการนี้ มีจำนวนทั้งสิ้น 7 เรื่อง



1. สำเนา Reprint ของงานวิจัยเรื่องที่ 1

Anan Tongraar, Supot Hannongbua and Bernd M. Rode "M/MM MD simulations of iodide ion (I) in aqueous solution: A delicate balance between ion-water and water-water H-bond interactions" J. *Phys. Chem. A*, **2010**, 114, 4334-4339.

QM/MM MD Simulations of Iodide Ion (I⁻) in Aqueous Solution: A Delicate Balance between Ion-Water and Water-Water H-Bond Interactions

Anan Tongraar,*,† Supot Hannongbua,‡ and Bernd Michael Rode§

School of Chemistry, Institute of Science, Suranaree University of Technology, Nakhon Ratchasima 30000, Thailand, Department of Chemistry, Faculty of Science, Chulalongkorn University, Bangkok 10330, Thailand, and Theoretical Chemistry Division, Institute of General, Inorganic and Theoretical Chemistry, University of Innsbruck, Innrain 52a, A-6020 Innsbruck, Austria

Received: November 01, 2009; Revised Manuscript Received: February 17, 2010

The characteristics of an iodide ion (I⁻) in aqueous solution were investigated by means of HF/MM and B3LYP/MM molecular dynamics simulations, in which the ion and its surrounding water molecules were treated at HF and B3LYP levels using the LANL2DZdp and D95 V+ basis sets for I⁻ and water, respectively. According to both the HF/MM and B3LYP/MM results, the ion—water interactions are relatively weak, compared to the water—water hydrogen bonds, thus causing an unstructured nature of the hydration shell. Comparing the HF and B3LYP treatments for the description of this hydrated ion, the overestimation of the ion—water hydrogen-bond strength by the B3LYP method is recognizable, yielding a remarkably more compact and too rigid ion—water complex.

1. Introduction

The properties of aqueous electrolyte solutions containing ions have been investigated for a long time by both experimental and theoretical approaches.^{1–4} In contrast to the extensive studies of cations solvated in aqueous solution, a detailed picture of anion hydration is available for only a few anions. It is known that the interactions of anions with water are generally weaker than those of most cations and are energetically comparable with the water—water interactions in bulk water. Consequently, this leads to the interesting question as to whether the anion—water complexes, X⁻(H₂O)_n, adopt "interior" (I) or "surface" (S) states.⁵ Experimental data, from photoelectron detachment studies,^{6,7} of anion—water clusters have been interpreted in such a way that, except for F⁻, all halogen anions are believed to reside at such surfaces. However, these studies do not provide any structural details.

Time-dependent simulation methods, in particular molecular dynamics (MD), have been employed to provide molecular level data that is not experimentally accessible. For more than three decades, such simulations have been carried out, relying mostly on empirical force fields. Thus, the quality and accuracy of the simulation results depend strongly on the reliability of the anion-water and water-water potentials employed in the simulations.^{8–13} For example, the use of different parametrized potentials, that is, with and without treatment of molecular polarizability, predicted quite different structural properties. 13,14 In most cases, polarizable models can provide qualitative predictions in good agreement with the currently available experimental data. However, it would indeed be a substantial advance, as well as difficulty, to obtain an appropriate value of halogen ion polarizability since there are no direct measurements of this quantity in aqueous solution, and the available data are usually extrapolations from ionic crystals and salt solutions. 15,16

With the current computational capacity, more sophisticated and accurate simulation techniques incorporating quantum mechanics, in particular a so-called combined quantum mechanics/molecular mechanics (QM/MM) approach, have become an elegant tool for studying structural and dynamical properties of various ions in solution.^{4,17–21} This technique treats the activesite region, for example, the solvation shell around the ions, quantum mechanically, while the environment consisting of further solvent molecules can be described by molecular mechanical potentials. By the QM/MM scheme, the complicated many-body contributions, which are mostly due to polarization effects within the first solvation sphere of the ions, can be reliably included. Recently, the QM/MM MD technique was applied to aqueous solutions of F⁻ and Cl⁻,^{20,21} revealing that both F--water and Cl--water hydrogen bonds are strong enough to surpass the water-water interactions, that is, these ions try to form hydrogen bonds to water ligands resulting in the preferred "internally" solvated species in aqueous solution. In the case of Cl⁻, however, the Cl⁻-water hydrogen bond is relatively weak, leading to mutual arrangements between the directional hydrogen bond(s) of neighboring water molecules to the ion and the hydrogen bonding among water molecules, which thus produces an asymmetrically solvated Cl⁻.²⁰

Besides F⁻ and Cl⁻, the behavior of iodide ion (I⁻) in aqueous solution is of considerable interest since it has a very large ionic radius compared to the other halides, and thus represents one of the ions preferring an asymmetric first hydration shell in aqueous solution due to its weak ion—water interactions.^{6,22} X-ray diffraction studies have reported scattered coordination numbers of I⁻ in water, ranging from 4 to 9.^{3,6,23} Using X-ray absorption near-edge structure (XANES) analysis, it was demonstrated that this ion forms a quite loosely arranged first hydration shell.²⁴ The diffuse character of the hydrated I⁻, with a large range of coordination numbers, is also apparent from most previous force-field-based simulation studies.^{8–13} By means of Car—Parrinello (CP) MD technique, a disruptive influence of I⁻ on the local structure of bulk water is predicted, leading to the formation of a quite unstructured solvation shell.²⁵

^{*} To whom correspondence should be addressed. E-mail: anan_tongraar@yahoo.com. Fax: 0066-44-224185.

[†] Suranaree University of Technology.

[‡] Chulalongkorn University.

[§] University of Innsbruck.

Recently, CP-MD simulations of halide ions (F⁻, Cl⁻, Br⁻, and I⁻) in water have been carried out, providing more insights into the role of ion and molecular polarization in describing ion—water interactions.²⁶ In the case of electrolyte solutions, however, severe limitations of the CP-MD technique, in particular the use of simple GGA functionals such as BLYP and PBE and of the relatively small system size in such simulations, have repeatedly been demonstrated.^{4,19,27} Hence, in the present work the ab initio QM/MM MD technique is applied to the aqueous solution of I⁻, in order to provide more structural details of this hydrated ion.

2. Methods

Schematic details of the QM/MM MD method are available elsewhere in the literature.^{4,17,18} Briefly, the system is divided into two parts, namely, QM and MM regions. The total interaction energy of the system is defined as:

$$E_{\text{total}} = \langle \Psi_{\text{OM}} | \hat{H} | \Psi_{\text{OM}} \rangle + E_{\text{MM}} + E_{\text{OM-MM}}$$
 (1)

where $\langle \Psi_{\rm QM} | \hat{H} | \Psi_{\rm QM} \rangle$ refers to the interactions within the QM region, and $E_{\rm MM}$ and $E_{\rm QM-MM}$ represent the interactions within the MM and between the QM and MM regions, respectively. The QM region, the most interesting part, which includes a central I⁻ and its nearest-neighbor water molecules, is treated quantum mechanically using HF and B3LYP methods, while the rest of the system (i.e., the $E_{\rm MM}$ and $E_{\rm QM-MM}$) is described by classical pair potentials. In practice, the total force of the system is described by the following formula:

$$F_{\text{tot}} = F_{\text{MM}}^{\text{sys}} + (F_{\text{OM}}^{\text{QM}} - F_{\text{MM}}^{\text{QM}})$$
 (2)

where $F_{\text{MM}}^{\text{NM}}$, $F_{\text{MM}}^{\text{NM}}$, and $F_{\text{MM}}^{\text{NM}}$ are the MM force of the total system, the QM force in the QM region, and the MM force in the QM region, respectively. In this respect, the $F_{\text{MM}}^{\text{NM}}$ term accounts for the coupling between the QM and MM region.

During QM/MM simulations, the exchange of water molecules between the QM and MM regions can occur frequently. With regards to this point, the forces acting on each particle in the system are switched according to which region the water molecule is entering or leaving and can be defined as:

$$F_i = S_{\rm m}(r)F_{\rm OM} + (1 - S_{\rm m}(r))F_{\rm MM} \tag{3}$$

where $F_{\rm QM}$ and $F_{\rm MM}$ are the quantum mechanical and molecular mechanical forces, respectively. $S_{\rm m}(r)$ is a smoothing function, ²⁸

$$S_{\rm m}(r) = 1, \text{ for } r \le r_1$$

$$S_{\rm m}(r) = \frac{(r_0^2 - r^2)^2 (r_0^2 + 2r^2 - 3r_1^2)}{(r_0^2 - r_1^2)^3}, \text{ for } r_1 < r \le r_0$$
(4)
$$S_{\rm m}(r) = 0, \text{ for } r > r_0$$

where r_1 and r_0 are the distances characterizing the start and the end of the QM region, respectively, and applied within an interval of 0.2 Å (i.e., between the I⁻O distances of 4.4–4.6 Å) to ensure a continuous change of forces at the transition between QM and MM regions. It has been demonstrated that the use of smoothing is essential for proper energy conservation.¹⁸

With regard to the QM/MM technique, it is commonly known that the quality of the simulation results depends crucially on the selected QM method, basis set, and QM region size. In general, all of these essential parameters must be optimized, forcing compromises between the quality of the simulation results and the CPU time required to attain them. Since correlated QM calculations, even at the simple MP2-level, are

still beyond the current computational feasibility, the description of all interactions within the QM region are restricted to the HF and hybrid density functional B3LYP methods using the LANL2DZdp^{29,30} and D95 V+³¹ basis sets for I⁻ and water, respectively. To preliminarily check the validity of the HF and B3LYP methods employed for this particular system, geometry optimizations of the $I^-(H_2O)_n$ complexes, where n = 1, 3, and 4, were carried out at HF, B3LYP, MP2, and CCSD levels of accuracy using the above-mentioned basis sets. Ab initio calculations of I^- (H_2O)_{n=1-6} clusters have been studied extensively, 32,33 revealing that most of the clusters for n = 2-6have several low energy conformations that are close to the minimum energy geometries. In addition, as the number of water molecules increases, the sum of ion-water interactions becomes weaker than the sum of water-water interactions. In the present study, some selected clusters for n = 1, 3, and 4 were optimized and only the structures correspond to the lowest energies, namely $1(C_s)$, $3(C_3)$, and $4(C_4)$ structures, are reported. All interaction energies were corrected for the basis set superposition error (BSSE).^{32,33} These minimum energy structures are of the same type as obtained by Kim et al.³² As can be seen from the data in Table 1, the HF stabilization energies, which are the most relevant data determining solute-solvent interactions, show good agreement with those of the correlated ab initio methods. In terms of the hydrogen-bond length, however, the HF method predicts a considerably longer I⁻-H-O distance, as a consequence of the neglect of electron correlation effects. In contrast to this, the B3LYP method, although it produces the hydrogen-bond length which is in better agreement with the correlated ab initio methods, is found to considerably overrate the stabilization energy. Overall, the HF and B3LYP methods employed in this work are expected to be reliable enough to achieve a sufficient level of accuracy in the QM/ MM simulations.

To define the size of the QM region, a classical MD simulation using pair potentials, that is, a simulation in which the ion-water and water-water interactions are described by means of newly generated pair potentials and a set of potential functions obtained from the published literature, ^{34,35} respectively, has been preliminarily performed. According to the resulting I-O radial distribution function (RDF), the first minimum of the I-O peak is exhibited at around 5 Å, implying that a QM region with radius of 5 Å seemed to be desirable for the present study. However, an integration up to first minimum of the I-O peak yields about 20-22 water molecules, which is too timeconsuming for each QM/MM MD step to evaluate the QM forces for all particles within this QM size for a simulation with 50 000 to 100 000 steps. Hence, a smaller QM size with a radius of 4.4 Å was chosen, which includes I⁻ and about 14–16 water molecules. This QM size is assumed to be large enough to include most effects of many-body contributions, that is, most of interactions beyond the QM region could be well accounted for based on pairwise additive approximations. As can be seen in the next section (cf. Figure 1), the smooth shape of the I-O RDF between 4.4 and 4.6 Å supports that there are no artifacts caused by the QM-MM border, and that transition of molecules between both regions occurs smoothly.

A flexible model, which describes intermolecular³⁴ and intramolecular³⁵ interactions, was employed for water, ensuring the compatibility and a smooth transition, when water molecules move from the QM region with full flexibility to the MM region. The pair potential functions for I⁻H₂O interactions were newly developed. The 1450 HF and 1400 B3LYP interaction points

TABLE 1: Stabilization Energies and Structural Parameters of the Minimum Energy I⁻-(H₂O)_{n=1,3,4} Structures

	0	2 / 1,5,0,1			
method I^- – $(H_2O)_n$	HF	B3LYP	MP2	CCSD	
		For $n = 1 [1(C_s)]$			
ΔE^{a} (kcal mol ⁻¹)	-10.39 ± 0.24	-12.45 ± 0.11	-10.36 ± 0.28	-10.48 ± 0.28	
$R_{\mathrm{I-H1}}$ (Å)	2.995	2.678	2.693	2.734	
$R_{\mathrm{O-H1}}$ (Å)	0.958	0.995	0.993	0.990	
$R_{\mathrm{O-H2}}$ (Å)	0.952	0.978	0.980	0.980	
$A_{\mathrm{I-H1-O}}$ (°)	138.91	155.88	154.72	152.19	
$A_{\mathrm{H1-O-H2}}$ (°)	108.15	106.20	106.81	106.59	
		For $n = 3$ [(3C ₃)]			
ΔE^a (kcal mol ⁻¹)	-33.82 ± 1.63	-41.80 ± 1.4	-34.70 ± 1.80	-34.80 ± 1.74	
$R_{\mathrm{I-H1}}$ (Å)	3.116	2.925	2.895	2.910	
$R_{\mathrm{O-H1}}$ (Å)	0.956	0.986	0.987	0.986	
$R_{\mathrm{O-H2}}$ (Å)	0.958	0.992	0.988	0.986	
$A_{\mathrm{I-H1-O}}$ (°)	137.88	139.15	141.18	141.66	
$A_{\mathrm{H1-O-H2}}$ (°)	109.84	107.04	107.59	107.58	
		For $n = 4 [(4C_4)]$			
ΔE^a (kcal mol ⁻¹)	-50.85 ± 6.72	-64.32 ± 8.13	-52.81 ± 7.07	-48.88 ± 3.02	
$R_{\mathrm{I-H1}}$ (Å)	3.283	3.150	3.114	3.083	
$R_{\mathrm{O-H1}}$ (Å)	0.955	0.982	0.985	0.984	
$R_{\mathrm{O-H2}}$ (Å)	0.962	1.006	0.997	0.991	
$A_{\mathrm{I-H1-O}}$ (°)	130.08	127.09	128.51	131.78	
$A_{\mathrm{H1-O-H2}}$ (°)	109.62	107.13	107.48	107.40	

 $[^]a$ $\Delta E = (\Delta E_{\rm N} + \Delta E_{\rm B})/2 \pm {\rm BSSE}/2$, where $\Delta E_{\rm N}$ and $\Delta E_{\rm B}$ are energies without and with BSSE correction, respectively.³²

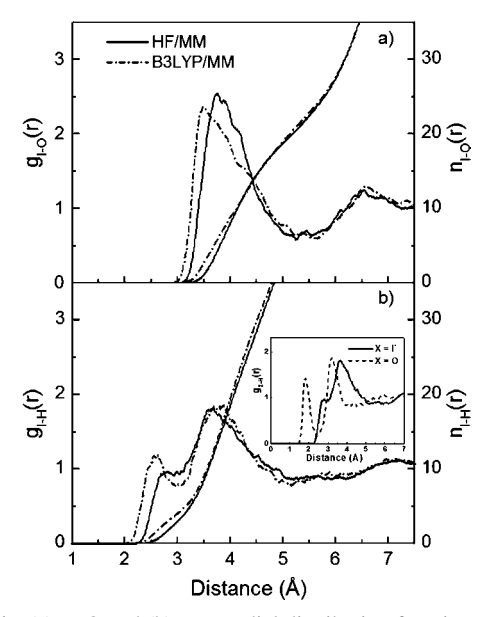


Figure 1. (a) I—O and (b) I—H radial distribution functions and their corresponding integration numbers obtained from the HF/MM and B3LYP/MM MD simulations.

for I⁻H₂O energy surfaces obtained from Gaussian03³⁶ calculations were fitted to the analytical forms of

$$\Delta E_{\text{I--H}_2\text{O}}^{\text{HF}} = \sum_{i=1}^{3} \left(\frac{A_{ia}}{r_{ia}^5} + \frac{B_{ia}}{r_{ia}^8} + C_{ia} \exp(-D_{ia} r_{ia}) + \frac{q_i q_a}{r_{ia}} \right)$$
(5)

and

$$\Delta E_{\text{I}-\text{H}_2\text{O}}^{\text{B3LYP}} = \sum_{i=1}^{3} \left(\frac{A_{ia}}{r_{ia}^5} + \frac{B_{ia}}{r_{ia}^9} + C_{ia} \exp(-D_{ia}r_{ia}) + \frac{q_i q_a}{r_{ia}} \right)$$
(6)

respectively, where A_{ia} , B_{ia} , C_{ia} , and D_{ia} are the fitting parameters (see Table 2), r_{ia} denotes the distances between the anions and the *i*th atom of water, and q are the respective atomic net

charges. The charge on the anion was set to -1.0, and the charges on O and H of water to -0.6598 and 0.3299, respectively. With regard to eqs 5 and 6, although the forms of pair potentials may not reflect the actual physical terms of interactions, their fitting to the ab initio energy surface led to an accurate basis for calculating the interaction energies within the defined area.

All MD simulations were performed in a canonical ensemble at 298 K with a time step of 0.2 fs. The system's temperature was kept constant using the Berendsen algorithm.³⁷ The cubic box, with a box length of 18.19 Å, employed in the simulations contained 1 I⁻ and 199 water molecules, assuming the experimental density of pure water. Long-range interactions were treated using the reaction-field procedure.³⁸ Starting from the equilibrium configuration obtained by the classical MD simulation, the corresponding HF/MM and B3LYP/MM simulations were separately performed with re-equilibration for 50 000 time steps. Then, the HF/MM and B3LYP/MM simulations were continued for 180 000 and 120 000 time steps, respectively, collecting the configuration data every 10th step.

3. Results and Discussion

The hydration shell structure of I⁻ is characterized through I-O and I-H RDFs, together with their corresponding integration numbers, as shown in Figure 1. With regard to the I-O RDFs (Figure 1a), both HF/MM and B3LYP/MM simulations reveal broad and unsymmetrical first peaks with maxima at 3.75 and 3.45 Å, respectively. The shape and height of I-O RDFs clearly suggests a high flexibility of I⁻ hydration. In addition, the first I-O peaks are not well separated from the bulk, implying that water molecules surrounding the ion can easily exchange with bulk water. Flexibility of the I- hydration is apparent when the I-O RDF is compared to that of smaller halide ions, like F⁻ and Cl⁻, obtained by analogous QM/MM MD simulations,^{20,21} as shown in Figure 2a. Comparing the HF/ MM and B3LYP/MMs I-O RDF, the observed shorter I-O maximum, of about 0.3 Å less, in the B3LYP/MM simulation implies that the DFT method predicts too strong ion-water interactions and thus a more structured first shell. According to

TABLE 2: Optimized Parameters of the Analytical Pair Potentials for the Interactions of Water with I^{-a}

pair HF-based Method	$\begin{array}{c} A \\ (kcal\ mol^{-1}\ \mathring{A}^5) \end{array}$	$\begin{array}{c} B \\ (kcal\ mol^{-1}\ \mathring{A}^8) \end{array}$	C (kcal mol ⁻¹)	$\mathop{D}_{(\mathring{A}^{-1})}$
I–H	-3202.3283	3387.7704	12 064.111	2.105 4279
	-2065.6868	7360.3925	-3144.580	2.098 5796
B3LYP-based Method	(kcal $\text{mol}^{-1} \text{ Å}^5$)	(kcal $\text{mol}^{-1} \text{ Å}^9$)	(kcal mol ⁻¹)	$(\mathring{\mathrm{A}}^{-1})$
I-H	-3953.7934	24 506.7233	-10 431.904	2.025 3397
I-O	-1721.8645	9327.24134	-4018.5833	2.222 7220

^a Interaction energies are in kcal mol⁻¹ and distances are in Å.

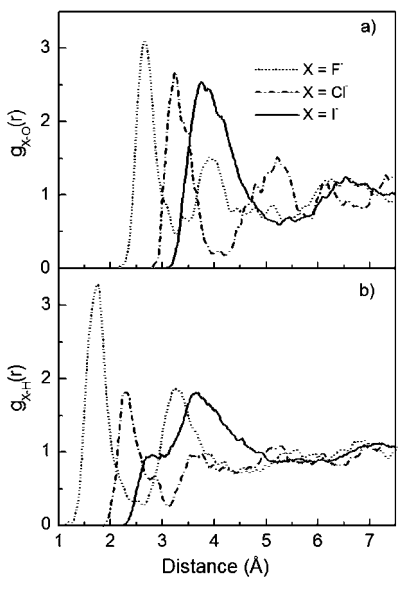


Figure 2. (a) X-O and (b) X-H radial distribution functions (X =F-, Cl-, and I-), as obtained from the compatible HF/MM MD

X-ray diffraction studies, 2,3,6 in which the I-O distance was measured to be in the range of 3.60–3.76 Å, the B3LYP method apparently overestimates the H-bond strength and thus predicts a too rigid solvation shell. The overestimation of H-bond strength by the B3LYP method has repeatedly been demonstrated in recent B3LYP/MM simulations of several other ions in solution.^{4,18,20} In both the HF/MM and B3LYP/MM simulations, integration up to the first I-O minimum yields about 19-20 water molecules. However, according to the observed unsymmetrical first I-O peaks, this large number of water molecules can certainly not be considered as the first shell coordination number of I-. Instead, it could be considered as the number of nearest-neighbor water molecules that are arranged within the (rather disordered) vicinity of the ion. Consequently, a different definition is needed for determining the "real" coordination numbers of I⁻, that is, to distinguish between the nearest-neighbor waters, whose arrangement is influenced by the mere presence of I- and those that are directly bound to the ion by hydrogen bonds and can thus be considered as "coordinated".

In this context, an analysis of the I-H RDF, as this reflects the characteristics of I-H-O hydrogen bonds, appears more appropriate in order to estimate the number of hydrogen-bonding waters. Further differences between the HF/MM and B3LYP/ MM simulations become obvious in the I-H RDFs, as depicted in Figure 1b. Concerning the feature of I⁻H⁻O interactions, a distance of about 1 Å between the first I-H and the first I-O peaks can be seen as an indication for a certain contribution of linear hydrogen-bond formation between I⁻ and its nearestneighbor water molecules, which will be further analyzed,

TABLE 3: Positions of $I-H1(R_{H1})$, $I-H2(R_{H2})$, and $I-O(R_0)$ Maxima in the RDFs, and the Coordination Numbers Calculated up to Their Corresponding I-H1 and I-O Minima $(n_{H1}(R) \text{ and } n_{O}(R))$

$R_{\rm H1}/\text{Å} (n_{\rm H1}(R))$	$R_{ m H2}$ /Å	$R_{\rm O}/{\rm \mathring{A}}\ (n_{\rm O}(R))$	method
2.80 (3.0)	3.60	3.75 (8.0 ^a)	HF/MM MD
2.60 (4.1)	3.80	$3.45 (8.8^a)$	B3LYP/MM MD
2.61 (5.1)	4.10	3.55 (6.6)	CP-MD ²⁵
2.70		3.60 (7.3)	SPC/E MD ¹¹
		3.60 (7.9)	SPC/E MD ¹³
2.77		3.71 (9.7)	TIP4P MD ⁸
2.71 (6)		3.64 (8.3)	MCDHO MC12
		3.60-3.76 (4.2-9.6)	$XRD^{2,3,6}$

^a Values obtained with respect to I-O distance of 4.0 Å.

however, later on. According to Figure 1b, the HF/MM simulation shows two distinguishable I-H peaks with maxima at 2.80 \pm 0.05 and 3.60 \pm 0.05 Å, respectively. The first I-H peak is less pronounced, in particular when compared to the first F-H and Cl-H RDFs, as depicted in Figure 2b. This confirms that the hydrogen bonds between I⁻ and its surrounding water molecules are quite weak. Compared to the characteristics of the O-H RDF of pure water obtained from a similar QM/ MM scheme (see insert in Figure 1b), 19 the first I-H peak indicates that the hydrogen bonds between the I- anion and adjacent water molecules, besides being longer, are of a lower strength compared to those between water molecules. In the B3LYP/MM simulation, the corresponding I—H RDF peak starts at a distance of about 0.25 Å shorter than that observed in the HF/MM simulation. In addition, the first I-H peak is more pronounced, with its maximum located at a shorter distance (2.60 Å) and consequently with a wider separation of the first and second I-H peaks (about 1.2 Å compared to the HF/MM value of 0.8 Å). These B3LYP/MM results clearly point at a more pronounced linear I-H-O hydrogen bond formation. The observed difference between the HF/MM and B3LYP/MM results cannot be solely attributed to the inclusion of some electron correlation effects at the DFT level of theory. Considering the experimental ion-water distance,3,6 it is rather the approximations and the parametrization of the B3LYP functional—which have been identified as a reason for the too rigid estimation of the hydration shells of other ions in solution as well^{4,18,20}—that cause this artificial stabilization. Recently, it has been demonstrated that the simple DFT functionals BLYP and PBE usually employed in the CP-MD scheme are even not capable to describe the solvent water itself, as the use of these functionals yields a glassy state rather than a liquid at room temperature and up to 400 K.²⁷

Quantitative comparisons of the I-O and I-H RDFs with classical and CP-MD simulations are summarized in Table 3. With regard to classical MC and MD simulations, 8,11-13 the observed differences in the shape and width of the I-O and I-H RDFs clearly indicate a significant sensitivity to the applied

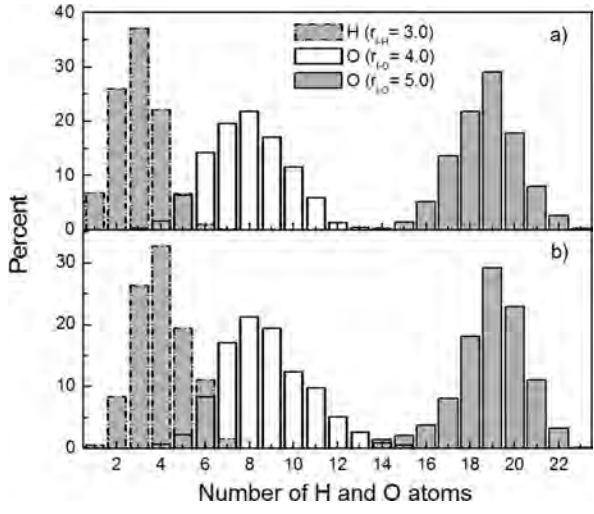


Figure 3. Probability distributions of hydrogen and oxygen atoms of water molecules surrounding the I^- ion, calculated up to first minimum of the I-H RDFs as well as to the I-O distances of 4 and 5 Å, respectively, as obtained from (a) HF/MM and (b) B3LYP/MM simulations.

empirical force field models. In the CP-MD simulation, ²⁵ although the characteristics of I—O and I—H RDFs had led to the conclusion that the solvation shell of I⁻ is rather unstructured and diffuse, the overestimation of ion—water hydrogen bonds is recognizable from a strong pronounced first I—H RDF at relatively shorter I—H distance compared to the HF/MM results. Further, the CP-MD method also predicts too short I—O distance when compared to the corresponding experimental data.^{2,3,6}

Figure 3 shows the probability distributions of hydrogen and oxygen atoms of surrounding water molecules, calculated up to first minimum of the I-H RDFs as well as to the I-O distances of 4 and 5 Å, respectively. Here, the values obtained within the I-O distance of 4 Å are assumed to represent water molecules able to form hydrogen bonds to the ion, that is, the water molecules corresponding to the first I-H peak. In both HF/MM and B3LYP/MM simulations, the probability distributions of the hydrogen and oxygen atoms of water are rather broad, showing clear evidence for the formation of a quite weak, unstructured solvation shell of I-, which has to be seen in relation to the ion's disruptive influence on the local structure of the solvent. According to the shape and height of the RDFs (Figure 1), the first-shell coordinated water molecules are defined by an I-H distance of about 3.0 Å. Integrations up to this I-H distance yield coordination numbers of 3.0 and 4.1 for the HF/ MM and B3LYP/MM simulations, respectively. In fact, a small shift in the selected I—H distance will have a significant impact on the number of water molecules counted. For example, at the slightly larger I-H distance of 3.3 Å, the most frequently observed numbers of hydrogen bonding waters increase from 3.0 to 5.8 (HF/MM) and from 4.1 to 6.4 (B3YP/MM). In comparison to the corresponding values of 8.0 and 8.8 water molecules, as obtained with respect to the I-O distance of 4.0 Å (i.e., a distance where the nearest-neighbor water molecules can involve in the linear I-H-O H-bond formation), these data compare well, however, with the experimentally estimated values ranging from 4.2 to 9.6.²

To provide more details on the structure of the hydrated I^- , the orientations of water molecules within the first hydration sphere of I^- were investigated, and the results are depicted in Figure 4. Here, the waters' orientations are described in terms of angle α (Figure 4a), which corresponds to the distributions of I^- O-H angles, and angle θ (Figure 4b), as defined by the

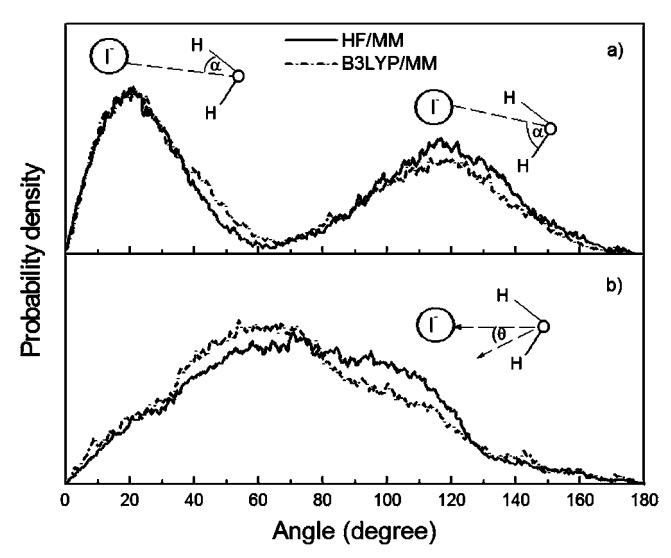


Figure 4. Probability distributions of the (a) α and (b) θ angles, calculated within the I–O distance of 4 Å.

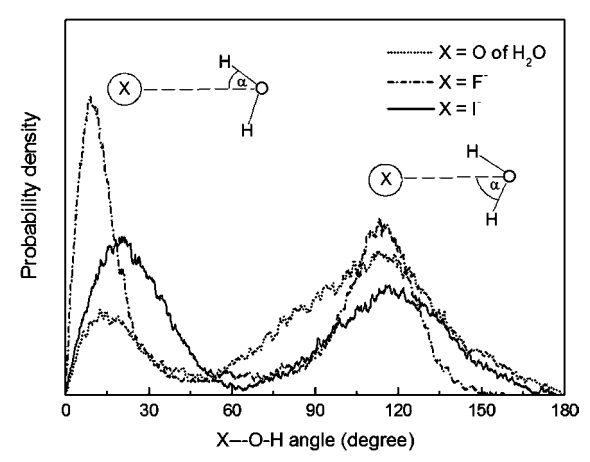


Figure 5. Distributions of X-O-H angle ($X=O, F^-$, and I^-), calculated up to the first minimum of the O-O and F-O RDFs and within the I-O distance of 4 Å.

dipole vector of the water molecule and the I ^-O vector. In both the HF/MM and B3LYP/MM simulations, the distributions of the α angle (Figure 4a) display a significant deviation from a linear ion—water hydrogen bond, in good agreement with the observed nonlinear I–H–O angle of the XANES experiments. 24 In Figure 4b, the observed broad θ distributions clearly confirm a highly flexible arrangement of water molecules in the hydration sphere of I $^-$.

Figure 5 displays the arrangement of water molecules around I⁻ and F⁻ compared to those in the bulk water itself, as obtained by the similar QM/MM methodology.²¹ For F⁻, it is obvious that F-water hydrogen bonds are predominantly linear in aqueous solution. In the case of I⁻, however, the observed broad distribution of the I-O-H angle clearly indicates the flexibility of the weak I⁻-water hydrogen bonds. In comparison to the QM/MM data for pure water, especially in terms of the shape and height of the O-O and O-H RDFs (cf., Figure 4 in ref 19), the "structure-breaking" behavior of I⁻ is well-reflected. In this context, the water—water interactions appear to dominate over ion-water hydrogen bonding, that is, most of the water molecules surrounding the ion are arranged by the forces exerted by the neighboring water molecules in the same shell and/or the bulk, rather than by the influence of I-. To confirm this statement, the hydrogen bond lifetimes of water molecules surrounding the ion were estimated via the mean residence times

TABLE 4: Positions of X-H1($R_{\rm H1}$), X-H2 ($R_{\rm H2}$), and X-O ($R_{\rm O}$) Maxima in the RDFs, Where X = I, F, Cl, or O, and the Coordination Numbers Calculated up to Their Corresponding X-H1 and X-O Minima ($n_{\rm HI}(r)$ and $n_{\rm O}(r)$), and Lifetime of X···H Hydrogen Bonds of the Anions Compared to Those in Bulk Water

solute/ion $(n_{\rm O}(R))$	$R_{\mathrm{H}1}/\mathrm{\mathring{A}}$ $(n_{\mathrm{H}1}(R))$	$R_{ m H2}/{ m \AA}$	$R_{ m O}/{ m \AA}$	H-bond lifetime $ au_{ m H_2}^0{ m O}$	method
I-	2.80 (3.0)	3.60	3.75 (8.0*)	0.13*	HF/MM
	2.60 (4.1)	3.80	3.45 (8.8*)	0.18^{*}	B3LYP/MM
F^-	1.74 (4.8)	3.21	2.68 (4.6)	0.40	HF/MM ²¹
Cl^-	2.42 (4.9)		3.24 (5.6)	0.22	HF/MM^{21}
H_2O	1.83 (2.2)		2.78(4.7)	0.20	HF/MM^{21}
	2.06 (3.5)		2.92 (4.2)	0.33	HF/MM^{17}

^{*} Values obtained with respect to I-O distance of 4.0 Å.

(MRT). The MRT values of water molecules surrounding the ion were evaluated using the direct method,³⁹ with a time parameter t^* of 0.0 ps. Due to the diffuse character of the solvation shell of I^- , an I-O distance of 4.0 Å was selected, which was assumed to be a rough estimate of the first solvation shell and a limit for significant ion—water interactions. According to this evaluation limit, the HF/MM and B3LYP/MM simulations produced MRT values of 0.13 and 0.18 ps, respectively, compared to the corresponding value of between 0.20 and 0.33 ps for pure water obtained by the methodically compatible HF/MM simulations. ^{17,21} These data clearly show that the water molecules surrounding the I^- ion are more mobile than those in the pure solvent, and that the ion forms an unstructured first solvation shell in aqueous solution.

Table 4 compares the data obtained for I^- with those resulting from similar HF/MM simulations for F^- and $Cl^-,^{20,21}$ outlining the transition from structure-forming to structure-breaking properties within this series of halogenide ions, and the corresponding trends in hydrogen bond characteristics and hydrate structure.

4. Conclusion

On the basis of both HF/MM and B3LYP/MM simulations, the iodide—water interactions can be characterized as weak, leading to a high flexibility of the loosely bound first solvation shell and a permanent competition between hydrogen bonding of surrounding water to the ion and hydrogen bonding among water molecules. Consequently, this induces the well-known structure-breaking ability of I⁻. Comparing the HF and B3LYP treatments for the QM part of the system, the overestimation of ion-water hydrogen bonds by the B3LYP method is evident, in accordance with the reported tendency of the DFT scheme to predict too rigid ion solvation complexes. According to the fact that the solvation shell of I is rather unstructured and diffuse, and that the QM size employed in the present study is relatively small, the corresponding dynamical data, and in particular the mechanism for the shell-bulk water exchange process, may not be accurately obtainable by the present QM/ MM study. To obtain such details, a larger QM size and an improved methodology seems desirable, although it would seriously expand the computational effort.

Acknowledgment. This work was financially supported by the Thailand Research Fund (TRF) and Suranaree University of Technology (SUT). B.M.R. acknowledges support by the Austrian Science Foundation (FWF).

References and Notes

- (1) Impey, R. W.; Madden, P. A.; McDonald, I. R. J. Phys. Chem. 1983, 87, 5071.
 - (2) Ohtaki, H.; Radnai, T. Chem. Rev. 1993, 93, 1157.
- (3) Enderby, J. E.; Neilson, G. W. Water a Comprehensive Treatise; Plenum: New York, 1979, vol. 1.
- (4) Rode, B. M.; Schwenk, C. F.; Tongraar, A. J. Mol. Liq. 2004, 110, 105
 - (5) Stuart, S. J.; Berne, B. J. J. Phys. Chem. 1996, 100, 11934.
- (6) Markovich, G.; Pollack, S.; Giniger, R.; Cheshnovsky, O. *J. Chem. Phys.* **1994**, *101*, 9344.
 - (7) Markovich, G.; Cheshnocsky, O. J. Phys. Chem. 1994, 98, 3550.
 - (8) Tóth, G. J. Chem. Phys. 1996, 105, 5518.
- (9) Brodskaya, E.; Lyubartsev, A. P.; Laaksonen, A. J. Chem. Phys. 2002, 116, 7879.
 - (10) Lee, S. H.; Rasaiah, J. C. J. Phys. Chem. 1996, 100, 1420.
 - (11) Dang, L. X.; Garrett, B. C. J. Chem. Phys. 1993, 99, 2972.
- (12) Ayala, R.; Martinez, J. M.; Pappalardo, R. R.; Marcos, E. S. J. Chem. Phys. 2003, 119, 9538.
- (13) Koneshan, S.; Rasiah, J. C.; Lynden-Bell, R. M.; Lee, S. H. J. Phys. Chem. B 1998, 102, 4193.
- (14) Yeh, I.-C.; Perera, L.; Berkowitz, M. L. Chem. Phys. Lett. 1997, 264, 31.
 - (15) Jungwirth, P.; Tobias, D. J. J. Phys. Chem. A 2002, 106, 379.
- (16) Tobias, D. J.; Jungwirth, P.; Parrinello, M. J. Chem. Phys. 2001, 114, 7036.
- (17) Xenides, D.; Randolf, B. R.; Rode, B. M. J. Chem. Phys. 2005, 122, 174506.
- (18) Kerdcharoen, T.; Liedl, K. R.; Rode, B. M. Chem. Phys. 1996, 211, 313.
- (19) Tongraar, A.; Tangkawanwanit, P.; Rode, B. M. J. Phys. Chem. A 2006, 110, 12918.
 - (20) Tongraar, A.; Rode, B. M. Phys. Chem. Chem. Phys. 2003, 5, 357.
 - (21) Tongraar, A.; Rode, B. M. Chem. Phys. Lett. 2005, 403, 314.
- (22) Koch, D. M.; Peslherbe, G. H. *Chem. Phys. Lett.* **2002**, *359*, 381. (23) Markovich, G.; Giniger, R.; Levin, M.; Cheshnovsky, O. *J. Chem.*
- (23) Markovich, G.; Giniger, R.; Levin, M.; Cheshnovsky, O. J. Chem Phys. **1991**, *95*, 9416.
- (24) Tanida, H.; Kato, K.; Watanabe, I. Bull. Chem. Soc. Jpn. 2003, 76, 1735.
 - (25) Heuft, J. M.; Meijer, E. J. J. Chem. Phys. 2005, 123, 94506.
- (26) Guàrdia, E.; Skarmoutsos, I. J. Chem. Theory Comput. 2009, 5, 1449.
- (27) Yoo, S.; Zeng, X. C.; Xantheas, S. S. J. Chem. Phys. **2009**, 130, 221102.
- (28) Brooks, B. R.; Bruccoleri, R. E.; Olafson, B. D.; States, D. J.; Swaminathan, S.; Karplus, M. J. Comput. Chem. 1983, 4, 187.
 - (29) Hay, P. J.; Wadt, W. R. J. Chem. Phys. 1985, 82, 284.
- (30) Check, C. E.; Faust, T. O.; Bailey, J. M.; Wright, B. J.; Gilbert, T. M.; Sunderlin, L. S. J. Phys. Chem. A 2001, 105, 8111.
- (31) Dunning Jr., T. H.; Hay, P. J. Modern Theoretical Chemistry; Plenum Press: New York, 1976.
- (32) Kim, J.; Lee, H. M.; Suh, S. B.; Majumdar, D.; Kim, K. S. *J. Chem. Phys.* **2000**, *113*, 5259.
 - (33) Lee, H. M.; Kim, D.; Kim, K. S. J. Chem. Phys. 2002, 116, 5509.
 - (34) Stillinger, F. H.; Rahman, A. J. Chem. Phys. **1978**, 68, 666.
- (35) Bopp, P.; Jancsó, G.; Heinzinger, K. Chem. Phys. Lett. 1983, 98, 129.
- (36) Frisch, M. J.; Trucks, G. W.; Schlegel, H. B.; Scuseria, G. E.; Robb, M. A.; Cheeseman, J. R.; Montgomery, J. A.; Vreven, T.; Kudin, K. N.; Burant, J. C.; Millam, J. M.; Iyengar, S. S.; Tomasi, J.; Barone, V.; Mennucci, B.; Cossi, M.; Scalmani, G.; Rega, N.; Peterson, G. A.; Nakatsuji, H.; Hada, M.; Ehara, M.; Toyota, K.; Fukuda, R.; Hasegawa, J.; Ishida, M.; Nakajima, T.; Honda, Y.; Kitao, O.; Nakai, H.; Klene, M.; Li, X.; Knox, J. E.; Hratchian, H. P.; Cross, J. B.; Bakken, V.; Adamo, C.; Jaramillo, J.; Gomperts, R.; Stratmann, R. E.; Yazyev, O.; Austin, A. J.; Cammi, R.; Pomelli, C.; Ochterski, J. W.; Ayala, P. Y.; Morokuma, K.; Voth, G. A.; Salvador, P.; Dannenberg, J. J.; Zakrzewski, V. G.; Dapprich, S.; Daniels, A. D.; Strain, M. C.; Farkas, O.; Malick, D. K.; Rabuck, A. D.; Raghavachari, K.; Foresman, J. B.; Ortiz, J. V.; Cui, Q.; Baboul, A. G.; Clifford, S.; Cioslowski, J.; Stefanov, B. B.; Liu, G.; Liashenko, A.; Piskorz, P.; Komaromi, I.; Martin, R. L.; Fox, D. J.; Keith, T.; Al-Laham, M. A.; Peng, C. Y.; Nanayakkara, A.; Challacombe, M.; Gill, P. M. W.; Johnson, B.; Chen, W.; Wong, M. W.; Gonzalez, C.; Pople, J. A. GAUSSIAN 03, Revision D.1; Gaussian, Inc.: Wallingford, CT, 2005.
- (37) Berendsen, H. J. C.; Grigera, J. R.; Straatsma, T. P. J. Phys. Chem. **1987**, 91, 6269.
- (38) Adams, D. J.; Adams, E. H.; Hills, G. J. *Mol. Phys.* **1979**, *38*, 387. (39) Hofer, T. S.; Tran, H. T.; Schwenk, C. F.; Rode, B. M. *J. Comput. Chem.* **2004**, *25*, 211.

JP910435D

1. สำเนา Reprint ของงานวิจัยเรื่องที่ 2

Anan Tongraar, Jiraroj T-Thienprasert, Saroj Rujirawat and Sukit Limpijumnong "Structure of the hydrated Ca²⁺ and Cl̄: Combined X-ray absorption measurements and QM/MM MD simulations study" *Phys. Chem. Chem. Phys.* **2010**, 12, 10876-10887.

Structure of the hydrated Ca²⁺ and Cl⁻: Combined X-ray absorption measurements and QM/MM MD simulations study

Anan Tongraar,* a Jiraroj T-Thienprasert, bc Saroj Rujirawat cd and Sukit Limpijumnong cd

Received 6th April 2010, Accepted 28th May 2010 DOI: 10.1039/c0cp00136h

A combination of X-ray absorption spectroscopy (XAS) measurements and quantum mechanical/molecular mechanical (OM/MM) molecular dynamics (MD) simulations has been applied to elucidate detailed information on the hydration structures of Ca²⁺ and Cl⁻. The XAS spectra (extended X-ray absorption fine structure, EXAFS, and X-ray absorption near-edge structure, XANES) measured from aqueous CaCl₂ solution were analyzed and compared to those generated from snapshots of QM/MM MD simulations of Ca²⁺ and Cl⁻ in water. With regard to this scheme, the simulated QM/MM-EXAFS and QM/MM-XANES spectra, which correspond to the local structure and geometrical arrangement of the hydrated Ca²⁺ and Cl⁻ at molecular level show good agreement with the experimentally observed EXAFS and XANES spectra. From the analyses of the simulated QM/MM-EXAFS spectra, the hydration numbers for Ca²⁺ and Cl⁻ were found to be 7.1 \pm 0.7 and 5.1 \pm 1.3, respectively, compared to the corresponding values of 6.9 ± 0.7 and 6.0 ± 1.7 derived from the measured EXAFS data. In particular for XANES results, it is found that ensemble averages derived from the QM/MM MD simulations can provide reliable QM/MM-XANES spectra, which are strongly related to the shape of the experimental XANES spectra. Since there is no direct way to convert the measured XANES spectrum into details relating to geometrical arrangement of the hydrated ions, it is demonstrated that such a combined technique of XAS experiments and QM/MM MD simulations is well-suited for the structural verification of aqueous ionic solutions.

1. Introduction

The characteristics of ions solvated in polar solvents, in particular water, have long been a topic of scientific interest in order to understand the role of these ions in chemical and biological processes.^{1,2} In general, such detailed knowledge can be obtained from a variety of experimental and theoretical techniques. In experiments, powerful techniques from a structural viewpoint are neutron and X-ray diffraction because they offer a direct probe of the ionic structure.^{3–9} However, especially for multi-component systems, discrepancies in the established data exist, even for fundamental properties such as the mean ion-oxygen nearest-neighbor distance and the average number of coordinating solvent molecules. Some explicit reasons are due to the uncertainty in modeling the scattering data as well as to the lack of direct information relating to the static and dynamics properties of solvent molecules surrounding the ions.

Besides the diffraction techniques, X-ray absorption spectroscopy (XAS) is a powerful tool for an accurate structural

In addition, since most of the diffraction techniques restrict their use only for relatively high concentrations, the XAS technique can be applied to a wider range of concentrated solutions. With respect to the XAS analysis, the spectra have been subdivided into a high-energy region (50-1000 eV), termed extended X-ray absorption fine structure (EXAFS), and a low-energy region (0-50 eV), which is called X-ray absorption near-edge structure (XANES). For relatively large disordered systems, like aqueous ionic solutions, the EXAFS spectra can provide a good resolution in detecting a near-neighbor solvent environment, especially for systems with a high degree of local order, while the XANES spectra correspond to the geometrical arrangement of the solvated ions. However, it is known that the presence of multiple scattering (MS) effects^{10,11} in the spectra as well as the errors from asymmetric distributions 12,13 are major problems in the analysis of XAS data. To simplify the process of XAS data analysis and interpretation, the use of information derived from other sources, such as molecular simulations, is of special interest.

determination of solvated ions, because of its element selectivity.

Molecular simulations, in particular the molecular dynamics (MD) technique, have been employed to generate partial pair distributions, g(R)'s, from which a model $\chi(k)$ is constructed and then used as a starting model in the analysis of XAS data. In this respect, the accuracy in the XAS data analysis depends crucially on the quality of the simulation results, *i.e.*, the reliability of the ensemble averages. The combined XAS

^a School of Chemistry, Institute of Science, Suranaree University of Technology, Nakhon Ratchasima 30000, Thailand

^b Department of Physics, Faculty of Science, Kasetsart University, Bangkok 10900, Thailand

^c Thailand Center of Excellence in Physics (ThEP Center), Commission on Higher Education, Bangkok 10400, Thailand

^d School of Physics, Institute of Science, Suranaree University of Technology, and Synchrotron Light Research Institute, Nakhon Ratchasima 30000, Thailand

measurements, in particular EXAFS, and the MD simulations technique have been successfully applied to several aqueous and non-aqueous ionic solutions, providing a more comprehensive understanding of the structural properties of solvated ions. 13-25 By this scheme, however, the detailed information derived from molecular simulations relies mostly on molecular mechanical (MM) force fields, i.e., the potential functions describing the ion-water and water-water interactions are usually constructed with respect to a set of experimental data or to ab initio calculations. For strong interacting systems, like aqueous ionic solutions, it has been demonstrated that "quantum effects" are significant and that the inclusion of these effects in the simulations is mandatory. 26,27 Nowadays, a high-level quantum mechanics/molecular mechanics (QM/MM) MD technique has been shown to be an elegant approach for studying condensed-phase systems, in particular the aqueous ionic solutions. ^{26–36} With regard to the QM/MM MD technique, the most interesting region, a sphere which includes the ion and its surrounding solvent molecules, is treated quantum mechanically. As a result, the complicated many-body contributions as well as the polarization effects, which are hardly accessible through the basic assumptions underlying the MM potentials, can be reliably included into the defined QM region.

Consequently, the aim of this study is to apply a combined technique of XAS (EXAFS and XANES) measurements and high-accuracy QM/MM MD simulations for studying the hydration shell structure of Ca²⁺ and Cl⁻. For Ca²⁺. established results in the literature, both experimental and theoretical investigations, reveal a rather inhomogeneous picture of this hydrated ion. X-Ray diffraction (XRD) experiments on calcium halide aqueous solutions reported hydration numbers between 5.9 and 8,^{37–43} whereas neutron diffractions (ND) yielded larger deviated values, ranging from 5.5 to 10.37,38 With regard to the XRD and ND experiments, the ion-oxygen distances are reported between 2.39 and 2.46 Å. Although the observed difference in these experimental data is considered mainly a consequence of concentration dependence, the discrepancies in the coordination number, as well as in the ion-oxygen distance, exist even at similar concentrated solutions. 37,38,42 Recently, EXAFS measurements have demonstrated that this ion has coordination numbers between 6.8 and 8, with ion-oxygen distances between 2.43 and 2.46 Å. 17,43,44

Apart from experiments, theoretical studies contributed even larger discrepancies. Classical simulations based on MM force fields provided large deviations in the coordination numbers, ranging from 6 to 10, with varying ion-oxygen distances between 2.39 and 2.54 Å. 29,41,45-48 In the broadest sense, the variation in results can be attributed to the use of different theoretical models. On the other hand, the inhomogeneous picture of this hydrated ion clearly indicates the important sensitivity to the applied potential functions. For quantum-mechanics-based simulations, different Car-Parrinello MD (CP-MD) simulations also gave variations in the coordination numbers of Ca2+ from 6 to 8, and in the ion-oxygen distance from 2.39 to 2.64 Å. 49-52 The observed difference found among CP-MD simulations has been attributed to the use of different simulation protocols and density

functionals. For the treatment of electrolyte solutions, severe limitations of the CP-MD technique, in particular the use of simple generalized gradient approximations (GGA), such as Becke's exchange in conjunction with Lee-Yang-Parr's correlation functionals (BLYP) and the functionals of Perdew, Burke and Ernzerhof (PBE), combined with the relatively small system size employed in some simulations, have been well demonstrated.^{27,53}

Alternatively, the QM/MM MD technique using the HF method as a benchmark has been applied for studying Ca²⁺ in water, revealing that this ion conducts coordination numbers of 8.3, with ion-oxygen distance of 2.45 Å.31 Later on, analogous QM/MM MD simulations of Ca²⁺ in water using the HF and B3LYP methods have reported Ca²⁺ coordination numbers of 7.6 and 8.1, with corresponding ion-oxygen distances of 2.46 and 2.51 Å, respectively. 54,55 Note that the observed difference, in particular the coordination number, of two QM/MM simulations using the same HF method is not surprising, since the latter one has been performed with the use of a larger QM region. This clearly suggests that inclusion of quantum mechanical treatment beyond the first hydration shell is important in order to obtain a reliable and accurate description of this solvated ion.

In the case of Cl⁻, the interactions of this ion with its surrounding water molecules are generally weaker than that of Ca²⁺, and even energetically comparable with waterwater interactions in bulk water. This makes the structural determination of Cl hydrate become more difficult. Consequently, the uncertainty in the coordination number of Cl in water is found both in experimental and theoretical studies, varying from 4 to 9^{7,8} and from 5.1 to 8.4, ^{33,56-63} respectively. Previous QM/MM MD simulation of Cl in water³³ indicated that the hydration structure of this ion is quite flexible as a consequence of weak Cl⁻-water hydrogen bonds, especially when compared to that of F⁻. This leads to a combination of linear and bridged forms, together with a competition between the solvation of the ion and hydrogen bonding among water molecules. The QM/MM results clearly indicate the importance of QM treatment in order to correctly describe such a delicate balance between Cl--water and water-water interactions.

In the present study, the QM/MM MD simulations of Ca²⁺ and Cl in water will be revisited by using an enlarged QM region's size, together with a sufficiently long simulation period. One of the significant contributions of this study is to benchmark the performance of the QM/MM MD approach in order to generate reliable ensemble averages of such systems, from which the simulated XAS spectra are constructed and supplied in the analysis of measured XAS spectra. In addition, a set of configurations corresponding to the geometrical arrangement of the hydrated ions, as obtained from the QM/MM MD simulations, is expected to provide useful information in the process of XANES data interpretation.

Experimental details

XAS measurements

The experimental Ca and Cl K-edge XAS spectra of 2.0 M aqueous CaCl₂ solutions were measured at beamline 8 of Siam Photon Laboratory, Synchrotron Light Research Institute (SLRI) in Nakhon Ratchasima, Thailand. The Siam Photon storage ring was operating at the electron energy of 1.2 GeV and the electron beam current between 80–120 mA. A Si(111) double crystal monochromator was used to select the X-ray photon energy. The solutions were kept in U-shape liquid cells with Kapton windows. All EXAFS and XANES spectra were collected at the ambient temperature and atmospheric pressure. The spectra were recorded in the transmission mode using ionization chambers as the detectors. The scanning photon energy step is set at 1 eV for the EXAFS region and 0.25 eV for the XANES region. To improve the signal-to-noise ratio, several scans were recorded and averaged. For comparison purposes, the measured XAS spectra were aligned to the corresponding spectra reported in the literature. ^{17,39,44}

2.2 XAS data analysis

2.2.1 EXAFS. According to the standard EXAFS data analysis.^{2,7} the structure factor can be described by

$$\chi(E) = \frac{\mu(E) - \mu_0(E)}{\Delta \mu_0(E_0)},\tag{1}$$

where $\mu(k)$ is the absorption coefficient, $E = E_0 + \hbar^2 k^2 / 2m_e$ is the X-ray energy, $\mu_0(E)$ is the background absorption coefficient, and $\Delta\mu_0(E_0)$ is an absorption edge height. It is more common to write the structure factor as a function of the photoelectron wave vector k, $\chi(k)$. In general, $\chi(k)$ can be expressed by the classical EXAFS equation,

$$\chi(k) = \sum_{j} \frac{S_{\circ}^{2} N_{j}}{k R_{j}^{2}} |f_{j}^{eff}(k, R_{j})| \sin[2kR_{j} + \varphi_{j}(k)] e^{-2\sigma_{j}^{2}k^{2}} e^{-2R_{j}/\lambda(k)},$$
(2)

where the summation goes over all paths j, N_j is the coordination number, $S_0^2(k)$ is the amplitude reduction factor, f_j^{eff} is the curved-wave scattering amplitude, R_j is the path length, $\lambda(k)$ is the electron mean free path, $\sigma(k)$ is the Debye–Waller factor, and $\varphi(k)$ accounts for the total phase shift. Basically, if the correct geometrical configuration around the absorber atom can be obtained, the structural parameters such as path length and coordination number could be fitted with high accuracy.

To obtain the EXAFS spectra of Ca and Cl K-edge, the measured raw X-ray absorption spectra were processed using an interactive program for XAFS analysis called IFEFFIT package. ^{64,65} This includes (1) a background subtraction in the pre-edge and post-edge regions; (2) creating a spline curve above the threshold energy with a four-segment polynomial; and (3) extracting the oscillation by subtracting the spline from the spectra and normalizing the remaining. To enhance the EXAFS in the high k region, we choose to plot $k^2 \chi(k)$. The plots are windowed between $2.0 < k < 8.0 \text{ Å}^{-1}$ using a Hanning window W(k) with $dk = 1.0 \text{ Å}^{-1}$.

To obtain a real-space representation of the EXAFS spectra, Fourier transformations (FT), as implemented in the IFEFFIT package, of the structural factors were carried out using

$$\tilde{\chi}(R) = \frac{1}{\sqrt{2\pi}} \int_{0}^{\infty} k^2 \chi(k) W(k) e^{i2kR} dk$$
 (3)

Once the EXAFS spectra are processed, information on the local structure of the absorber atom can be obtained by fitting with predetermined local structure models. If all absorber atoms are expected to have the same local structure, a single local structure model can be used to fit the measured spectra with some parameters, such as the neighboring distances and coordination numbers, allowed to relax.⁶⁶ If two or more local structure models are expected, such models can be used in combination for the fit which allows more degrees of freedom.⁶⁷ For aqueous ionic solutions, however, water molecules surrounding the ions are quite labile, i.e., there are uncountable forms of local structures. Consequently, the measured spectra are regarded as the statistical average of all structures. ⁶⁸ Several groups have reported success in finding the proper configuration averages of ionic hydration structures with shells of water molecules. 17,21,39,44,66,68 Such models, with appropriate parameters (i.e., neighboring distances and coordination numbers), can produce good fits to the experimental measurements. In this work, the structural parameters from EXAFS spectra were extracted using nonlinear least squares fitting procedure in IFEFFIT. In the fitting process, the interatomic distances (R) of each shell, coordination number, mean-square thermal, static deviation in $R(\sigma^2)$, and the threshold energy (E_0) were allowed to vary. To obtain the best fit, the amplitude reduction factors (S_0^2) for Ca^{2+} and Cl^- ions were set to 0.83 and 0.91, respectively. The theoretical phase and amplitude functions were calculated using FEFF codes. 64,65,69,70 In fact, it should be noted that the neighboring distance and the coordination number of a representative structure that best fit the experimental EXAFS do not necessarily equal the average values of all structures that comprise the measured EXAFS.

2.2.2 XANES. The IFEFFIT utility program was employed to process the measured raw X-ray absorption spectra of Ca and Cl *K*-edge. In the XANES region, the background subtractions based on the information from the pre-edge regions are performed. Then, the XANES spectra are normalized and compared with the simulated spectra.

3. Computational details

3.1 QM/MM MD simulations

Using the QM/MM MD technique, ^{26–36} the system is divided into two parts, namely QM and MM regions. The total interaction energy of the system is defined as

$$E_{\text{total}} = \langle \Psi_{\text{OM}} | \hat{H} | \Psi_{\text{OM}} \rangle + E_{\text{MM}} + E_{\text{OM-MM}}, \tag{4}$$

where $\langle \Psi_{\rm QM} | \hat{H} | \Psi_{\rm QM} \rangle$ refers to the interactions within the QM region, while $E_{\rm MM}$ and $E_{\rm QM-MM}$ represent the interactions within the MM and between the QM and MM regions, respectively. The QM region, the most interesting part which contains the ion and its surrounding water molecules, is treated quantum mechanically, while the rest of the system is described by classical pair potentials. In practice, the total force of the system is described by the following formula:

$$F_{\text{tot}} = F_{\text{MM}}^{\text{sys}} + F_{\text{OM}}^{\text{QM}} - F_{\text{MM}}^{\text{QM}}$$
 (5)

where $F_{\text{MM}}^{\text{sys}}$, $F_{\text{QM}}^{\text{QM}}$, and $F_{\text{MM}}^{\text{QM}}$ are the MM force of the total system, the QM force in the QM region and the MM force in

the QM region, respectively. In this respect, the F_{MM}^{QM} term accounts for the coupling between the QM and MM region.

In principle, the post-HF methods with the extended basis sets are most suitable for the OM treated region but it turns out to be computationally prohibitive. With regard to this point, some essential parameters such as the level of quantum mechanics calculations, basis set and size of QM region must be optimized, compromising between the quality of the simulation results and the requirement of CPU time. Since the performance of correlated ab initio methods is still far too time-consuming, the Hartree-Fock (HF) method was employed for the treatment of all interactions within the QM region. The HF method has been well validated in previous QM/MM studies, 26-36 even for the treatment of anions.³³ Density functionals, such as B3LYP, are not taken into consideration since it has been demonstrated that these functionals often overestimate the ion-water interactions, which leads to a remarkably more compact and too rigid ion-water complex. 26,27 All quantum mechanical calculations were carried out using DZV+, ⁷¹ LANL2DZ, ^{71,72} and 6-31+ $G^{73,74}$ basis sets for H_2O , Ca^{2+} , and Cl^- , respectively. The QM sizes with diameters of 8.8 and 9.2 Å were chosen for the systems of aqueous Ca²⁺ and Cl⁻ solutions, respectively. These QM sizes, which contain the ion and about 12-15 (for Ca²⁺) and 11-16 (for Cl⁻) water molecules, were considered large enough to ensure that the quantum mechanical forces beyond the QM region smoothly converge to pair potential forces. For the treatment of all interactions within the MM and between the QM and MM regions, a flexible model, which describes intermolecular⁷⁵ and intramolecular⁷⁶ interactions, was employed for water and the pair potential functions for describing Ca²⁺-H₂O and Cl⁻-H₂O interactions were obtained from previous works. 31,33

During the QM/MM MD simulations, exchange of water molecules between the QM and MM regions took place frequently. With regard to this point, the forces acting on each particle in the system were switched according to which region the water molecule was entering or leaving the QM region and are defined as

$$F_i = S_m(r)F_{QM} + (1 - S_m(r))F_{MM},$$
 (6)

where $F_{\rm QM}$ and $F_{\rm MM}$ are quantum mechanical and molecular mechanical forces, respectively. $S_m(r)$ is a smoothing function 77 described by

$$S_m(r) = 1, for r \le r_1,$$

$$S_m(r) = \frac{(r_0^2 - r^2)^2 (r_0^2 + 2r^2 - 3r_1^2)}{(r_0^2 - r_1^2)^3}, for r_1 < r \le r_0, (7)$$

$$S_m(r) = 0, for r > r_0,$$

where r_1 and r_0 are distances characterizing the start and end of the QM region, applied within an interval of 0.2 Å (*i.e.*, between the Ca–O and Cl–O distances of 4.2–4.4 and 4.4–4.6 Å, respectively).

In this work, the QM/MM MD simulations for aqueous Ca²⁺ and Cl⁻ solutions were separately performed in a

canonical ensemble at 298 K with periodic boundary conditions. The system's temperature was kept constant using the Berendsen algorithm. A periodic box, with a box length of 18.17 Å, contains one ion and 199 water molecules, corresponding to the experimental density of pure water. The reaction-field method was employed for the treatment of long-range interactions. The Newtonian equations of motions were treated by a general predictor–corrector algorithm. The time step size was set to 0.2 fs, which allows for the explicit movement of the hydrogen atoms of water molecules. For both aqueous Ca²⁺ and Cl⁻ solutions, the simulations were started with the system's re-equilibration for 25 000 time steps, followed by another 250 000 (Ca²⁺) and 100 000 (Cl⁻) time steps to collect the configurations every 10th step.

3.2 Calculations of QM/MM-EXAFS and QM/MM-XANES spectra

Once the QM/MM MD simulations have been performed, sets of molecular configurations (for both aqueous Ca²⁺ and Cl⁻ solutions) obtained from the simulations are used to produce theoretical XAS spectra. With regard to the QM/MM MD simulations, the periodic box contains only one ion (Ca²⁺ or Cl⁻) surrounded by water molecules and the time evolution of the system is studied. Since the systems of this kind are *ergodic*, we can sample the system at various times to represent the ensemble average that can be used to compare with measured XAS spectra. In this work, the OM/MM MD frames, obtained at every 0.5 ps, are sampled, from which the positions of oxygen and hydrogen atoms with respect to the central ion in each chosen frame were used to construct the OM/MM-EXAFS and QM/MM-XANES spectra. All the calculated QM/MM-EXAFS and QM/MM-XANES spectra are generated using the FEFF codes.^{69,70}

For EXAFS calculations, we employed most of the default setting in the FEFF codes and restricted the scattering path to the length of 5.0 Å. In the case of XANES, the codes utilize a full multiple scattering approach based on ab initio overlapping muffin-tin potentials. The muffin-tin potentials were obtained using self-consistent calculations with a Hedin–Lundqvist (HL) exchange–correlation function.⁸⁰ The (time-consuming) self-consistent calculations were performed in a sphere with a radii of 5.6 Å centering on the absorbing ion. Such a sphere contains about 25-30 water molecules, which is sufficient to take into account the influence from the outer solvation shell. Test calculations show that further increasing the sphere radii leads to an exponential increase in computational time, but without a significant change on the XANES spectra. The full multiple scattering calculations include all possible paths within a larger cluster radius of 9.2 Å (consisting of 105–110 water molecules).

In addition, the established QM/MM-EXAFS spectra provide an opportunity to test how well the usual EXAFS, fitted by a model containing two shells of water molecules, can describe the systems. This can be done by simply treating the QM/MM-EXAFS spectra as experiment spectra and fitting them. After the fit, the obtained neighbor distances and the coordination numbers can be used to compare with the values obtained from the QM/MM MD analysis. In general, it should

be noted that the XAS techniques are employed to study the local structure around the absorber atoms, where there are only one or two (at most a few) different configurations in the sample. In the fitting (using a theoretical model), one generates the corresponding spectra from an assumed configuration (or the mixture of a few configurations) where the species of neighbors, number of neighbors, and neighboring distances can be varied to produce the results that fit the measured data. For aqueous ionic solutions, especially for the case where water molecules are less bounded to the ion, the situation is much more different since there are virtually infinite different configurations, i.e., the ion is surrounded differently by water molecules during the measurement. Therefore, it is unexpected that a single representative shell model, as usually assumed in the EXAFS fitting, can be fitted to the spectra and represent correctly the average parameters (for instance, the coordination number). This will be discussed again in the Results section.

4. Results and discussion

4.1 QM/MM MD results

Structural properties of the hydrated Ca²⁺ and Cl⁻ can be explained in terms of Ca-O and Cl-O radial distribution functions (RDFs) and their corresponding integration numbers, as shown in Fig. 1. For Ca²⁺, the first Ca-O maximum is centered at 2.45 Å, where integration up to the first minimum of the Ca-O peak yields an average coordination number of 7.4. In addition, the first solvation shell is well separated from the outer region, suggesting that first-shell water molecules are rather arranged with respect to the strong influence of Ca²⁺. Compared to the earlier QM/MM MD work,³¹ which reported a broad minimum of the first Ca-O RDF with an average number of first-shell waters of 8.3, the observed lower coordination number of Ca²⁺ could be attributed to the use of larger QM size (i.e., in eqn (7) $r_0 = 4.4 \text{ Å} \text{ versus } 3.6 \text{ Å} \text{ used in}$ ref. 31). A similar trend is found in the analogous QM/MM MD simulation of Ca²⁺ in water using r_0 of 4.0 Å, ^{54,55} which also predicted the rather well-defined first hydration shell with an average coordination number of 7.6. In this respect, it could be demonstrated that the QM treatment for the non-additive contributions beyond the first hydration shell is somewhat

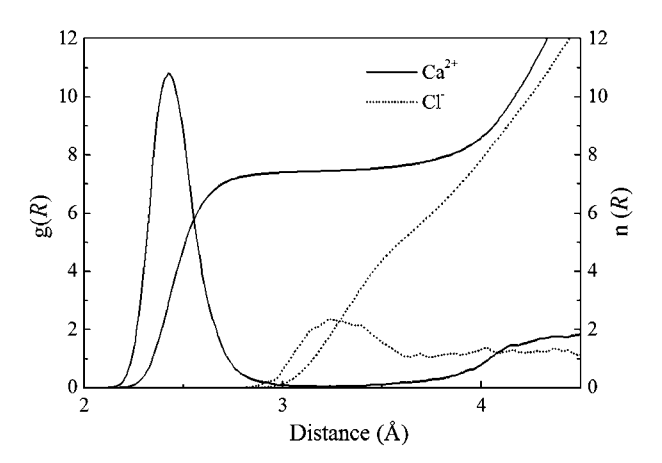


Fig. 1 Ca-O and Cl-O RDFs and their corresponding integration numbers.

important in determining the hydration shell structure of Ca²⁺. Recently, a new QM/MM framework using an *ab initio* quantum mechanical charge field (QMCF) has been applied for aqueous Ca²⁺ solutions.⁸¹ The Ca–O distance and the coordination number were found to be 2.55 Å and 7.9, respectively. Compared to the previous OM/MM results, the observed difference in the structural properties has been demonstrated due to the use of solute-solvent potentials in the conventional QM/MM MD scheme, which probably reflect in slight artificial pressure on the primary hydration layer. In terms of CP-MD simulations, coordination numbers between 6 and 8 are reported, with observed large variations in the Ca-O distances, ranging from 2.39 to 2.64. 49-52 In most cases, the shape and width of the resulting Ca-O RDFs are rather sensitive to the density functionals applied, showing too rigid an arrangement of the hydration shell of Ca²⁺ (i.e., compared to the present QM/MM MD results). Recently, it has been demonstrated that the simple density functionals BLYP and PBE usually employed in the CP-MD scheme are not even capable of describing the solvent water itself, as the use of these functionals yields a glassy state rather than a liquid at room temperature and up to 400 K.⁵³

In the case of Cl⁻, a less pronounced first Cl-O RDF, with a maximum at 3.24 Å, is observed. The shape and height of the first Cl-O peak clearly indicate a high flexibility of this hydrated ion. In addition, the first peak of Cl-O RDF is not distinctly separated from the bulk, which suggests an easy exchange of water molecules between the first hydration shell and the outer region. An integration up to the first Cl-O minimum leads to an average coordination number of 5.5. In fact, as a consequence of the broad Cl-O minimum, the observed coordination number of Cl⁻ could be regarded as a rough estimate, i.e., a small shift in the position of the Cl-O minimum could lead to a significant difference in the average coordination number. For example, as can be seen in Fig. 1, the integrations up to the Cl-O distances of 3.5 and 4.0 Å yield 4.5 and 8.0 water molecules, respectively. Fig. 2 shows the arrangement of water molecules around Cl compared to those in the bulk water itself, as obtained by the similar

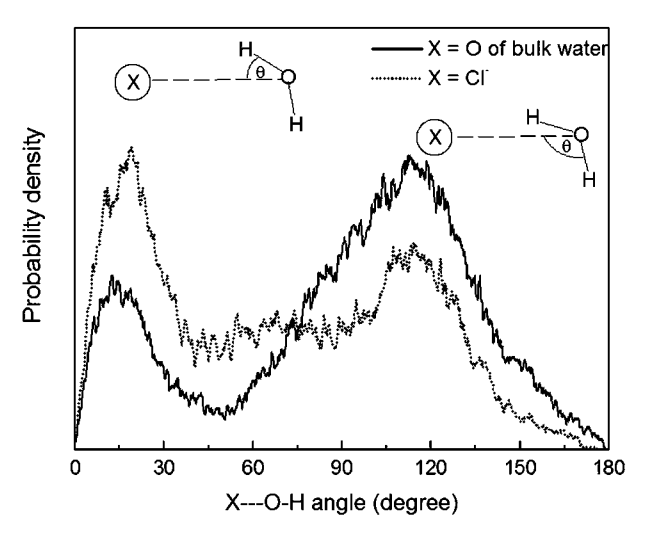


Fig. 2 Distributions of the X—O–H angle (X = O and Cl^-), calculated within the first minimum of the O–O and Cl–O RDFs.

QM/MM methodology.⁸² It is obvious that water molecules in the hydration shell of Cl⁻ are not bound by classical hydrogen bonds to the ion. Instead, they are rather arranged with respect to a combination of linear and bridged forms. Consequently, this leads to a competition between the solvation of the ion and hydrogen bonding among water molecules. The results obtained by the present QM/MM MD simulation are in good accord with the previous QM/MM MD study,³³ which demonstrated the relative weak Cl⁻—water hydrogen bonds and a high flexibility of the hydration shell structure. According to a recent CP–MD study,⁸³ the overestimation of ion–water hydrogen bonds is recognizable, *i.e.*, by the strong pronounced first Cl–O and Cl–H RDFs.

Fig. 3 shows probability distributions of the coordination numbers, calculated within first minimum of the Ca-O and Cl-O RDFs, respectively. For Ca²⁺, the most frequent coordination number for this ion is 7, followed by 8 in a smaller amount. In addition, a slight distribution for the coordination number of 6 (\sim 5%) clearly indicates lesser significance of Ca²⁺(H₂O)₆ formation. In the case of Cl⁻, although the 5- and 6-fold coordinated complexes are most frequently found during the QM/MM MD simulation, numerous possible species of the hydrated Cl⁻ exist, varying from 3 to 9. The observed large variation in the coordination numbers clearly indicates high flexibility of the hydration structure of Cl⁻ as well as high mobility of its first-shell water molecules. Fig. 4 displays the O–X–O angular distributions, calculated up to the first minimum of the X-O RDFs for $X = Ca^{2+}$ and Cl⁻, respectively. For Ca²⁺, the structural arrangement of this hydrated ion with respect to the distinct coordination numbers between 7 and 8 is well reflected, i.e., by the two pronounced peaks between 60–90° and between 130–150°. Unlike Ca²⁺, the observed broad O-Cl-O peak corresponds to the numerous species of hydrated Cl⁻ complexes formed in aqueous solution. In fact, it should be noted that water molecules in the hydration shell of Cl⁻ are organized differently from that of Ca²⁺ hydration, *i.e.*, they are arranged with respect to the resultant force of the competition between the Cl--H-O hydrogen bonds (see Fig. 2) and the hydrogen bonding among water molecules in the same shell and/or the bulk.

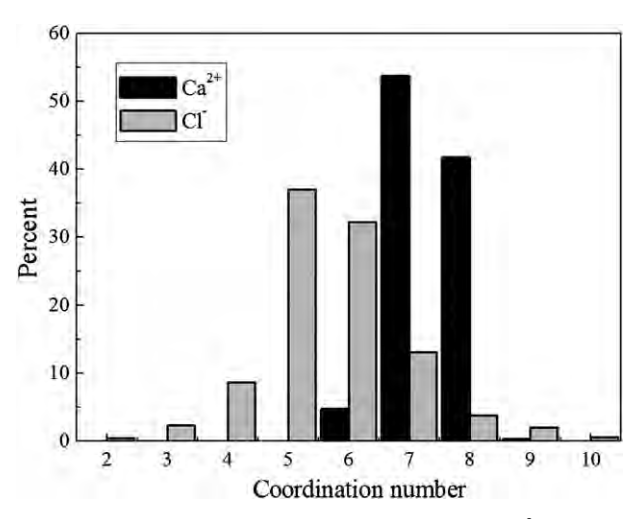


Fig. 3 Distributions of the coordination numbers of Ca²⁺ and Cl⁻, calculated within the first minimum of the Ca–O and Cl–O RDFs.

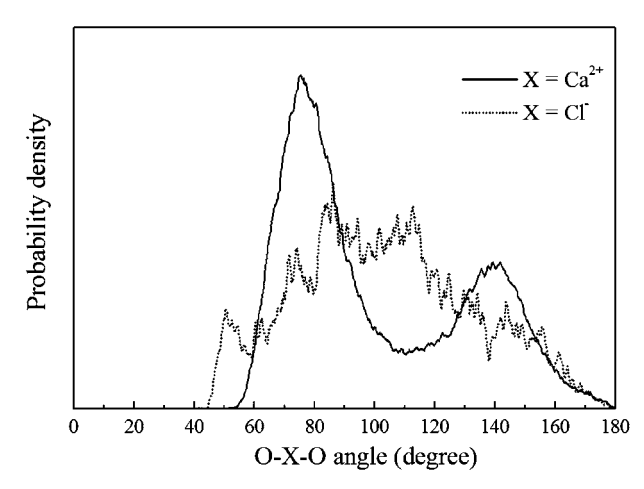


Fig. 4 Distributions of the O-X-O angle ($X = Ca^{2+}$ and Cl^{-}), calculated within the first minimum of the Ca–O and Cl–O RDFs.

More detailed information on the structural arrangement of the hydrated Ca²⁺ and Cl⁻ complexes can be visualized through the plots of the Ca–O and Cl–O distances against the simulation times, as shown in Fig. 5 and 6, respectively. According to Fig. 5, it is obvious that the Ca²⁺ (H₂O)₇ and Ca²⁺ (H₂O)₈ complexes are dominantly formed in aqueous solution. Within a simulation time of 50 ps, only 12 water molecules are found to be involved in about 27 water exchange processes, indicating that most of the first-shell waters are tightly bound to the ion. In contrast to Ca²⁺, water molecules surrounding Cl⁻ are quite labile (see Fig. 6), showing numerous water exchange processes during the QM/MM MD simulation. This clearly anticipates fast water-exchange rates of the first hydration shell, and thus shows large variations in the coordination number of this ion.³⁴

4.2 EXAFS and QM/MM-EXAFS spectra

With respect to the short-range nature of XAS, this technique is suitable for studying local geometry, especially for the disordered systems. In the EXAFS region, the single back-scattering processes are mostly dominant. Making use of

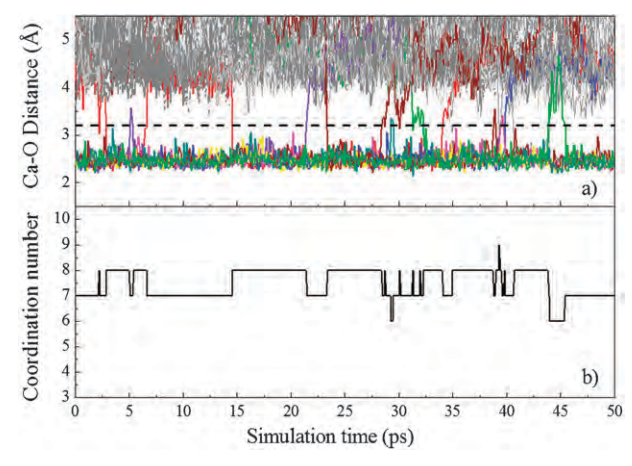


Fig. 5 Time dependences of (a) Ca^{2+} —O distance and (b) number of first-shell waters, as obtained from 50 ps of the QM/MM MD simulation. In Fig. 5a), the dash line parallel to the *x*-axis indicates the first minimum of the Ca–O RDF.

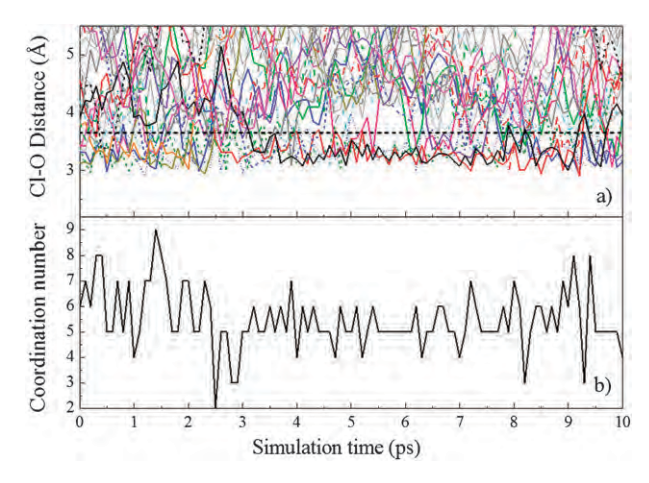


Fig. 6 Time dependences of (a) Cl⁻—O distance and (b) number of first-shell waters, selecting only for first 10 ps of the QM/MM MD simulation. In Fig. 6a), the dash line parallel to the *x*-axis indicates the first minimum of the Cl–O RDF.

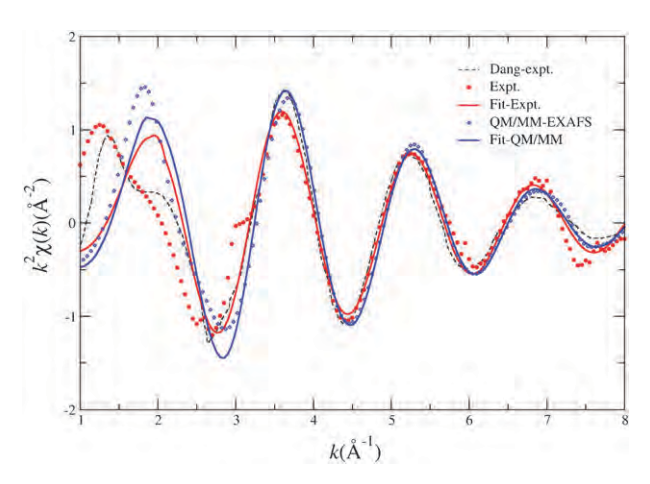


Fig. 7 Structural factors and the corresponding fitted curves for Ca^{2+} in water, as obtained from the QM/MM MD simulation and the experimental measurements.

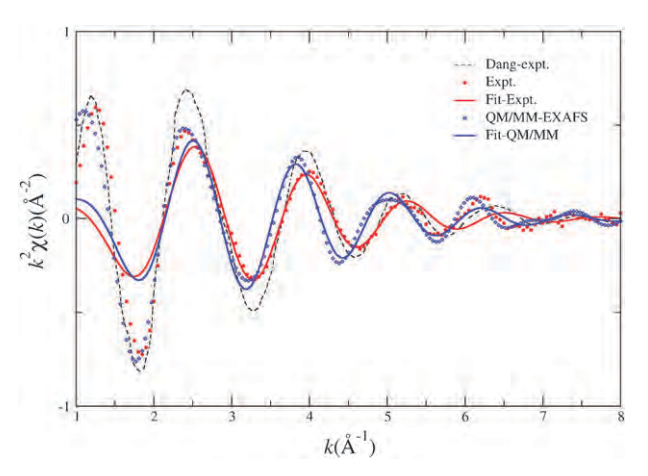


Fig. 8 Structural factors and the corresponding fitted curves for Cl^- in water, as obtained from the QM/MM MD simulation and the experimental measurements.

Table 1 Ion-oxygen distances, Debye-Waller factors and coordination numbers, as derived from the ion-O RDFs of QM/MM MD simulations and from the fitting of QM/MM-EXAFS and measured EXAFS spectra

Ion	Technique	$R_0/ ext{Å}$	$\sigma^2/\text{Å}^2$	N
Ca ²⁺	QM/MM MD QM/MM–EXAFS EXAFS	2.425 ± 0.013	$ \begin{array}{c} -\\ 0.011 \pm 0.002 \\ 0.010 \pm 0.002 \\ 0.0115 \pm 0.002^{a} \end{array} $	7.4 7.1 \pm 0.7 6.9 \pm 0.7 6.8 \pm 1.0 ^a
Cl ⁻	QM/MM MD QM/MM–EXAFS EXAFS	3.047 ± 0.040	$\begin{array}{c}$	5.5 5.1 ± 1.3 6.0 ± 1.7 6.4 ± 1.0^{a}

^a EXAFS measurements from Dang et al. 17

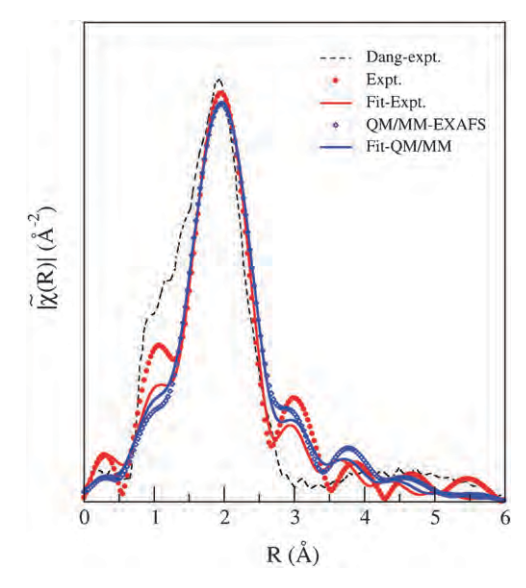


Fig. 9 Fourier transformations of the structural factors and the corresponding fitted curves for Ca²⁺ in water, as obtained from the QM/MM MD simulation and the experimental measurements.

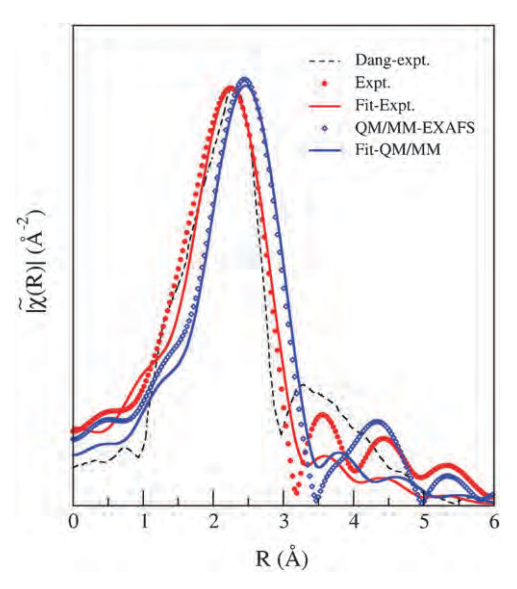


Fig. 10 Fourier transformations of the structural factors and the corresponding fitted curves for Cl⁻ in water, as obtained from the QM/MM MD simulation and the experimental measurements.

combined QM/MM MD simulations and the EXAFS measurements technique, however, it should be realized that the measured XAS spectra of ions in aqueous solution (where there are virtually infinite different configurations) may not necessarily be well fitted by one configuration model. Even if there is a configuration model that can fit the spectra well, the result obtained from the model might not represent the average of all configurations in the sample.

In this work, the QM/MM MD technique is expected to be an elegant simulation approach in order to generate reliable OM/MM-EXAFS spectra. The QM/MM-EXAFS spectra are generated by averaging 30 snapshot frames of the QM/MM MD simulations. (Test calculations show that increasing the snapshot frames does not significantly change the averaged spectra.) In this respect, it is worth noting that all major

structural details of the ion-water structures inherent in the simulations are mutually represented in the QM/MM-EXAFS spectra. The QM/MM-EXAFS spectra are also fitted with respect to classical EXAFS in eqn (2). The general reason is to gauge how well the nearest neighbor distance and the coordination number, as obtained from the simulated EXAFS spectra, fit a single configuration resembling the values determined from the analysis of the full QM/MM MD data.

Fig. 7 and 8 show the k^2 -weighted $\gamma(k)$ spectra for Ca²⁺ and Cl in water, respectively, comparing between the QM/MM-EXAFS and the experimental measurements along with their corresponding fits. For the EXAFS spectra, the data measured by Dang et al. 17 were also given for comparison. For Ca²⁺ (Fig. 7), the oscillation periods of the measured EXAFS and the QM/MM-EXAFS spectra are in good agreement,

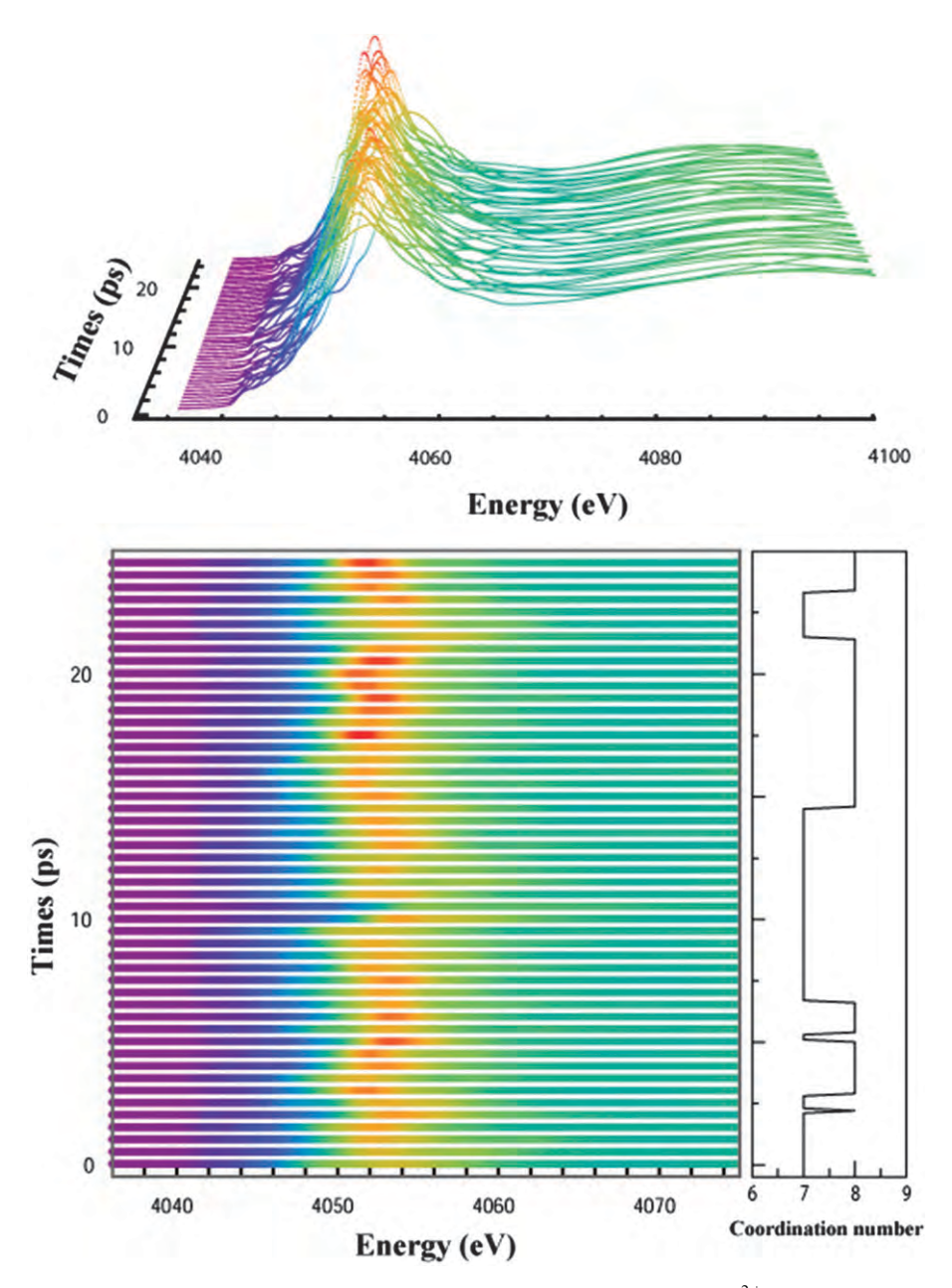


Fig. 11 Examples of the simulated QM/MM-XANES spectra for Ca²⁺ in water.

i.e., implying good accordance in the average Ca–O distances. The observed disagreement in the low k region between the QM/MM-EXAFS and the measured EXAFS spectra (this work and Dang et al.) can be described due to the residue of a different atomic background subtraction and treatment of anomalous features in the EXAFS signal processing steps. In addition, this region of the spectra belongs to the XANES region, in which the algorithm employed cannot generate accurate EXAFS spectra. In the case of Cl⁻ (Fig. 8), the observed discrepancy between our experimental $\gamma(k)$ spectrum and that measured by Dang et al. becomes more apparent, compared to that of the aqueous Ca²⁺ system. This can be explained by the high noise level of our measurement due to a low photon flux as well as strong water absorption at Cl⁻ Kedge region (2800-3000 eV). With regard to the present EXAFS data, the noise level of the spectrum remains actually the same throughout the spectrum. However, the signal decays rapidly at high k, leading to a higher signal-to-noise ratio. In addition, since the plot is k^2 -weighted, the noise is also significantly amplified. In this study, the QM/MM-EXAFS spectrum shows fair agreement in the oscillation periods when compared to the curves measured by experiments.

Following the expression given by eqn (2), the theoretical fit based on a single configuration is applied to the measured EXAFS and simulated QM/MM-EXAFS spectra. Some essential parameters for both Ca2+ and Cl- systems are summarized in Table 1. In comparison to the data by Dang et al., 17 good agreement in the fitting results is visible, especially for the case of Ca^{2+} . In addition, the parameters R_0 and N derived from the analysis of the QM/MM MD simulation (average overall ensemble) are in good accord with the values obtained from the fit of the QM/MM-EXAFS spectra. For Ca²⁺, the structural parameters obtained from the fit are in good agreement with the analysis of the simulation data (Table 1). This is not surprising because most of the frames used for generating the QM/MM-EXAFS spectra are expected to have similar local hydration structures due to the tight binding of the first hydration shell. In contrast to Ca²⁺, the observed larger variation in the fitting results could be ascribed to the rather weak Cl⁻-water interactions, which lead to high flexibility of this ion hydrate. As a result, the QM/MM-EXAFS spectra are constructed with respect to the frames that are distinctive in the hydration shell structures. Thus, they are not expected to fit well by a single configuration in the EXAFS equation. On the other hand, the fitting process forces a configuration that gives an overall feature in the best agreement with the average spectrum obtained from distinctive frames. However, as mentioned previously, the configuration obtained from the fit does not necessarily represent the average of all ion configurations in the sample. For both Ca²⁺ and Cl⁻ systems, our results show that the configurations obtained from the fits of QM/MM–EXAFS spectra can provide data in good accord with the average values derived from the simulated ensembles. Overall, it could be demonstrated that, for a tightly bound hydration structure like Ca²⁺, the EXAFS fit can yield the configuration that well represents the average of the ensemble. For more labile hydration structures like Cl⁻, however, the EXAFS fit may not be able to precisely represent the average of the ensemble as a consequence of numerous

possible species of the hydrated Cl⁻ found in aqueous solution.

The Fourier transformations (eqn (3)) of the QM/MM–EXAFS and the corresponding measured EXAFS spectra yield the real space distribution plots, as shown in Fig. 9 and 10 for the aqueous $\mathrm{Ca^{2+}}$ and $\mathrm{Cl^{-}}$ solutions, respectively. The main peak of the $\tilde{\chi}(R)$ spectra is primarily corresponding to the scattering originated from the oxygen atoms of first-shell water molecules. For $\mathrm{Ca^{2+}}$ systems, the peak position and shape obtained from the QM/MM–EXAFS spectrum are in good accord with the experimental measurements. For the $\mathrm{Cl^{-}}$ system, the peak position obtained from the QM/MM–EXAFS spectrum is exhibited at a slightly larger distance, compared to the experimental measurements. This can be ascribed due partly to the neglect of the electron correlation in the HF calculations, which generally diminishes the $\mathrm{Cl^{-}}$ –water interactions.

4.3 XANES and QM/MM-XANES spectra

In the XANES region, since the kinetic energy of the photoelectron is low, the excited electron density of states plays a dominant role. In order to obtain the correct partial density of states, detailed atomic potentials have to be correctly calculated and an extensive MS approach has been used. For the case of aqueous Ca²⁺ and Cl⁻ solutions, the densities of states are strongly sensitive to the detailed arrangement of water molecules surrounding the ions. In general, XANES spectra are considered to be insensitive to long-range disorder, but related to characteristics of the geometrical arrangement of the hydrated ions. Consequently, these spectra are often used as fingerprint for characterizing the neighborhood of the ions. For Ca²⁺, examples of the XANES spectra generated from every 0.5 ps of the QM/MM MD snapshots are plotted in Fig. 11. Obviously, each QM/MM-XANES spectrum generated from each QM/MM MD snapshot, which corresponds to a different hydration structure of Ca²⁺, is different. This confirms that each of the QM/MM-XANES spectra is sensitive

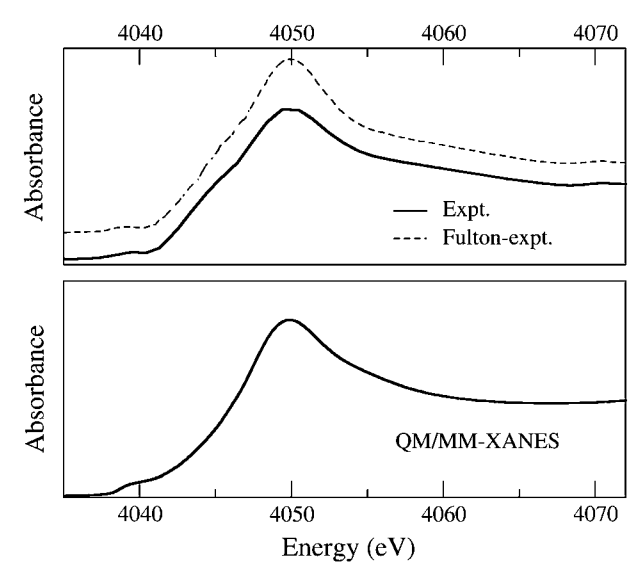


Fig. 12 Comparison between the experimental Ca *K*-edge XANES spectra and the averaged QM/MM–XANES spectrum.

to the details of the hydration structure around the ion. A comparison between the measured and the average QM/MM-XANES spectra is shown in Fig. 12. For the experimental data, the spectrum measured by Fulton et al.84 was also given for comparison. It should be noted that, in principle, the representative set of hydration structures used for generating the average QM/MM-XANES spectrum has to be extracted with proper statistics from the QM/MM MD trajectories that cover all possible configurations. In this work, the set of snapshots is taken from the QM/MM MD simulation of a time-scale that is sufficient to provide a reliable ensemble average. As can be seen in Fig. 12, despite the observed difference among the isolated QM/MM-XANES spectra obtained from each of the QM/MM MD snapshots, the average QM/MM-XANES spectrum gives satisfactory agreement with the measured XANES spectra.

For the case of Cl⁻, examples of the simulated XANES spectra with respect to each of 0.5 ps QM/MM MD snapshots are shown in Fig. 13. The average QM/MM-XANES spectrum is plotted and compared to the corresponding XANES measurements, as depicted in Fig. 14. According to the high flexibility (less defined) of the Cl hydrate, the distinction among the XANES from each snapshot becomes more prominent as compared to the Ca²⁺ case. In this respect, the statistical information regarding all possible hydration shell structures from the QM/MM MD simulation has an even more important effect on the average spectrum. As can be seen in Fig. 14, it is clear that the main features in the average XANES spectrum show good agreement with the experimental ones. This clearly indicates that the geometrical arrangements of the hydrated Cl⁻ obtained by the QM/MM MD simulation are realistic.

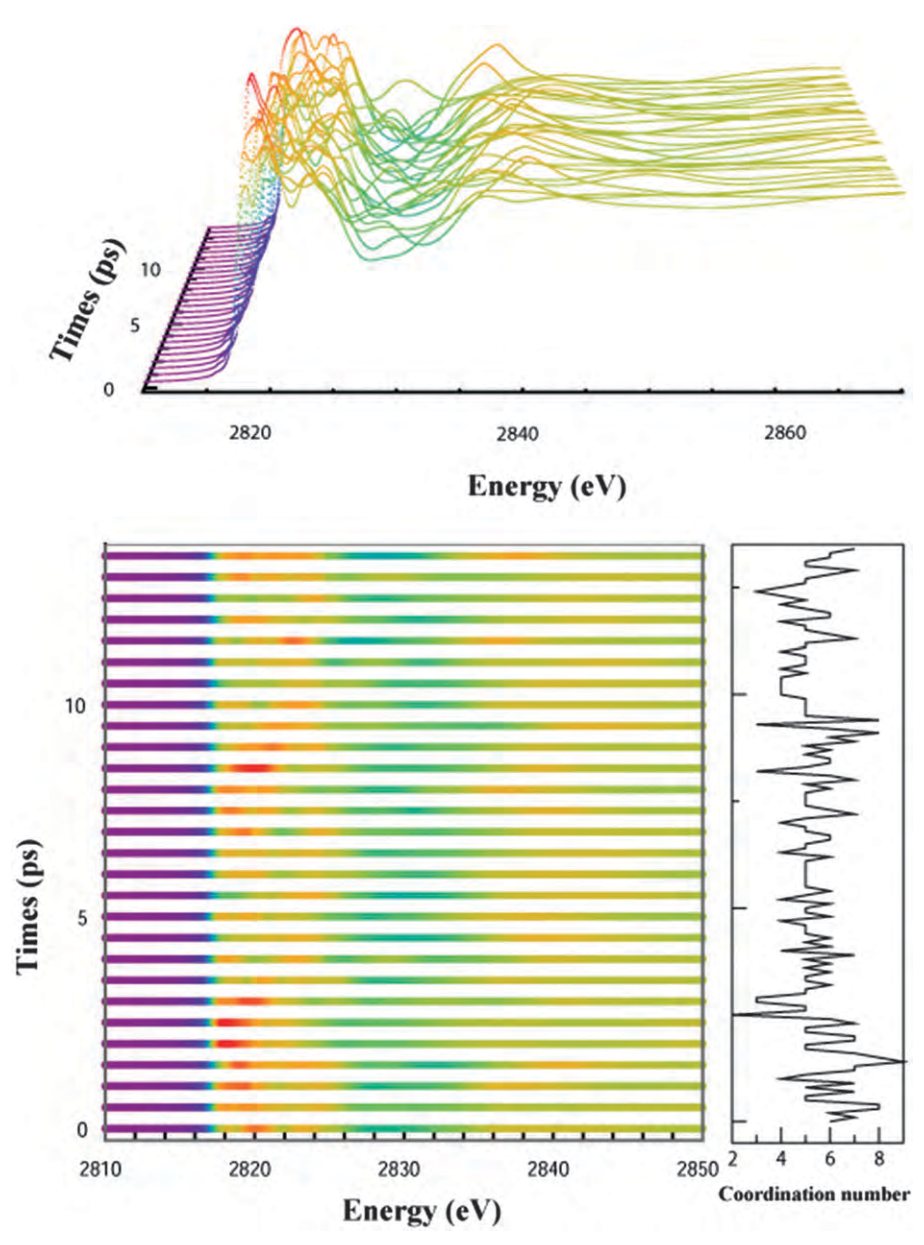


Fig. 13 Examples of the simulated QM/MM-XANES spectra for Cl⁻ in water.

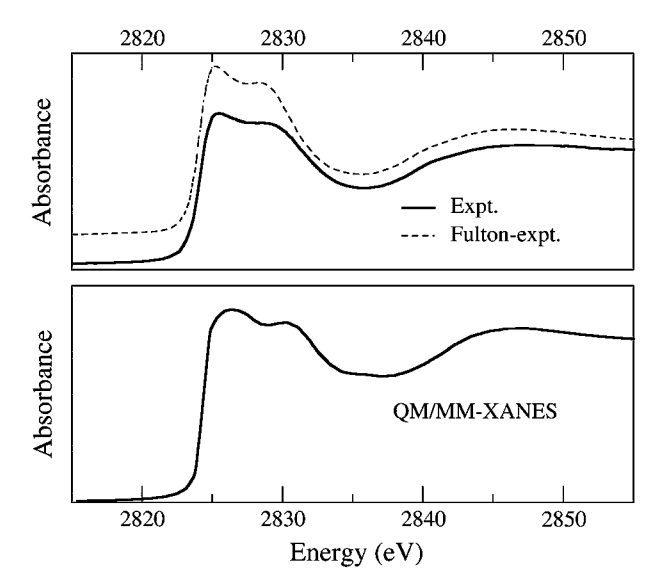


Fig. 14 Comparison between the experimental Cl *K*-edge XANES spectra and the averaged QM/MM–XANES spectrum.

Because the equally spaced (in time) snapshots are obtained from the QM/MM MD simulation without bias or any fitting to the experimental XANES, this agreement supplies information that the trajectory derived from the QM/MM MD simulation can realistically represent the actual system. This illustrates that the fact for an ergodic system, like the case at hand, we can calculate a temporal average XANES spectrum by choosing a sufficiently large number of equally spaced (in time) snapshots and compare with the measured spectrum which represent both the temporal and ensemble average. The agreement confirms that the overall simulation, i.e., both the dynamic behavior and the static details of each snapshot, is consistent with reality. With regard to this point, if the dynamics details obtained from the simulation are wrong, the resulting average XANES spectrum would be dominated by the feature of the wrong configuration and would not agree with that of the experiments. In this context, the molecular configurations obtained by the QM/MM MD simulation can be used as reliable representatives for the geometrical arrangement of the Ca²⁺ and Cl⁻ hydrations.

5. Conclusions

In this work, we combine the QM/MM MD technique with the XAS measurements for studying the hydration shell structures of Ca²⁺ and Cl⁻. The QM/MM MD results and the detailed analysis on the measured XAS spectra clearly indicate the characteristically low symmetry and disordered nature of the first coordination shell of these ions, especially for the case of Cl⁻. In terms of XAS measurements, the presence of MS effects in the measured spectra and the errors from asymmetric distributions are the major problems in the analysis of XAS data. To simplify these problems, QM/MM MD simulations have been performed to generate theoretical XAS spectra, from which these spectra have been used as starting models in the XAS data analysis. Since the accuracy in the interpretation of XAS data depends crucially on the

reliability of the simulated XAS models, the use of a more sophisticated QM/MM MD technique is highly recommended over other MM approaches in order to generate a reliable ensemble average, *i.e.*, a better theoretical $\chi(k)$. In particular for XANES, since there is no direct relationship between the XANES spectrum and the dynamic details relating to the geometrical arrangement of the hydrated ion, a representative set of geometries extracted from the QM/MM MD trajectories is extremely useful in order to simplify the process of XANES data interpretation.

Acknowledgements

This work was supported by the Thailand Research Fund (TRF, Grant No. RTA5280009). The corresponding author also acknowledges support from the Synchrotron Light Research Institute (SLRI) and TRF (Grant No. BRG5180018).

References

- 1 H. Frank, in Chemical Physics of Ionic Solutions, John Wiley & Sons, New York, 1956.
- 2 R. J. P. Williams, in *Bio-inorganic Chemistry*, American Chemical Society, Washington DC, 1971.
- 3 J. E. Enderby and G. W. Neilson, Rep. Prog. Phys., 1981, 44, 593.
- 4 I. Howell and G. W. Neilson, J. Phys.: Condens. Matter, 1996, 8, 4455.
- 5 M. Magini, G. Licheri, G. Paschina and G. Piccaluga, in X-ray Diffraction of Ions in Aqueous Solutions: Hydration and Complex Formation, CRC Press, Boca Raton, 1988.
- 6 G. W. Neilson, Pure Appl. Chem., 1988, 60, 1797.
- 7 G. W. Neilson and R. H. Tromp, Annu. Rep. Prog. Chem., Sect. C, 1991, 88, 45.
- 8 H. Ohtaki and T. Radnai, Chem. Rev., 1993, 93, 1157.
- 9 N. T. Skipper, G. W. Neilson and S. C. Cummings, J. Phys.: Condens. Matter, 1989, 1, 3489.
- 10 D. E. Crozier, J. J. Rehr and R. Ingalls, in X-ray Absorption: Principles, Applications, Techniques of EXAFS, SEXAFS and XANES, Wiley, New York, 1988, ch. 9.
- 11 P. D'Angelo, A. Di Nola, A. Filipponi, N. V. Pavel and D. Roccatano, *J. Chem. Phys.*, 1994, **100**, 985.
- 12 D. E. Crozier, Physica B, 1995, 208-209, 330.
- 13 D. E. Crozier, Nucl. Instrum. Methods Phys. Res., Sect. B, 1997, 133, 134.
- 14 P. D'Angelo, A. Di Nola, E. Giglio, M. Mangoni and N. V. Pavel, J. Phys. Chem., 1995, 99, 5471.
- 15 P. D'Angelo and N. V. Pavel, J. Chem. Phys., 1999, 111, 5107.
- 16 P. D'Angelo and N. V. Pavel, J. Synchrotron Radiat., 2001, **8**, 173.
- 17 L. X. Dang, G. K. Schenter, V.-A. Glezakou and J. L. Fulton, J. Phys. Chem. B, 2006, 110, 23644.
- 18 A. Di Cicco, J. Phys.: Condens. Matter, 1996, 8, 9341.
- 19 A. Di Cicco, M. J. Rosolen, R. Marassi, R. Tossici, A. Fillipponi and J. Rybicki, *J. Phys.: Condens. Matter*, 1996, **8**, 10779.
- 20 A. Di Cicco, M. Taglienti, M. Minicucci and A. Filipponi, *Phys. Rev. B: Condens. Matter Mater. Phys.*, 2000, 62, 12001.
- 21 J. L. Fulton, M. M. Hoffmann, J. G. Darab, B. J. Palmer and E. A. Stern, J. Phys. Chem. A, 2000, 104, 11651.
- 22 A. Kuzmin, S. Obst and J. Purans, J. Phys.: Condens. Matter, 1997 9 10065
- 23 S. Rossano, A. Ramos, J.-M. Delaye, A. Filipponi, C. Brouder and G. Calas, J. Synchrotron Radiat., 1999, 6, 247.
- 24 A. Trapananti, A. Di Cicco and M. Minicucci, *Phys. Rev. B: Condens. Matter Mater. Phys.*, 2002, **66**, 014202.
- 25 S. L. Wallen, B. J. Palmer and J. L. Fulton, J. Chem. Phys., 1998, 108, 4039
- 26 B. M. Rode, C. F. Schwenk, T. S. Hofer and B. R. Randolf, *Coord. Chem. Rev.*, 2005, **249**, 2993.
- 27 B. M. Rode, C. F. Schwenk and A. Tongraar, J. Mol. Liq., 2004, 110, 105.

- 28 P. Intharathep, A. Tongraar and K. Sagarik, J. Comput. Chem., 2005, 26, 1329.
- 29 T. Kerdcharoen, K. R. Liedl and B. M. Rode, Chem. Phys., 1996, **211**. 313.
- 30 A. Payaka, A. Tongraar and B. M. Rode, J. Phys. Chem. A, 2009, **113**, 3291.
- 31 A. Tongraar, K. R. Liedl and B. M. Rode, J. Phys. Chem. A, 1997, 101 6299
- 32 A. Tongraar, K. R. Liedl and B. M. Rode, J. Phys. Chem. A, 1998, **102**, 10340.
- 33 A. Tongraar and B. M. Rode, Phys. Chem. Chem. Phys., 2003, 5,
- 34 A. Tongraar and B. M. Rode, Chem. Phys. Lett., 2005, 403, 314.
- 35 A. Tongraar, K. Sagarik and B. M. Rode, Phys. Chem. Chem. Phys., 2002, 4, 628.
- 36 D. Xenides, B. R. Randolf and B. M. Rode, J. Chem. Phys., 2005, **122**, 174506.
- 37 S. Cummings, J. E. Enderby and R. A. Howe, J. Phys. C: Solid State Phys., 1980, 13, 1.
- 38 N. A. Hewish, G. W. Neilson and J. E. Enderby, *Nature*, 1982, 297, 138
- 39 F. Jalilevand, D. Spangberg, P. Lindqvist-Reis, K. Hermansson, I. Persson and M. Sandström, J. Am. Chem. Soc., 2001, 123, 431.
- 40 G. Licheri, G. Piccaluga and P. Pinna, J. Chem. Phys., 1976, 64,
- 41 M. M. Probst, T. Radnai, K. Heinzinger, P. Bopp and B. M. Rode, J. Phys. Chem., 1985, 89, 753.
- 42 P. Smirnov, M. Yamagami, H. Wakita and T. Yamaguchi, J. Mol. Liq., 1997, 73-74, 305.
- 43 D. Spangberg, K. Hermansson, P. Lindqvist-Reis, F. Jalilevand, M. Sandström and I. Persson, J. Phys. Chem. B, 2000, 104, 10467.
- 44 J. L. Fulton, M. S. Heald, Y. S. Badyal and J. M. Simonsom, J. Phys. Chem. A, 2003, 107, 4688.
- 45 F. M. Floris, M. Persico, A. Tani and J. Thomasi, Chem. Phys. Lett., 1994, 227, 126.
- 46 S. G. Kalko, G. Sesé and J. A. Padro, J. Chem. Phys., 1996, 104, 9578
- 47 S. Obst and H. Bradaczek, J. Phys. Chem., 1996, 100, 15677
- 48 G. Pálinkás and K. Heinzinger, Chem. Phys. Lett., 1986, 126, 251.
- 49 I. Bakó, J. Hutter and G. Pálinkás, J. Chem. Phys., 2002, 117,
- 50 M. M. Naor, K. V. Nostrand and C. Dellago, Chem. Phys. Lett., 2003, **369**, 159.
- 51 F. C. Lightstone, E. Schwegler, M. Allesch, F. Gygi and G. Galli, ChemPhysChem, 2005, 6, 1745.
- 52 T. Todorova, P. Hűnenberger and J. Hutter, J. Chem. Theory Comput., 2008, 4, 779.
- 53 S. Yoo, X. C. Zeng and S. S. Xantheas, J. Chem. Phys., 2009, 130, 221102.
- 54 C. F. Schwenk, H. Loeffler and B. M. Rode, J. Chem. Phys., 2001, 115, 10808.
- 55 C. F. Schwenk and B. M. Rode, Pure Appl. Chem., 2004, 76, 37.

- 56 J. Chandrasekhar, D. C. Spellmayer and W. L. Jorgensen, J. Am. Chem. Soc., 1984, 106, 903.
- E. Clementi, R. Barsotti, J. Fromm and R. O. Watts, Theor. Chim. Acta, 1976, 43, 101.
- 58 K. Heinzinger, Pure Appl. Chem., 1985, 57, 1031.
- 59 A. Ignaczak, J. A. N. F. Gomes and M. N. D. S. Cordeiro, Electrochim. Acta, 1999, 45, 659.
- 60 R. W. Impey, P. A. Madden and I. R. McDonald, J. Phys. Chem., 1983, 87, 5071.
- 61 S. Koneshan, J. C. Rasaiah, R. M. Lynden-Bell and S. H. Lee, J. Phys. Chem. B, 1998, 102, 4193.
- 62 M. Mezei and D. L. Beveridge, J. Chem. Phys., 1981, 74, 6902.
- 63 D. E. Smith and L. X. Dang, J. Chem. Phys., 1994, 101, 7873.
- 64 M. Newville, B. Ravel, D. Haskel, J. J. Rehr, E. A. Stern and Y. Yacoby, Phys. B, 1995, 208-209, 154.
- 65 J. J. Rehr, R. C. Albers and S. I. Zabinsky, Phys. Rev. Lett., 1992, **69** 3397
- 66 P. J. Merkling, A. Munoz-Paez and E. Sanchez Marcos, J. Am. Chem. Soc., 2002, 124, 10911.
- P. Wernet, D. Nordlund, U. Bergmann, M. Cavalleri, M. Odelius, H. Ogasawara, L. A. Naslund, T. K. Hirsch, L. Ojamae, P. Glatzel, L. G. M. Pettersson and A. Nilsson, Science, 2004, 304, 995.
- 68 P. D'Angelo, O. M. Roscioni, G. Chillemi, S. Della Longa and M. Benfatto, J. Am. Chem. Soc., 2006, 128, 1853.
- 69 A. L. Ankudinov, C. E. Bouldin, J. J. Rehr, J. Sims and H. Hung, Phys. Rev. B: Condens. Matter Mater. Phys., 2002, 65, 104107.
- A. L. Ankudinov, B. Ravel, J. J. Rehr and S. D. Conradson, Phys. Rev. B: Condens. Matter Mater. Phys., 1998, 58, 7565.
- T. H. Dunning and P. J. Hay, in Modern Theoretical Chemistry, Plenum, New York, 1976.
- 72 P. J. Hay and W. R. Wadt, J. Chem. Phys., 1985, 82, 270.
- 73 M. J. Frisch, J. A. Pople and J. S. Binkley, J. Chem. Phys., 1984, 80, 3265.
- 74 W. J. Hehre, R. Ditchfield and J. A. Pople, J. Chem. Phys., 1972, **56** 2257
- 75 F. H. Stillinger and A. Rahman, J. Chem. Phys., 1978, 68, 666.
- 76 P. Bopp, G. Jancsó and K. Heinzinger, Chem. Phys. Lett., 1983,
- 77 B. R. Brooks, R. E. Bruccoleri, B. D. Olafson, D. J. States, S. Swaminathan and M. Karplus, J. Comput. Chem., 1983, 4, 187.
- 78 H. J. C. Berendsen, J. P. M. Postma, W. F. van Gunsteren, A. DiNola and J. R. Haak, J. Chem. Phys., 1984, 81, 3684.
- 79 D. J. Adams, E. H. Adams and G. J. Hills, Mol. Phys., 1979, 38, 387.
- 80 L. Hedin and S. Lundqvist, Solid State Phys., 1970, 23, 1.
- 81 L. H. V. Lim, A. B. Pribil, A. E. Ellmerer, B. R. Randolf and B. M. Rode, J. Comput. Chem., 2010, 31, 1195.
- 82 A. Tongraar, P. Tangkawanwanit and B. M. Rode, J. Phys. Chem. A, 2006, 110, 12918.
- 83 J. M. Heuft and E. J. Meijer, J. Chem. Phys., 2003, 119, 11788.
- 84 J. L. Fulton, Y. Chen, S. M. Heald and M. Balasubramanian, J. Chem. Phys., 2006, 125, 94507.

1. สำเนา Reprint ของงานวิจัยเรื่องที่ 3

Apirak Payaka, **Anan Tongraar** and Bernd M. Rode "QM/MM dynamics of CH₃COO-water hydrogen bonds in aqueous solution" J. *Phys. Chem. A*, **2010**, 114 10443-10453.

QM/MM Dynamics of CH₃COO⁻-Water Hydrogen Bonds in Aqueous Solution

Apirak Payaka,† Anan Tongraar,*,† and Bernd Michael Rode‡

School of Chemistry, Institute of Science, Suranaree University of Technology, Nakhon Ratchasima 30000, Thailand, and Department of Theoretical Chemistry, Institute of General, Inorganic and Theoretical Chemistry, University of Innsbruck, Innrain 52a, A-6020 Innsbruck, Austria

Received: June 19, 2010; Revised Manuscript Received: August 20, 2010

Two combined QM/MM molecular dynamics (MD) simulations, namely, HF/MM and B3LYP/MM, in which the central CH₃COO⁻ and its surrounding water molecules were treated at HF and B3LYP levels of accuracy, respectively, using the DZV+ basis set, have been performed to investigate the characteristics of CH₃COO⁻—water hydrogen bonds in dilute aqueous solution. Both HF/MM and B3LYP/MM simulations clearly indicate relatively strong hydrogen bonds between CH₃COO⁻ oxygens and their nearest-neighbor waters compared with those of water—water hydrogen bonds in the bulk. In addition, it is observed that first-shell waters are either "loosely" or "tightly" bound to their respective CH₃COO⁻ oxygen atoms, leading to large fluctuations in the coordination number, ranging from 2 to 5, with the prevalent value of 3. Among the HF and B3LYP methods for the description of the QM-treated region, the latter predicts slightly higher hydrogen-bond strength in the CH₃COO⁻—water complex.

1. Introduction

Detailed knowledge of ions solvated in aqueous electrolyte solutions is essential for understanding the role of ions in chemical and biological processes. 1-3 Besides much attention on the interactions between simple ions and water, characteristics of carboxylate (RCOO⁻) functional groups that form hydrogen bonds with surrounding water have also been a matter of interest.^{4,5} According to nuclear magnetic resonance (NMR) experiments with carboxylate acids, it has been suggested that each RCOO⁻ group binds about 5.0 to 6.5 water molecules.⁶ For acetate ion (CH₃COO⁻), the biological species of our interest, X-ray diffraction studies of concentrated divalent transition metal acetates, that is, in the presence of transition metal-acetate complexes, have demonstrated the formation of hydrogen bonds between the oxygen atoms of CH₃COO⁻ and water molecules, with nearest-neighbor distances between 2.77 and 2.95 Å.⁷ The hydration number of CH₃COO⁻ has been evaluated to be in the range of 3.0-6.1, depending on the concentration and the type of metal ion. Later, X-ray diffraction measurements were carried out for aqueous 8 mol % CH₃COONa solution, in which the nearest-neighbor O₀-O_w (O₀: carboxylate oxygen atom, Ow: water oxygen atom) distance was determined to be 2.78 Å, with the coordination number of 4.0 per CH₃COO^{-.8} Recently, the hydration structure around the -COO[−] group of CH₃COO[−] has been investigated by means of neutron diffraction (ND) measurements of the aqueous 8 mol % CH₃COONa solution in D₂O.⁹ According to the ND results, the nearest-neighbor C_o-D_w (C_o: carboxylate carbon atom, D_w: water deuterium atom) and Co-Ow distances were obtained to be 2.63 and 3.23 Å, respectively, with the average coordination number of 4.0.

In terms of theoretical investigations, classical Monte Carlo (MC) and molecular dynamics (MD) simulations using different sets of molecular mechanical (MM) force fields have been

performed for CH₃COO⁻ in water.¹⁰⁻¹² However, because most of the MM force fields are usually constructed with respect to simple atomic interaction terms, the simulation results, even for the fundamental data as the hydration number, have been found to depend crucially on the quality and reliability of the MM models employed in the simulations. For example, MC simulations by Alagona et al.¹¹ and by Jorgensen et al.¹⁰ using TIP4P and OPLS potentials for water, respectively, have predicted that there are about six and seven tightly bound waters for the CH₃COO⁻, whereas MD simulations by Meng et al.¹² using two different water models, namely, a pairwise additive SPC/E potential and the related POL3 model, which includes nonadditive terms, led to the average coordination numbers of 6.6 and 6.2, respectively.

To obtain more reliable simulation results, an elegant approach is to apply a combined quantum mechanical/molecular mechanical (OM/MM) technique. 13-16 A major attractive feature of this technique is that a small, chemically most relevant region, that is, a sphere including the ion and its surrounding solvent molecules, is treated as accurately as needed using quantum mechanics (QM), whereas the rest of the system is described by MM force fields. By this scheme, the complicated nonadditive contributions as well as the polarization effects, which are hardly represented by the basic assumptions underlying the classical MM models, can be reliably included in the specific region. In recent years, a number of QM/MM MD simulations have been carried out for various ions in solutions, providing many new insights into the solvation structure and dynamics of the solvated ions. 17-26 Recently, two QM/MM MD simulations, namely, HF/MM and B3LYP/MM, have been performed for formate ion (HCOO⁻) in water, ²⁶ providing microscopic details with respect to hydrogen bonds between HCOOoxygens and first-shell waters. Analogous QM/MM MD simulations were performed in the present study to obtain a detailed picture of CH₃COO⁻-water hydrogen bonds in dilute aqueous solution.

^{*} Corresponding author. E-mail: anan_tongraar@yahoo.com. Fax: 0066-44-224017.

[†] Suranaree University of Technology.

[‡] University of Innsbruck.

2. Methods

By the QM/MM MD technique, ^{17–26} the system's interactions can be written as

$$E_{\text{total}} = \langle \Psi_{\text{QM}} | \hat{H} | \Psi_{\text{QM}} \rangle + E_{\text{MM}} + E_{\text{QM-MM}}$$
 (1)

where $\langle \Psi_{\rm QM} | \hat{H} | \Psi_{\rm QM} \rangle$ refers to the interactions within the QM region, whereas $E_{\rm MM}$ and $E_{\rm QM-MM}$ represent the interactions within the MM and between the QM and MM regions, respectively. The QM region, the most interesting subsystem that includes ${\rm CH_3COO^-}$ and its nearest-neighbor water molecules, is treated quantum mechanically, whereas the rest of the system is described by classical pair potentials. Considering the exchange of water molecules between the QM and MM regions, which can occur frequently during the QM/MM simulations, the forces acting on each particle in the system are switched according to which region the water molecule is entering or leaving and can be defined as

$$F_i = S_m(r)F_{\text{OM}} + (1 - S_m(r))F_{\text{MM}}$$
 (2)

where F_{QM} and F_{MM} are quantum mechanical and molecular mechanical forces, respectively. $S_m(r)$ is a smoothing function²⁷

$$S_m(r) = 1 \quad \text{for} \quad r \le r_1$$

$$S_m(r) = \frac{(r_0^2 - r^2)^2 (r_0^2 + 2r^2 - 3r_1^2)}{(r_0^2 - r_1^2)^3} \quad \text{for} \quad r_1 < r \le r_0$$

$$S_m(r) = 0 \quad \text{for} \quad r > r_0$$
(3)

where r_1 and r_0 are distances characterizing the start and the end of the QM region, applied within an interval of 0.2 Å to ensure a continuous change of forces at the boundary between QM and MM regions.

Because the performance of QM/MM MD simulations with correlated ab initio methods as well as with relatively large QM size and basis set is still far too time-consuming, the HF and hybrid density functional B3LYP methods with a moderate QM region and basis set were chosen as a compromise. To check the validity of the HF and B3LYP methods for this particular system, geometry optimizations of cyclic, anti-, and syn-CH₃COO⁻-H₂O clusters (Figure 1) were carried out at HF, B3LYP, MP2, and CCSD levels of accuracy using DZV+28 and aug-cc-pvdz²⁹⁻³¹ basis sets. As can be seen from the optimized parameters in Table 1, the B3LYP hydrogen-bond lengths and energies are close to that of the correlated ab initio methods using the same large basis set, whereas the HF results show good agreement with the correlated data when the smaller basis set, DZV+, is employed. Overall, the H-bond length and energy ordering of the three CH₃COO⁻-H₂O clusters predicted by the HF and B3LYP methods are in good accord with the correlated results. This suggests that quantum mechanical calculations based on both HF and B3LYP methods would be reliable enough to achieve a sufficient level of accuracy in the QM/ MM simulations. The quality of the HF method has been well demonstrated in previous QM/MM studies,17-26 even for the treatment of anions, implying that the effects of electron correlation are small enough to be neglected. 19,20,26 In recent QM/MM MD simulations of pure water,32 it has been shown that the HF method with a sufficiently large QM region could provide detailed information for pure water, in particular,

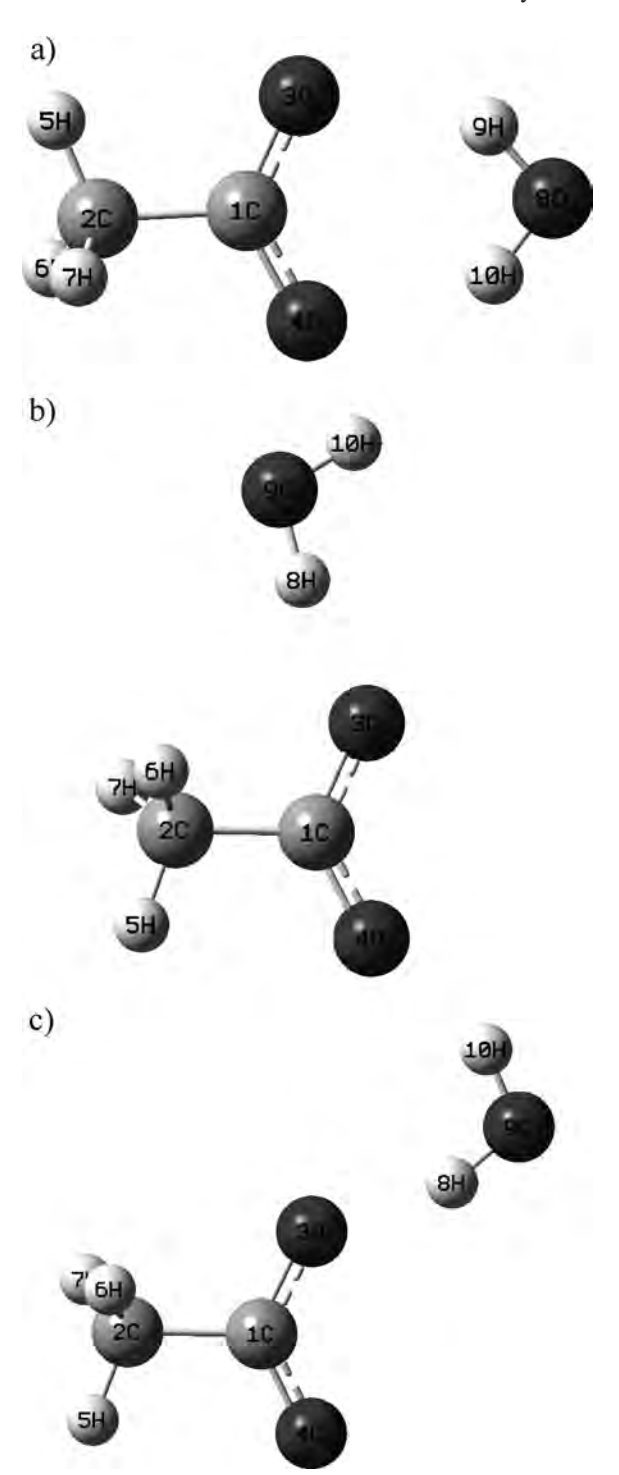


Figure 1. (a) Cyclic, (b) *anti-*, and (c) $syn\text{-CH}_3COO^-\text{-H}_2O$ complexes.

hydrogen-bond structure and lifetime, in good agreement with the MP2-based simulation and with experimental data. The B3LYP method, although inferior for most of hydrated cations, ^{23,24} was also employed in this work because it has been shown that this method could predict reasonable data for weakly bound H-bond systems. ^{25,26,33}

In the present study, the DZV+ basis set²⁸ was chosen and considered to be a suitable compromise between the quality of the simulation results and the requirement of CPU time. To determine the appropriate size of the QM region, preliminary HF/MM and B3LYP/MM simulations, that is, the simulations in which only the CH₃COO⁻ was treated

TABLE 1: Stabilization Energies and Some Selected Structural Parameters of the Optimized Cyclic, anti-, and syn-CH₃COO⁻-H₂O Complexes Calculated at HF, B3LYP, MP2, and CCSD Methods Using DZV+ and aug-cc-pvdz (Data in Parentheses) Basis Sets

method	HF	B3LYP	MP2	CCSD
<u> </u>		Cyclic Complex		
$\Delta E (\text{kcal} \cdot \text{mol}^{-1})$	-20.66(-16.47)	-22.65(-18.41)	-21.78(-19.64)	-21.65(-19.12)
R_{1-2} (Å)	1.5326 (1.5368)	1.5491 (1.5474)	1.5655 (1.5452)	1.5652 (1.5480)
R_{1-3} (Å), R_{1-4} (Å)	1.2710 (1.2410)	1.2961 (1.2647)	1.3158 (1.2750)	1.3087 (1.2682)
R_{2-5} (Å), R_{2-6} (Å), R_{2-7} (Å)	1.0842 (1.0913)	1.0980 (1.6501)	1.1043 (1.1020)	1.1080 (1.1043)
R_{3-9} (Å), R_{4-10} (Å)	2.1155 (2.1185)	1.9991 (1.9888)	2.0770 (1.9791)	2.0921 (2.0092)
R_{8-9} (Å), R_{8-10} (Å)	0.9594 (0.9516)	0.99173 (0.9795)	0.9918 (0.9805)	0.9895 (0.9761)
A_{3-1-4} (deg)	126.17 (127.58)	126.34 (127.51)	126.40 (127.66)	126.43 (127.73)
A_{3-9-8} (deg), A_{4-10-8} (deg)	138.14 (141.41)	140.89 (143.78)	140.31 (144.74)	139.95 (143.94)
A_{9-8-10} (deg)	104.19 (98.51)	100.83 (96.01)	101.83 (95.08)	102.06 (95.89)
		anti Complex		
$\Delta E (\text{kcal} \cdot \text{mol}^{-1})$	-18.52 (-14.06)	-20.74(-16.47)	-19.17 (-17.34)	-18.90(-16.71)
R_{1-2} (Å)	1.5368 (1.5379)	1.5520 (1.5476)	1.5696 (1.5465)	1.5689 (1.5496)
R_{1-3} (Å), R_{1-4} (Å)	1.2681 (1.2278)	1.2928 (1.2636)	1.3123 (1.2735)	1.3182 (1.3055)
R_{2-5} (Å), R_{2-6} (Å), R_{2-7} (Å)	1.0842 (1.0914)	1.0978 (1.0999)	1.1043 (1.1020)	1.1079 (1.1043)
$R_{3-8} (\text{Å})$	1.7002 (1.7777)	1.5688 (1.6390)	1.6710 (1.6419)	1.6939 (1.6784)
R_{8-9} (Å), R_{9-10} (Å)	0.9645 (0.9541)	1.0038 (0.9863)	0.9993 (0.9870)	0.9956 (0.9811)
A_{3-1-4} (deg)	126.81 (127.50)	126.19 (126.83)	126.49 (127.10)	126.69 (127.31)
A_{3-8-9} (deg)	167.12 (168.96)	172.08 (172.96)	170.50 (174.37)	169.47 (173.31)
A_{8-9-10} (deg)	109.28 (103.44)	108.26 (102.76)	108.26 (102.02)	107.86 (102.21)
		syn Complex		
$\Delta E (\text{kcal} \cdot \text{mol}^{-1})$	-18.30 (-13.77)	-20.16(-15.79)	-18.93(-16.31)	-18.79 (-15.88)
$R_{1-2}(\text{Å})$	1.5364 (1.5382)	1.5528 (1.5497)	1.5687 (1.5477)	1.5680 (1.5503)
$R_{1-3}(\text{Å}), R_{1-4}(\text{Å})$	1.2682 (1.2393)	1.2920 (1.2625)	1.3119 (1.2724)	1.3052 (1.2659)
R_{2-5} (Å), R_{2-6} (Å), R_{2-7} (Å)	1.0843 (1.0917)	1.0981 (1.1004)	1.1045 (1.1024)	1.6622 (1.1046)
$R_{3-8} (\text{Å})$	1.7448 (1.8357)	1.6273 (1.7002)	1.7338 (1.7106)	1.7540 (1.7420)
R_{8-9} (Å), R_{9-10} (Å)	0.9638 (0.9531)	0.9990 (0.9827)	0.9958 (0.9828)	0.9933 (0.9782)
A_{3-1-4} (deg)	127.18 (127.99)	127.27 (127.95)	127.19 (127.96)	127.23 (128.05)
A_{3-8-9} (deg)	158.62 (160.16)	161.87 (164.63)	158.86 (164.26)	157.69 (163.08)
A_{8-9-10} (deg)	108.43 (102.79)	106.77 (102.01)	106.72 (101.12)	106.38 (101.30)

quantum mechanically using HF and B3LYP methods while the rest of the system was described by classical pair potentials, were performed. According to the resulting Co-Ow radial distribution functions (RDFs) (data not shown), both HF/MM and B3LYP/MM simulations reveal first C_o-O_w minima between 4.1 and 4.2 Å, in which integrations up to these C_o-O_w distances yield about 10-13 water molecules. In this work, therefore, the QM size with radius of 4.2 Å was chosen (i.e., the values of r_1 and r_0 in eq 3 were set with respect to the C_o-O_w distances of 4.0 and 4.2 Å, respectively). It should be noted that the position of the C₀ atom was set as the center of QM region during the simulations.

A flexible model, which describes intermolecular34 and intramolecular35 interactions, was employed for water. This flexible water model allows explicit hydrogen movements, thus ensuring a smooth transition, when water molecules move from the QM region with its full flexibility to the MM region. The

TABLE 2: Optimized Parameters of the Analytical Pair Potentials for the Interaction of Water with CH₃COO⁻ (Interaction Energies in kilocalories per mole and Distances in angstroms)

	A	В	C	D			
pair	$(\text{kcal} \cdot \text{mol}^{-1} \text{ Å}^4)$	$(\text{kcal} \cdot \text{mol}^{-1} \text{ Å}^5)$	$(\text{kcal} \cdot \text{mol}^{-1} \text{ Å}^6)$	$(\text{kcal} \cdot \text{mol}^{-1} \text{ Å}^{12})$			
HF-Based Method							
$C_H - O_w$	6.25575×10^6	-2.80636×10^7	3.66359×10^7	-2.11546×10^8			
$C_o - O_w$	-3.24728×10^6	1.87939×10^7	-2.86738×10^7	4.74720×10^8			
$O-O_{w}$	6.65129×10^5	-6.72760×10^6	1.30700×10^7	-6.88407×10^7			
$H-O_{w}$	-5.70606×10^5	1.68140×10^6	-1.08799×10^6	-3.39850×10^{5}			
$C_H - H_w$	-1.07945×10^6	3.37053×10^6	-2.79560×10^6	1.72989×10^6			
C_o-H_w	2.98361×10^{5}	-7.82658×10^{5}	7.53084×10^{5}	-5.07991×10^5			
$O-H_{w}$	6.58235×10^4	-2.19426×10^5	2.21554×10^{5}	-4.43483×10^4			
$H-H_{\rm w}$	1.87543×10^4	-1.39169×10^3	-6.36335×10^3	5.11901×10^2			
		B3LYP-Based Method	l				
$C_H - O_w$	6.09669×10^6	-2.78939×10^7	3.65314×10^7	-2.00914×10^{8}			
$C_{o}-O_{w}$	-4.90291×10^6	2.45331×10^7	-3.36074×10^7	3.84037×10^{8}			
$O-O_{w}$	7.97158×10^{5}	-7.60038×10^6	1.43174×10^7	-8.17032×10^7			
$H-O_{w}$	-5.56079×10^5	1.77187×10^6	-1.27320×10^6	-1.87559×10^4			
$C_H - H_w$	-7.51684×10^5	2.37607×10^6	-1.91117×10^6	8.07782×10^{5}			
C_o-H_w	1.02899×10^6	-3.38311×10^6	3.26716×10^6	-2.67571×10^6			
$O-H_w$	6.93278×10^4	-2.68761×10^{5}	2.65680×10^{5}	-4.26558×10^4			
$H-H_{\rm w}$	-3.34025×10^4	8.37539×10^4	-4.57267×10^4	1.07909×10^3			

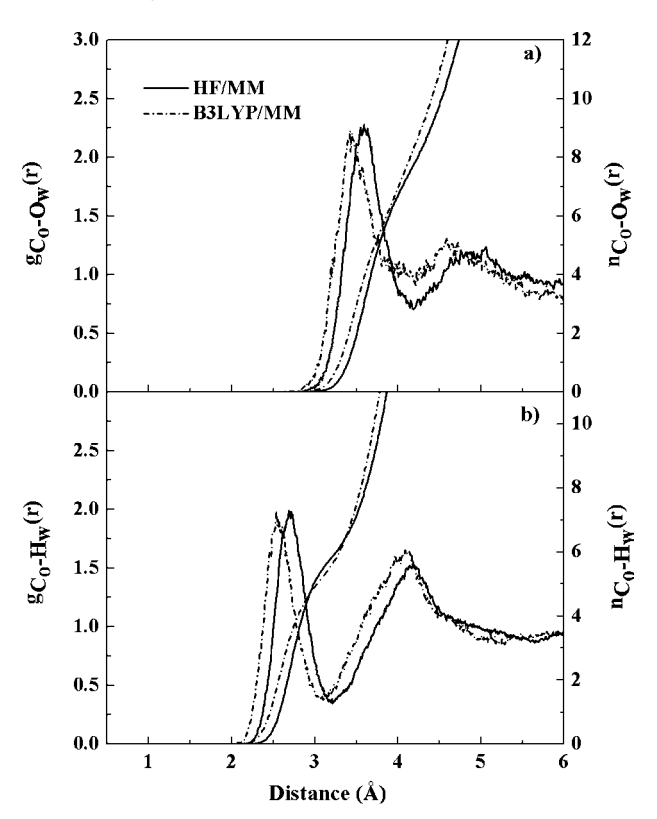


Figure 2. (a) C_o-O_w and (b) C_o-H_w RDFs and their corresponding integration numbers.

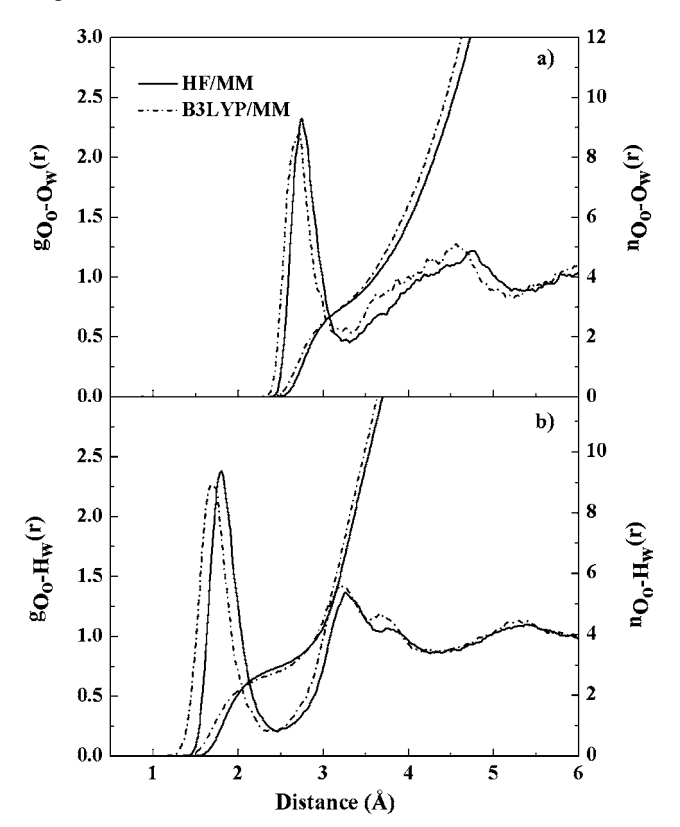


Figure 3. (a) O_o-O_w and (b) O_o-H_w RDFs and their corresponding integration numbers.

pair potential functions for describing $CH_3COO^--H_2O$ interactions were newly constructed. The 24 637 HF and 22 038 B3LYP interaction energy points for various $CH_3COO^--H_2O$ configurations, obtained from Gaussian03³⁶ calculations using aug-cc-pvdz basis set,^{29–31} were fitted to the analytical form of

$$\Delta E_{\text{CH}_3\text{COO}^--\text{H}_2\text{O}} = \sum_{i=1}^{7} \sum_{j=1}^{3} \left[\frac{A_{ij}}{r_{ij}^4} + \frac{B_{ij}}{r_{ij}^5} + \frac{C_{ij}}{r_{ij}^6} + \frac{D_{ij}}{r_{ij}^{12}} + \frac{q_i q_j}{r_{ij}} \right]$$
(4)

where A, B, C, and D are fitting parameters (Table 2), r_{ij} denotes the distances between the ith atoms of CH_3COO^- and the jth atoms of water molecule, and q are atomic net charges. In the present study, the charges on C_H (methyl carbon atom), C_o , O_o , and O_o of the corresponding O_o or bital (NBO) analysis O_o of the corresponding HF and O_o and O_o of the corresponding HF and O_o of the corresponding the angle of O_o of O_o of the corresponding the O_o of O_o

Both HF/MM and B3LYP/MM simulations were performed in a canonical ensemble at 298 K with a time step of 0.2 fs. The system's temperature was kept constant using the Berendsen algorithm.⁴⁰ The periodic box, with a box length of 18.17 Å, contained one CH₃COO⁻ and 199 water molecules, corresponding to the experimental density of pure water. Long-range interactions were handled using the reaction-field procedure.⁴¹ In the present study, the HF/MM and B3LYP/MM simulations were carried out independently with system's re-equilibration for 25 000 time steps, followed by another 300 000 (HF/MM)

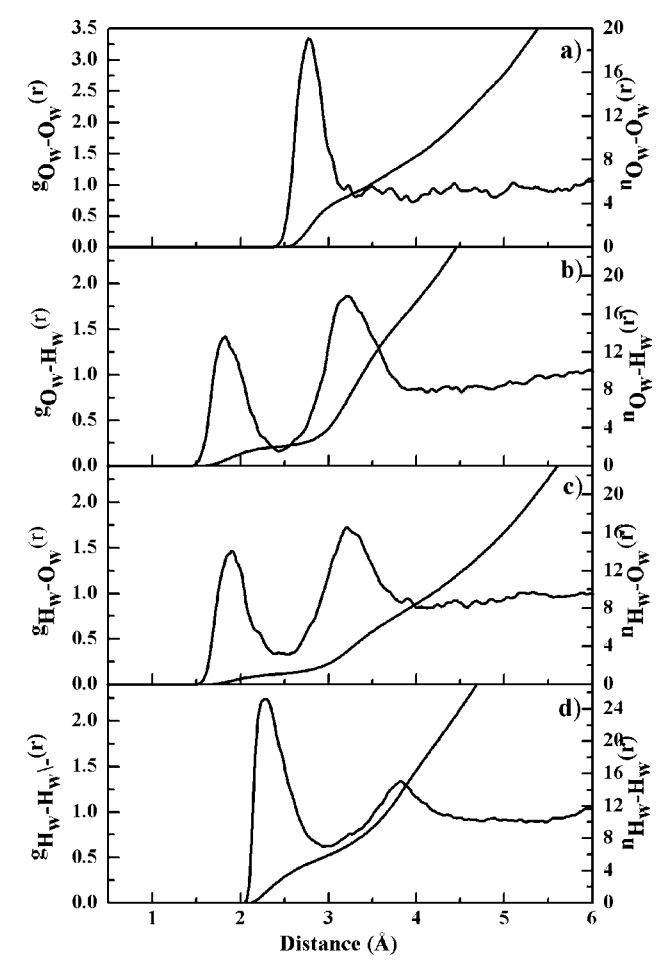


Figure 4. (a) $O_w - O_w$, (b) $O_w - H_w$, (c) $H_w - O_w$, and (d) $H_w - H_w$ RDFs and their corresponding integration numbers. The first atom of each pair refers to the atoms of the water molecule, whose oxygen position was defined as the center of the QM region during the QM/MM simulation of pure water.



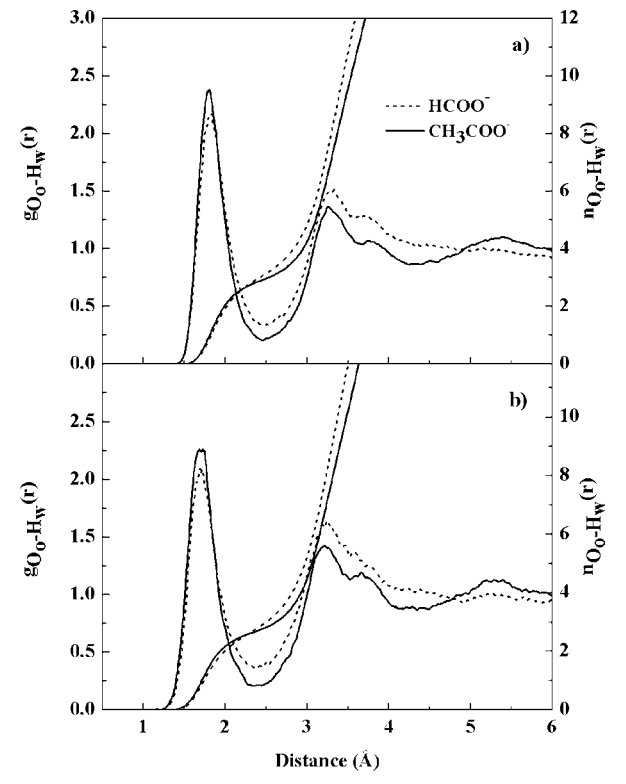


Figure 5. Comparisons of O₀-H_w RDFs and their corresponding integration numbers for aqueous HCOO⁻ and CH₃COO⁻ solutions, as obtained from (a) HF/MM and (b) B3LYP/MM simulations, respectively.

and 250 000 (B3LYP/MM) time steps to collect configurations every 10th step.

3. Results and Discussion

3.1. Structural Details. The hydration structure around the -COO group of CH₃COO can be interpreted through the $C_o {-} O_w$ and $C_o {-} H_w$ RDFs, together with their corresponding integration numbers, as depicted in Figure 2a,b, respectively. In the HF/MM simulation, the first C_o-O_w peak is exhibited at 3.60 Å, and integration up to the corresponding first C_o-O_w minimum yields an average coordination number of 7.6 \pm 0.2. The first C_o-H_w peak is found at ~ 2.68 Å, with the corresponding coordination number (i.e., calculated up to first minimum of the C_0 - H_w RDF) of 5.8 \pm 0.1. In the B3LYP/ MM simulation, the first Co-Ow peak is found to start at a distance of ~ 0.1 Å shorter than that observed in the HF/MM simulation, with the maximum at 3.44 Å. Compared with the HF/MM results, the first C_o-O_w minimum is rather broad, giving an average coordination number of 8.3 ± 0.4 . In accord with the C_o-O_w RDF, the B3LYP/MM simulation reveals a shorter C_o-H_w distance of 2.53 Å, with an average coordination number of 5.3 ± 0.1 . On the basis of both HF/MM and B3LYP/ MM simulations, the feature of C_o-O_w and C_o-H_w RDFs clearly suggests an arrangement where each of the first-shell water molecules donates one of its hydrogen atoms to hydrogen to bind with the CH₃COO⁻ oxygens. Such phenomenon is similar to that observed in the ND study of aqueous 8 mol % CH₃COONa solution in D₂O.9 Comparing the HF and B3LYP methods for the description of the QM-treated region, however, the latter one predicts a slightly more compact hydration structure around the -COO group.

The characteristics of hydrogen bonds between the CH₃COO⁻ oxygen atoms and their nearest-neighbor waters can be visual-

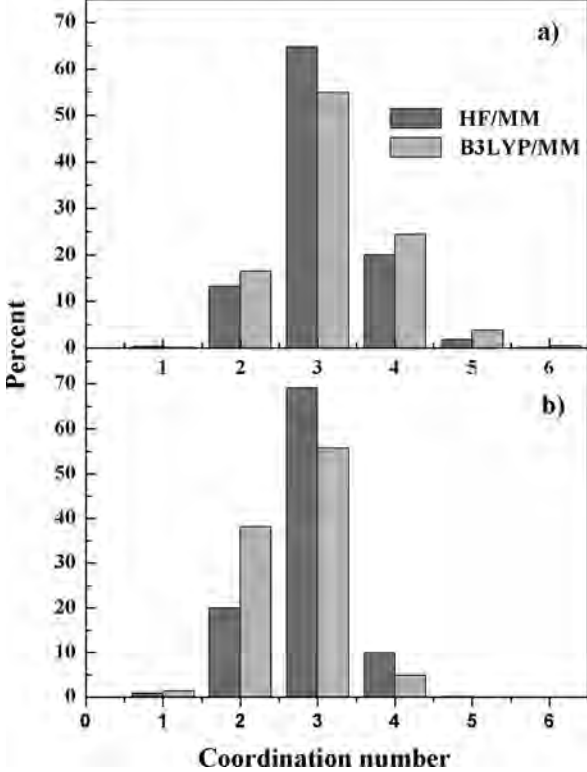


Figure 6. Distributions of (a) oxygen and (b) hydrogen atoms of firstshell waters at each of the CH₃COO⁻ oxygens, calculated within first peak of the Oo-Ow and Oo-Hw RDFs, respectively.

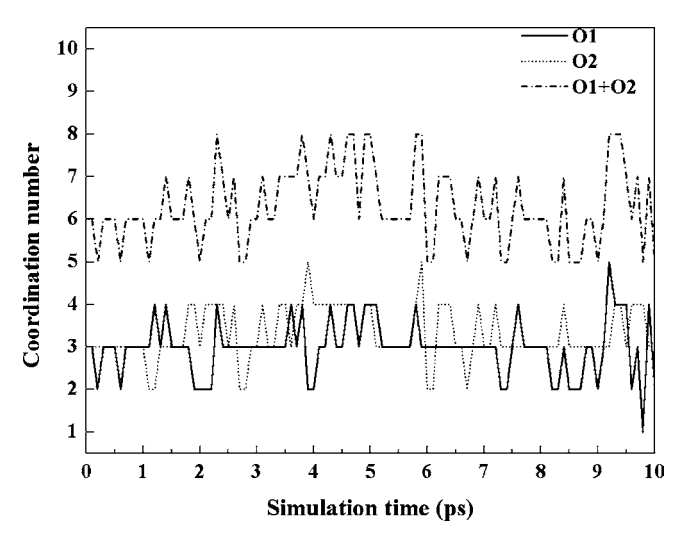


Figure 7. Time dependence of the number of first-shell waters at CH₃COO⁻ oxygen atoms, selecting only the first 10 ps of the HF/MM simulation.

ized from the O_o-O_w and O_o-H_w RDFs, as given in Figure 3a,b, respectively. To better illustrate the behavior of CH₃COO⁻—water hydrogen bonds, we utilized the corresponding atom-atom RDFs for pure water obtained at similar QM/ MM level of accuracy⁴² for comparison, as shown in Figure 4. In the HF/MM simulation, the first O_o-O_w peak is exhibited at 2.74 Å, and integration up to the corresponding first $O_0 - O_w$ minimum yields an average coordination number of 3.0 ± 0.1 . The position of the O_o-O_w peak obtained by the HF/MM simulation is in good agreement with the X-ray study, which reported the O_o-O_w distance to be 2.78 Å.⁴³ In the B3LYP/ MM simulation, the first O_o-O_w peak is observed at a shorter distance of 2.66 Å, with a lower coordination number of 2.9 \pm

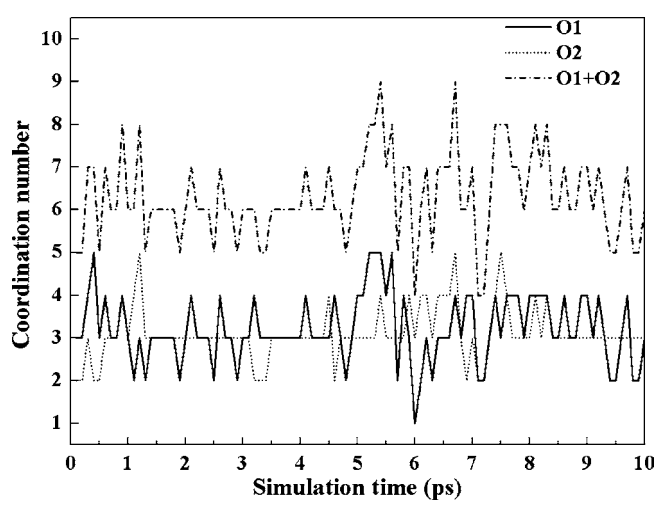


Figure 8. Time dependence of the number of first-shell waters at CH₃COO⁻ oxygen atoms, selecting only the first 10 ps of the B3LYP/MM simulation.

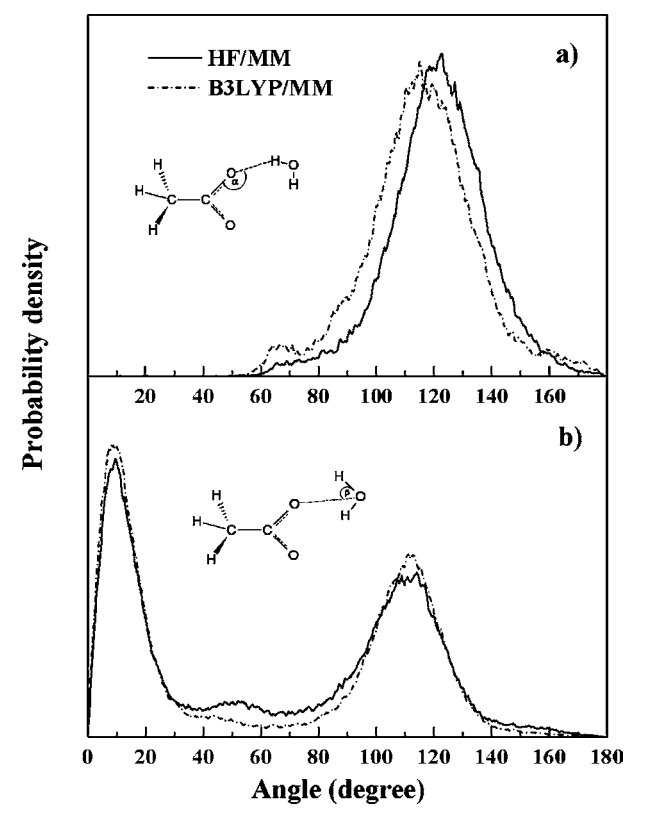


Figure 9. Distributions of (a) $C_o - O_o \cdots H_w$ and (b) $O_o \cdots O_w - H_w$ angles calculated within first peak of the $O_o - O_w$ RDFs.

0.1. Supposing that the "shells" for the two CH_3COO^- oxygens are not overlapping, it can be concluded that the maximum numbers of water molecules in the first hydration sphere near the $-COO^-$ group are about 6.0 (HF/MM) and 5.8 (B3LYP/MM), respectively. These data are in good accord with Kuntz's NMR results. In both HF/MM and B3LYP/MM simulations, the second peaks in the $O_o^-O_w$ RDFs are broad and less pronounced, which correspond to the contributions of both bulk waters and water molecules in the first hydration layer of another CH_3COO^- oxygen atom.

For O_o-H_w RDFs, the HF/MM and B3LYP/MM simulations reveal first O_o-H_w peaks with maxima at 1.78 and 1.67 Å, respectively. The position of the O_o-H_w RDFs is \sim 1 Å inward from the O_o-O_w peaks, demonstrating hydrogen-bond donation

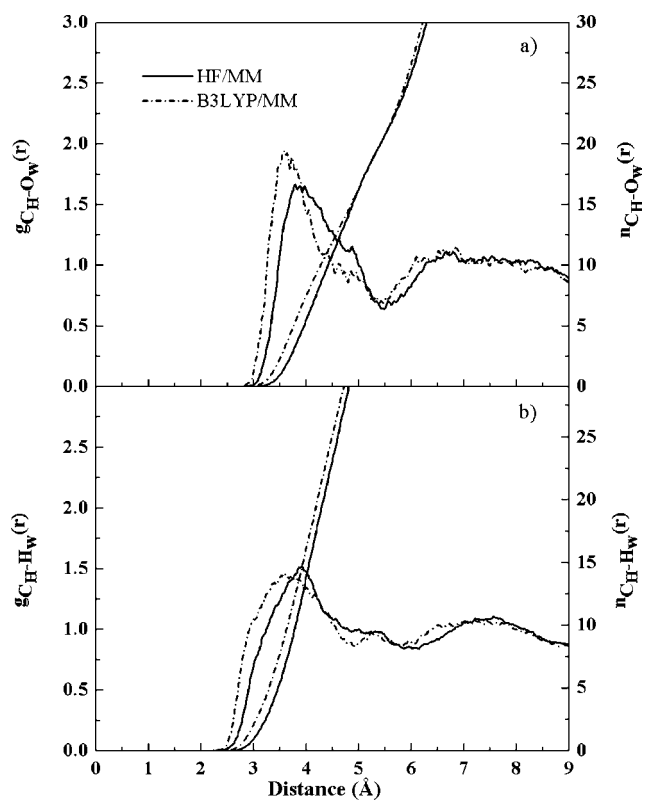


Figure 10. (a) $C_H - O_w$ and (b) $C_H - H_w$ RDFs and their corresponding integration numbers.

by the nearest-neighbor water molecules. Integrations up to the corresponding first Oo-Hw minima give average hydrogen atom numbers of 2.9 \pm 0.1 and 2.7 \pm 0.1, respectively. With regard to both HF/MM and B3LYP/MM results, the observed numbers of water oxygen and hydrogen atoms clearly demonstrate that the first-shell waters are linearly hydrogen bonded to each of the CH₃COO⁻ oxygens. In comparison with the first peak of the pure water O_w-H_w RDF (cf. Figure 4b), in terms of shape and peak height, it is obvious that the $O_0 \cdots H_w - O_w$ hydrogen bond interactions are relatively strong. In the HF/MM and B3LYP/MM simulations, the closest O₀···H_w distances are 1.35 and 1.13 Å, respectively, compared with the shortest O_w···H_w distance of 1.45 Å for bulk water. The second peak in the O₀-H_w RDFs around 3.2 Å can be assigned to the hydrogen atoms of first-shell waters that are not hydrogen-bonded with the CH₃COO⁻ oxygen atoms. Figure 5 shows the comparison of Oo-Hw RDFs for aqueous CH3COO- and HCOO-26 solutions, as obtained from similar HF/MM and B3LYP/MM simulations. Comparing both HF/MM and B3LYP/MM results, the strength of CH₃COO⁻-water hydrogen bonds appears slightly higher than that in the aqueous HCOO⁻ system. This phenomenon could be ascribed to the electronic effect of the -CH₃ group that acts as the electron-donating group, which release electrons into the -COO⁻ group when CH₃COO⁻ oxygen atoms form hydrogen bonds with their first-shell water molecules.

The distributions of oxygen and hydrogen atoms of first-shell waters, calculated with respect to the first minima of the O_o-O_w and O_o-H_w RDFs, are depicted in Figure 6a,b, respectively. Both HF/MM and B3LYP/MM simulations clearly show that the most frequent number of water molecules per CH_3COO^- oxygen atom is 3, followed by 4 and 2 (for water oxygens) and by 2 and 4 (for water hydrogens) in decreasing amounts. As compared with the corresponding data for aqueous $HCOO^-$

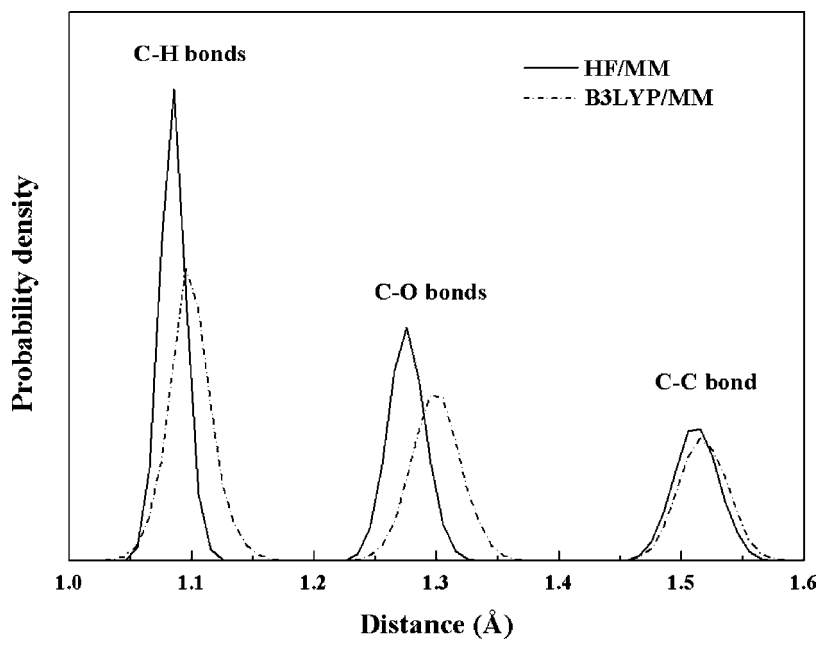


Figure 11. Distributions of C-H, C-O, and C-C bond lengths of CH₃COO⁻.

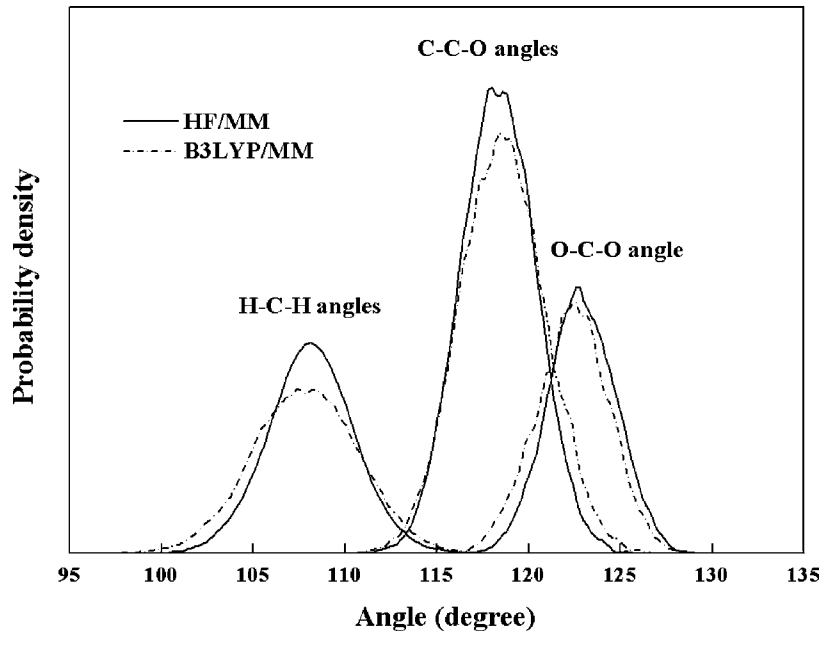


Figure 12. Distributions of H-C-H, C-C-O, and O-C-O angles of CH₃COO⁻.

system,26 the present study clearly confirms the expectation that the steric hindrance arising from the -CH₃ group of CH₃COO⁻ should result in a lower coordination number at the -COOgroup. Figures 7 and 8 show examples of time dependences of the hydration number at each of the CH₃COO⁻ oxygens occurring within the first 10 ps of the HF/MM and B3LYP/ MM simulations, respectively. From the analysis of the HF/ MM and B3LYP/MM trajectories, it is found that the two CH₃COO⁻ oxygen atoms simultaneously form asymmetric solvation shells, that is, each of them hydrogen bond to different numbers of water molecules. Consequently, this causes numerous possible species of the CH₃COO⁻-water complexes to exist in aqueous solution. As can be seen from Figures 7 and 8, the total numbers of water molecules in the vicinity of CH₃COO⁻ oxygens show large fluctuations, ranging from 5 to 8 and from 4 to 9 for the HF/MM and B3LYP/MM simulations, respectively.

More detailed interpretation of the CH₃COO⁻—water hydrogen bonds can be seen from the probability distributions of the $C_o - O_o \cdots H_w$ and $O_o \cdots O_w - H_w$ angles, calculated up to the first minimum of the O₀-O_w RDFs, as shown in Figure 9a,b, respectively. In cases where solvent effects cause strong charge localization at CH₃COO⁻, an asymmetrical charge distribution at the two CH₃COO⁻ oxygens, that is, a formation of C_o-O_o single and double bonds, could exist in aqueous solution. With regard to this point, one could expect the arrangement of directional C_o-O_o···H_w hydrogen bonds that causes the Co-Oo···Hw angle to peak at 109.5 and 120°. According to both HF/MM and B3LYP/MM simulations, the observed broad C_o-O_o····H_w angular distributions (Figure 9a) suggest that the -COO- group would preferentially adopt the "resonance structure" in aqueous solution, which may be stabilized because of fluctuations in the solvent environments. Figure 9b shows the distributions of the Oo ··· Ow - Hw angle, which clarify the preference for linear $O_o \cdots H_w - O_w$ arrangements.

To investigate the solvation structure around the hydrophobic site of acetate, the C_H-O_w and C_H-H_w RDFs and their

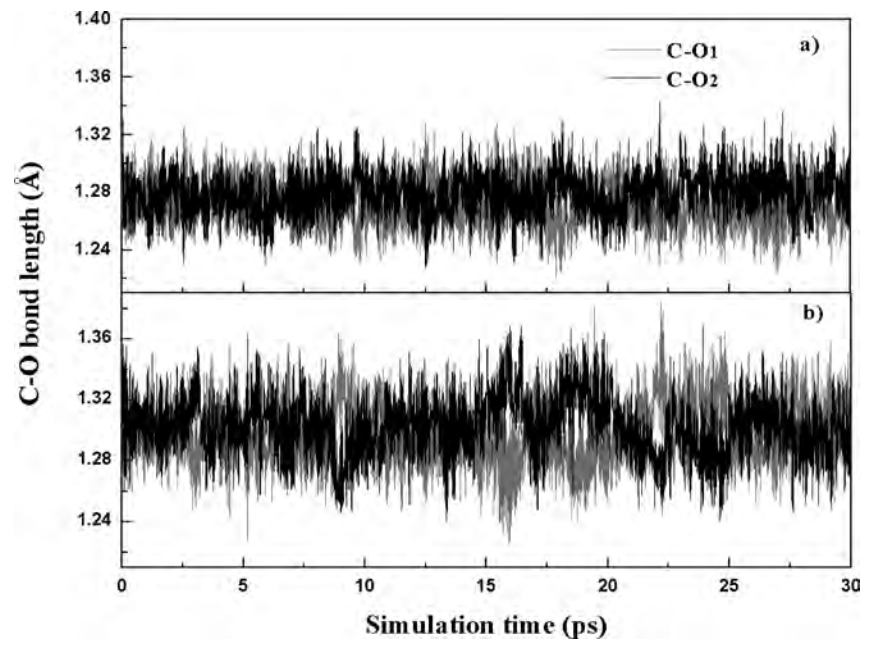


Figure 13. Time dependence of the C-O bond lengths of CH₃COO⁻, as obtained from first 30 ps of (a) HF/MM and (b) B3LYP/MM simulations, respectively.

corresponding integration numbers, as obtained from the HF/ MM and B3LYP/MM simulations, have been plotted in Figure 10a,b, respectively. As in this work, the center of the QM-treated region (with the radius of 4.2 Å) was set with respect to the position of C_o, water molecules surrounding the -CH₃ group are located beyond the QM sphere, and the interactions between the -CH₃ group and its surrounding waters are fully described by means of pair potentials and should be fairly accurate as well. According to the HF/MM results, the observed broad and less pronounced C_H-O_w and C_H-H_w peaks compared with the C_o-O_w and C_o-H_w RDFs for the -COO⁻ group clearly indicate no binding effects of the -CH₃ group on its surrounding waters but rather a repulsive interaction keeping the solvent at a larger distance. In this respect, water molecules in this region would prefer to form water—water hydrogen bonds rather than to form hydrogen bonds with the -CH₃ group. In the B3LYP/MM simulation, however, the solvent around the -CH3 group becomes more structured compared with the HF/MM results. This can be ascribed to the overestimation of the solute—solvent interactions by the B3LYP method. The observed weak interactions between the -CH₃ group and waters are in good accord with the recent ND measurements of aqueous 8 mol % CH₃COONa solution in D₂O,⁹ which reported the weak hydration nature of the $-CH_3$ group.

3.2. Dynamical Details. 3.2.1. Intramolecular Geometry of CH₃COO⁻. In both HF/MM and B3LYP/MM simulations, it is observed that the instantaneous environments of the two CH₃COO⁻ oxygens are somewhat different because of fluctuations in their respective solvation shells. The geometrical arrangement of CH₃COO⁻ in aqueous solution is explained in terms of the distributions of bond lengths and bond angles, as shown in Figures 11 and 12, respectively. In comparison with the gas-phase CH₃COO⁻ structure, both HF/MM and B3LYP/ MM simulations clearly indicate a substantial change in the local structure of CH₃COO⁻ according to the influence of water environment, in particular, an elongation of the C-O bond and a decrease in C-H bond length and O-C-O angle. With regard to the change in internal C-O bond, time dependence of the C-O bond lengths, as obtained from the HF/MM and B3LYP/ MM simulations, is shown in Figure 13. Compared with the HF/MM results, the B3LYP/MM simulation shows relatively larger variation of the C–O bond length. This supplies information that an arrangement of C_o – O_o single and double bonds could possibly be formed along with the CH₃COO⁻–water hydrogen-bond formation. In conjunction with the detailed analysis of the structural parameters and Mulliken charges of some selected B3LYP/MM CH₃COO⁻–water complexes, as shown in Figure 14, it is likely that the "resonance structure" of the –COO⁻ group can frequently convert to C_o – O_o single and double bonds. In the HF/MM simulation, however, this phenomenon is less observed. The difference could be ascribed to either the lack of electron correlation in the HF scheme or to the overestimation of ion–water hydrogen bond interactions by the B3LYP method.

3.2.2. Exchange Process of Water Molecules at CH₃COO⁻ Oxygens. According to Figure 3, the nonzero first minimum of the $O_o\!-\!O_w$ and $O_o\!-\!H_w$ RDFs obtained by both HF/MM and B3LYP/MM simulations clearly suggests an easy exchange of water molecules between the first hydration shell and the bulk. The exchange processes of first-shell waters at each of the CH₃COO⁻ oxygen atoms can be visualized through the plots of the Oo-Ow distances against the simulation time, as shown in Figures 15 and 16 for the HF/MM and B3LYP/MM simulations, respectively. During the first 10 ps of HF/MM and B3LYP/MM trajectories, numerous water molecules were exchanged between the first shell and the bulk, showing large fluctuations in the hydration number at each of the CH₃COO⁻ oxygen atoms (e.g., see insertions in Figures 15 and 16). Of particular interest, water molecules in the first hydration shell are either loosely or tightly bound to CH₃COO⁻ oxygen; that is, some first-shell waters transiently form a hydrogen bond with COO oxygen (and then leaving or even entering again) and some form weaker hydrogen bonds within the shell. With regard to both HF/MM and B3LYP/MM simulations, the arrangement of bifurcated hydrogen bonds (cf. Figure 1a) is rarely found in aqueous solution. The first-shell water molecules preferentially associate with one CH₃COO⁻ oxygen atom or the other rather than adopting a bifurcated arrangement.

The rates of water exchange processes at each of oxygen and hydrogen atoms of CH₃COO⁻ were evaluated through mean

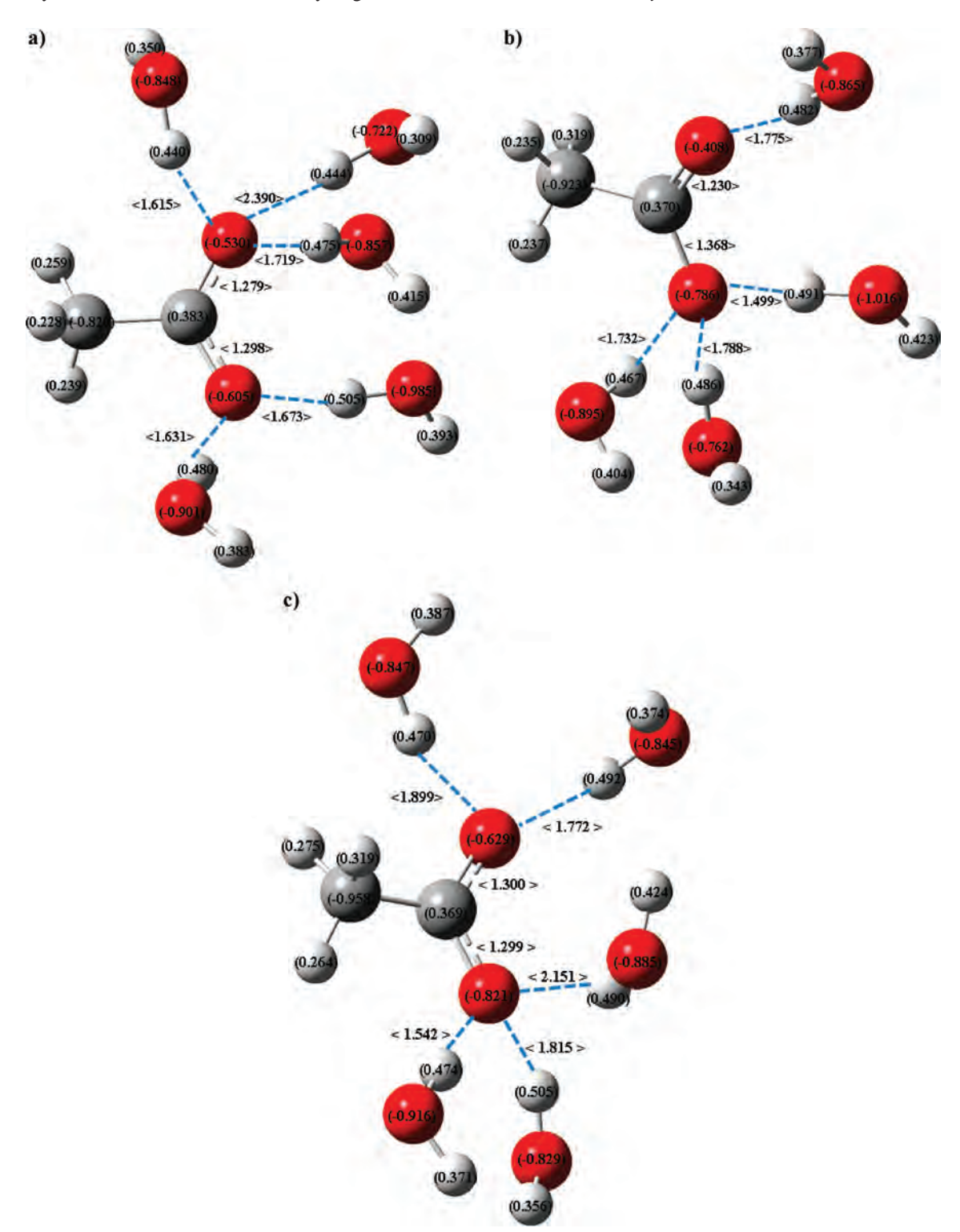


Figure 14. C-O bond lengths, $O_0 \cdots H_w$ distances, and atomic charges on the CH₃COO⁻-water complexes, as obtained at (a) 15.48, (b) 15.96, and (c) 16.54 ps of the B3LYP/MM simulation.

residence times (MRTs) of the surrounding water molecules. In this work, the MRT data were calculated using the direct method,⁴⁴ which is the product of the average number of nearestneighbor water molecules located within the first minimum of the O_o-O_w and H_H-O_w RDFs during the simulation divided by the number of exchange events. With respect to time parameters t^* (i.e., the minimum duration of a ligand's displacement from its original coordination shell to be accounted) of 0.0 and 0.5 ps, the calculated MRT values are summarized in Table 3. In general, the MRT data obtained using $t^* = 0.0 \text{ ps}$ are used for an estimation of hydrogen bond lifetimes, whereas the data obtained with $t^* = 0.5$ ps are considered to be a good estimate for sustainable ligand exchange processes.⁴⁴ In both HF/MM and B3LYP/MM simulations, the calculated MRT values with respect to $t^* = 0.0$ and 0.5 ps at each of the CH₃COO⁻ oxygens are relatively larger than those of HCOO⁻ oxygens²⁶ and of pure water.⁴² These data correspond to the observed stronger hydrogen bonds between CH₃COO⁻ oxygens and their first-shell water molecules when compared with those of HCOO-water and water-water hydrogen bonds. In the

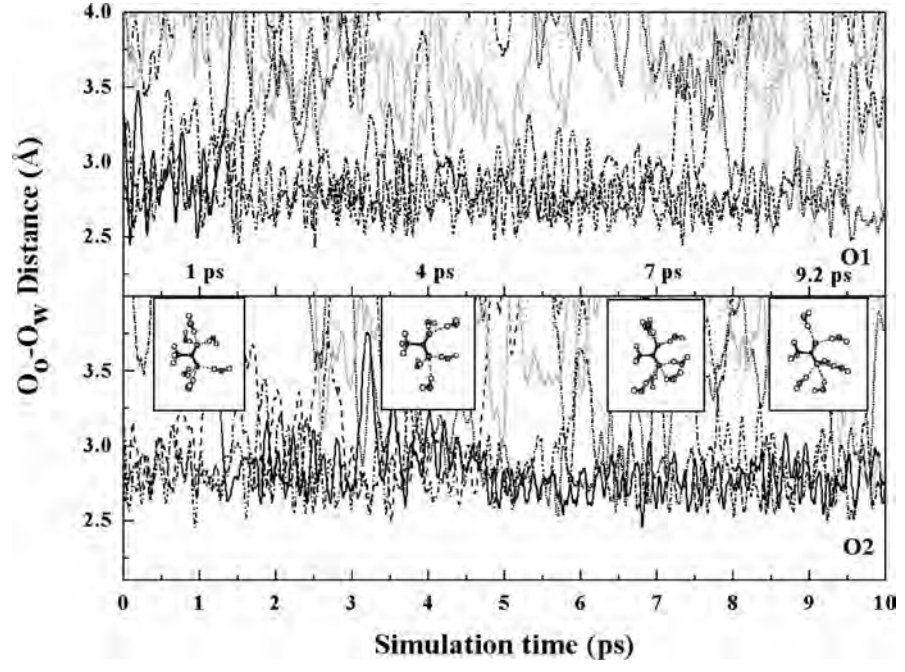


Figure 15. Time dependence of $O_0 \cdots O_w$ distances, selecting the first 10 ps of the HF/MM trajectory.

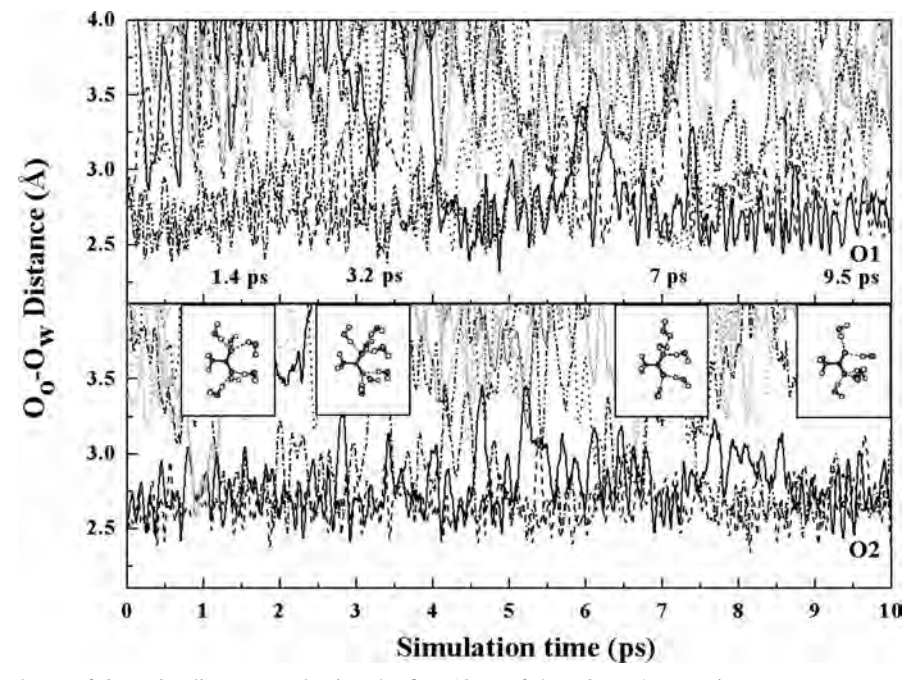


Figure 16. Time dependence of $O_o \cdots O_w$ distances, selecting the first 10 ps of the B3LYP/MM trajectory.

B3LYP/MM simulation, the observed slower exchange rate at each of CH₃COO⁻ oxygens, that is, compared with the HF/MM results, could be attributed to the overestimation of CH₃COO⁻—water hydrogen bond interactions, as the recent B3LYP/MM simulation for pure water³² has predicted a too-slow exchange rate compared with the experimental values.⁴⁵ The failure of the B3LYP method to predict the dynamics properties of pure water³² could be considered to be an example indicating the inadequacy of the DFT methods to describe correctly the characteristics of such aqueous hydrogen-bond systems.

In contrast with the observed strong hydrogen bonds between −COO⁻ group and waters, the calculated MRT values at each of hydrogen atoms of CH₃COO⁻ (Table 3) clearly reveal that the interactions between hydrogen atoms of −CH₃ group and

their nearest-neighbor water molecules are relatively weak, that is, compared with the MRT values of pure water. In this respect, it could be demonstrated that water molecules in this region preferentially form water—water hydrogen bonds rather than form hydrogen bonds with the $-CH_3$ group.

4. Conclusions

The HF/MM and B3LYP/MM MD simulations have been performed to obtain detailed knowledge of CH₃COO⁻—water hydrogen bonds in dilute aqueous solution. On the basis of both HF and B3LYP simulations, it can be concluded that the hydrogen bonds between CH₃COO⁻ oxygens and first-shell waters are relatively strong compared with the water—water hydrogen bonds in the bulk. The structure of CH₃COO⁻ is found

TABLE 3: Mean Residence Time of Water Molecules in the Bulk and in the Vicinity of Oxygen and Hydrogen Atoms of CH_3COO^- Calculated within the First Peak of the O_o-O_w and H_H-O_w RDFs, respectively

11 11	/	I	- 0			
			$t^* = 0$	0.0 ps	$t^* =$	0.5 ps
atom/solute	CN	$t_{\rm sim}$	$N_{ m ex}^{0.0}$	$ au_{ m H_2O}^{0.0}$	$N_{\rm ex}^{0.5}$	$ au_{ m H_{2}o}^{0.5}$
		HF/N	MM MD			
CH ₃ COO ⁻						
01	3.01	65.0	633	0.31	76	2.57
O2	3.02	65.0	530	0.37	75	2.62
H1	4.80	65.0	3172	0.10	203	1.54
H2	4.82	65.0	3184	0.10	215	1.46
H3	4.95	65.0	3301	0.10	213	1.51
$HCOO^{-26}$						
O1	3.45	70.0	970	0.25	132	1.83
O2	3.44	70.0	1042	0.23	112	2.15
pure H_2O^{42}	4.60	12.0	292	0.20	31	1.80
pure H_2O^{32}	4.20	40.0		0.33		1.51
		B3LYI	P/MM MI)		
$\mathrm{CH_{3}COO^{-}}$						
O1	2.93	55.0	644	0.25	54	2.98
O2	2.90	55.0	590	0.27	49	3.25
H1	4.27	55.0	2745	0.09	162	1.45
H2	4.26	55.0	2578	0.09	149	1.57
H3	4.29	55.0	2733	0.09	169	1.40
$HCOO^{-26}$						
O1	2.84	50.0	810	0.17	57	2.49
O2	2.97	50.0	799	0.19	63	2.36
pure H ₂ O ³²	4.20	30.0		1.07		7.84

to be rather flexible according to the influence of solvent environment. In addition, the first-shell water molecules are observed to be either "loosely" or "tightly" bound to each of CH₃COO⁻ oxygen atoms, forming asymmetric solvation shells with different number of hydrogen bonds, with the prevalent value of three. As compared with the HF/MM results, however, the B3LYP/MM simulation seems to predict slightly stronger CH₃COO⁻—water hydrogen bonds. With regard to the reported failure of the B3LYP method in describing the dynamics details of pure water, the observed stronger CH₃COO⁻—water hydrogen bonds in the B3LYP/MM simulation can be attributed to an inadequacy of the B3LYP method rather than the neglect of electron correlations in the HF scheme. In this respect, further improvement of the QM/MM results can be achieved by extending the OM size and basis set, in conjunction with the use of more sophisticated ab initio correlated methods, such as MP2, which are presently still beyond computational feasibility for such simulations.

Acknowledgment. This work was supported by the Thailand Research Fund (TRF). A.T. also acknowledges support from the Synchrotron Light Research Institute (SLRI) and Suranaree University of Technology (SUT). B.M.R. acknowledges support from the Austrian Science Foundation (FWF).

References and Notes

- (1) Frank, H. Chemical Physics of Ionic Solutions; John Wiley & Sons: New York, 1956.
- (2) Williams, R. J. P. *Bio-Inorganic Chemistry*; American Chemical Society: Washington, DC, 1971.
 - (3) Cowan, J. A. Chem. Rev. 1998, 98, 1067.
- (4) Shah, D. O. In *Micelles, Microemulsions, and Monolayers: Quarter Century Progress at the University of Florida*; Shad, D. O., Ed.; Marcel Dekker: New York, 1998; pp 1–52.
- (5) Ulman, A. Introduction to Ultrathin Films: from Langmuir–Blodgett Films to Self-Assembly; Academic Press: Boston, MA, 1991.
 - (6) Kuntz, I. D. J. Am. Chem. Soc. 1971, 93, 514.

- (7) Caminiti, R.; Cucca, P.; Monduzzi, M.; Saba, G.; Crisponi, G. *J. Chem. Phys.* **1984**, *81*, 543.
- (8) Naganuma, H.; Kameda, Y.; Usuki, T.; Uemura, O. J. Phys. Soc. Jpn. 2001, 70, 356.
- (9) Kameda, Y.; Sasaki, M.; Yaegashi, M.; Tsuji, K.; Oomori, S.; Hino, S.; Usuki, T. J. Solution Chem. 2004, 33, 733.
 - (10) Jorgensen, W. L.; Gao, J. J. Phys. Chem. 1986, 90, 2174.
- (11) Alagona, G.; Ghio, C.; Kollman, P. J. Am. Chem. Soc. 1986, 108, 185.
 - (12) Meng, E. C.; Kollman, P. J. Phys. Chem. 1996, 100, 11460.
 - (13) Warshel, A.; Levitt, M. J. Mol. Biol. 1976, 103, 227.
 - (14) Singh, U. C.; Kollman, P. A. J. Comput. Chem. 1986, 7, 718.
- (15) Field, M. J.; Bash, P. A.; Karplus, M. J. Comput. Chem. 1990, 11, 700.
 - (16) Gao, J. Rev. Comput. Chem. 1996, 7, 119.
- (17) Kerdcharoen, T.; Liedl, K. R.; Rode, B. M. Chem. Phys. 1996, 211, 313.
- (18) Tongraar, A.; Liedl, K. R.; Rode, B. M. J. Phys. Chem. A 1998, 102, 10340.
 - (19) Tongraar, A.; Rode, B. M. Phys. Chem. Chem. Phys. 2003, 5, 357.
 - (20) Tongraar, A.; Rode, B. M. Chem. Phys. Lett. 2005, 403, 314.
 - (21) Tongraar, A.; Rode, B. M. Chem. Phys. Lett. **2005**, 405, 514.
- (22) Intharathep, P.; Tongraar, A.; Sagarik, K. J. Comput. Chem. 2005, 26, 1329.
- (23) Rode, B. M.; Schwenk, C. F.; Tongraar, A. J. Mol. Liq. 2004, 110, 105.
- (24) Rode, B. M.; Schwenk, C. F.; Hofer, T. S.; Randolf, B. R. *Coord. Chem. Rev.* **2005**, 249, 2993.
- (25) Tongraar, A.; Tangkawanwanit, P.; Rode, B. M. J. Phys. Chem. A 2006, 110, 12918.
- (26) Payaka, A.; Tongraar, A.; Rode, B. M. J. Phys. Chem. A 2009, 113, 3291.
- (27) Brooks, B. R.; Bruccoleri, R. E.; Olafson, B. D.; States, D. J.; Swaminathan, S.; Karplus, M. J. Comput. Chem. 1983, 4, 187.
- (28) Dunning, T. H., Jr.; Hay, P. J. In *Modern Theoretical Chemistry*; Plenum: New York, 1976; Vol. III.
 - (29) Dunning, T. H. J. Chem. Phys. 1989, 90, 1007.
- (30) Kendall, R. A.; Dunning, T. H.; Harrison, R. J. J. Chem. Phys. 1992, 96, 6769.
- (31) Woon, D. E.; Dunning, T. H. J. Chem. Phys. 1993, 98, 1358.
- (32) Xenides, D.; Randolf, B. R.; Rode, B. M. J. Chem. Phys. 2005, 122, 174506.
- (33) Tongraar, A.; Kerdcharoen, T.; Hannongbua, S. J. Phys. Chem. A **2006**, 110, 4924.
 - (34) Stillinger, F. H.; Rahman, A. J. Chem. Phys. 1976, 68, 666.
- (35) Bopp, P.; Jancsó, G.; Heinzinger, K. Chem. Phys. Lett. 1983, 98,
- (36) Frisch, M. J.; Trucks, G. W.; Schlegel, H. B.; Scuseria, G. E.; Robb, M. A.; Cheeseman, J. R.; Montgomery, J. A., Jr.; Vreven, T.; Kudin, K. N.; Burant, J. C.; Millam, J. M.; Iyengar, S. S.; Tomasi, J.; Barone, V.; Mennucci, B.; Cossi, M.; Scalmani, G.; Rega, N.; Peterson, G. A.; Nakatsuji, H.; Hada, M.; Ehara, M.; Toyota, K.; Fukuda, R.; Hasegawa, J.; Ishida, M.; Nakajima, T.; Honda, Y.; Kitao, O.; Nakai, H.; Klene, M.; Li, X.; Knox, J. E.; Hratchian, H. P.; Cross, J. B.; Bakken, V.; Adamo, C.; Jaramillo, J.; Gomperts, R.; Stratmann, R. E.; Yazyev, O.; Austin, A. J.; Cammi, R.; Pomelli, C.; Ochterski, J. W.; Ayala, P. Y.; Morokuma, K.; Voth, G. A. D.; Strain, M. C.; Farkas, O.; Malick, D. K.; Rabuck, A. D.; Raghavachari, K.; Foresman, J. B.; Ortiz, J. V.; Cui, Q.; Baboul, A. G.; Clifford, S.; Cioslowski, J.; Stefanov, B. B.; Liu, G.; Liashenko, A.; Piskorz, P.; Komaromi, I.; Martin, R. L.; Fox, D. J.; Keith, T.; Al-Laham, M. A.; Peng, C. Y.; Nanayakkara, A.; Challacombe, M.; Gill, P. M. W.; Johnson, B.; Chen, W.; Wong, M. W.; Gonzalez, C.; Pople, J. A. *GAUSSIAN 03*, revision D.1; Gaussian, Inc.: Wallingford, CT, 2005.
 - (37) Carpenter, J. E.; Weinhold, F. THEOCHEM 1988, 169, 41.
- (38) Reed, A. E.; Weinstock, R. B.; Weinhold, F. J. Chem. Phys. 1985, 83, 735.
- (39) Reed, A. E.; Curtiss, L. A.; Weinhold, F. Chem. Rev. 1988, 88, 899.
- (40) Berendsen, H. J. C.; Postma, J. P. M.; van Gunsteren, W. F.; DiNola, A.; Haak, J. R. *J. Phys. Chem.* **1984**, *81*, 3684.
 - (41) Adams, D. J.; Adams, E. H.; Hills, G. J. Mol. Phys. 1979, 38, 387.
 - (42) Tongraar, A.; Rode, B. M. Chem. Phys. Lett. 2004, 385, 378.
- (43) Naganuma, H.; Kameda, Y.; Usuki, T.; Uemura, O. J. Phys. Soc. Jpn. 2001, 70, 356.
- (44) Hofer, T. S.; Tran, H. T.; Schwenk, C. F.; Rode, B. M. J. Comput. Chem. 2004, 25, 211.
- (45) Lock, A. J.; Wouterson, S.; Bakker, H. J. Femtochemistry and Femtobiology; World Scientific: Singapore, 2001.

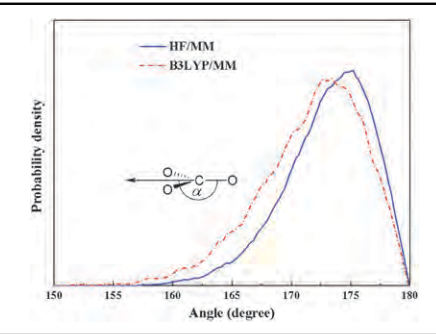
JP105671F

1. สำเนา Reprint ของงานวิจัยเรื่องที่ 4

Anan Tongraar, Pathumwadee Yotmanee and Apirak Payaka, "Characteristics of CO₃²-water hydrogen bonds in aqueous solution: Insights from HF/MM and B3LYP/MM MD simulations" *Phys. Chem. Chem. Phys.* **2011**, In press, DOI: 10.1039/C1CP21802F.

Physical Chemistry Chemical Physics

c1cp21802f



Characteristics of CO₃²-water hydrogen bonds in aqueous solution: insights from HF/MM and B3LYP/MM MD simulations

Anan Tongraar,* Pathumwadee Yotmanee and Apirak Payaka

Distributions of α , as defined by a vector along one C–O bond and a vector pointing outwards between the other two C–O bonds.

Please check this proof carefully. **Our staff will not read it in detail after you have returned it.** Translation errors between word-processor files and typesetting systems can occur so the whole proof needs to be read. Please pay particular attention to: tabulated material; equations; numerical data; figures and graphics; and references. If you have not already indicated the corresponding author(s) please mark their name(s) with an asterisk. Please e-mail a list of corrections or the PDF with electronic notes attached – do not change the text within the PDF file or send a revised manuscript.

Please bear in mind that minor layout improvements, e.g. in line breaking, table widths and graphic placement, are routinely applied to the final version.

Please note that, in the typefaces we use, an italic vee looks like this: ν , and a Greek nu looks like this: ν .

We will publish articles on the web as soon as possible after receiving your corrections; no late corrections will be made.

Please return your final corrections, where possible within 48 hours of receipt, by e-mail to: pccp@rsc.org.

Reprints—Electronic (PDF) reprints will be provided free of charge to the corresponding author. Enquiries about purchasing paper reprints should be addressed via: http://www.rsc.org/publishing/journals/guidelines/paperreprints/. Costs for reprints are below:

Reprint costs		
No of pages	Cost (pe	er 50 copies)
	First	Each additional
2-4 5-8 9-20 21-40 >40	£225 £350 £675 £1250 £1850	£125 £240 £550 £975 £1550
Cost for including cover of £55 per 50 copies		2.000

Queries are marked on your proof like this Q1, Q2, etc. and for your convenience line numbers are indicated like this 5, 10, 15, ...

Query reference	Query	Remarks
Q1	For your information: You can cite this article before you receive notification of the page numbers by using the following format: (authors), Phys. Chem. Chem. Phys., (year), DOI: 10.1039/c1cp21802f.	
Q2	In the caption to Table 1 should 'HF, B3LYP, MP2 and CCSD methods' be changed to 'HF, B3LYP, MP2 and CCSD levels'?	



10

15

20

25

30

55

Cite this: DOI: 10.1039/c1cp21802f

www.rsc.org/pccp PAPER

Characteristics of ${\rm CO_3}^{2-}$ -water hydrogen bonds in aqueous solution: insights from HF/MM and B3LYP/MM MD simulations

Anan Tongraar,* Pathumwadee Yotmanee and Apirak Payaka

Received 3rd June 2011, Accepted 3rd August 2011 DOI: 10.1039/c1cp21802f

Two combined quantum mechanics/molecular mechanics (QM/MM) molecular dynamics simulations, namely HF/MM and B3LYP/MM, have been performed to investigate the local hydration structure and dynamics of carbonate (CO₃²⁻) in dilute aqueous solution. With respect to the QM/MM scheme, the QM region, which contains the CO₃²⁻ and its surrounding water molecules, was treated at HF and B3LYP levels of accuracy, respectively, using the DZV+ basis set, while the rest of the system is described by classical MM potentials. For both the HF/MM and B3LYP/MM simulations, it is observed that the hydrogen bonds between CO₃²⁻ oxygens and their nearest-neighbor waters are relatively strong, *i.e.*, compared to water–water hydrogen bonds in the bulk, and that the first shell of each CO₃²⁻ oxygen atom somewhat overlaps with the others, which allows migration of water molecules among the coordinating sites to exist. In addition, it is observed that first-shell waters are either "loosely" or "tightly" bound to the respective CO₃²⁻ oxygen atoms, leading to large fluctuations in the number of first-shell waters, ranging from 1 to 6 (HF/MM) and 2 to 7 (B3LYP/MM), with the prevalent value of 3. Upon comparing the HF and B3LYP methods in describing this hydrated ion, the latter is found to

overestimate the hydrogen-bond strength in the ${\rm CO_3}^{2-}$ -water complexes, resulting in a slightly

1. Introduction

35 Detailed knowledge of ions solvated in aqueous electrolyte solution has long been a topic of special interest for scientists in order to understand the role and reactivity of these ions in chemical and biological processes. 1-3 Consequently, several experimental and theoretical techniques have been employed to elucidate such details. In experiments, the most powerful techniques from the structure viewpoint are neutron and X-ray diffractions because they offer a direct probe of the ionic structure, 4-9 while other techniques such as Nuclear Magnetic Resonance (NMR), Infrared (IR) and Ultraviolet (UV) spectroscopy can provide dynamical details about the ions in solution. 10 With regard to recent advances in timeresolved spectroscopic techniques, X-ray absorption spectroscopy (XAS) is a powerful tool for an accurate determination of the ion hydration structure, because it is element-specific. This technique has been successfully used to probe the local structure of several specific systems. 11,12

more compact hydration structure at each of the CO₃²⁻ oxygens.

In conjunction with experiments, the results obtained by Monte Carlo (MC) and molecular dynamics (MD) simulations can provide detailed interpretation and prediction of

experimental observations, in particular at the molecular level. With regard to early MC and MD simulations, however, the classical potentials based on molecular mechanical (MM) force fields are usually employed. 13-16 These potentials are mostly constructed with respect to a set of experimental data or to ab initio energy surface calculations. In this sense, the reliability of the potentials is, therefore, one of the crucial factors when we discuss the quality and accuracy of the simulation results. 17,18 To obtain more reliable simulation data, a more sophisticated simulation technique is to apply a well-known combined quantum mechanical and molecular mechanical (QM/MM) method. 19-22 For the treatment of aqueous ionic solutions, the most interesting part of the system, i.e., the sphere which includes the ion and its surrounding water molecules, is treated at an appropriate level of quantum mechanics, while the rest of the system is described by classical MM potentials. Using this scheme, the complicated many-body interactions and ion polarizability can be reliably included within the defined QM region, i.e., at least within the hydration sphere of the ions. This QM/MM technique has been proven to be an elegant simulation approach, which can provide many new insights into the structure and dynamics of various solvated ions. 23-32

In the present study, the characteristics of carbonate (CO_3^{2-}) solvated in aqueous electrolyte solution was our interest. This carbonate species is ubiquitous in the natural environment, especially in seawater,³³ and can react with many

School of Chemistry, Institute of Science, Suranaree University of Technology, Nakhon Ratchasima 30000, Thailand. E-mail: anan_tongraar@yahoo.com; Fax: +66-44-224750

This journal is © the Owner Societies 2011

Phys. Chem. Chem. Phys., 2011, ■■, 1-10 | 1

metals to form various aqueous and solid state complexes.³⁴ In seawater, the amount of ${\rm CO_3}^{2-}$ is related to the atmospheric CO_2 . In this respect, a detailed knowledge of CO_3^{2-} in aqueous solution is essential in order to understand the role 5 of CO₂ in the global carbon cycle. Recently, Car-Parrinello (CP) MD simulations have been performed for aqueous carbonate species, namely H₂CO₃, HCO₃⁻, CO₃²⁻ and CO₂, providing quantitative information with respect to hydrogenbond environments for these important species and their effects on the structure and dynamics of the surrounding water molecules.³⁵ In the case of electrolyte solutions, however, some limitations of the CP-MD technique come from the use of simple generalized gradient approximation (GGA) functionals such as BLYP and PBE and of the relatively small system size. 27,36 15 Recently, it has been shown that the use of simple density functionals in the CP-MD scheme results in poor structural and dynamical data even for the underlying liquid water. 37,38 In this work, two combined QM/MM MD simulations, namely HF/MM and B3LYP/MM, have been performed to investigate the local hydration structure and dynamics of the CO₃²-water hydrogen bonds in aqueous solution.

2. Methods

40

25 The QM/MM technique divides the systems into two parts, namely the QM and MM regions. The total interaction energy of the system is defined as:

$$E_{\text{total}} = \langle \Psi_{\text{QM}} | \hat{H} | \Psi_{\text{QM}} \rangle + E_{\text{MM}} + E_{\text{QM-MM}}, \qquad (1)$$

where $\langle \Psi_{\rm QM} | \hat{H} | \Psi_{\rm QM} \rangle$ refers to the interactions within the QM region, and $E_{\rm MM}$ and $E_{\rm QM-MM}$ represent the interactions within the MM and between the QM and MM regions, respectively. The QM region, the most interesting part which contains a central ${\rm CO_3}^{2-}$ and its nearest-neighbor water molecules, is treated quantum mechanically using the HF and B3LYP methods, while the rest of the system (i.e., the $E_{\rm MM}$ and $E_{\rm QM-MM}$) is described by classical pair potentials. Then, the total force of the system is described by the following formula:

$$F_{\text{tot}} = F_{\text{MM}}^{\text{sys}} + (F_{\text{OM}}^{\text{QM}} - F_{\text{MM}}^{\text{QM}}),$$
 (2)

where $F_{\rm MM}^{\rm sys}$, $F_{\rm QM}^{\rm QM}$ and $F_{\rm MM}^{\rm QM}$ are the MM force of the total system, the QM force in the QM region and the MM force in the QM region, respectively. In this respect, the $F_{\rm MM}^{\rm QM}$ term accounts for the coupling between the QM and MM regions.

During the QM/MM simulations, since the interchange of water molecules between the QM and MM regions can take place frequently, the forces acting on each particle in the system are switched according to which region the water molecule is entering or leaving and can be defined as:

$$F_i = S_m(r)F_{QM} + (1 - S_m(r))F_{MM},$$
 (3)

where F_{QM} and F_{MM} are the quantum mechanical and molecular mechanical forces, respectively. $S_m(r)$ is a smoothing function,³⁹

$$\begin{split} S_m(r) &= 1, & \text{for } r \leq r_1, \\ S_m(r) &= \frac{(r_0^2 - r^2)^2 (r_0^2 + 2r^2 - 3r_1^2)}{(r_0^2 - r_1^2)^3}, & \text{for } r_1 < r \leq r_0, \\ S_m(r) &= 0, & \text{for } r > r_0, \end{split} \tag{4}$$

where r_1 and r_0 are the distances characterizing the start and the end of the QM region, respectively, and applied within an interval of 0.2 Å (*i.e.*, between the C···O_w distances of 3.8–4.0 Å) to ensure a continuous change of forces at the transition between the QM and MM regions.

5

15

With respect to the QM/MM scheme, it is known that the quality of the simulation results depends crucially on the selection of the QM method, basis set and QM size. In several cases, all of these essential parameters must be optimized, compromising between the quality of the simulation results and the computational feasibility. Since the correlated QM calculations, even at the MP2 level of accuracy, are still too time-consuming, the HF and hybrid density functional B3LYP methods become the possible alternatives for the present study. The HF method has been well recommended in previous QM/MM studies, ^{23–32} even for the treatment of anions. 27,31,32 In recent QM/MM MD simulations of pure water, 40 it has been demonstrated that the HF method with a sufficiently large QM size could provide detailed information of liquid water in good accord with the MP2/MM simulation and with experimental data concerning the H-bond structure and lifetime. In contrast to the HF calculations, the B3LYP method proved inferior in several cases. 27,28,36 However, this method was employed in this work in order to test its validity for the description of CO₃²⁻ hydrate, as it has been shown that this level of calculation can provide reasonable results for some hydrated anions. 31,32 In this respect, it should be realized that while the HF scheme could produce an error due to the neglect of electron correlation effects, the DFT methods, although including such effects to a certain (uncontrollable) extent, are often found to overestimate the correlation energy.

Regarding the QM calculations, the use of a larger basis set is a key factor for obtaining better results. In practice, however, the computational expense for QM force calculations using large basis sets is significant. Thus, moderate basis sets have been employed in most of the previous QM/MM studies. 36,40,23-32 In this work, since a satisfactory description of anions requires diffuse basis functions, the DZV+ basis set⁴¹ was chosen for CO₃²⁻ and water. To preliminarily check the validity of the OM methods and the basis set employed for this particular system, geometry optimizations of the CO_3^{2-} – $(H_2O)_n$ complexes, where n = 0-3 (see Fig. 1), were carried out at HF, B3LYP, MP2 and CCSD levels of accuracy using DZV+ and $6-311++G(d,p)^{42}$ basis sets, and the results are summarized in Table 1. Using a moderate basis set, like DZV+, the HF calculation can provide the stabilization energy in good accord with the data obtained by the MP2 and CCSD methods using the 6-311++G(d,p) basis set, but with slightly longer hydrogenbond lengths. For the B3LYP calculation, while the hydrogenbond lengths show better agreement with the correlated methods, the interactions between the CO₃²⁻ and water are considerably overrated. Overall, according to the limit of our computational feasibility, the selection of the HF and B3LYP methods and the use of the DZV+ basis set are expected to be reliable enough to achieve a sufficient level of accuracy in the QM/MM simulations.

To define the size of the QM region, a preliminary HF/MM simulation, *i.e.*, the simulation in which only the ${\rm CO_3}^{2-}$ was treated quantum mechanically using the HF method while the

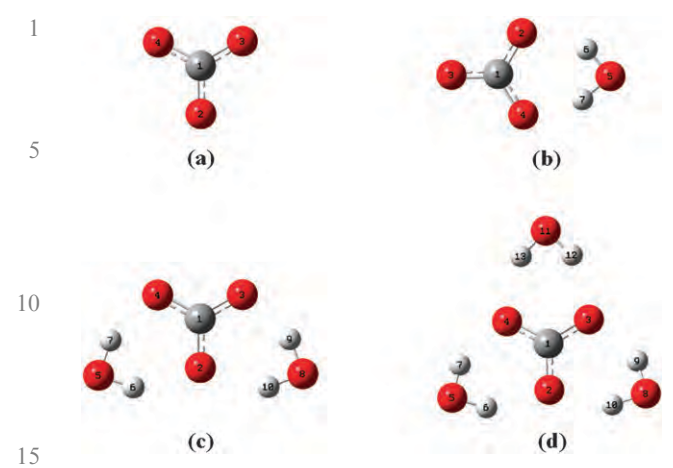


Fig. 1 Optimized structures of (a) CO_3^{2-} , (b) CO_3^{2-} – H_2O , (c) CO_3^{2-} – $(H_2O)_2$ and (d) CO_3^{2-} – $(H_2O)_3$ complexes.

rest of the system is described by classical pair potentials, 20 was performed (data not shown). According to the resulting C-O_w radial distribution function (RDF), the first minimum of the C-O_w peak is exhibited at around 4.4 Å, in which the integration up to the first minimum of the C-O_w peak yields

about 16–18 water molecules. This implies that a QM size with a diameter of 8.8 Å seemed to be desirable for the present study. However, the evaluation of QM forces for all particles within this QM size is still too time-consuming. In this study, therefore, a slightly smaller QM size with a diameter of 8.0 Å was chosen, which includes CO_3^{2-} and about 10–14 water molecules. This QM size is assumed to be large enough to include most many-body effects within the short-range ion-water interactions, that is, most of the interactions beyond the QM region could be reasonably described based on pairwise additive approximations. As can be seen in the next section (cf. Fig. 2a), the smooth shape of the C-O_w RDFs between 3.8–4.0 Å supports that there are no artifacts caused by the QM-MM boundary, and that the transition of molecules between the QM and MM regions occurs smoothly.

A flexible model, which describes intermolecular⁴³ and intramolecular⁴⁴ interactions, was employed for water. This flexible water model allows explicit hydrogen movements, thus ensuring a smooth transition, when water molecules move from the QM region with full flexibility to the MM region. The pair potential functions for describing the CO_3^{2-} – H_2O interactions were newly constructed using a fitting procedure similar to that employed for the construction of NO_3^- – H_2O

15

Table 1 Stabilization energies and some selected structural parameters of the optimized CO_3^{2-} – $(H_2O)_n$ complexes, where n = 0–3, calculated at HF, B3LYP, MP2 and CCSD methods using DZV+ and 6-311++G(d,p) (data in parentheses) basis sets

	Method	HF	B3LYP	MP2	CCSD	
	(a) CO ₃ ²⁻					
30	R_{1-2} , R_{1-3} , R_{1-4}/A	1.3158 (1.2823)	1.3432 (1.3077)	1.3642 (1.3100)	1.3572 (1.3042)	30
50	A ₂₋₁₋₃ , A ₂₋₁₋₄ , A ₃₋₁₋₄ /deg	120.00 (120.00)	120.00 (120.00)	120.00 (120.00)	120.00 (120.00)	50
	(b) $CO_3^{2-}-H_2O$					
	$\Delta E/\text{kcal mol}^{-1}$	-39.86 (-36.75)	-46.06 (-42.73)	-42.51 (-42.56)	-41.04 (-40.79)	
	R_{1-2}/\mathring{A}	1.3217 (1.2878)	1.3490 (1.3157)	1.3717 (1.3138)	1.3644 (1.3111)	
	R_{1-3}/\mathring{A}	1.2974 (1.2666)	1.3184 (1.2870)	1.3384 (1.2891)	1.3334 (1.2849)	
	R_{1-4}/\mathring{A}	1.3217 (1.2878)	1.3537 (1.3141)	1.3738 (1.3207)	1.3655 (1.3111)	
35	R_{2-6}/\mathring{A}	1.9150 (1.8990)	1.8425 (1.7601)	1.8962 (1.8454)	1.9124 (1.7932)	35
	R_{4-7}/\mathring{A}	1.9150 (1.8999)	1.7291 (1.8003)	1.8403 (1.6855)	1.8755 (1.7930)	
	A_{2-1-3}/deg	120.87 (120.66)	121.05 (120.60)	120.93 (121.06)	120.88 (120.70)	
	A_{2-1-4}/deg	118.27 (118.67)	118.27 (118.63)	118.32 (118.54)	118.33 (118.61)	
	A_{3-1-4}/deg	120.87 (120.67)	120.68 (120.77)	120.75 (120.40)	120.79 (120.70)	
	(c) CO_3^{2-} – $(H_2O)_2$					
40	$\Delta E/\text{kcal mol}^{-1}$	-76.92 (-70.27)	-86.57 (-79.67)	-81.28 (-79.41)	-78.88 (-76.79)	40
	R_{1-2}/\mathring{A}	1.3289 (1.2923)	1.3567 (1.3173)	1.3831 (1.3186)	1.3735 (1.3137)	
	R_{1-3}/\mathring{A}	1.3029 (1.2730)	1.3286 (1.2964)	1.3470 (1.2997)	1.3414 (1.2940)	
	R_{1-4}/\mathring{A}	1.3025 (1.2725)	1.3275 (1.2968)	1.3454 (1.2991)	1.3407 (1.2941)	
	R_{2-6}/\mathring{A}	1.8921 (1.9339)	1.8331 (1.8874)	1.8353 (1.8683)	1.8811 (1.8911)	
	R_{4-7}/\mathring{A}	2.0012 (1.9321)	1.8230 (1.7754)	1.9764 (1.7576)	1.9719 (1.7910)	
45	$R_{/2-10}/A$	1.9071 (1.9597)	1.8717 (1.8758)	1.8870 (1.8897)	1.9091 (1.8871)	45
43	R ₃₋₉ /Å	1.9810 (1.9100)	1.7876 (1.7840)	1.9200 (1.7417)	1.9464 (1.7937)	43
	A_{2-1-3}/deg	119.04 (119.35)	119.19 (119.56)	118.96 (119.50)	119.05 (119.49)	
	A_{2-1-4}/deg	119.08 (119.42)	119.30 (119.54)	119.08 (119.57)	119.11 (119.47)	
	A_{3-1-4}/\deg	121.88 (121.22)	121.51 (120.90)	121.95 (120.93)	121.84 (121.03)	
	(d) CO_3^{2-} – $(H_2O)_3$					
	$\Delta E/\text{kcal mol}^{-1}$	-111.35 (-110.95)	-123.25 (-112.80)	-116.72 (-113.12)	-113.89 (-109.81)	
50	R_{1-2}/\mathring{A}	1.3093 (1.2780)	1.3348 (1.3019)	1.3544 (1.3048)	1.3491 (1.2992)	50
	R_{1-3}/\mathring{A}	1.3097 (1.2779)	1.3349 (1.3017)	1.3576 (1.3042)	1.3492 (1.2993)	
	R_{1-4}/\mathring{A}	1.3090 (1.2781)	1.3355 (1.3024)	1.3542 (1.3043)	1.3490 (1.2993)	
	R_{2-6}/A	1.9742 (1.9651)	1.8764 (1.8742)	1.9389 (1.8477)	1.9549 (1.8780)	
	$R_{4-7}/\mathring{A}_{\circ}$	1.9731 (1.9658)	1.8566 (1.8657)	1.9374 (1.8552)	1.9604 (1.8745)	
	$R_{/2-10}/\mathring{A}$	1.9737 (1.9665)	1.8646 (1.8665)	1.9710 (1.8448)	1.9592 (1.8778)	
55	R_{3-9}/A	1.9726 (1.9650)	1.8713 (1.8756)	1.9035 (1.8581)	1.9554 (1.8735)	55
00	$R_{/3-12}/A$	1.9528 (1.9707)	1.8668 (1.8750)	1.8939 (1.8512)	1.9552 (1.8775)	55
	R_{4-13}/A	1.9945 (1.9626)	1.8662 (1.8609)	1.9834 (1.8506)	1.9594 (1.8751)	
	A_{2-1-3}/deg	119.98 (120.00)	120.00 (120.03)	119.89 (119.99)	119.99 (120.00)	
	A_{2-1-4}/deg	120.03 (119.99)	120.00 (119.98)	120.16 (119.98)	120.01 (120.00)	
	A_{3-1-4}/deg	119.99 (120.00)	120.00 (119.99)	119.94 (120.03)	120.00 (120.00)	

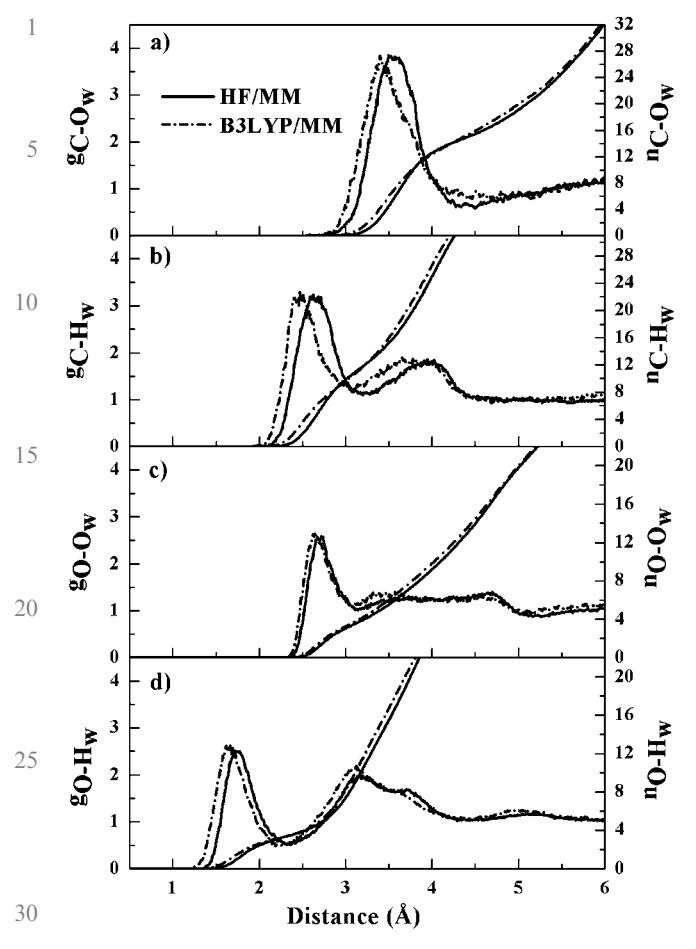


Fig. 2 (a) C–O_w, (b) C–H_w, (c) O–O_w and (d) O–H_w radial distribution functions and their corresponding integration numbers.

pair potentials.³¹ The 4500 MP2 interaction energy points for various CO₃²⁻–H₂O configurations, obtained from Gaussian03⁴⁵ calculations using the aug-cc-pvdz basis set,⁴⁶⁻⁴⁸ were fitted to an analytical form of

40
$$\Delta E_{\text{CO}_3^{2-}-\text{H}_2\text{O}} = \sum_{i=1}^4 \sum_{j=1}^3 \left[\frac{A_{ij}}{r_{ij}^4} + \frac{B_{ij}}{r_{ij}^5} + C_{ij} \exp(-D_{ij}r_{ij}) + \frac{q_i q_j}{r_{ij}} \right],$$
(5)

where A, B, C and D are fitting parameters (see Table 2), r_{ij} denotes the distances between the ith atoms of $\mathrm{CO_3}^{2-}$ and the jth atoms of the water molecule and q are atomic net charges. In this work, the charges on C and O of $\mathrm{CO_3}^{2-}$ were obtained from natural bond orbital (NBO) analysis $^{49-51}$ of the MP2 calculations using the aug-cc-pvdz basis set, while the charges on O and H of the water molecule were adopted from the flexible

Table 2 Optimized parameters of the analytical pair potential for the interaction of water with CO_3^{2-} (interaction energies in kcal mol⁻¹ and distances in Å)

55	Pair	$A/\text{kcal mol}^{-1} \text{ Å}^4$	$B/\text{kcal mol}^{-1} \text{ Å}^5$	$C/\text{kcal mol}^{-1}$	$D/\text{Å}^{-1}$
	C-O _w	-676.7561	1367.0807	205.5809	0.7958
	C-H _w O-O _w	-416.9094 -3316.4919	305.4097 6979.2169	1913.8424 13.6609	2.4620 0.3973
	$O-H_w$	-70.3719	90.1658	99.0753	1.4615

water model. The charges were set to 1.2424 (C), -1.0808 (O), -0.6598 (O_w) and 0.3299 (H_w), respectively.

5

20

All MD simulations were performed in a canonical ensemble at 298 K with a time step of 0.2 fs. The periodic box, with a box length of 18.17 Å, contained one CO₃²⁻ and 199 water molecules, corresponding to the experimental density of pure water. Since there are no counterions present, the aqueous CO₃²⁻ solution is not electrostatically neutral, i.e., the structure and dynamics obtained in this work do not account for the effects of dissolved cations. Long-range interactions were treated using the reaction-field procedure. 52 The system was initially equilibrated by performing a preliminary HF/MM MD simulation, in which only the CO₃²⁻ was treated quantum mechanically using the HF method, for 200 000 time steps. Then, the HF/MM and B3LYP/MM simulations with the QM diameter of 8.0 Å were started independently with the system's re-equilibration for 30 000 time steps, followed by another 200 000 (HF/MM) and 135 000 (B3LYP/MM) time steps to collect configurations every 10th step.

3. Results and discussion

3.1 Structural details

Structural aspects of the CO₃²⁻ hydrate can be analyzed from C-Ow, C-Hw, O-Ow and O-Hw RDFs, together with their corresponding integration numbers, as depicted in Fig. 2. Regarding the C-O_w RDFs (Fig. 2a), both the HF/MM and B3LYP/MM simulations reveal broad and rather unsymmetrical first peaks with a maximum at 3.48 and 3.39 Å, respectively. These observed C-O_w distances are in good accord with the corresponding value of 3.35 Å estimated by neutron diffraction measurement.⁵³ The feature of the first C-O_w peaks clearly suggests a high flexibility of the CO₃²⁻ hydration. In addition, the first minimum of the C-Ow peaks is not well separated from the bulk, implying that water molecules in the hydration sphere of CO₃²⁻ are quite labile and they can exchange with bulk waters. In Fig. 2b, the characteristics of C-H_w peaks are somewhat useful, providing a detailed picture with respect to the distributions of water's hydrogen atoms surrounding the ion. Comparing the HF/MM and B3LYP/MM's C-Ow and C-H_w RDFs, it is apparent that the density functional B3LYP method predicts a relatively more compact structure of the CO₃²⁻ hydration. This can be ascribed to the overestimation of the CO₃²-water interactions (cf. Table 1). In both the HF/ MM and B3LYP/MM simulations, the integration up to the first minimum of the C-O_w peaks yields about 15-16 water molecules. However, according to the unsymmetrical first $C-O_w$ peaks and the planarity with D_{3h} symmetry of CO_3^{2-} , the observed large number of water molecules cannot be considered as the first shell coordination number of CO_3^{2-} . Instead, it could be demonstrated as the number of nearestneighbor waters, whose arrangement is influenced by the direct CO₃²-water hydrogen bonds, and those that are arranged with respect to the hydrogen bonds among nearest-neighbor water molecules, rather than by the presence of the ion. In recent classical MD simulation,⁵⁴ it has been shown that the location of water molecules in the vicinity of CO₃²⁻ lies preferably between or above and below oxygen atoms of

 ${\rm CO_3}^{2-}$, with less probability positioning straight in front of the ${\rm CO_3}^{2-}$ oxygens. In addition, an exclusion area was found in the first hydration sphere of ${\rm CO_3}^{2-}$, which was located above and below the ${\rm CO_3}^{2-}$ plane.

and below the CO_3^{2-} plane. A detailed description of the hydrogen bonds between CO₃²⁻ oxygen atoms and their nearest-neighbor waters can be obtained from the O-O_w and O-H_w RDFs (Fig. 2c and d). In the HF/MM simulation, the first O-O_w peak is exhibited at 2.71 Å, and integration up to the corresponding first O-O_w minimum yields an average coordination number of 3.7 ± 0.1 . In the B3LYP/MM simulation, the first O-O_w peak is observed at a slightly shorter distance of 2.64 Å, with an average coordination number of 3.5 \pm 0.1. In both the HF/ MM and B3LYP/MM simulations, the O-O_w RDFs do not 15 show distinct minima after the first shell, indicating that a clear determination of the first shell coordination number for each oxygen atom of ${\rm CO_3}^{2-}$ is not feasible. Nevertheless, if one supposes that the "shells" for each of the CO₃²⁻ oxygens are not overlapping, it could be demonstrated that the maximum 20 numbers of water molecules that directly form hydrogen bonds with CO_3^{2-} are about 11.1 (HF/MM) and 10.5 (B3LYP/MM), respectively. For O-H_w RDFs, the HF/MM and B3LYP/MM simulations reveal first O-H_w peaks with a maximum at 1.74 and 1.67 Å, respectively. The position of the 25 O-H_w RDFs of about 1 Å inward from the O-O_w peaks clearly reveals the hydrogen bond donation by nearestneighbor water molecules. Integrations up to the corresponding first O-H_w minima give average hydrogen atom numbers of 3.4 ± 0.1 and 3.2 ± 0.1 , respectively. In both the HF/MM and B3LYP/MM simulations, the observed numbers of water oxygen and hydrogen atoms clearly indicate that most first-shell waters are linearly hydrogen bonded to each of the CO₃²⁻ oxygens. According to Fig. 2d, the second peak in the O-H_w RDFs around 3.1 Å can then be assigned to the hydrogen 35 atoms of first-shell waters that are not hydrogen bonded with the CO₃²⁻ oxygen atoms. In comparison to the O_w-H_w RDFs of pure water, as obtained at similar QM/MM levels of accuracy, 30,40 it is apparent that the hydrogen bonds between CO₃²⁻ oxygens and their nearest-neighbor waters are relatively 40 strong. The strength of the hydrogen bonds between CO₃²⁻ oxygen atoms and their nearest-neighbor waters was also demonstrated in the recent CP-MD study, 35 but the shape and height of the resulting O-H_w RDFs reveal relatively stronger CO₃²-water hydrogen bonds, *i.e.*, compared to the 45 HF/MM and B3LYP/MM results, and thus, a more ordered

The distributions of oxygen and hydrogen atoms of first-shell waters, calculated with respect to the first minima of the O-O_w and O-H_w RDFs, are depicted in Fig. 3a and b, respectively.

50 Both the HF/MM and B3LYP/MM simulations clearly show that the most frequent number of water molecules per CO₃²⁻ oxygen atom is 3, followed by 4 and 2 in decreasing amounts. Fig. 4 and 5 show examples of time dependence of the hydration number of each of the CO₃²⁻ oxygens occurring within the first 10 ps of the HF/MM and B3LYP/MM simulations, respectively. From the analysis of the HF/MM and B3LYP/MM trajectories, it is found that each of the CO₃²⁻ oxygen atoms simultaneously forms asymmetric solvation shells, *i.e.*, each of them forms hydrogen bonds with different

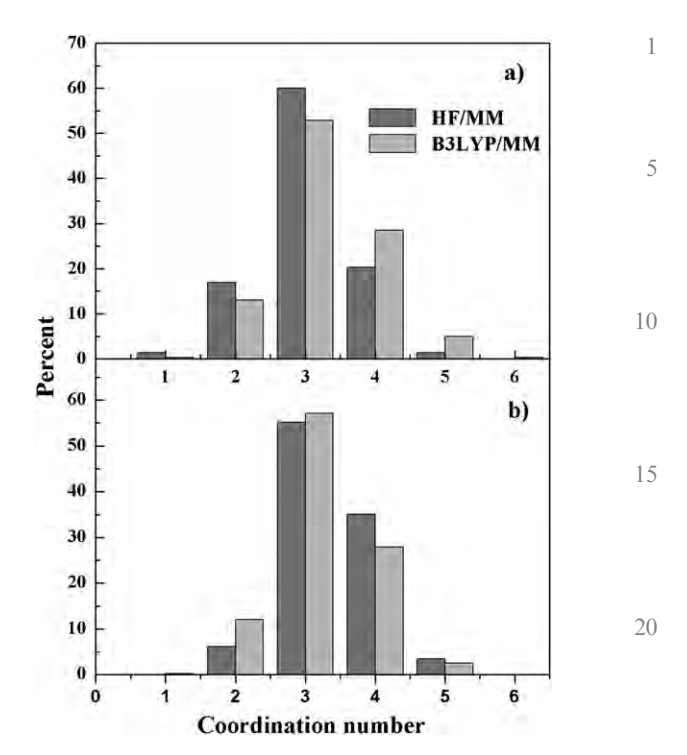


Fig. 3 Distributions of (a) oxygen and (b) hydrogen atoms of first-shell waters at each of the ${\rm CO_3}^{2-}$ oxygens, calculated within the first minimum peak of the O-O_w and O-H_w RDFs, respectively.

25

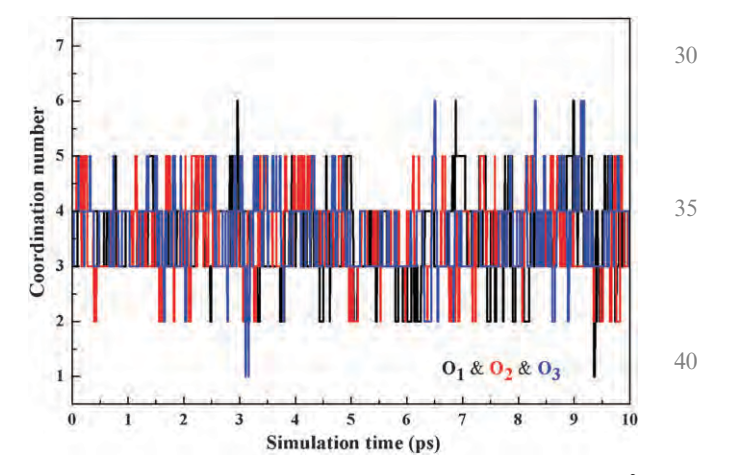


Fig. 4 Time dependence of the number of first-shell waters at ${\rm CO_3}^{2-}$ oxygen atoms, selecting only the first 10 ps of the HF/MM simulation.

numbers of water molecules. As a consequence, this causes numerous possible species of the ${\rm CO_3}^2-$ -water complexes to exist in aqueous solution. According to Fig. 4 and 5, the total numbers of water molecules in the vicinity of the ${\rm CO_3}^2-$ oxygens show large fluctuations, ranging from 1 to 6 and from 2 to 7 for the HF/MM and B3LYP/MM simulations, respectively.

More information about the ${\rm CO_3}^{2-}$ —water hydrogen bonds can be visualized from the probability distributions of the C–O···H_w and O···O_w–H_w angles, calculated within the first minimum of the O–O_w RDFs, as shown in Fig. 6a and b, respectively. In both the HF/MM and B3LYP/MM simulations, since the instantaneous environments of each of the ${\rm CO_3}^{2-}$

solvation structure.

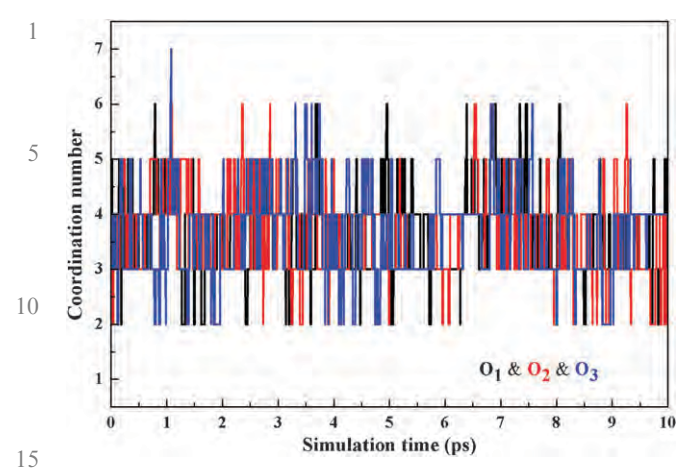


Fig. 5 Time dependence of the number of first-shell waters at CO_3^{2-} oxygen atoms, selecting only the first 10 ps of the B3LYP/MM simulation.

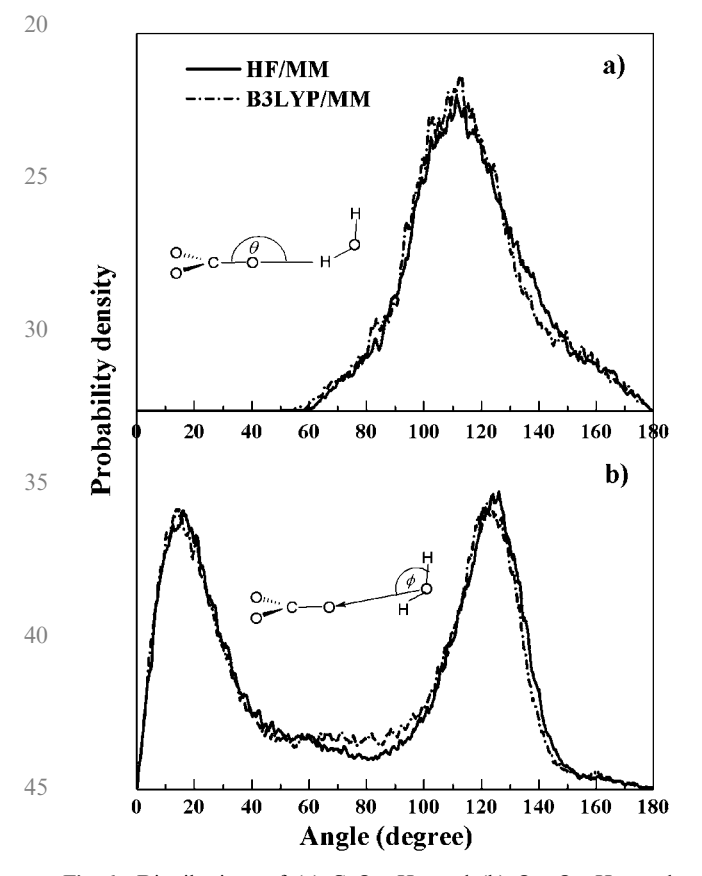


Fig. 6 Distributions of (a) $C-O\cdots H_w$ and (b) $O\cdots O_w-H_w$ angles, calculated within the first minimum of the $O-O_w$ RDFs.

oxygens are somewhat different because of fluctuations in their respective solvation shells (*cf*. Fig. 4 and 5), the solvent effects can be expected to cause strong charge localization at CO₃²⁻. Consequently, an asymmetrical charge distribution at each of the CO₃²⁻ oxygens, *i.e.*, the formation of C-O single and double bonds, could exist in aqueous solution. In this respect, one could anticipate the arrangement of directional C-O···H_w hydrogen bonds that causes the C-O···H_w angle to pronounce at 109.5° and 120°. In both the HF/MM and B3LYP/MM

simulations, however, the observed broad $C\text{--}O\cdots H_w$ angular distributions clearly indicate the absence of such a phenomenon. In addition, with regard to the Mulliken charge analyses of several CO_3^{2-} —water complexes, there is no substantial charge concentration at each of the CO_3^{2-} oxygens. In this context, the CO_3^{2-} would adopt an electronically delocalized structure in aqueous solution, which may fluctuate due to solvent exchange processes. Fig. 6b shows the distributions of the $O\cdots O_w$ – H_w angle, which prove the preference for linear $O\cdots H_w$ – O_w arrangements.

5

10

15

3.2 Dynamical details

3.2.1 Intramolecular geometry of CO_3^{2-} . The geometrical arrangement of CO₃²⁻ in aqueous solution is described in terms of the distributions of the C-O bond length and O-C-O angle, as shown in Fig. 7a and b, respectively. To visualize the change in the internal C-O bond, time dependence of the C-O bond lengths, as obtained by the HF/MM and B3LYP/MM simulations, are plotted in Fig. 8 and 9, respectively. In addition, the distribution of the α angle, as defined by a vector along any C-O bond and a vector pointing outwards between the other two C-O bonds, is also given in Fig. 10. According to Fig. 8 and 9, the observed C-O distances of 1.29 (HF/MM) and 1.31 Å (B3LYP/MM) are in good agreement with the recent neutron diffraction experiments of K₂CO₃ solutions, which reported the corresponding C-O distance of 1.3 Å.54 The HF/MM and B3LYP/MM results clearly indicate a high flexibility of the CO₃²⁻ structure. As compared to the structure

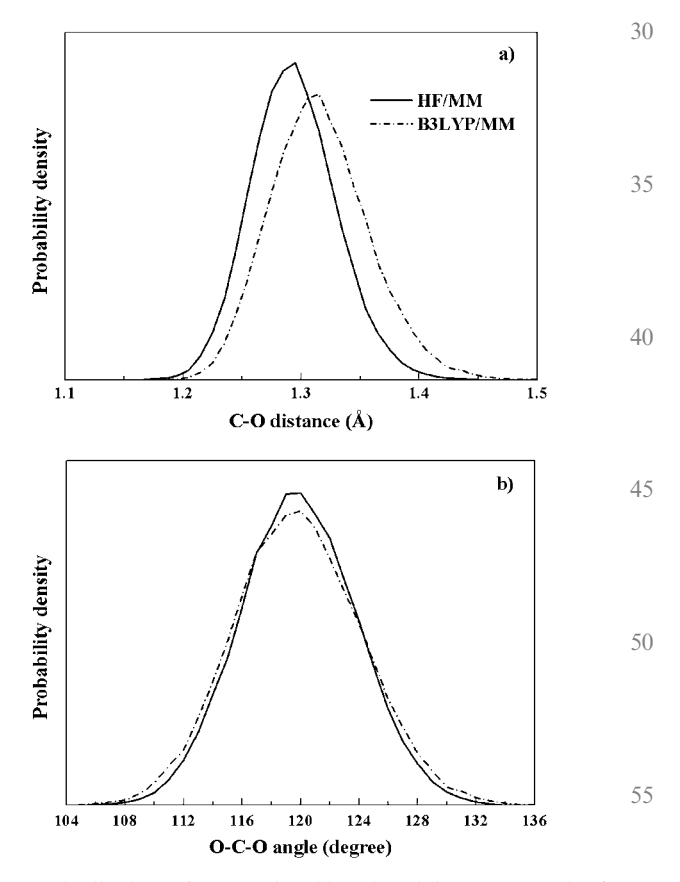


Fig. 7 Distributions of (a) C–O bond length and (b) O–C–O angle of ${\rm CO_3}^{2-}$.

50

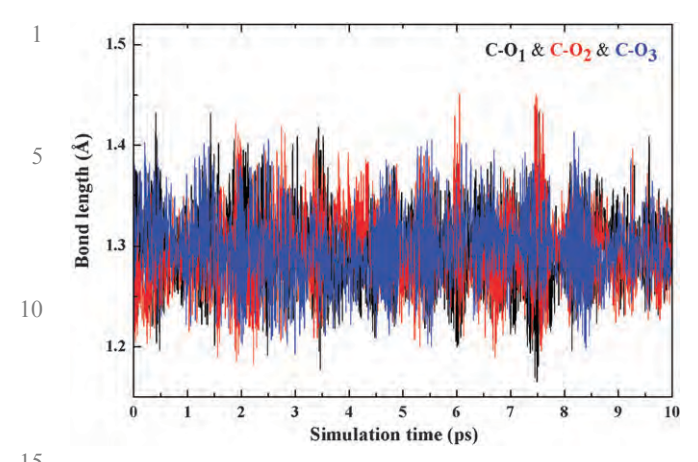


Fig. 8 Time dependence of the C–O bond lengths of CO₃²⁻, as obtained from the first 10 ps of the HF/MM simulation.

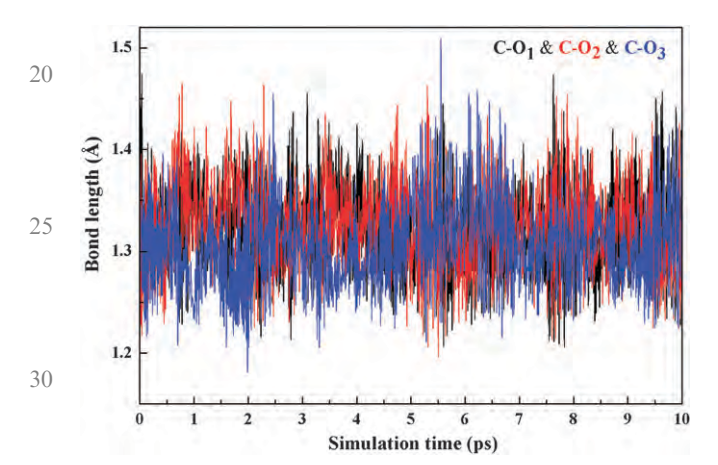


Fig. 9 Time dependence of the C–O bond lengths of CO₃²⁻, as obtained from the first 10 ps of the B3LYP/MM simulation.

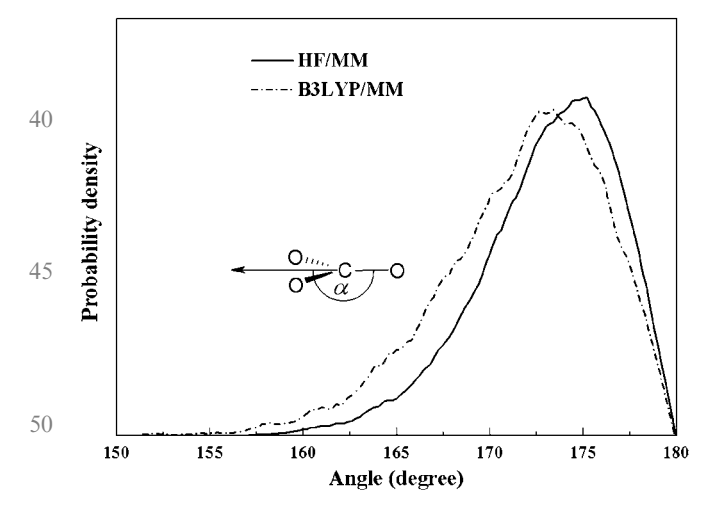


Fig. 10 Distributions of α , as defined by a vector along one C–O bond and a vector pointing outwards between the other two C–O bonds.

of gas-phase $\mathrm{CO_3}^{2-}$ (cf. Table 1), both the HF/MM and B3LYP/MM simulations reveal a substantial change in the local structure of $\mathrm{CO_3}^{2-}$ (i.e., due to the influence of water

environments), being either planar or non-planar geometry with equivalent and/or in-equivalent C–O bonds. On the other hand, this supplies information that water molecules in the first hydration shell of CO₃²⁻ oxygens break the *D*_{3h} symmetry of the ion. This phenomenon has been detected by IR and Raman spectra. ⁵⁵ According to the plots in Fig. 8 and 9, the B3LYP/MM simulation shows a relatively larger variation of the C–O bond length, *i.e.*, compared to the HF/MM results. With regard to the relatively too strong CO₃²⁻—water interactions predicted by the B3LYP method (see Table 1), the observed difference between the HF/MM and B3LYP/MM simulations can be regarded as a consequence of the approximations of the functional and the parameterizations of the B3LYP method, rather than as a consequence of the lack of electron correlation in the HF scheme.

5

15

20

55

3.2.2 Exchange processes of water molecules in the hydration shell of CO₃²⁻ oxygens. According to Fig. 2c and d, the nonzero first minimum of the O-Ow and O-Hw RDFs, as obtained by both the HF/MM and B3LYP/MM simulations, clearly suggests an easy exchange of water molecules between those in the first hydration shell of CO₃²⁻ oxygens and in the outer region. The exchange processes of water molecules at each oxygen atom of CO₃²⁻ can be visualized through the plots of the O-O_w distances against the simulation time, as depicted in Fig. 11 and 12 for the HF/MM and B3LYP/MM simulations, respectively. During the first 10 ps of the HF/MM and B3LYP/MM trajectories, a number of water exchange processes were observed at each of the CO₃²⁻ oxygens. Interestingly, as can be seen from the examples of water exchange processes shown in Fig. 11 and 12, it is found that each of the water exchange processes displays significant different dynamics of the exchange mechanisms, together with either short-lived or long-lived exchange periods. These results supply information that first-shell water molecules can be either "loosely" or "tightly" bound to each of the CO₃²⁻ oxygens.

The rates of water exchange processes at each of the CO₃²⁻ oxygens were evaluated via mean residence times (MRT) of the surrounding water molecules. In this work, the MRT data were calculated using the direct method, 56 as the product of the average number of nearest-neighbor waters located within the first minimum of the O-Ow RDFs with the duration of the simulation, divided by the number of exchange events. With respect to time parameters t^* (i.e., the minimum duration of a ligand's displacement from its original coordination shell to be accounted) of 0.0 and 0.5 ps, the calculated MRT values are summarized in Table 3. In general, the MRT data obtained using $t^* = 0.0$ ps are used for an estimation of hydrogen bond lifetimes, whereas the data obtained with $t^* = 0.5$ ps are considered as a good estimate for sustainable ligand exchange processes. ⁵⁶ With respect to $t^* = 0.0$ ps, both the HF/MM and B3LYP/MM simulations reveal rather similar MRT values with $\tau_{H_2O}(O_i) < \tau_{H_2O}(H_2O)$, whereas the reverse order of $\tau_{\text{H},\text{O}}(\text{O}_i) > \tau_{\text{H},\text{O}}(\text{H}_2\text{O})$ is observed for $t^* = 0.5$ ps. In this respect, since the hydration shell of each CO₃²⁻ oxygen atom can somewhat overlap with the others, some of the first-shell water molecules can be expected to rapidly migrate back and forth among the different coordinating sites according to the strong influence of each CO₃²⁻ oxygen atom. As a consequence,

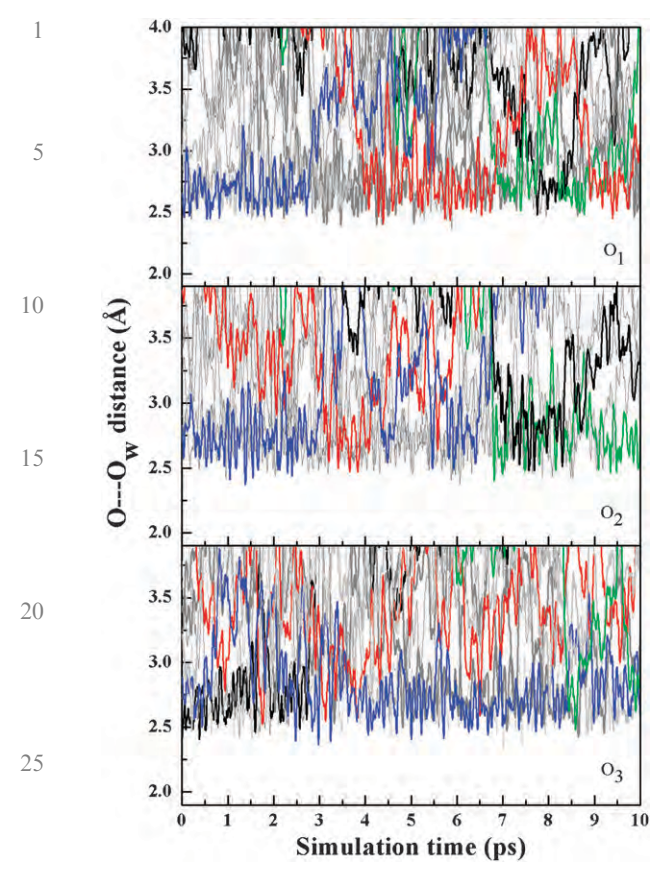


Fig. 11 Time dependence of O···Ow distances, selecting the first 0 10 ps of the HF/MM trajectory. Examples of observed water exchange processes are highlighted in color.

this reflects in the observed relatively large numbers of $N_{\rm ex}$ for $t^* = 0.0$ ps, i.e., compared to the $N_{\rm ex}$ for $t^* = 0.5$ ps. The 35 migration of water molecules between the coordinating sites have also been demonstrated for aqueous HCO3-57 and HSO₄⁻⁵⁸ anions. With regard to the data in Table 3, the number of processes needed for one successful water exchange, $R_{\rm ex}$, being the ratio of $N_{\rm ex}^{0.0}$ to $N_{\rm ex}^{0.5}$, for an individual ${\rm CO_3}^{2-}$ oxygen atom clearly confirms the strong hydrogen bonds between the CO₃²⁻ oxygens and their nearest-neighbor water molecules. In this context, the MRT results clearly point out the evidence for the "structure making" ability of CO₃²⁻ in aqueous solution. Compared to the HF/MM results, the 45 relatively higher MRT values predicted by the B3LYP/MM simulation are in accordance with the observed tendency of the B3LYP method to overestimate the stabilization energy of gas-phase CO_3^{2-} -water complexes (cf. Table 1).

Finally, a comparison of the results with other anions, in particular the bicarbonate ion, HCO₃⁻, appears to be useful. Recently, an *ab initio* quantum mechanical charge field (QMCF) formalism has been applied to simulate the HCO₃⁻ ion in aqueous solution, revealing the high flexibility of the HCO₃⁻ hydration structure as well as the "structure-breaking" behavior of this ion in water. Such a phenomenon is understandable since, unlike CO₃²⁻, the HCO₃⁻ ion has lower symmetry and its interactions with waters are relatively weak. As a consequence, this reflected in the different hydration sites, and thus in the lower range of MRT values for the individual HCO₃⁻

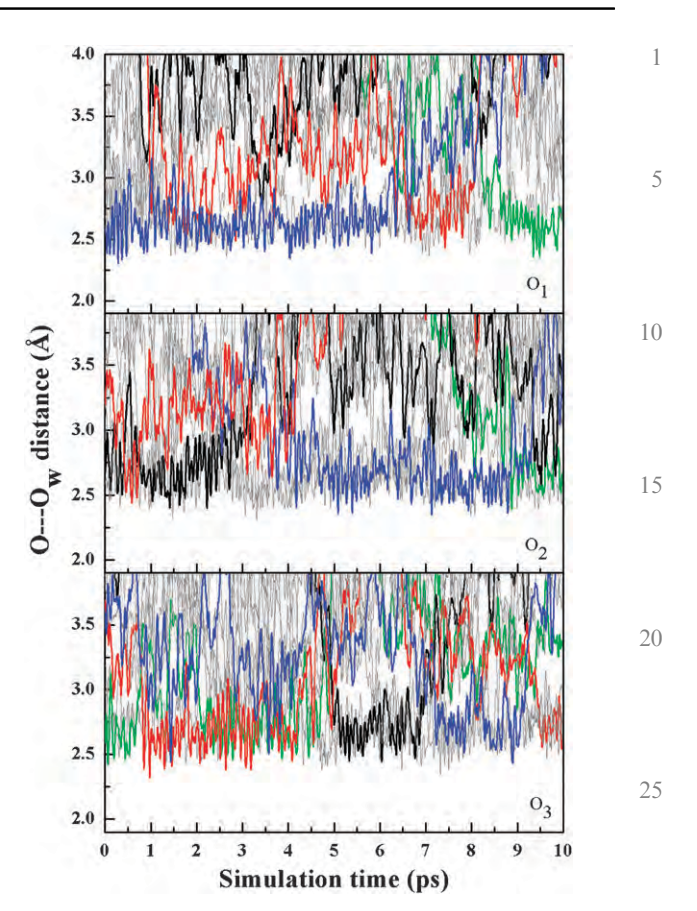


Fig. 12 Time dependence of $O \cdot \cdot \cdot O_w$ distances, selecting the first 10 ps of the B3LYP/MM trajectory. Examples of observed water exchange processes are highlighted in color.

30

55

Table 3 Number of water exchange events (N_{ex}) , mean residence time of water molecules in the bulk and in the vicinity of ${\rm CO_3}^{2-}$ oxygens (τ) and total number of processes needed for one successful water exchange (R_{ex}) , calculated within the first minimum of each of the O–O $_{\rm w}$ RDFs

			$t^* = 0$	0.0 ps	<i>t</i> * =	$t^* = 0.5 \text{ ps}$		
Atom/solute	CN	$t_{\rm sim}$	$N_{ m ex}^{0.0}$	$\tau_{\rm H_2O}^{0.0}$	$N_{ m ex}^{0.5}$	$\tau_{\rm H_2O}^{0.5}$	$R_{\rm ex}$	4
HF/MM MD								
O1	3.56	40.0	977	0.15	85	1.67	11.5	
O2	3.71	40.0	1115	0.13	62	2.39	18.0	
O3	3.50	40.0	980	0.14	73	1.92	13.4	
Pure H ₂ O ²⁹	4.6	12.0	292	0.20	31	1.80	9.4	4:
Pure H ₂ O ⁴⁰	4.2	40.0	_	0.33	_	1.51		т.
B3LYP/MM	MD							
O1	3.37	27.0	632	0.14	33	2.76	19.2	
O2	3.84	27.0	800	0.13	48	2.16	16.7	
O3	3.81	27.0	733	0.14	42	2.45	17.5	
Pure H ₂ O ⁴⁰	4.2	30.0	_	1.07	_	7.84		51

hydrogen and oxygen atoms.⁵⁷ The contrasting behavior of these isoelectronic species is very crucial, which is an important basis for further study of their molecular scale reactivity.

4. Conclusion

In this study, we have performed two combined QM/MM MD simulations, namely HF/MM and B3LYP/MM, for obtaining

- detailed knowledge on the local hydration structure and dynamics of CO₃²⁻ in aqueous solution. Both the HF/MM and B3LYP/MM simulations clearly show relatively strong hydrogen bonds between the CO₃²⁻ oxygens and their nearest- neighbor waters, *i.e.*, when compared to water–water hydrogen bonds in the bulk. The geometrical arrangement of CO₃²⁻ in aqueous solution is found to be rather flexible and first-shell waters can be either "loosely" or "tightly" bound to each of the CO₃²⁻ oxygens, forming an asymmetric solvation structure
- with a varying number of hydrogen bonds, with the prevalent value of 3. With regard to the observed tendency of the B3LYP method to overestimate the stabilization energy of gas-phase CO₃²—water complexes, the HF method seems to be more reliable for the description of such a particular
- system. Significant weaknesses of the B3LYP scheme could be attributed to the incompleteness of the kinetic energy term, the self-interaction error and the parameterization of the B3LYP method which did not contain any H-bonded system. As a consequence of the rapid development in computer
- 20 capacity and performance, a further improvement of the simulation results could be achieved by increasing the QM region and basis set, together with the use of correlated methods, *i.e.*, at the MP2 level of accuracy.

Acknowledgements

This work was supported by the Thailand Research Fund (TRF), Suranaree University of Technology (SUT) and Office of the Higher Education Commission under an NRU project.

References

25

- H. Frank, Chemical Physics of Ionic Solutions, John Wiley & Sons, New York, 1956.
- 2 R. J. P. Williams, *Bio-inorganic Chemistry*, American Chemical Society, Washington DC, 1971.
- 3 E. Clementi, Determination of Liquid Water Structure, Coordination Number of Ions and Solvation for Biological Molecules, Springer-Verlag, New York, 1976, p. 107.
- 4 G. W. Neilson and R. H. Tromp, *Annu. Rep. Prog. Chem., Sect. C: Phys. Chem.*, 1991, **88**, 45.
 - 5 M. Magini, X-Ray Diffraction of Ions in Aqueous Solution: Hydration and Complex Formation, CRC Press Inc., Boca Raton, Florida, 1988.
 - 6 G. W. Neilson and N. T. Skipper, Chem. Phys. Lett., 1985, 114, 35.
- 45 7 I. Howell and G. W. Neilson, J. Phys.: Condens. Matter, 1996, 8, 4455.
 - 8 G. W. Neilson, Pure Appl. Chem., 1988, 60, 1797.
 - 9 N. T. Skipper, G. W. Neilson and S. C. Cummings, J. Phys.: Condens. Matter, 1989, 1, 3489.
 - 10 F. Franks, *Water. A Comprehensive Treatise*, Plenum, New York, 1972, vol. 1–7.
 - J. 11 A. Kuzmin, S. Obst and J. Purans, J. Phys.: Condens. Matter, 1997, 9, 10065.
 - 12 C. J. Fecko, J. D. Eaves, J. J. Loparo, A. Tokmakoff and P. L. Geissler, Science, 2003, 301, 1698.
 - 13 E. Spohr, G. Pálinkás, K. Heinzinger, P. Bopp and M. M. Probst, J. Phys. Chem., 1988, 92, 6754.
- 55 14 P. Bopp, *The Physics and Chemistry of Aqueous Ionic Solutions*, Reidel Publishing Company, Dordrecht, 1987, p. 217.
 - 15 S. H. Lee and J. C. Rasaiah, J. Phys. Chem., 1996, 100, 1420.
 - 16 S. Obst and H. Bradaczek, J. Phys. Chem., 1996, 100, 15677.
 - 17 E. Clementi, H. Kistenmacher, W. Kolos and S. Romano, *Theor. Chim. Acta*, 1980, 55, 257.

- 18 L. A. Curtiss, J. W. Halley and J. Hautman, *Chem. Phys.*, 1989, 133, 89.
- 19 A. Warshel and M. Levitt, J. Mol. Biol., 1976, 103, 227.
- 20 U. C. Singh and P. A. Kollman, J. Comput. Chem., 1986, 7, 718.
- 21 M. J. Field, P. A. Bash and M. Karplus, J. Comput. Chem., 1990, 11, 700.
- 22 J. Gao, Rev. Comput. Chem., 1996, 7, 119.
- 23 T. Kerdcharoen, K. R. Liedl and B. M. Rode, *Chem. Phys.*, 1996, 211, 313.
- 24 A. Tongraar, K. R. Liedl and B. M. Rode, J. Phys. Chem. A, 1997, 101, 6299.
- 25 A. Tongraar, K. R. Liedl and B. M. Rode, J. Phys. Chem. A, 1998, 102, 10340.
- 26 A. Tongraar and B. M. Rode, Phys. Chem. Chem. Phys., 2003, 5, 357.
- 27 B. M. Rode, C. F. Schwenk and A. Tongraar, J. Mol. Liq., 2004, 110, 105.
- 28 B. M. Rode, C. F. Schwenk, T. S. Hofer and B. R. Randolf, *Coord. Chem. Rev.*, 2005, **249**, 2993.

15

30

35

- 29 A. Tongraar and B. M. Rode, *Chem. Phys. Lett.*, 2004, **385**, 378.
- 30 P. Intharathep, A. Tongraar and K. Sagarik, *J. Comput. Chem.*, 2005, **26**, 1329.
- 31 A. Tongraar, P. Tangkawanwanit and B. M. Rode, *J. Phys. Chem.* A, 2006, 110, 12918.
- 32 P. Payaka, A. Tongraar and B. M. Rode, *J. Phys. Chem. A*, 2010, 114, 10453.
- 33 H. Elderfield, Science, 2002, 296, 1618.
- 34 J. R. Bargar, J. D. Kubicki, R. Reitmeyer and J. A. Davis, *Geochim. Cosmochim. Acta*, 2005, **69**, 1527.
- 35 P. P. Kumar, A. G. Kalinichev and R. J. Kirkpatrick, J. Phys. Chem. B, 2009, 113, 794.
- 36 A. Tongraar and S. Hannongbua, J. Phys. Chem. B, 2008, 112, 885.
- 37 S. Yoo, X. C. Zeng and S. S. Xantheas, J. Chem. Phys., 2009, 130, 221102.
- 38 J. X. Grossman, E. Schwegler, E. W. Draeger, F. Gygi and G. Galli, J. Chem. Phys., 2004, 120, 300.
- 39 B. R. Brooks, R. E. Bruccoleri, B. D. Olafson, D. J. States, S. Swaminathan and M. Karplus, J. Comput. Chem., 1983, 4, 187.
- D. Xenides, B. R. Randolf and B. M. Rode, J. Chem. Phys., 2005, 122, 174506.
- 41 T. H. Dunning, Jr and P. J. Hay, *Modern Theoretical Chemistry*, *III*, Plenum, New York, 1976.
- 42 M. J. Frisch, J. A. Pople and J. S. Binkley, *J. Chem. Phys.*, 1984, 80, 3265.
- 43 F. H. Stillinger and A. Rahman, J. Chem. Phys., 1976, 68, 666.
- 44 P. Bopp, G. Jancsó and K. Heinzinger, *Chem. Phys. Lett.*, 1983, 98 129
- 45 M. J. Frisch, G. W. Trucks, H. B. Schlegel, G. E. Scuseria, M. A. Robb, J. R. Cheeseman, J. A. Montgomery, T. Vreven, K. N. Kudin, J. C. Burant, J. M. Millam, S. S. Iyengar, J. Tomasi,
- V. Barone, B. Mennucci, M. Cossi, G. Scalmani, N. Rega, G. A. Peterson, H. Nakatsuji, M. Hada, M. Ehara, K. Toyota, R. Fukuda, J. Hasegawa, M. Ishida, T. Nakajima, Y. Honda,
- O. Kitao, H. Nakai, M. Klene, X. Li, J. E. Knox, H. P. Hratchian, J. B. Cross, V. Bakken, C. Adamo, J. Jaramillo, R. Gomperts,
- R. E. Stratmann, O. Yazyev, A. J. Austin, R. Cammi, C. Pomelli, J. W. Ochterski, P. Y. Ayala, K. Morokuma, G. A. Voth, P. Salvador, J. J. Dannenberg, V. G. Zakrzewski, S. Dapprich,
- A. D. Daniels, M. C. Strain, O. Farkas, D. K. Malick, A. D. Rabuck, K. Raghavachari, J. B. Foresman, J. V. Ortiz,
- Q. Cui, A. G. Baboul, S. Clifford, J. Cioslowski, B. B. Stefanov, G. Liu, A. Liashenko, P. Piskorz, I. Komaromi, R. L. Martin, D. J. Fox, T. Keith, M. A. Al-Laham, C. Y. Peng,
- A. Nanayakkara, M. Challacombe, P. M. W. Gill, B. Johnson, W. Chen, M. W. Wong, C. Gonzalez and J. A. Pople, *GAUSSIAN 03 (Revision D.1)*, Gaussian, Inc., Wallingford, CT, 2005.
- 46 T. H. Dunning, J. Chem. Phys., 1989, 90, 1007.
- 47 R. A. Kendall, T. H. Dunning and R. J. Harrison, *J. Chem. Phys.*, 1992, **96**, 6769.
- 48 D. E. Woon and T. H. Dunning, J. Chem. Phys., 1993, 98, 1358.
- 49 J. E. Carpenter and F. Weinhold, THEOCHEM, 1988, 169, 41.
- 50 A. E. Reed, R. B. Weinstock and F. Weinhold, J. Chem. Phys., 1985, 83, 735.

- 1 51 A. E. Reed, L. A. Curtiss and F. Weinhold, Chem. Rev., 1988, 88, 899.
 - 52 D. J. Adams, E. H. Adams and G. J. Hills, Mol. Phys., 1979, **38**, 387.
- 53 Y. Kameda, M. Sasaki, S. Hino, Y. Amo and T. Usuki, Physica B
- 55 W. W. Rudolph, D. Fischer and G. Irmer, Appl. Spectrosc., 2006, **60**, 130.
- 56 T. S. Hofer, H. T. Tran, C. F. Schwenk and B. M. Rode, J. Comput. Chem., 2004, 25, 211.
- 57 V. Vchirawongkwin, A. B. Pribil and B. M. Rode, J. Comput. Chem., 2010, 31, 249.

(Amsterdam), 2006, 385, 279. 5 58 V. Vchirawongkwin, C. Kritayakornupong and B. M. Rode, 54 F. Bruneval, D. Donadio and M. Parrinello, J. Phys. Chem. B, J. Phys. Chem. B, 2010, 114, 11561. 2007, **111**, 12219. 10 10 15 15 20 20 25 25 30 30 35 35 40 40 45 45 50 50 55 55

1. สำเนา Manuscript ของงานวิจัยเรื่องที่ 5

Viwat Vchirawongkwin, Chinapong Kritayakornupong and **Anan Tongraar**, "Characterization of the structure and dynamics of an aqueous Hg²⁺ solution by an *ab initio* molecular dynamics study" *J. Mol. Liq.*, **2011**, 115, 12527-12536.

1. สำเนา Manuscript ของงานวิจัยเรื่องที่ 6

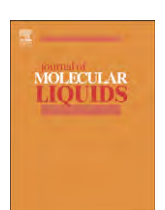
Viwat Vchirawongkwin, Chinapong Kritayakornupong, **Anan Tongraar** and Bernd M. Rode, "Symmetry breaking and hydration structure of carbonate and nitrate in aqueous solution: A study by *ab initio* quantum mechanical charge field molecular dynamics" J. *Phys. Chem. B*, **2011**, 115, 12527-12536.

FISEVIER

Contents lists available at SciVerse ScienceDirect

Journal of Molecular Liquids

journal homepage: www.elsevier.com/locate/molliq



Characterization of the structure and dynamics of an aqueous Hg^{2+} solution by an ab initio molecular dynamics study

Viwat Vchirawongkwin ^a, Chinapong Kritayakornupong ^b, Anan Tongraar ^{c,*}

- ^a Department of Chemistry, Faculty of Science, Chulalongkorn University, Bangkok 10330, Thailand
- ^b Department of Chemistry, Faculty of Science, King Mongkut's University of Technology Thonburi, Bangkok 10140, Thailand
- ^c School of Chemistry, Institute of Science, Suranaree University of Technology, Nakhon Ratchasima 30000, Thailand

ARTICLE INFO

Article history: Received 16 June 2011 Received in revised form 12 August 2011 Accepted 31 August 2011 Available online 17 September 2011

Keywords: QMCF MD Dissociative interchange Structure-making

ABSTRACT

Quantum mechanical charge field (QMCF) MD simulation has been performed to investigate the structure and dynamics of ${\rm Hg^{2+}}$ hydrate. The first-shell hexacoordinated ${\rm [Hg(H_2O)_6]^{2+}}$ complex with an average ${\rm Hg^{2+}}$ -O distance of 2.40 Å is dominantly found, which corresponds to the neutron diffraction and extended X-ray absorption fine structure (EXAFS) experiments. Other species, in particular the 7-fold coordinated complexes, can be formed transiently, according to the water exchange processes with an associative interchange (I_a) mechanism. The second hydration shell exhibits a ${\rm Hg^{2+}}$ -O distance of 4.6 Å with a coordination number of ~14. The mean residence times (MRTs) of first- and second-shell waters clearly indicate a strong "structure-forming" ability of ${\rm Hg^{2+}}$ in aqueous solution.

© 2011 Elsevier B.V. All rights reserved.

1. Introduction

Due to the chemical and toxicological importance of Hg²⁺ in aqueous solution [1], a number of experimental and theoretical techniques have been employed to obtain detailed knowledge of this ion hydrate. In experiments, the hydration structure of Hg²⁺ in Hg (BF₄)₂ solution has been investigated using X-ray scattering measurement, showing that Hg^{2+} in aqueous solution has an octahedralhexaaquo coordination with a mean Hg²⁺-O distance of 2.33 Å [2]. Using the proton NMR technique, a coordination number of 4.9 was predicted for the first hydration shell of Hg²⁺[3]. According to X-ray scattering data obtained from concentrated solutions (2, 3.5 and 4.6 M) of hydrolyzed and non-hydrolyzed mercury (II) perchlorate, the first-shell Hg²⁺-O distance is found between 2.41 and 2.44 Å, with the coordination numbers varying from 4.9 to 6.8 [4]. In addition, it has been shown that the hydrolysis leads to the shortening of two Hg²⁺-O bonds, at 2.0 Å, and the elongation of other four bonds at 2.5 Å.

Subsequently, more consistent X-ray scattering data and Raman spectra of aqueous and dimethyl sulfoxide (DMSO) solutions of mercury (II) perchlorate were analyzed, showing an average Hg^{2+} -O bond lengths of 2.41 and 2.39 Å, respectively [5]. Comparing to solid hydrates, the X-ray crystal structure of [Hg $(H_2O)_6](ClO_4)_2$ is consistent with a Hg^{2+} -O bond length of 2.34 Å, with a small deviation from the regular octahedral O_b

symmetry [6]. Later, extended X-ray absorption fine structure (EXAFS) spectra were taken for aqueous solutions of $HgCl_2$, $HgBr_2$ and $Hg(CN)_2$, highlighting dynamic distortions of the first hydration shell caused by second-order Jahn–Teller effects [7]. Recently, a neutron diffraction study of Hg^{2+} in a solution of DNO_3/D_2O has reported the first hydration shell to be located at 2.48 Å, with a coordination number of 5.8 [8]. The neutron diffraction data proved that the average Hg^{2+} -O bond length in the solutions is significantly longer than that evaluated from the solid structure.

Besides the experiments, computer simulations, in particular molecular dynamics (MD), have been carried out to characterize the hydration structure and dynamics of Hg²⁺ in aqueous solution [9–12]. However, most of the early simulation works relied on classical molecular mechanics models. For example, an MD simulation based on effective two-body potential function has predicted a relatively large coordination number of 9, while the inclusion of three-body corrections reduces the coordination number to 6 [9]. The observed difference in the coordination number clearly indicates the importance of three-body contributions, i.e., the inclusion of these terms in the simulation appears necessary in predicting a more reliable first-shell coordination number of Hg2+. Recently, a pair potential-based MD simulation has shown evidence for a heptacoordinated $[Hg(H_2O)_7]^{2+}$ complex with C_2 symmetry for the first hydration shell, which coincides with the X-ray absorption spectroscopy (XAS) observation [11]. Regarding to such MM-based MD simulations, however, it should be realized that the quality of the simulation results depends crucially on the reliability of the interaction potentials employed in the simulations.

^{*} Corresponding author. Fax: +66 44 224185. E-mail address: anan_tongraar@yahoo.com (A. Tongraar).

In terms of quantum-mechanics-based simulations, an elegant simulation approach is to employ a hybrid ab initio quantum mechanics/molecular mechanics (QM/MM) MD technique. According to the recent QM/MM study [9], an octahedral $[Hg(H_2O)_6]^{2+}$ complex with the Hg²⁺-O distance of 2.42 Å has been reported for the first hydration shell of Hg²⁺, which is in good agreement with most experimental data [4,5]. In addition, fast dynamics ligand exchange processes in the first hydration shell of Hg^{2+} were detected, together with several observed migrations of water molecules between the second hydration shell and the bulk [10]. With regard to the QM/MM results [9,10], however, the QM region employed in the simulation is relatively small, i.e., only a sphere which includes the ion and its firstshell water molecules are described by QM calculations. In addition, the analytical potentials employed for describing the ion-solvent interactions in the QM/MM simulation can be considered as a further error source, e.g., due to the use of fixed changes in the potential

In the present study, the characteristics of Hg²⁺ in aqueous solution were re-investigated by performing a more accurate *ab initio* quantum mechanical charge field (QMCF) MD simulation. The QMCF MD technique has been successfully employed to evaluate the structure and dynamics of ions, composite ions, and acids in aqueous solution [13–19]. The aim of this study is to provide more reliable details regarding the structure and dynamics of the Hg²⁺ hydrate. The vibrational frequency of the Hg²⁺-O interactions in the first hydration shell was also calculated and compared to the available experimental data. A subsequent evaluation of mean residence times (MRTs) was carried out to describe the dynamics of the ligand exchange processes in the first and second hydration shells.

2. QMCF MD simulation

The QMCF MD technique has been developed in order to eliminate a difficulty in the construction of solute-solvent potentials [20,21]. In line with the QM/MM MD scheme [22-24], the QMCF MD technique divides the system into two parts, namely the QM and MM regions, in which different levels of approximation are applied. In addition, the OM region is also separated into two sub-regions, called the "core" and "layer" zones. In this respect, the solute and the first-shell solvents are embedded in the core zone, whereas the layer zone consists of further neighboring solvent molecules. The layer zone has been introduced in order to be able to neglect the non-Coulombic interactions between the core zone and the MM region. By the OMCF formalism, the OM region employing an ab initio quantum mechanical method is enlarged to include the second hydration shell, while the interactions among solvent molecules in the MM region can be described by the flexible BJH-CF2 water model [25,26]. The Coulombic interactions between particles in the QM zone and in the MM region are calculated by quantum chemically evaluated Mulliken partial charges on the atoms in the QM region and the model point charges on the atoms in the MM region. The charges of the particles in the MM region are embedded in the calculation of the core energy gradients as a perturbation potential into the core Hamiltonian operator:

$$H_{CF} = H_{HF} + V_{i}^{'} \tag{1}$$

$$V'_{i} = \sum_{i=1}^{M} \frac{q_{i}}{r_{ii}} \tag{2}$$

where q_j is the partial charges of each atom in the MM region, *i.e.*, -0.65966 and +0.32983 for oxygen and hydrogen, respectively, according to the BJH-CF2 model of water [25,26]. The

contributions of all forces acting on each particle in the different regions are thus defined as following:

$$F_{j}^{core} = F_{j}^{QM} + \sum_{i=1}^{M} \frac{q_{j}^{QM} q_{i}^{MM}}{r_{ij}^{2}}$$
 (3)

$$F_{j}^{layer} = F_{j}^{QM} + \sum_{i=1}^{M} \frac{q_{j}^{QM} q_{i}^{MM}}{r_{ij}^{2}} + \sum_{i=1}^{M} F_{ij}^{BJHnC}$$
(4)

$$F_{j}^{MM} = \sum_{\substack{i=1\\i\neq j}}^{M} F_{ij}^{BJH} + \sum_{i=1}^{N_{1}+N_{2}} \frac{q_{i}^{QM} \cdot q_{j}^{MM}}{r_{ij}^{2}} + \sum_{i=1}^{N_{2}} F_{ij}^{BJHnC}$$
(5)

where F_{j}^{core} , F_{j}^{layer} , and F_{j}^{MM} correspond to the forces acting on particle jlocated in the core region, the solvation layer, and the MM region, respectively. M represents the number of atoms in the MM region. With regard to Eqs. (3) and (4), the evaluation of ab initio quantum mechanical forces acting on each particle in the core and in the layer regions (F_i^{core} and F_i^{layer}) is affected by the Coulombic interactions of all MM particles. Due to the long range of Coulombic interactions, compared to the non-Coulombic components, the non-Coulombic forces between the core particles and the MM particles are neglected. This is justifed by the distance between the core and the MM region of at least 3 Å. The QM forces in the layer (F_i^{layer}) are influenced by the non-Coulombic forces and are evaluated from the MM particles, i.e., according to the BJH-CF2 water model [25,26]. Finally, the forces acting on each particle in the MM region (F_i^{MM}) are described by means of the BIH-CF2 water model [25,26], with additionally the inclusion of the Coulombic forces generated by all particles in the core (N_1) and in the layer (N_2) regions, and the non-Coulombic forces (F_{ii}^{BJHnC}) produced by the particles in the layer region (N_2) .

Since the QMCF methodology allows a continuous transition of particles between the QM and MM regions, smooth forces acting on each particle in the system are defined as:

$$F_j^{Smooth} = S_m(r) \times \left(F_j^{layer} - F_j^{MM}\right) + F_j^{MM}$$
 (6)

where F_j^{layer} and F_j^{MM} are the forces acting on particle j in the solvation layer and those located in the MM region, respectively, r is the distance of the water molecule from the ion, and S_m is a smoothing function [27],

$$S_m(r) = 1, \qquad \qquad for \ r \le r_1$$

$$S_m(r) = \frac{\left(r_0^2 - r^2\right)^2 \left(r_0^2 + 2r^2 - 3r_1^2\right)}{\left(r_0^2 - r_1^2\right)^3}, for \ r_1 < r \le r_0$$
 (7)

where r_1 and r_0 are distances defining the start and the end of the smoothing region. The thickness of the boundary between the QM and MM regions was set to 0.2 Å, which has been found to be optimal to ensure a continuous transition at such boundaries [9].

 $S_m(r)=0$,

The QMCF simulation was performed using similar parameters as employed in the previous QM/MM simulation [9]. All forces acting on each particle in the QM region were evaluated at the restricted Hartree-Fock (RHF) level of accuracy using the TURBOMOLE 5.9 program [28–30]. The effective core potential plus double- ζ valence basis set developed by Stevens, Krauss and Basch [31] (SBKJC VDZ ECP) was employed for Hg²⁺, and Dunning double- ζ valence (DZV) basis sets [32,33] were employed for the oxygen and hydrogen atoms of water. A periodic boundary cubic box with a dimension of 24.8 Å was used, consisting of one Hg²⁺ and 499 water molecules. The density of the system was fixed at 0.997 g/cm³, which corresponds to the density of pure water at the temperature of 298.15 K. Since there are

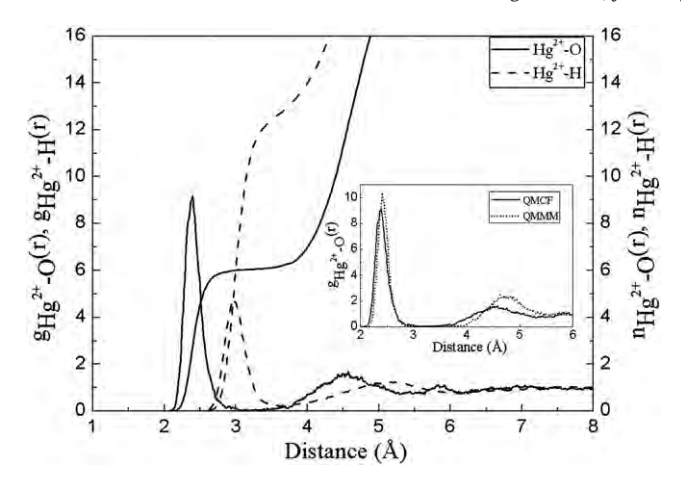


Fig. 1. ${\rm Hg^{2+}}$ -O and ${\rm Hg^{2+}}$ -H RDFs and their corresponding integration numbers determined from the QMCF MD simulation.

no counterions present, the aqueous Hg^{2+} solution is not electrostatically neutral, i.e., the structure and dynamics obtained in this work do not account for the effects of dissolved anions. The canonical (NVT) ensemble was controlled by applying the Berendsen temperature-scaling algorithm [34] with a relaxation time of 0.1 ps. Newton's equations of motions were integrated with a predictor-corrector algorithm. Since the flexible BJH-CF2 water model [25,26] was used for the MM region, a time step of 0.2 fs was chosen to allow for explicit movement of water's hydrogens. Cutoff distances of 5 Å and 3 Å were used for the non-Coulombic O-H and H-H interactions, respectively. The radial cutoff limit for Coulombic interactions was set to half of the box length, and the reaction field procedure [35] was applied for their treatments. According to the structural aspects of the Hg^{2+} hydrate observed in the previous QM/MM study [9], a cutoff radius of 3.3 Å was used for the core region and the layer region extends from 3.3 to 5.8 Å. The smoothing function [27] was applied between r_0 (6.0 Å) and r_1 (5.8 Å), which corresponds to the QM diameter of 12.0 Å. This QM sphere includes the Hg²⁺ ion and its first- and second-shell water molecules. The QMCF simulation of the aqueous Hg^{2+} solution was started using a configuration taken from the previous QM/MM study [9]. The system was re-equilibrated for 4 ps and a further 28 ps were performed for the sampling procedure.

In this work, the structural properties of the hydrated Hg^{2+} were analyzed in terms of radial distribution functions (RDF), coordination numbers, angular distributions, θ -angle and tilt angle distributions, whereas dynamical data regarding ligand exchange processes between the first and second hydration shells of Hg^{2+} were determined by mean residence time using the "direct" method [36]. In addition, the vibrational frequency of the Hg^{2+} -O distances in the first hydration shell was obtained from the Fourier transformations of the velocity autocorrelation functions (VACFs). The normalized VACF, C(t), is defined by

$$C(t) = \frac{\sum_{i}^{N_{t}} \sum_{j}^{N} \nu_{j}(t_{i})\nu_{j}(t_{i} + t)}{N_{t}N\sum_{i}^{N} \sum_{j}^{N} \nu_{j}(t_{i})\nu_{j}(t_{i})},$$
(8)

where N is the number of particles, N_t is the number of time origins t_i , and v_j denotes a certain velocity component of the particle j. The power spectrum of C(t) was evaluated using a correlation length of 2.0 ps.

3. Results and discussion

3.1. Structural properties

Fig. 1 displays the Hg²⁺-O and Hg²⁺-H RDFs derived from the QMCF simulation, together with a comparison of the Hg²⁺-O RDFs as

obtained from the present QMCF study and the previous QM/MM simulation (see insertion in Fig. 1) [9]. The structural parameters of the hydrated Hg²⁺ ion evaluated from the QMCF simulation are summarized in Table 1, together with the available theoretical and experimental data. With regard to the QMCF's Hg²⁺-O RDF in Fig. 1, the two main peaks are well pronounced, indicating well-defined first and second hydration shells. The first sharp peak of the Hg²⁺-O RDF is centered at 2.40 Å and is rather well separated from the second one, while the second peak is located in a wider range between 3.2 and 5.3 Å, with a maximum value at 4.6 Å. In fact, the minimum of the first Hg²⁺-O peak does not completely reach zero, implying that water exchange processes can be occurred between the first and the second hydration shells. As compared to the previous QM/MM's Hg²⁺-O RDF [9], the shape and height of the first Hg²⁺-O peak are almost identical, whereas a significant difference is found for the second peak. The OMCF simulation shows a broader and less pronounced second Hg²⁺-O peak, with a maximum at a shorter distance. The observed difference in the second Hg²⁺-O RDF can certainly be ascribed to the inclusion of "quantum effects" in the second hydration shell according to the QMCF scheme. On the other hand, this clarifies the need for a more accurate simulation technique, like QMCF, in order to correctly describe such hydrated ion in aqueous solution. According to Fig. 1, a slight pronounced Hg²⁺-O peak exhibited at around 5.7–6.0 Å can be considered as a small artifact of the smoothed transition between the QM and MM regions.

In experiments, the average ${\rm Hg^{2+}\text{-}O}$ distance for the first hydration shell was measured in a span from 2.33 to 2.48 Å, depending on the method, concentration and the type of salts in the solutions [2–8]. The first-shell ${\rm Hg^{2+}\text{-}O}$ distance of 2.40 Å obtained by the QMCF simulation in this work is in good accord with the octahedral ${\rm [Hg(H_2O)_6]^{2+}}$ structure determined by the X-ray diffraction study [4]. In addition, the ${\rm Hg^{2+}\text{-}H}$ peak for the first hydration shell is centered at 3.00 Å, which is in good agreement with the neutron diffraction data with isotopic substitution ($d_{\rm Hg-D}$ = 3.08 Å) [8]. The second ${\rm Hg^{2+}\text{-}H}$ peak is relatively broad, with a range of 3.5–5.3 Å with a maximum at 4.57 Å. Overall, the features of the ${\rm Hg^{2+}\text{-}O}$ and ${\rm Hg^{2+}\text{-}H}$ RDFs clearly support information that the orientation of water molecules in the first and second hydration shells of ${\rm Hg^{2+}}$ is mostly determined by the strong ion-dipole interactions.

To clarify the number of water molecules surrounding the Hg²⁺ ion, the distributions of the coordination numbers in the first and the second hydration shells are evaluated, as depicted in Fig. 2. For the first

Table 1Characteristic data of the Hg-O RDFs, as obtained from different MD simulations and experiments.

	* /							24.1.1
Solute	Ion/water ratio or molarity (M)	$r_{\rm M1}$	$r_{\rm m1}$	n_1	$r_{\rm M2}$	r _{m2}	n ₂	Method
Hg ²⁺	1/499	2.40	3.09	6.1	4.6	5.3	14.1	QMCF-MD
	1/499	2.42	3.58	6.2	4.6	5.6	21.7	QM/MM-MD [9]
	1/499	2.46	3.21	6.0	4.8	6.3	32.7	three-body
								MD [9]
	1/449	2.29	3.10	9.0	4.2	5.4	23.9	two-body
								MD [9]
	1/819	2.28		7				two-body
								MD [12]
	1/819	2.26		6.9				two-body
								MD [12]
$Hg (BF)_2$	2.0	2.33		6				XRD [2]
$Hg (ClO_4)_2$	3.5	2.42		5.7	4.1		18.4	XRD [4]
$Hg (ClO_4)_2$	2.8	2.34		6				XRD [6]
$Hg (ClO_4)_2$	3.5	2.41		6.0				LAXS [5]
$Hg (ClO_4)_2$	0.1	2.31		7				XANES [11]
Hg (DNO ₃)	0.225	2.48		6				ND [8]
Hg ²⁺	1.000			4.9				NMR [3]

 $r_{\rm M1}$, $r_{\rm M2}$ and $r_{\rm m1}$, $r_{\rm m2}$, are the distance in Å, where $g_{\rm Hg}^{2+}$ - $_{\rm O}(r)$, has the first and second maximum and the first and second minimum, respectively. n_1 and n_2 are average coordination numbers of the first and second hydration shells, respectively.

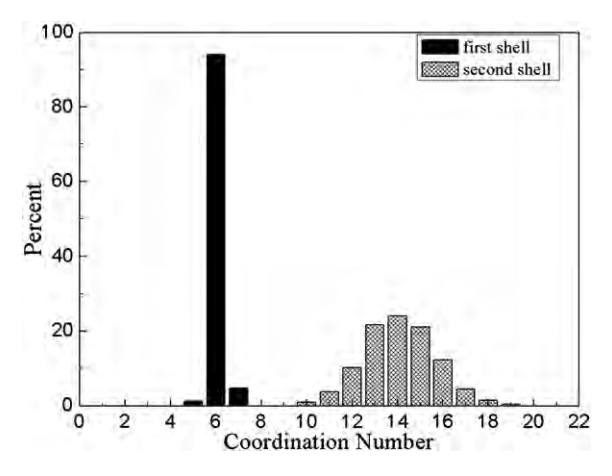


Fig. 2. First and second shell coordination number distributions of the ${\rm Hg}^{2+}$ hydrate obtained from the QMCF MD simulation.

hydration shell, probability distribution of the coordination number calculated up to the minimum of the Hg^{2+} –O RDF reveals three main species, namely 5-, 6- and 7-fold coordinated complexes, with a prevalent value of 6. According to Fig. 2, the 5- and 7-fold coordinated species are rarely detected, with 1.2% and 4.7% occurrences, respectively. In this respect, the presence of 5- and 7-fold coordinated complexes in aqueous solution supplies information that the first hydration shell of Hg^{2+} is not exclusively octahedral $[Hg(H_2O)_6]^{2+}$ arrangement. In the second hydration shell, a large variation of the coordination number ranging from 10 to 18 is observed, with a mean value of 14.1 ± 0.3 .

To interpret the arrangements of first-shell water molecules around the Hg^{2+} ion, the distribution of O- Hg^{2+} -O angle, calculated up to the first minimum of the Hg^{2+} -O RDF, is plotted in Fig. 3. The QMCF results show a recognizable distortion of the octahedral [Hg $(H_2O)_6]^{2+}$ complex, with the O- Hg^{2+} -O peaks centered at 87° and 167°. The flexibility and orientation of first-shell water molecules are further characterized in terms of the distributions of θ and tilt angles, as depicted in Fig. 4a and b, respectively. In this context, the angle θ is defined as the angle between the Hg^{2+} -O bond axis and the dipole vector of water molecules, while the tilt angle is the angle between the Hg^{2+} -O axis and the plane defined by the O-H vectors of water molecules. According to Fig. 4a, the distribution of the θ angle for the first hydration shell is centered at 169°, spanning a broad range of 110–180°.

According to the ability of Hg^{2+} to bind instead of Zn^{2+} in many essential biomolecules, a comparison of the orientations of first-shell waters in the Hg^{2+} and Zn^{2+} hydrates might be useful. In this work, it is found that the distribution of the θ angle for the first hydration

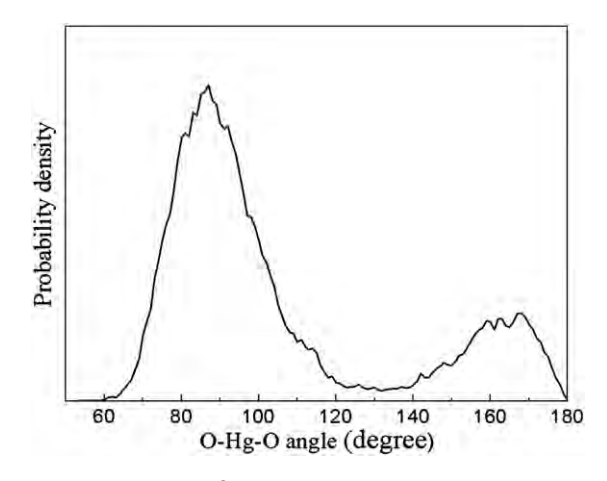


Fig. 3. Distributions of the O-Hg $^{2+}$ -O angles for the first hydration shell obtained from the QMCF MD simulation.

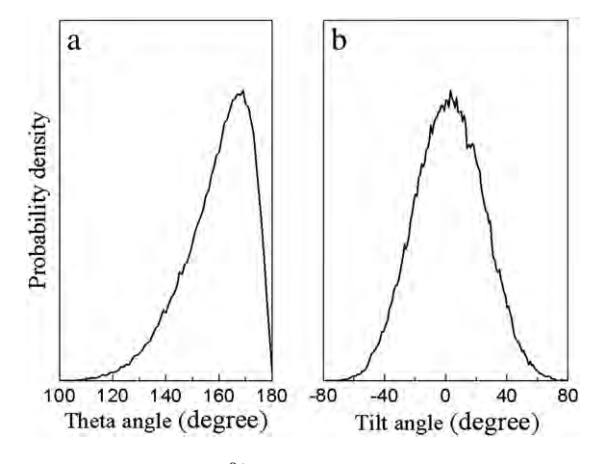


Fig. 4. Angular distributions of Hg²⁺-water configurations for the first hydration shell: a) θ and b) tilt angle, as obtained from the QMCF MD simulation.

shell of Hg^{2+} is almost identical to that obtained from the two-shell QM/MM MD simulation of aqueous Zn^{2+} solution [37]. However, a slight difference is visible in the case of the tilt angle (Fig. 4b). For Hg^{2+} , a maximum value of 3° is observed, with the peak reaching zero at $\pm 70^\circ$, while a maximum value of -2° , ranging from -60 to $+60^\circ$ is reported for the case of Zn^{2+} [37]. In this context, the QMCF results indicate slightly more flexibility of the first-shell Zn^{2+} hydration structure, *i.e.*, compared to the Zn^{2+} hydrate.

3.2. Dynamical properties

3.2.1. Hg^{2+} -O vibrations

The strength of ion–water interactions can be described by means of the vibrational frequency, which can be determined from the velocity autocorrelation functions (VACFs) and their Fourier transformations. The power spectra of the ${\rm Hg^2}^+-{\rm O_w}{\rm vibrational}$ mode obtained by the QMCF simulation are scaled by the standard factor of 0.89 [38–40], as shown in Fig. 5. This scaling factor has been applied in order to compensate the rather constant systematic error of quantum mechanical calculations at HF level of accuracy, i.e., for scaling the computed frequencies to be in agreement with the experiment. The calculated frequencies of the ${\rm Hg^2}^+-{\rm O_w}$ vibrational mode in the first hydration shell has its maximum at 290 cm $^{-1}$ with a shoulder peak at around 174 cm $^{-1}$, corresponding to a Hg-O stretching force constants of 73.4, and 26.4 N/m, respectively. Without the applied scaling factor, a maximum value of 326 cm $^{-1}$ is estimated, leading to a force constant of 92.8 N/m. These data are in fair

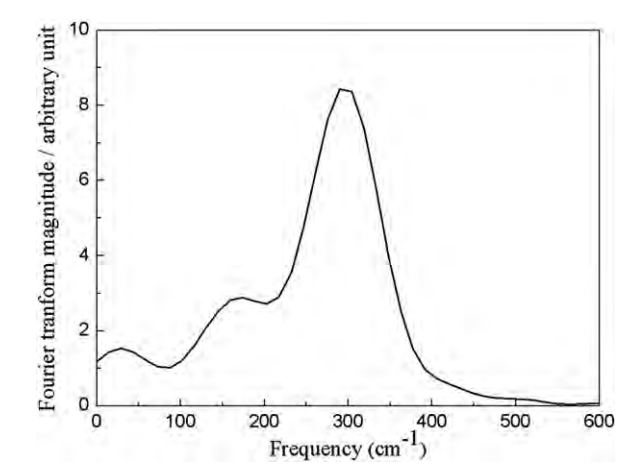


Fig. 5. Power spectra of Hg²⁺-O vibrational mode in the first hydration shell obtained from the QMCF MD simulation.

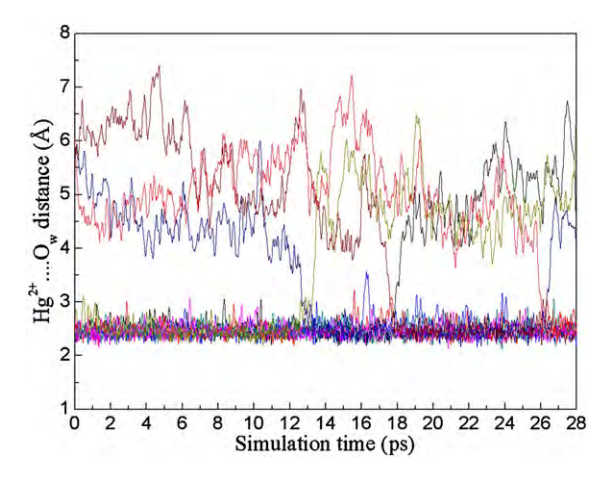


Fig. 6. Time dependence of Hg²⁺-Oxygen distances during the QMCF MD simulation, showing three water exchange processes between the first and second hydration shells.

agreement with the experimental value of $370\,\mathrm{cm}^{-1}$, with a force constant of $119.5\,\mathrm{N/m}$ [5]. In this work, the scaled force constant of $73.4\,\mathrm{N/m}$ evaluated by the QMCF simulation is slightly larger than the QM/MM value of $64\,\mathrm{N/m}$ [10]. This difference confirms the significance of the QMCF treatment for obtaining a more accurate description of this hydrated ion. Comparing to the two-shell QM/MM simulation of $\mathrm{Zn^{2+}[37]}$, which has a force constant of $60\,\mathrm{N/m}$ and a vibrational frequency of $282\,\mathrm{cm}^{-1}$, it is obvious that the $\mathrm{Hg^{2+}}$ ion can form a stronger ion-ligand complex in aqueous solution.

3.2.2. Ligand exchange processes in the first and second hydration shells During the QMCF simulation, several ligand exchange processes are observed, in particular for water molecules in the second hydration shell and the bulk. To investigate the water exchange processes around the Hg^{2+} ion, the variation of the $\mathrm{Hg} ext{-}\mathrm{O}$ distances in the first hydration shell was evaluated, as plotted in Fig. 6. As mentioned, the 6-fold coordinated complex $[Hg(H_2O)_6]^{2+}$ appears to be the most frequent structure exhibited during the 28 ps of the QMCF simulation. At around 12.5 ps, the first water migration from the second hydration shell takes place, giving a heptacoordinated $[Hg(H_2O)_7]^{2+}$ complex with a life time of about 0.6 ps. Similarly, the second and the third water exchange processes occur at the simulation times of 17.5 and 26.0 ps, respectively, with a fast water substitution reaction at the ion of about 0.3 ps. As shown in Fig. 5, these three exchange processes can be classified as an associative interchange (I_a) mechanism. In addition, the transient arrangement of the pentacoordinated $[Hg(H_2O)_5]^{2+}$ intermediate is also visible in aqueous solution, i.e., at the simulation time ~ 16 ps. The I_a mechanism identified by the QMCF simulation is in contrast to the results obtained by the MD simulation using two-body potentials performed by D'Angelo and coworkers [11,12], in which a stable 7-fold coordinated complex of the Hg²⁺ ion in aqueous solution was determined for the first-shell coordination, and the ligand exchange reactions which took place in the first hydration shell displayed the dissociative mechanism. This discrepancy can be understood due to the use of different treatments for the solute-solvent and solvent-solvent interactions in the system. In this context, the more accurate QMCF formalism yielded the quantum mechanical forces calculated for both the first and second hydration shell and, thus, can be expected to provide more reliable data.

To further analyze the dynamics details of the Hg^{2+} hydrate, the mean residence times (MRTs) of water molecules surrounding the ion were calculated using the "direct" method [36]. The number of ligand exchange processes, the mean residence times and the number of attempts needed for a sustainable ligand migration from the hydration shells of Hg^{2+} with respect to the time parameters t^* = 0.0 and 0.5 ps are summarized in Table 2. The first-shell MRT values

Table 2 Mean ligand residence times and sustainability of migration processes to and from the first and second hydration shells of the Hg^{2+} ion.

Solute	t _{sim} (ps)	$t^* = 0.0 \text{ ps}$		$t^* = 0.5$	R_{ex}	
		N_{ex}^0	$ au_{H_2O}^0$	$N_{ex}^{0.5}$	$ au_{H_{2}O}^{0.5}$	
First shell	28.0	10	16.9	6	28.2	1.7
Second shell	28.0	904	0.4	123	3.2	7.3
Bulk ^a	10.0	131	0.2	20	1.3	6.5

^a Values obtained from a QMCF MD simulation of pure water [41].

evaluated by the QMCF simulation are 16.9 and 28.2 ps for t^* =0.0 and 0.5 ps, respectively. These data correspond to 10 and 6 ligand exchange processes, respectively. For the exchange processes of water molecules in the second hydration shell, MRT values of 0.4 and 3.2 ps for t^* =0.0 and 0.5 ps are observed. Compared to the QM/MM's MRT values of 0.2–0.3 and 1.5–1.8 ps for t^* =0.0 and 0.5 ps evaluated for pure water [41], the Hg²⁺ ion clearly exhibits a strong "structure-making" ability up to its second hydration shell. The QMCF results are significantly different from the recent MD simulations using TIP5P and SPC/E water models, in which the corresponding MRT data with t^* =25 fs are predicted to be 6.1 and 7.0 ns for the first hydration shell, and 0.8 and 1.3 ps for the second hydration shell, respectively [11,12].

4. Conclusion

In this study, an *ab initio* QMCF MD simulation, which includes the complete first and second hydration shells of $\mathrm{Hg^{2+}}$ into the QM treated region, was performed to provide detailed knowledge on the structure and dynamics of the $\mathrm{Hg^{2+}}$ hydrate. With regard to the QMCF results, the observed structural parameters for the hydrated $\mathrm{Hg^{2+}}$ ion are in good agreement with the experimental data. The six-coordinated $[\mathrm{Hg(H_2O)_6}]^{2+}$ complex, is found to be the most dominant species in aqueous solution, while the arrangements of 7-fold and 5-fold coordinated complexes can transiently be formed as intermediate species. A detailed analysis of the QMCF trajectories clearly demonstrates an associative interchange (I_a) mechanism for ligand exchange processes in the first hydration shell of $\mathrm{Hg^{2+}}$. In addition, the observed MRT data for ligand migrations in the first and second hydration shells of $\mathrm{Hg^{2+}}$ clearly reveal the strong "structure-forming" ability of this ion.

Acknowledgments

This work was supported by the Higher Education Research Promotion and National Research University Project of Thailand, Office of the Higher Education Commission. V.V. would like to thank the Center for Petrochemicals and Advanced Materials, Chulalongkorn University. A.T. also acknowledges support by the Thailand Research Fund (TRF) and Suranaree University of Technology (SUT).

References

- [1] W. Stopford, L.J. Goldwater, Environmental Health Perspectives 12 (1975) 115.
- [2] C.L. van Panthaleon van Eck, H.B.M. Wolters, W.J.M. Jaspers, Recueil des Travaux Chimiques 75 (1956) 802.
- [3] T.J. Swift, W.G. Sayre, Journal of Chemical Physics 44 (1966) 3567.
- [4] G. Johansson, Acta Chemica Scandinavica, Series A 25 (1971) 2787.
- [5] M. Sandström, I. Persson, S. Ahrland, Acta Chemica Scandinavica, Series A 32 (1978) 607.
- [6] G. Johansson, M. Sandström, Acta Chemica Scandinavica, Series A 32 (1978) 109.
- [7] R. Åkesson, I. Persson, M. Sandström, U. Wahlgren, Inorganic Chemistry 33 (1994)
- [8] O. Sobolev, G.J. Cuello, G. Román-Ross, N.T. Skipper, L. Charlet, The Journal of Physical Chemistry A 111 (2007) 5123.
- [9] C. Kritayakornupong, B.M. Rode, Journal of Chemical Physics 118 (2003) 5065.
- [10] C. Kritayakornupong, K. Plankensteiner, B.M. Rode, Chemical Physics Letters 371 (2003) 438.

- [11] G. Chillemi, G. Mancini, N. Sanna, V. Barone, S.D. Longa, M. Benfatto, N.V. Pavel, P. D'Angelo, Journal of the American Chemical Society 129 (2007) 5430.
- [12] G. Mancini, N. Sanna, V. Barone, V. Migliorati, P. D'Angelo, G. Chillemi, The Journal of Physical Chemistry B 112 (2008) 4694.
- [13] S.T. Moin, T.S. Hofer, A.B. Pribil, B.R. Randolf, B.M. Rode, Inorganic Chemistry 49 (2010) 5101.
- [14] V. Vchirawongkwin, A.B. Pribil, B.M. Rode, Journal of Computational Chemistry 31 (2010) 249.
- [15] C. Kritayakornupong, V. Vchirawongkwin, T.S. Hofer, B.M. Rode, The Journal of Physical Chemistry B 112 (2008) 12032.
- [16] C. Kritayakornupong, V. Vchirawongkwin, B.M. Rode, Journal of Computational Chemistry 31 (2010) 1785.
- [17] R.J. Frick, T.S. Hofer, A.B. Pribil, B.R. Randolf, B.M. Rode, The Journal of Physical Chemistry A 113 (2009) 12496.
- [18] L.H.V. Lim, A.B. Pribil, A.E. Ellmerer, B.R. Randolf, B.M. Rode, Journal of Computational Chemistry 31 (2010) 1200.
- [19] C. Kritayakornupong, V. Vchirawongkwin, B.M. Rode, The Journal of Physical Chemistry B 114 (2010) 12883.
- [20] B.M. Rode, T.S. Hofer, B.R. Randolf, C.F. Schwenk, D. Xenides, V. Vchirawongkwin, Theoretical Chemistry Accounts 115 (2006) 77
- Theoretical Chemistry Accounts 115 (2006) 77.

 [21] T.S. Hofer, A.B. Pribil, B.R. Randolf, B.M. Rode, Ab Initio Quantum Mechanical Charge Field Molecular Dynamics-A Nonparameterized First-Principle Approach to Liquids and Solutions, Academic Press, Elsevier Inc., 2001.
- [22] M.J. Field, P.A. Bash, M. Karplus, Journal of Computational Chemistry 11 (1990)
- [23] J. Gao, Journal of the American Chemical Society 115 (1993) 2930.
- [24] D. Bakowies, W. Thiel, Journal of Physical Chemistry 100 (1996) 10580.

- [25] P. Bopp, G. Janscó, K. Heinzinger, Chemical Physics Letters 98 (1983) 129.
- [26] F.H. Stillinger, A. Rahman, Journal of Chemical Physics 68 (1978) 666.
- [27] B.R. Brooks, R.E. Bruccoleri, B.D. Olafson, D.J. States, S. Swaminathan, M. Karplus, Journal of Computational Chemistry 4 (1983) 187.
- [28] R. Ahlrichs, M. Bär, M. Häser, H. Horn, C. Kölmel, Chemical Physics Letters 162 (1989) 165.
- [29] R. Ahlrichs, M. von Arnim, Methods and Techniques in Computational Chemistry: METECC-95, , 1995 (Cagliari, Sardinia).
- [30] M. von Arnim, R. Ahlrichs, Journal of Computational Chemistry 19 (1998)
- [31] W.J. Stevens, M. Krauss, H. Basch, P.G. Jasien, Canadian Journal of Physics 70 (1992) 612
- [32] T.H. Dunning Jr., Journal of Chemical Physics 53 (1970) 2823.
- [33] T.H. Dunning Jr., P.J. Hay, in: H.F. Schaefer III (Ed.), Methods of Electronic Structure Theory, Vol. 3. Plenum. New York. 1977.
- ture Theory, Vol. 3, Plenum, New York, 1977.

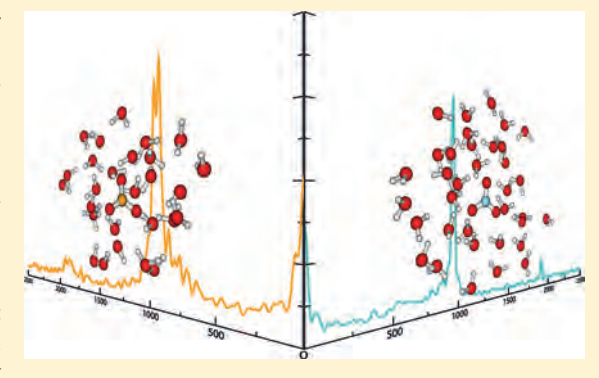
 [34] H.J.C. Berendsen, J.P.M. Postma, W.F. van Gunsteren, A. DiNola, J.R. Haak, Journal of Chemical Physics 81 (1984) 3684.
- [35] D.J. Adams, E.H. Adams, G. Hills, Journal of Molecular Physics 38 (1979) 387.
- [36] T.S. Hofer, H.T. Tran, C.F. Schwenk, B.M. Rode, Journal of Computational Chemistry 25 (2004) 211.
- [37] M.Q. Fatmi, T.S. Hofer, B.M. Rode, B.R. Randolf, Journal of Chemical Physics 123 (2005) 054514.
- [38] R.S. Grev, C.L. Janssen, H.F. Schaefer III, Journal of Chemical Physics 95 (1991) 5128.
- [39] A.P. Scott, L. Random, Journal of Physical Chemistry 100 (1996) 16502.
- [40] D.J. DeFrees, A.D. McLean, Journal of Chemical Physics 82 (1985) 333.
- [41] B.R. Randolf, T.S. Hofer, B.M. Rode, Unpublished results.

pubs.acs.org/JPCB

Symmetry Breaking and Hydration Structure of Carbonate and Nitrate in Aqueous Solutions: A Study by Ab Initio Quantum Mechanical Charge Field Molecular Dynamics

Viwat Vchirawongkwin, *Chinapong Kritayakornupong, *Anan Tongraar, *, * and Bernd M. Rode|

ABSTRACT: The ab initio quantum mechanical charge field molecular dynamics (QMCF MD) formalism was applied to simulate carbonate and nitrate anions in aqueous solution. The out-of-plane (ν_2) spectra obtained from the velocity autocorrelation functions (VACFs) and the torsion angle—time functions indicate that the symmetry of carbonate is reduced from D_{3h} to a lower degree by breaking up the molecular plane, whereas the planarity of nitrate anion is retained. The calculated frequencies are in good agreement with the Raman and IR data. Carbonate shows a stronger molecular hydration shell than the nitrate anion with the average molecular coordination numbers of 8.9 and 7.9, respectively. A comparison with the average number of ion—solvent hydrogen bonds (H-bonds) indicates the extra water molecules within the hydration shell of carbonate (~ 2) and nitrate (~ 3) , readily



migrating from one coordinating site to another. The mean residence times for water ligands in general classify carbonate and nitrate as moderate and weak structure-making anions, while the specific values for individual sites of nitrate reveal local weak structure-breaking properties.

■ INTRODUCTION

The carbonate and nitrate anions play an important role in biological and environmental systems. 1-3 The level of carbonate anion in seawater relates to atmospheric CO₂. The carbonate is an ubiquitous and reactive anion and reacts to form aqueous and solid state complexes with a majority of metals in the periodic table.4 The nitrate anion is one of the reactive nitrogen forms, occurring in many biological systems,³ and a strong oxidizing agent. All nitrate salts are highly soluble. The nitrate anion is also produced in the human body by the oxidation of nitric oxide obtained from the reaction between the enzyme nitric oxide synthase and L-arginine. 5,6 It is interesting that X-ray scattering experiments have investigated many nitrate solutions, 7-11 while experimental data are rare for the carbonate anion. Recent neutron diffraction studies with isotopic substitution were performed for the CsNO₃ and Cs₂CO₃ solutions, concluding that hydrogen bonds between water molecules and carbonate are stronger than those formed with nitrate. 12 The reported average coordination number of nitrate is in the range of 5.9 to 9, 13 while it is close to unavailable for carbonate.

The isolated structure of these anions is normally planar with D_{3h} symmetry, which has six normal modes consisting of two single modes, namely, the symmetric stretch (ν_1) and out-of-plane

deformation (v_2) , and two doubly degenerate modes, namely, the antisymmetric stretch (ν_3) and in-plane deformation (ν_4) . Rudolph et al. reported the symmetry breaking from the D_{3h} to lower symmetry in the concentrated 14 and dilute 15 carbonate solutions due to a strong and asymmetric hydration via Raman and infrared experiments and also optimized the carbonate water cluster with two water molecules employing density functional theory at the B3LYP level with the 6-31+G* basis set in the gas phase, resulting in $C_{2\nu}$ symmetry. ¹⁴ The far-ultraviolet resonance Raman spectroscopy indicates the planarity of nitrate ion in several polar solvents, but with the symmetry being broken from D_{3h} to $C_{2\nu}$ or C_s due to a very broad band of ν_3 . ^{16,17} The results of photoelectron spectroscopy suggested the first hydration consisting of three water molecules with C_{3h} symmetry for the nitrate ion in aqueous solution.¹⁸ Raman studies have reported that the splitting of v_3 vanishes for dilute nitrate solutions. ^{19–21} Recent infrared multiple photon photodissociation experiments of $NO_3^-(H_2O)_n$ clusters, n = 1-6, observed the splitting of v_3 band due to the perturbation of water molecules, showing the

Received: May 24, 2011
Revised: September 8, 2011
Published: September 20, 2011

[†]Department of Chemistry, Faculty of Science, Chulalongkorn University, Phayathai Road, Patumwan, Bangkok 10330, Thailand

[‡]Department of Chemistry, Faculty of Science, King Mongkut's University of Technology, Thonburi, Bangkok 10140, Thailand

[§]School of Chemistry, Institute of Science, Suranaree University of Technology, Nakhon Ratchasima 30000, Thailand

Theoretical Chemistry Division, Institute of General, Inorganic and Theoretical Chemistry, University of Innsbruck, Innrain 52a, A-6020 Innsbruck, Austria

possible lowering of symmetry to C_1 .²² The weighted average IR spectra of the optimized geometries for the microhydration of carbonate and nitrate anion presented an effect of explicit waters on symmetry lowering. ^{23,24} The optimization of the carbonate ion in aqueous solution as a dielectric medium employing the electron correlated method with the generalized conductorlike screening model indicated a slight effect of solvent on the geometry compared with the gaseous state.²⁵ An empirical force field including the out-of-plane displacement of the carbon atom within the carbonate ion was developed to investigate the phase transition of calcite.²⁶ This potential function was adopted by increasing the stiffness of carbonate ion utilized in the classical molecular dynamics (MD) simulation of calcium carbonate.² Recent investigations of the carbonate ion in aqueous solution based on Car-Parrinello (CP) MD simulation discussed the structural properties of the hydration shell without addressing symmetry breaking.^{28,29} The inclusion of an intramolecular anharmonic force field in the classical MD simulation³⁰ and a combined quantum mechanics/molecular mechanics (QM/ MM) MD simulation³¹ of hydrated nitrate ion presented a splitting of v_3 in agreement with the spectroscopic results. The reference interaction site model self-consistent field spatial electron density distribution (RISM-SCF-SEDD) provided the evidence of symmetry breaking for the carbonate in the isotropic environment, while the planarity of nitrate anion was claimed.³² All of these results here motivated us to reinvestigate the influence of hydration on the symmetry breaking and also the characteristics of the hydration structures of both anions by a contemporary ab initio simulation method.

Due to the limitations of conventional QM/MM methods to study composite solutes due to the tedious task to construct intermolecular potential functions accounting for the interactions between each site of solute and water, we applied the ab initio quantum mechanical charge field molecular dynamics (QMCF MD) formalism^{33,34} that has already been successfully employed to investigate the structural and dynamical properties of hydrated sulfate, ^{35,36} phosphate, ^{37,38} perchlorate, ^{37,39} bicarbonate, ^{40,41} and bisulfate ⁴² anions. The vibrational spectra of the anions in water are evaluated from the velocity autocorrelation functions (VACFs) to investigate the evidence of broken symmetry. The structural properties for each hydration site and the whole molecular shell were obtained via radial distribution functions (RDFs) and coordination number distributions (CNDs). The average number of hydrogen bonds (H-bonds) was also evaluated for each coordinating site to clarify the actual coordination of the solvent. The dynamics were characterized by ligand mean residence times (MRTs). In addition, we evaluated structural and dynamical properties by means of the molecular approach. 40,42

METHODS

The ab initio QMCF MD formalism has been summarized in detail elsewhere. 33,34 Due to the inclusion of an additional quantum mechanically treated solvent *layer zone* located beyond the first hydration shell of the solute species, the QMCF method avoids the construction of potential functions between the solute and the water molecules; that is, it evades a time-consuming and sometimes hardly tractable task essential in the conventional QM/MM MD formalism. 43-46 The involvement of the point charges of the atoms in the MM region with their changing positions in the core Hamiltonian for the QM calculations is a

useful feature of the QMCF MD method with a perturbation term,

$$V' = \sum_{i=1}^{n} \sum_{j=1}^{m} \frac{q_j^{\text{MM}}}{r_{ij}} \tag{1}$$

where n is the number of atoms in the QM region, m is the number of atoms in the MM region, $q_j^{\rm MM}$ is the partial charges of these atoms according to the selected water model, and r_{ij} refers to the distance between a pair of particles in the QM (i) and MM (j) regions. On the other hand, the dynamically changing charges of QM particles, $q_i^{\rm QM}$, determined by population analysis contribute to the force on each atom j in the MM region as Coulombic forces,

$$F_j^{\text{QM} \to \text{MM}} = \sum_{i=1}^n \frac{q_i^{\text{QM}} \cdot q_j^{\text{MM}}}{r_{ij}}$$
 (2)

As the conventional QM/MM MD formalism, the QMCF MD method permits the migration of water molecules between the QM and the MM region. For this process, one has to apply a smoothing function, 47

$$S(r) = \begin{cases} 0 & \text{for } r > r_{\text{on}} \\ \frac{(r_{\text{off}}^2 - r^2)^2 (r_{\text{off}}^2 + 2r^2 - 3r_{\text{on}}^2)}{(r_{\text{off}}^2 - r_{\text{on}}^2)^3} & \text{for } r_{\text{on}} \le r \le r_{\text{off}} \\ 1 & \text{for } r < r_{\text{off}} \end{cases}$$

where r is the distance of a given solvent molecule from the center of the simulation box, $r_{\rm off}$ is the radius of the QM region, and $r_{\rm on}$ is the inner border of the smoothing region. The formalism is applied to all atoms of molecules located in the smoothing region, ensuring a continuous transition and change of forces for these molecules according to

$$F_{j}^{\text{smooth}} = F_{j}^{\text{MM}} + (F_{j}^{\text{layer}} - F_{j}^{\text{MM}}) \times S(r)$$
 (4)

where F_j^{layer} is the force acting on a particle j located in the (outer QM) smoothing zone and F_j^{MM} is the force acting on a particle j in the MM region. In this context it has to be mentioned that energy is not rigorously conserved, but the related error can be considered very minor due to the short simulation time and the large size of the quantum mechanical region.

The systems consisted of 496 water molecules with one carbonate and one nitrate anion in the carbonate and nitrate solution, respectively. Both solutions were represented by a cubic box of 24.65 Å with periodic boundary conditions. The density of the simulation boxes was 0.997 g cm⁻³, that is, the experimental value of pure water at 298 K. The simulation was performed in the NVT ensemble using a general predictor-corrector algorithm with a time step of 0.2 fs. The system temperature was maintained at 298.16 K by the Berendsen temperature-scaling algorithm⁴⁸ with a relaxation time of 100 fs. Although this temperature-scaling algorithm requires, in principle, a long simulation period to sufficiently describe the phase space, a large number of successful publications of QMCF MD simulations 35-42 indicate that our simulation period of 10 ps is adequate to reproduce the properties of hydrated ions well. The QM subregions, namely, the core and laver zone, extended for the carbonate and nitrate anions to 3.5 and 6.0 Å and 3.5 and 6.8 Å, respectively. The structural and dynamical results obtained from our previous

QMCF MD studies^{35–42} have also indicated the Hartree–Fock (HF) method to be a good compromise between accuracy and affordable computational effort; thus the quantum mechanical calculation was performed by the HF method with the Dunning double-ζ plus polarization (DZP)^{49,50} basis sets for hydrogen and oxygen atoms of water molecules and the Dunning double- ζ plus polarization and diffuse functions (DZP+)^{49,50} basis sets for carbon, nitrogen, and oxygen atoms of the carbonate and nitrate anions. Although HF and the methodical problems associated with the thermostat probably leads to slightly underestimated values, our previous study indicated that the associated errors are probably within a 10% to 20% range. 42 The thickness of the smoothing region was chosen as 0.2 Å, corresponding with the smooth exchange of a water between the QM and MM regions of the conventional QM/MM MD formalism. 51 The values of $r_{\rm on}$ and $r_{\rm off}$ are 5.8 and 6.0 Å and 6.6 and 6.8 Å for the carbonate and nitrate anions, according to the RDFs obtained from the equilibrated simulations. The large size of the QM region ensures that it is possible to neglect the interactions between the solute and the solvent molecules in the MM region.³³ The flexible BJH-CF2 water model^{52,53} was applied to calculate the interactions between pairs of water in the MM region, with the cutoff distances of 3.0 and 5.0 Å for non-Coulombic interactions between H atoms and between O and H atoms, respectively. According to the verification process by the water simulations in the development of the QMCF MD formalism, this water model satisfied to describe several microscopic and macroscopic properties of water.³³ The partial charges for oxygen and hydrogen atoms in the water molecule according to this model are -0.65966 and +0.32983. This water model supports the fully flexible geometries of water molecules transiting between the QM and MM region. The Coulombic interactions between the Mulliken charges on the atoms within the QM region and the point charges of water molecules according to the BJH-CF2 model are evaluated providing an electrostatic description by a dynamically changing field of point charges, which change according to the movements of atoms inside the QM region and water molecules in the MM region during the simulation. This ensures the continuous adaptation of the Coulombic interactions to all polarization and chargetransfer effects within the solute and surrounding solvent layers. 33,34 In addition, the reaction field method combined with the shiftedforce potential technique were applied to account for long-range electrostatic potentials and forces, with a spherical cutoff limit of 12.350 Å. The systems were equilibrated with the QMCF MD method for 50 000 steps (10 ps), and a further 50 000 steps (10 ps) were collected as data sampling for analyzing the structural and dynamical properties. The average number of water molecules in the QM region was 23.6 and 36.6 for the carbonate and nitrate solution, respectively.

The structural and dynamical properties for the hydration shell of carbonate and nitrate anions were evaluated in individual and molecular manners. The molecular hydration shell of these anions was constructed by the combination of all atomic hydration spheres of each anion. The coordinating site for each water molecule to the anions was defined by searching for the shortest distance between the oxygen atom of water molecule and each atom within each anion. The molecular RDFs, molecular CNDs, and molecular ligand MRTs for the hydration shell of carbonate and nitrate anions are thus presented in this article. All MRT values were evaluated by the direct method, counting the water exchange processes between hydration shell and bulk. The most appropriate time span to record a water displacement from

its original coordination sphere as an exchange process is 0.5 ps, ^{54,55} which corresponds to the average lifetime of a hydrogen bond in the solvent. ⁵⁶

The dynamical properties of a fluid system related to macroscopic transport coefficients can be evaluated from the VACFs, and their Fourier transformations deliver the vibrational spectra via normal-coordinate analysis. ⁵⁷ The normalized VACF, C(t), is defined as

$$C(t) = \frac{\sum_{i}^{N_{t}} \sum_{j}^{N} \nu_{j}(t_{i}) \nu_{j}(t_{i} + t)}{N_{t} N \sum_{i}^{N_{t}} \sum_{j}^{N} \nu_{j}(t_{i}) \nu_{j}(t_{i})}$$
(5)

where N is the number of particles, N_t is the number of time origins t_i , and v_j denotes a certain velocity component of the particle j. A correlation length of 2.0 ps was used to obtain the power spectra with 4000 averaged time origins.

■ RESULTS AND DISCUSSION

Structural and Dynamical Properties of CO₃²⁻ and NO₃⁻ Anions. According to the dynamic movement of all atoms within the systems throughout the simulation period, the averaged geometric parameters such as bond distances, angles, and torsion angles of carbonate and nitrate anions indicate the quality of the selected theoretical level, HF/DZP+, for the QM calculations. The C- and N-torsion angles were defined to investigate the planarity of the solutes as the C-O(1)-O(2)-O(3) and N-O(1)-O(2)-O(3) dihedral angles, respectively. The average C-O distances varying within 0.003 Å are slightly longer than those in the HCO₃ by 0.04 Å, ⁴⁰ while the N-O distances varying within 0.002 Å are slightly shorter than those obtained from the conventional HF/MM simulation of nitrate solution by 0.03 Å.31 These tiny deviations show the similarity of the bonds within each anion. The bond and torsion angles were collected in the form of angular distribution functions (AFDs). The average bond angles around the center atoms again indicate the equivalence of oxygens within each anion. The average C-torsion and N-torsion angles with their deviation of $1^{\circ} \pm 4^{\circ}$ and $0^{\circ} \pm 2^{\circ}$ reflect the planarity of both anions. Table 1 reports the averaged geometric parameters with their statistical deviation obtained from the QMCF MD simulation, comparing with those parameters obtained from various methods evaluated in the gas phase and solution utilizing the polarizable continuum model (PCM).58 Our geometry parameters were also compared with those obtained from the reference interaction site model self-consistent field (RISM-SCF) at the HF and B3LYP level with the 6-311+G* basis set.³² The hybrid B3LYP exchange-correlation functional coupling with the tzvp+ basis set⁵⁹ was employed to verify the interpretation of the spectra of photoelectron spectroscopy for the HSO_4^- ion, ⁶⁰ and this was also applied to verify the theoretical level in our previous work. 42 Thus, we again utilized this basis set coupling with the Hartree-Fock (HF), B3LYP, and quadratic CI calculation including single and double substitutions (QCISD) levels to optimize the geometries of carbonate and nitrate in both phases. The HF/DZP+ level was also employed to investigate the effect of isotropic and uniform field generated by the PCM on the geometries of both anions. The bond distances of anions in the solution phase treated with PCM are shorter than those in gas phase by ca. 0.01 Å, whereas these averaged distances obtained

Table 1. Structural Parameters for the Geometry of ${\rm CO_3}^{2-}$ and ${\rm NO_3}^-$ Ions Obtained from Averaging Their Distributions with Their Variations

		HF/	DZP+	HF	tzvp+	B3LY	P/tzvp+	QCIS	D/tzvp+	RISM-SCI	F/6-311+G* ³²
structural parameter	QMCF MD	gas	PCM	gas	PCM	gas	PCM	gas	PCM	HF	B3LYP
					CO ₃ ²⁻						
C-O(1) (Å)	1.290 ± 0.035	1.288	1.279	1.286	1.277	1.312	1.302	1.314	1.303	1.267	1.288
C-O(2) (Å)	1.287 ± 0.032	1.288	1.279	1.286	1.277	1.312	1.302	1.314	1.303	1.267	1.288
C-O(3) (Å)	1.290 ± 0.035	1.288	1.279	1.286	1.277	1.312	1.302	1.314	1.303	1.267	1.288
$\angle O(1)CO(2)$ (deg)	120 ± 4	120	120	120	120	120	120	120	120	120	120
∠O(2)CO(3) (deg)	120 ± 3	120	120	120	120	120	120	120	120	120	120
C-torsion (deg)	1 ± 4	0	0	0	0	0	0	0	0	7	8
					NO_3^-						
N-O(1) (Å)	1.231 ± 0.023	1.232	1.229	1.231	1.228	1.268	1.265	1.270	1.268	1.217	1.253
N-O(2) (Å)	1.232 ± 0.022	1.232	1.229	1.231	1.228	1.268	1.265	1.270	1.268	1.217	1.253
N-O(3) (Å)	1.233 ± 0.025	1.232	1.229	1.231	1.228	1.268	1.265	1.270	1.268	1.217	1.253
$\angle O(1)NO(2)$ (deg)	120 ± 3	120	120	120	120	120	120	120	120	120	120
$\angle O(2)NO(3)$ (deg)	120 ± 3	120	120	120	120	120	120	120	120	120	120
N-torsion (deg)	0 ± 2	0	0	0	0	0	0	0	0	0	0

Table 2. C-O and N-O Distances within the $CO_3^{2-}(H_2O)_n$ and $NO_3^{-}(H_2O)_n$ Clusters Obtained from the Optimizations in the Gas Phase at the HF, MP2, and CCSD Levels

	HF				MP2		CCSD		
n	X-O(1)	X-O(2)	X-O(3)	X-O(1)	X-O(2)	X-O(3)	X-O(1)	X-O(2)	X-O(3)
1	1.292	1.292	1.273	1.325	1.325	1.302	1.319	1.319	1.297
2	1.279	1.296	1.279	1.308	1.330	1.308	1.303	1.324	1.303
3	1.283	1.283	1.283	1.313	1.313	1.313	1.308	1.308	1.308
					NO ₃				
1	1.235	1.235	1.223	1.282	1.282	1.269	1.274	1.274	1.259
2	1.225	1.239	1.227	1.271	1.290	1.271	1.262	1.282	1.262
3	1.230	1.230	1.230	1.276	1.276	1.276	1.267	1.267	1.267

from the QMCF MD simulations affected by the explicit water molecules are close to those obtained from the HF/DZP+ optimized geometries in the gas phase. To clarify this point, we optimized each anion with one to three water molecules by applying the DZP+ basis set on the atoms within each anion and the DZP basis set on the H and O atoms in water molecules at the HF, MP2, and CCSD levels. The C-O and N-O distances in these small water clusters are listed in Table 2. Their average binding energies are also shown in Table 3. It indicates that the explicit waters with and without the electron correlation effect also affects the bonds in both anions by reducing the distances as in the PCM approach (cf. Table 1). Due to the intermolecular interaction described by the electron correlation method, the MP2 and CCSD levels give stronger binding energies than the HF calculations. With increasing number of water molecules in the system convergence of average binding energies from the HF calculations to the higher methods is observed, especially for the nitrate anion. There is evidence that the perturbation of the Hamiltonian from the point charges in the QMCF MD formalism improves the interactions within the solution, resulting in elongated bond distances that are a good agreement with the

Table 3. Average Binding Energies in kcal mol^{-1} for $\mathrm{CO_3}^{2-}$ - $(\mathrm{H_2O})_n$ and $\mathrm{NO_3}^-(\mathrm{H_2O})_n$ Clusters Obtained from the Optimizations in the Gas Phase at the HF, MP2, and CCSD Levels

n	HF	MP2	CCSD
	(CO ₃ ²⁻	
1	-34.9	-37.3	-36.8
2	-33.4	-35.5	-35.0
3	-32.2	-33.9	-33.4
	:	NO ₃	
1	-13.9	-14.1	-14.2
2	-13.3	-13.5	-13.6
3	-12.7	-12.7	-12.8

 $C-O_C$ of 1.3 Å and $N-O_N$ in a range from 1.21 \pm 0.02 to 1.24 \pm 0.02 Å, respectively, reported from the recent neutron diffraction experiments of $K_2CO_3^{~61}$ and $NaNO_3^{~11}$ solutions.

The C-torsion and N-torsion angles from the gas phase and PCM calculations show the planarity of each anion, but the

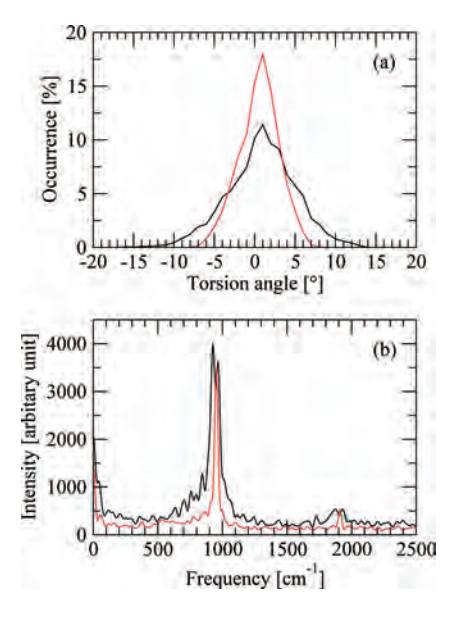


Figure 1. (a) Dihedral angle distribution of the torsion angles and (b) Fourier transformation of the function of time for their angles; the black and red solid lines refer to the C-torsion and N-torsion angles, respectively.

RISM-SCF results indicate a symmetry breaking of the carbonate anion.³² Although the average C-torsion obtained from the QMCF MD simulations ($1^{\circ} \pm 4^{\circ}$) shows a slight removal of the C atom from the molecular plane, it might be a consequence of the limited number of geometries in the short simulation period of 10 ps. It is interesting to investigate the possibility of the symmetry breaking for both anions. According to the motion of all atoms in the MD formalism, the center atoms also oscillate during the simulation period. The ADFs in Figure 1a present a higher flexibility of C-torsion $(-14^{\circ} \text{ to } 16^{\circ})$ compared to the N-torsion $(-8^{\circ} \text{ to } 8^{\circ})$. The Fourier transformations for the C-torsion and N-torsion as the function of time are shown in Figure 1b, presenting two peaks situated at 927 and 967 cm⁻¹ for the carbonate, and the peak at 953 cm⁻¹ for the nitrate anion. These values correspond to the out-of-plane deformation (ν_2) reported from Raman experiments at 884 and 832 cm⁻¹ for the carbonate and nitrate anions. The spectra in Figure 1b also display small peaks with a low intensity at 1873 and 1930 cm⁻¹ for the carbonate and at 1910 cm⁻¹ for the nitrate anion, corresponding to the Raman observations for the overtone of the out-of-plane deformation $(2\nu_2)$ at 1764 and 1658 cm⁻¹ in carbonate ^{14,15} and nitrate ^{16,17,21} solutions, respectively. The differences of v_2 frequencies between both anions and between the atomic masses of C and N are small; thus the harmonic motion and its force constant of C-torsion and N-torsion should be similar. Whereas a significant difference of both anions is observed, the range of C-torsion in Figure 1a is ca. two times that of the N-torsion ADF. The agreements of QM calculations, RISM-SCFs, and our QMCF MD simulation let us conclude that the nitrate anion mostly retains its planarity in the solution. The symmetric band of the N-torsion corresponds to an out-ofplane displacement of N atom around 0°, implying the amplitude of this oscillation in the QMCF MD simulation be 8°. The range of the C-torsion covers the value of $\pm 7^{\circ}$ reported from the RISM-SCF/HF³² and an oscillating amplitude of $\pm 8^{\circ}$, indicating the occurrence of symmetry breaking for the carbonate anion in solution during the simulation period.

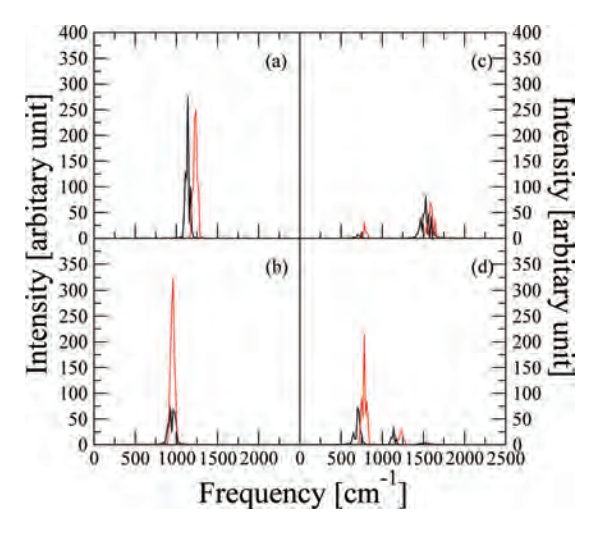


Figure 2. Power spectra of (a) ν_1 , (b) ν_2 , (c) ν_3 , and (d) ν_4 modes for the D_{3h} symmetry of ${\rm CO_3}^{2-}$ (black solid lines) and ${\rm NO_3}^-$ (red solid lines) anions.

One dynamical property, namely, the vibrational spectrum, is an important property as it can be compared with the Raman (R) and infrared (IR) data. The spectra calculated via VACFs from the QMCF MD simulation require an assignment of the point group to the solute. The nitrate anion has approximately identical bond distances and planar geometry of D_{3h} symmetry. Although there is evidence indicating symmetry breaking for the carbonate anion, we also assumed a molecular plane with the D_{3h} symmetry for this anion due to a low barrier of the free energy surface (less than 5 kcal mol⁻¹) obtained from the RISM-SCF calculations and a symmetric oscillation of the C atom throughout the simulation period. Four fundamental modes of the D_{3h} symmetry will span the following representation:

$$\Gamma(D_{3h}) = a'_{1}(R) + 2e'(R, IR) + a''_{2}(IR)$$
 (6)

These modes consist of the symmetric stretch, $\nu_1(a'_1)$, the outof-plane deformation, $\nu_2(a''_2)$, the antisymmetric stretch, $\nu_3(e')$, and the in-plane deformation, $\nu_4(e')$ modes. The power spectra of these normal modes for the carbonate and nitrate anions predicted by the QMCF MD simulations are displayed in Figure 2, and the frequencies of peaks for each mode are listed in Table 4.

The bands of v_2 in Figure 2b, showing a split peak for the carbonate anion, have a similar pattern with the Fourier transformations for the C-torsion and N-torsion as the function of time in Figure 1b; however, the overtone peaks disappear in the spectra obtained from the VACFs. This again confirms the broken symmetry of the carbonate anion's molecular plane, while the plane is still retained in the nitrate anion. The ν_3 and ν_4 are degenerate modes, presented by the dominant band with the appearance of a minor band of another mode in the spectrum of each mode. Furthermore, v_4 also appears as a minor peak of v_1 , according to a contamination of bond stretching in a vector projection. The calculated v_3 and v_4 spectra with a band characteristic interpreted as a reduction of symmetry to $C_{2\nu}$ or to $C_{\epsilon}^{16,17}$ correspond to the dynamical motions of these anions within the environment of explicit waters during the simulation period. The frequencies of the solutes within the optimized $CO_3^{2-}(H_2O)_3$ and $NO_3^{-}(H_2O)_3$ clusters evaluated at the MP2 and CCSD levels are also listed in Table 4. MP2 and CCSD

predict a lower ν_1 of the carbonate anion than the experimental value, reflecting an overestimated interaction of the solute with water molecules. However, these correlated methods indicate a weak interaction of nitrate anion with solvent resulting in a higher ν_1 than the Raman result. To further investigate the influence of correlation in the liquid state was impossible, as the application of these methods in the QMCF simulations is beyond present computational feasibility. All calculated frequencies obtained without applying a scaling factor from the QMCF MD simulations are higher than the values reported from the Raman experiment 14 by \sim 230 cm $^{-1}$. We also calculated the frequencies scaled with the factor 0.902 obtained from the correction of the QMCF MD results with the coupled-cluster singles and doubles (CCSD) level. 36 The scaled frequencies of carbonate anion are

Table 4. Vibration Frequencies (cm $^{-1}$) for Each Normal Mode of $\mathrm{CO_3}^{2-}$ and $\mathrm{NO_3}^{-}$ Anions Evaluated by the VACFs of QMCF MD Simulations, Given Scaled by the Factor 0.902 36 in Parentheses

		frequency (cm ⁻¹)						
	$v_1(a'_1)$	$v_2(a''_2)$	$\nu_3(e')$	$\nu_4(e')$				
	(CO ₃ ²⁻						
QMCF MD	1140	928, 961	1531	700				
	(1028)	(837, 867)	(1381)	(631)				
MP2	1026	841	1403	684				
CCSD	1046	864	1432	692				
$exptl^{14}$	1066	884	1385	684				
	1	NO_3^-						
QMCF MD	1238	961	1580	782				
	(1117)	(867)	(1425)	(705)				
MP2	1070	790	1529	712				
CCSD	1088	821	1440	715				
HF/MM MD ^{a,31}	1088	712	1401, 1441	709				
$B3LYP/MM MD^{b,31}$	965	710	1237, 1313	649				
$exptl^{14}$	1048	832	1348	718				

 $[^]a\mathrm{The}$ reported values are scaled by 0.9051. $^b\mathrm{The}$ reported values are scaled by 0.9614.

red-shifted by \sim 50 cm⁻¹, while the scaled ν_1 , ν_2 , and ν_3 of the nitrate anion are blue-shifted by \sim 80 cm⁻¹ compared with the experimental data. The agreement of calculated frequencies, especially the scaled values, for these modes with the experimental data again shows the reliability of the QMCF MD simulation to acquire dynamical properties of the solutes. $^{37-42}$

Structural and Dynamical Properties of the Hydration Shell. According to the preliminary equilibrations of system boxes, their RDFs, or $g_{\alpha\beta}(r)$, suggested that the boundary of QM region should be selected as 6.0 and 6.8 Å for the carbonate and nitrate solutions. The larger QM size for the nitrate system is caused by the weak interactions between the anion with its hydration shell, resulting in a larger number of water molecules within this region during the simulation period than in the case of carbonate anion (ca. 13 molecules). The boundary of the hydration shell from the $C \cdots O_{water}$ and $N \cdots O_{water}$ RDFs is located at 4.48 Å and 4.74 Å, respectively, which implies that the hydration shell of the center atom extends from the terminal oxygens to 3.19 and 3.51 Å for the carbonate and nitrate anion. The O(1), O(2), and O(3) atoms were assigned to represent the coordinating sites for both anions producing the hydration shell around each molecular solute. The individual RDF of each site associated with its CND for both anions are displayed in Figure 3. The height of $g_{\alpha\beta}(r_{\rm max})$ for the carbonate indicates a stronger structure of the individual hydration shells than those of the nitrate anion, agreeing with the results that the water molecules form stronger hydrogen bonds with carbonate than nitrate anion concluded from the neutron diffraction with isotopic substitution (NDIS) of Cs₂CO₃ and CsNO₃ in aqueous solutions. 12 It is in good agreement with average binding energies of the small water clusters for the carbonate and nitrate anions calculated at the various levels shown in Table 3, which also indicates the stronger hydration shell of carbonate than that of nitrate anion. The first peak of (site) \cdots O_{water} RDFs for the carbonate anion situated at 2.70 Å is in good agreement with those obtained from the first classical MD for this anion (2.69 Å),²⁷ while the slightly shorter (\sim 0.06 Å) peak of (site) \cdots H_{water} RDFs from the QMCF MD simulation than those from the classical MD $(1.78 \, \text{Å})^{27}$ reflects a stronger hydrogen bonding caused by quantum effects. For the nitrate anion, the first peak of (site) · · · O_{water} RDFs from the QMCF MD simulation is slightly longer than those obtained

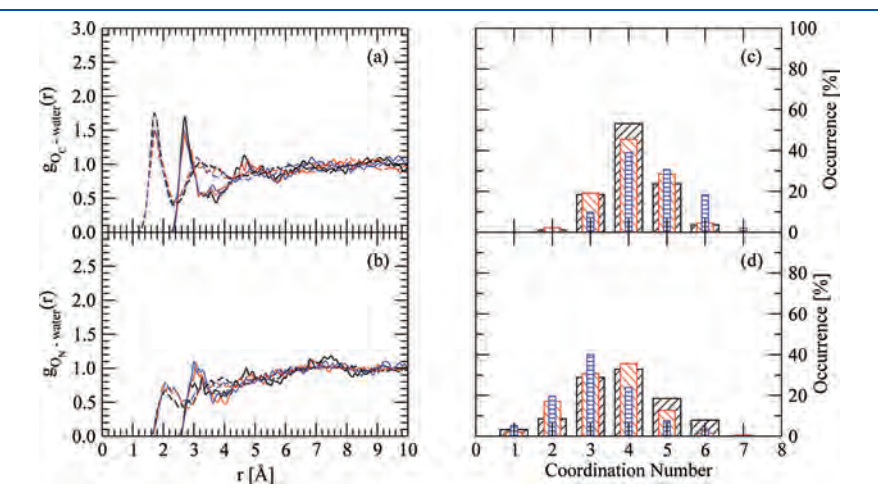


Figure 3. Individual RDF plots of (a) O_C —water and (b) O_N —water, which solid and dashed lines refer to the RDFs for the O and H atoms of water, for CO_3^{2-} and NO_3^{-} anions, respectively. Hydration shell CNDs of each O sites within the (c) CO_3^{2-} and (d) NO_3^{-} anions. The black, red, and blue colors refer to the O(1), O(2), and O(3) atoms within each anion, respectively.

Table 5. Characteristic Values of the Radial Distribution Function $g_{\alpha\beta}(r)$ for Each Site of ${\rm CO_3}^{2-}$ and ${\rm NO_3}^-$ Anions in the Hydration Shell Determined by the QMCF MD Simulation

coordinating site	$r_{\text{max}}(O_{\text{w}})^a$	$r_{\min}(O_w)^a$	$r_{\rm max}({\rm H_w})^a$	$r_{\min}(H_w)^a$	n^a
Ü	mux (W)	mm (11)	max (W)	IIII (117	
		CO_3^{2-}			
O(1)	2.70	3.72	1.71	2.38	4.1
O(2)	2.70	3.74	1.74	2.40	4.1
O(3)	2.68	3.87	1.72	2.30	4.6
surface	2.70	3.82	1.72	2.44	8.9
		$\mathrm{NO_3}^-$			
O(1)	3.28	3.90	2.07	2.66	3.8
O(2)	3.08	3.76	1.99	2.82	3.4
O(3)	3.00	3.62	2.08	2.86	3.2
surface	3.02	3.72	2.08	2.88	7.9

 $[^]a$ $r_{\rm max}$ and $r_{\rm min}$ are the distances of the maximum and minimum of $g_{\alpha\beta}\left(r\right)$ for the hydration shell in Å, and n is the averaged coordination numbers of the shell, respectively.

from the recent classical MD simulated NaNO₃ solution (2.83 Å).¹¹ However, our results are in good agreement with the distances obtained from the X-ray scattering measurements of 2.88, 2.87–2.95, 2.86–3.00, and 2.90–2.95 for the NH₄NO₃, NaNO₃, AgNO₃, and Rh(NO₃)₃ solutions, respectively. This again indicates the reliability of individual hydration structures for both anions obtained from the QMCF MD simulations. The individual CNDs were evaluated based on the minimum of RDFs for each site and are listed in Table 5. The range of averaged coordination numbers (CNs) from 4.1 to 4.6 for the carbonate also proves stronger interactions of each site with its hydration shell than those of nitrate anion with the range of 3.2-3.8. The observed small deviations of individual CNs are considered as insignificant due to the short sampling time, which would not cover all possible configurations. However, the individual CNs of water molecules coordinating with each oxygen of nitrate anion obtained from the QMCF MD simulation are larger than the values of 1-2 molecules expected from the averaged CN of 5.9–9 from the X-ray scattering results. 13 For the carbonate anion, no such experimental data have been reported yet.

According to the overlapping of all individual hydration spheres in the anions, the direct sum of these CNs is unable to refer to the molecular CN of solutes.⁶² We thus evaluated the molecular RDFs and CNDs for both anions, utilizing the radius of hydration spheres for each (site) · · · O_{water} RDF as the criterion to assign the coordinating site for each water molecule 35,40,42 shown in Figure 4. The density of water molecules presented in the molecular RDFs was evaluated in the domain produced by the union of spheres having the same radii, by assigning the coordination site with the shortest distance among the values obtained from the oxygen of water and each site within the solute. The molecular CNDs were evaluated on the molecular domain, constructed by applying the boundary obtained from the individual RDF for each site of the solute.⁶² The characteristic values of molecular hydration shells and their averaged CNs from the molecular surface-water RDFs and CNDs are also listed in Table 5. The height of molecular RDFs indicates that the molecular hydrations of both anions is well-defined with a more pronounced structure than in the separate investigations of each hydration site. The higher CNs of carbonate (12.8) and nitrate (10.4) anions from

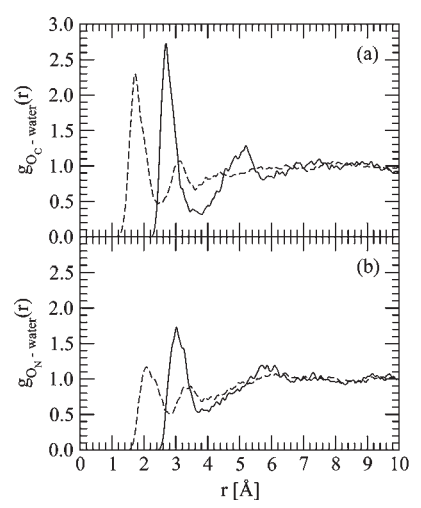
Table 6. Average Number of Hydrogen Bonds for Each O Site and Molecular Surface of ${\rm CO_3}^{2-}$ and ${\rm NO_3}^-$ Anions in the Simulation Period

	O(1)	O(2)	O(3)	surface
CO ₃ ²⁻	2.5 ± 0.6	2.3 ± 0.7 1.8 ± 0.9	2.2 ± 0.7	7.0 ± 1.1
NO ₃ ⁻	1.6 ± 0.9		1.8 ± 1.0	5.2 ± 1.4

the direct sum of individual CNs than in the corresponding molecular CN, differing by 3.9 and 2.5 molecules, indicate the location of waters in the intersection of the individual hydration spheres, causing on overcounting of CN as observed also in the hydration structures of sulfate, 35 bicarbonate, 40 and bisulfate 42 anions. These results support the possibility that the water molecules within the molecular hydration shell are able to rapidly change the coordinating site around the solute during the simulation period. The molecular CN of 7.9 for the nitrate anion is in excellent agreement with the accepted experimental data (5.9-9), 13 and hence the molecular CN of 8.9 produced for carbonate anion appears reliable as well.

To clarify the dynamical change of the water molecules between coordination sites, the number of H-bonds can be taken as a measure for the actual contacts between solute and hydrating water molecules, also indicating possible migrations of available extra molecules to other sites.⁴² Since the definition of H-bond has been expressed by two different ways, namely, by energetic and geometric criteria, 63,64 we utilized the structural criterion depending on the cutoff parameters (distances $R_{\rm HO}^{\rm (c)}$ and $R_{\rm OO}^{\rm (c)}$, and angle $\phi^{\rm (c)}$) in analogy to water-dimethyl sulfoxide mixtures and our previous studies. ^{41,42} The cutoff distances $R_{\rm HO}^{\rm (c)}$ and $R_{\rm OO}^{\rm (c)}$ for each oxygen site were obtained from the corresponding $((site)\cdots H_{water} \text{ and } (site)\cdots O_{water})$ RDFs. The angle $\phi^{(c)}$ was set to $30^{\circ}.65$ The average numbers of H-bonds for the carbonate and nitrate anions are listed in Table 6. The average H-bond numbers for the molecular hydration (or the surface) was calculated by averaging the summation of all H-bonds in each time step over the simulation period. The equivalence between the direct sum of each site and the surface values shows the formation of H-bond between the water molecule and the coordinating site ratio as 1:1, resulting in the actual CN for the carbonate (7.0) and nitrate (5.2) anions. These H-bond data compared with the molecular CNs (8.9 and 7.9 for the carbonate and nitrate anion, respectively) also point at some extra water molecules located in the molecular hydration shell of carbonate (~ 2) and nitrate (~ 3) anions without forming H-bonds to the solutes, readily changing the coordinating site, and representing a weaker hydration. The smaller number of extra waters for carbonate compared to nitrate also indicates a stronger hydration structure of the former than the latter anion. It is obvious that the molecular charge also affects the number of H-bonds formed to each oxygen site, resulting in this stronger hydration structure of carbonate compared to nitrate (also see Figure 4) as concluded also from the NDIS experiment.12

The dynamics of water molecules within the hydration shell of both anions were analyzed by the ligand MRT evaluated by the direct method, ⁵⁴ dividing the average number of water molecules within the hydration shell throughout the simulation time by the number of exchange events with two time parameters, $t^* = 0.0$ and 0.5 ps, corresponding to all displacements and to sustainable exchange events. ⁵⁶ MRT values for all coordinating sites of both anions are listed in Table 7, compared with the data of pure water



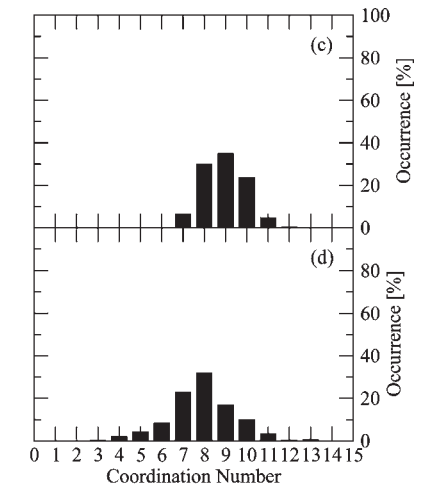


Figure 4. Molecular RDF plots of (a) CO_3^{2-} and NO_3^{-} anions obtained from the QMCF MD simulation evaluated by means of the combination of spheres; solid and dashed lines refer to the RDFs for the O and H atoms of water, respectively. The molecular hydration shell CND of (c) CO_3^{2-} and (d) NO_3^{-} anions is shown.

Table 7. Mean Ligand Residence Time τ (ps), Number of Accounted Ligand Exchange Events N, and Total Number of Processes Needed for One Successful Water Exchange $R_{\rm ex}$ Obtained from the QMCF MD Simulations

	$t^* = 0.0 \text{ ps}$				$t^* = 0.5 \text{ ps}$			
	$N_{\rm inv}^{a}$	$N_{\rm ex}^{0.0}/10~{\rm ps}^b$	$ au_{ m D}^{0.00}$	$N_{\rm inv}^a N$	$J_{\rm ex}^{0.5}/10~{\rm ps}^{1}$	$ au_{ m D}^{0.5c}$	$R_{\rm ex}^{d}$	
CO ₃ ²								
O(1)	29	170	0.25	16	27	1.56	6.3	
O(2)	30	195	0.22	17	27	1.58	7.2	
O(3)	32	222	0.22	14	23	2.08	9.6	
surface	40	171	0.53	26	39	2.31	4.4	
$\mathrm{NO_3}^-$								
O(1)	30	206	0.19	14	37	1.04	5.6	
O(2)	27	155	0.23	15	36	0.98	4.3	
O(3)	27	176	0.18	12	33	0.99	5.3	
surface	35	245	0.32	22	44	1.81	5.6	
H_2O^e		269 ⁵⁴	0.2, ⁵⁴ 0.	.33 ⁵⁵	24 ⁵⁴	1.7,54 1.5	51 ⁵⁵ 11.2 ⁵⁴	
H_2O		131^{f}	0.2^f , 0.5	5 ⁵⁶	20 ^f	1.3^{f}	6.5^{f}	

^a Number of ligands involved in the MRT evaluation according to the value of t*. ^b Number of accounted exchange events per 10 ps lasting at least 0.0 and 0.5 ps, respectively. ^c Mean residence time determined by the direct method⁵⁴ in picoseconds. ^d Average number of processes needed for one successful ligand exchange. ^c Values obtained from a QM/MM-MD simulation of pure water ^{54,55} in picoseconds. ^f Unpublished results: values obtained from a QMCF MD simulation of pure water in picoseconds.

simulations. S4,55 The number of involved ligands $(N_{\rm inv})$ represents the coordination of water molecules with the evaluated site in the criterion of t^* , while the number of accounted exchange events $(N_{\rm ex})$ accumulates the exchange processes of $N_{\rm inv}$ throughout the simulation period. The carbonate has a greater total number of individual and molecular $N_{\rm inv}$ than the nitrate anion, corresponding to the stronger hydration structure and larger CNs of the former as discussed from the RDFs and CNDs. The greater value of the total individual $N_{\rm inv}$ than the molecular $N_{\rm inv}$ includes the movements of waters among the coordinating sites

in the molecular hydration shell. The difference value between the total $N_{\rm ex}^{0.5}$ and the molecular $N_{\rm ex}^{0.5}$ implies that the migrations of water molecules between the coordinating sites were 38 and 62 processes (approximately half of the exchange events) for carbonate and nitrate, respectively, similar as for the HCO₃ and HSO_4^{-42} anions. The lower molecular $N_{\rm ex}$ of carbonate again indicates the stronger hydration shell than that of nitrate. The standard relaxation time used in the direct method with $t^* = 0.5$ ps leads to the MRT of water ligands at the coordinating sites, while the hydrogen bond lifetimes can be estimated with $t^* = 0.0 \text{ ps.}^{40,54} \text{ Our MRT results compared with the simulations}$ of pure water 54,55 classify carbonate as a structure-making anion, while the nitrate anion presents a more complicated situation. The individual MRTs of nitrate anion present a higher mobility of water molecules than those in pure water as reported in the previous conventional QM/MM MD study,³¹ while the molecular data indicate a stronger hydration structure. Thus, we can classify the nitrate anion as a weak structure-maker as a whole, but with local structure-breaking ability near the coordination sites. The number of processes needed for one successful water exchange, $R_{\rm ex}$, being the ratio of $N_{\rm ex}^{0.0}$ to $N_{\rm ex}^{0.5}$ for the carbonate anion also shows such peculiar processes, according to the significant difference between the individual and molecular $R_{\rm ex}$. The $R_{\rm ex}$ for the interchanging of coordinating site within the molecular hydration shell was 10.9 and 4.7 for carbonate and nitrate, respectively, reflecting the ease of migration for the water ligands within the hydration shell of the latter.

CONCLUSION

The aqueous solutions of carbonate and nitrate anion were simulated with the QMCF MD methodology to obtain structural and dynamical properties not only of their hydration shells, but also of the anions themselves. Our results give sufficient evidence of symmetry breaking from D_{3h} to a lower degree, while the nitrate anion seems to retain its planar structure. These results are also supported by the RISM-SCF-SEDD data. The vibrational spectra obtained from the VACFs are in good agreement with the experimental observations, $^{14-17,21}$ again indicating the validity of vector projections in the normal mode analysis. We also presented the correlation between the power spectrum of

the torsion angle—time functions and the out-of-plane (v_2) mode, showing a new possibility to obtain the vibration spectrum without the evaluation of VACFs. A good agreement of (site) · · · O_{water} RDFs was achieved with the X-ray scattering data for nitrate,7-10 indicating the accuracy of QMCF MD simulations to acquire the hydration structure of solutes as in previous studies. 35,37-40,42 Although such experimental data for the carbonate anion are missing to be compared with our results, the hydration structure of this anion is also assumed as reliable. The molecular approach 40,42 was applied to investigate the structural and dynamical properties for both anions. It indicates the location of water molecules within the intersection volumes of individual hydration spheres of both anions. The number of H-bonds shows the molecular hydration shell of anions consisting of the actual bound and extra water molecules readily migrating from one coordinating site to be other. The smaller number of such extra water for carbonate (\sim 2) than for nitrate (\sim 3) reflects the stronger hydration structure of the former, which is also confirmed by the MRTs for individual sites and the molecule as a whole. While carbonate is a structure-making anion, the individual MRTs of nitrate anion present a structure-breaking property, while the molecular value lets it appears as a weak structure-maker.

AUTHOR INFORMATION

Corresponding Author

*E-mail: anan tongraar@yahoo.com.

ACKNOWLEDGMENT

Generous financial support by the Austrian Science Foundation (FWF) and ASEA-UNINET, the National Research University (NRU) Project of Thailand's Office of the Higher Education Commission, and Centre for Petroleum, Petrochemicals and Advanced Materials, Chulalongkorn University are gratefully acknowledged. A.T. acknowledges support by the Thailand Research Fund (TRF) and Suranaree University of Technology (SUT). This work is also financial supported by the National Research Council of Thailand (NRCT) and the commission of Higher Education (CHE).

■ REFERENCES

- (1) Elderfield, H. Science 2002, 296, 1618-1621.
- (2) Bloom, A. J.; Burger, M.; Asensio, J. S. R.; Cousins, A. B. Science **2010**, 328, 899–903.
- (3) Sutton, M. A.; Oenema, O.; Erisman, J. W.; Leip, A.; van Grinsven, H.; Winiwarter, W. *Nature* **2011**, 427, 159–161.
- (4) Bargar, J. R.; Kubicki, J. D.; Reitmeyer, R.; Davis, J. A. Geochim. Cosmochim. Acta 2005, 69, 1527–1542.
- (5) Mitchell, H. H.; Shonle, H. A.; Grindley, H. S. J. Biol. Chem. 1916, 24, 461–490.
 - (6) Benjamin, N. Ann. Zootech. 2000, 49, 207-216.
- (7) Caminiti, R.; Licheri, G.; Piccaluga, G.; Pinna, G. J. Chem. Phys. 1978, 68, 1967–1970.
- (8) Caminiti, R.; Licheri, G.; Paschina, G.; Piccaluga, G.; Pinna, G. J. Chem. Phys. 1980, 72, 4522–4528.
- (9) Yamaguchi, T.; Johansson, G.; Holmberg, B.; Maeda, M.; Ohtaki, H. Acta Chem. Scand. 1984, A38, 437–451.
- (10) Caminiti, R.; Atzei, D.; Cucca, P.; Anedda, A.; Bongiovanni, G. J. Phys. Chem. 1986, 90, 238–243.
- (11) Megyes, T.; Bálint, S.; Peter, E.; Grósz, T.; Bakó, I.; Krienke, H.; Bellissent-Funel, M.-C. J. Phys. Chem. B 2009, 113, 4054–4064.
- (12) Mason, P. E.; Neilson, G. W.; Dempsey, C. E.; Brady, J. W. J. Am. Chem. Soc. **2006**, 128, 15136–15144.

- (13) Ohtaki, H.; Radnai, T. Chem. Rev. 1993, 93, 1157-1204.
- (14) Rudolph, W. W.; Fischer, D.; Irmer, G. Appl. Spectrosc. 2006, 60, 130-144.
- (15) Rudolph, W. W.; Irmer, G.; Königsberger, E. Dalton Trans. 2008, 900–908.
- (16) Waterland, M. R.; Kelley, A. M. J. Chem. Phys. 2000, 113, 6760–6773.
- (17) Waterland, M. R.; Stockwell, D.; Kelley, A. M. J. Chem. Phys. 2001, 114, 6249–6258.
- (18) Wang, X.-B.; Yang, X.; Wang, L.-S.; Nicholas, J. B. J. Chem. Phys. **2002**, 116, 561–570.
 - (19) Chang, T. G.; Irish, D. E. J. Phys. Chem. 1973, 77, 52-57.
- (20) Zhang, Y.-H.; Choi, M. Y.; Chan, C. K. J. Phys. Chem. A 2004, 108, 1712–1718.
- (21) Wahab, A.; Mahiuddin, S.; Hefter, G.; Kunz, W.; Minofar, B.; Jungwirth, P. *J. Phys. Chem. B* **2005**, *109*, 24108–24120.
- (22) Goebbert, D. J.; Garand, E.; Wende, T.; Bergmann, R.; Meijer, G.; Asmis, K. R.; Neumark, D. M. *J. Phys. Chem. A* **2009**, *113*, 7584–7592.
- (23) Pathak, A. K.; Mukherjee, T.; Maity, D. K. J. Phys. Chem. A 2008, 112, 3399–3408.
- (24) Pathak, A. K.; Maity, D. K. J. Phys. Chem. A 2009, 113, 13443–13447.
- (25) Stefanovich, E. V.; Boldyrev, A. I.; Truong, T. N.; Simons, J. J. Phys. Chem. B 1998, 102, 4205–4208.
- (26) Archer, T. D.; Birse, S. E. A.; Dove, M. T.; Redfern, S. A. T.; Gale, J. D.; Cygan, R. T. *Phys. Chem. Miner.* **2003**, *30*, 416–424.
- (27) Bruneval, F.; Donadio, D.; Parrinello, M. J. Phys. Chem. B 2007, 111, 12219–12227.
- (28) Tommaso, D. D.; de Leeuw, N. H. J. Phys. Chem. B 2008, 112, 6965–6975.
- (29) Kumar, P. P.; Kalinichev, A. G.; Kirkpatrick, R. J. J. Phys. Chem. B 2009, 113, 794–802.
- (30) Ebner, C.; Sansone, R.; Hengrasmee, S.; Probst, M. Int. J. Quantum Chem. 1999, 75, 805–814.
- (31) Tongraar, A.; Tangkawanwanit, P.; Rode, B. M. J. Phys. Chem. A **2006**, 110, 12918–12926.
- (32) Vchirawongkwin, V.; Sato, H.; Sakaki, S. J. Phys. Chem. B 2010, 114, 10513–10519.
- (33) Rode, B. M.; Hofer, T. S.; Randolf, B. R.; Schwenk, C. F.; Xenides, D.; Vchirawongkwin, V. *Theor. Chem. Acc.* **2006**, *115*, 77–85.
- (34) Hofer, T. S.; Pribil, A. B.; Randolf, B. R.; Rode, B. M. Ab Initio Quantum Mechanical Charge Field Molecular Dynamics: A Nonparametrized First-Principle Approach to Liquids and Solutions. In *Combining Quantum Mechanics and Molecular Mechanics. Some Recent Progresses in QM/MM Methods*; Sabin, J. R., Brändas, E., Eds.; Academic Press: New York, 2010; Vol. 59, pp 213–246.
- (35) Vchirawongkwin, V.; Rode, B. M.; Persson, I. J. Phys. Chem. B **2007**, 111, 4150–4155.
- (36) Vchirawongkwin, V.; Rode, B. M. Chem. Phys. Lett. 2007, 443, 4152–157
- (37) Pribil, A. B.; Vchirawongkwin, V.; Hofer, T. S.; Randolf, B. R. Structure and Dynamics of Composite Anions in Aqueous Solution. Computation in Modern Science and Engineering, Proceedings of the International Conference on Computational Methods in Science and Engineering, 2007; pp 921–923.
- (38) Pribil, A. B.; Hofer, T. S.; Randolf, B. R.; Rode, B. M. J. Comput. Chem. **2008**, 29, 2330–2334.
- (39) Pribil, A. B.; Hofer, T. S.; Vchirawongkwin, V.; Randolf, B. R.; Rode, B. M. Chem. Phys. 2008, 346, 182–185.
- (40) Vchirawongkwin, V.; Pribil, A. B.; Rode, B. M. J. Comput. Chem. **2010**, 31, 249–257.
- (41) Vchirawongkwin, V.; Kritayakornupong, C.; Ruangpornvisuti, V.; Rode, B. M. J. Mol. Struct.: THEOCHEM 2009, 913, 236–239.
- (42) Vchirawongkwin, V.; Kritayakornupong, C.; Rode, B. M. J. Phys. Chem. B **2010**, 114, 11561–11569.
 - (43) Warshel, A.; Levitt, M. J. Mol. Biol. 1976, 103, 227-249.
- (44) Field, M. J.; Bash, P. A.; Karplus, M. J. Comput. Chem. 1990, 11, 700-733.

- (45) Gao, J. J. Am. Chem. Soc. 1993, 115, 2930-2935.
- (46) Bakowise, D.; Thiel, W. J. Phys. Chem. 1996, 100, 10580-10594.
- (47) Brooks, B. R.; Bruccoleri, R. E.; Olafson, B. D.; States, B. D.; Swaminathan, S.; Karplus, M. J. Comput. Chem. 1983, 4, 187–217.
- (48) Berendsen, H. J. C.; Postma, J. P. M.; van Gunsteren, W. F.; DiNola, A.; Haak, J. R. *J. Chem. Phys.* **1984**, *81*, 3684–3690.
- (49) Dunning, T. H., Jr.; Hay, P. J. In Gaussian Basis Sets for Molecular Calculations; Schaefer, H. F., III, Ed.; Plenum Press: New York, 1977; Vol. 3, Chapter 1, pp 1–27.
 - (50) Dunning, T. H., Jr. J. Chem. Phys. 1970, 53, 2823–2833.
- (51) Tongraar, A.; Sagarik, K.; Rode, B. M. Phys. Chem. Chem. Phys. 2002, 4, 628-634.
 - (52) Stillinger, F. H.; Rahman, A. J. Chem. Phys. 1978, 68, 666-670.
- (53) Bopp, P.; Janscó, G.; Heinzinger, K. Chem. Phys. Lett. 1983, 98, 129-133.
- (54) Hofer, T. S.; Tran, H. T.; Schwenk, C. F.; Rode, B. M. J. Comput. Chem. 2004, 25, 211–217.
- (55) Xenides, D.; Randolf, B. R.; Rode, B. M. J. Chem. Phys. 2005, 122, 174506.
- (56) Lock, A. J.; Woutersen, S.; Bakker, H. J. J. Phys. Chem. A 2001, 105, 1238–1243.
 - (57) Bopp, P. Chem. Phys. 1986, 106, 205-212.
- (S8) Frisch, M. J. et al. *Gaussian 03*, Revision D.02; Gaussian, Inc.: Wallingford, CT, 2004.
- (59) Godbout, N.; Salahub, D. R.; Andzelm, J.; Wimmer, E. Can. J. Chem. 1992, 70, 560–571.
- (60) Wang, X.-B.; Nicholas, J. B.; Wang, L.-S. J. Phys. Chem. A 2000, 104, 504–508.
- (61) Kameda, Y.; Sasaki, M.; Hino, S.; Amo, Y.; Usuki, T. *Phys. B: Condens. Matter* **2006**, 385–386, 279–281; Proceedings of the Eighth International Conference on Neutron Scattering.
- (62) Vchirawongkwin, S.; Vchirawongkwin, V. Comput. Theoret. Chem. 2011, 974, 26–30.
 - (63) Sceats, M. G.; Rice, S. A. J. Chem. Phys. 1980, 72, 3236-3247.
 - (64) Mezei, M.; Beveridge, D. L. J. Chem. Phys. 1981, 74, 622-632.
 - (65) Luzar, A.; Chandler, D. J. Chem. Phys. 1993, 98, 8160-8173.

1. สำเนา Manuscript ของงานวิจัยเรื่องที่ 7

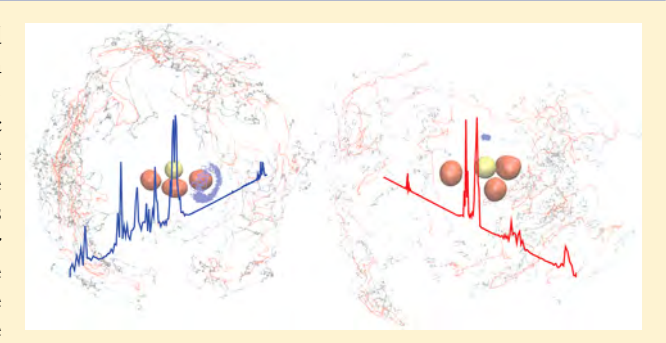
Viwat Vchirawongkwin, Chokchai Pornpiganon, Chinapong Kritayakornupong, **Anan Tongraar** and Bernd M. Rode, "The stability of bisulfite and sulfonate ions in aqueous solution characterized by hydration structure and dynamics" J. *Phys. Chem. B*, **2012**, 116, 11498-11507.



The Stability of Bisulfite and Sulfonate Ions in Aqueous Solution Characterized by Hydration Structure and Dynamics

Viwat Vchirawongkwin,*,† Chokchai Pornpiganon,† Chinapong Kritayakornupong,‡ Anan Tongraar,§ and Bernd M. Rode[⊥]

ABSTRACT: The aqueous solutions of bisulfite (SO₃H⁻) and sulfonate (HSO₃) were simulated by the ab initio quantum mechanical charge field molecular dynamics (QMCF MD) formalism. All superimposed trajectories for the atomic coordinates of solutes with three-dimensional alignment here illustrated the reactivities of the ions. Power spectra were evaluated on the basis of the velocity autocorrelation functions (VACFs) with the normal-mode analysis, presenting a higher frequency of the symmetric SO₃ deformation ($\delta_s(SO_3)$) than the asymmetric SO₃ deformation ($\delta_{as}(SO_3)$) modes for the sulfonate ion. The different influence of solvent on the frequency of the O-H and S-H stretching suggests a higher stability of hydrated



sulfonate ion. The bisulfite shows a slightly stronger molecular hydration shell than the sulfonate ion with the average number of ion-solvent hydrogen bonds (H-bonds) of 5.3 and 5.0, respectively. Extra water molecules within the molecular hydration shell are found for bisulfite (1.2) and for sulfonate (1.6). The mean residence times for the water ligands classify each ion as a structure maker, while the S-H bond within the sulfonate ion displays a hydrophobic behavior. No tautomerization was observed within the simulation period.

INTRODUCTION

The man-made emissions of sulfur dioxide (SO₂) in the atmosphere are one of the serious air pollutions; however, the winemaking process uses SO2 to inhibit the growth of indigenous yeasts and contaminating bacteria, and suppress the formation of quinones.2 The first protonation of dissolved SO₂ in water produces two tautomeric forms, namely bisulfite (SO_3H^-) and sulfonate (HSO_3^-) ions, identified by ultraviolet absorption³ and Raman^{4,5} studies. For the former, the proton attaches to one oxygen atom, whereas the hydrogen in the latter binds to the sulfur atom. The characterization of both ions was reported in many IR and Raman experiments. 4-9 Risberg et al. assigned seven and six frequencies for the bisulfite and sulfonate ion, respectively, via the Raman investigation of 1 M NaHSO₃ at pH 3.9.8 They also assigned the frequency of the symmetric SO_3 deformation $(\delta_s(SO_3))$, lower than the asymmetric SO_3 deformation ($\delta_{as}(SO_3)$), to the sulfonate ion, while the inclusion of the sulfur isotope effect⁶ suggested a reversed order. Varying assignments for the O-H stretching mode of the bisulfite ion were also reported from Raman experiments. 7-9 A recent FTIR spectroscopy in conjunction with a laminar flow-tube and the scanning mobility particle sizer measurements was also unable to assign the frequency to all normal modes for both ions.9

The oxygen-17 NMR spectroscopy reported the equilibrium quotient for the isomerization reaction between bisulfite and sulfonate ions $(Q = [SO_3H^-]/[HSO_3^-])$ to be 4.9 ± 0.1 at 298 K in solutions of ionic strength 1.0 m_1^{10} while the sulfur K-edge XANES experiment at the total concentration of 0.05 M without ionic medium gave this value as 2.6 ± 0.5 . Baird and Taylor¹¹ utilized the single-determinant SCF with a small basis set obtaining a more stable sulfonate than bisulfite ion by 5 kcal mol⁻¹, while the superior MC-SCF with double-ζ basis set predicted the bisulfite to be the more stable isomer. 12 The MP2 and MP4 calculations with a 6-31++G(d,p) basis set reported a higher stability of the bisulfite by approximately 8 kcal mol⁻¹ compared to the sulfonate ion in the gas phase. 13 The theoretical results including small water clusters also indicated that the bisulfite ion is more stable than the sulfonate ion.¹⁴ Calculations at the G2 and G2(MP2) level with the inclusion of multiple polarization functions on the sulfur atom indicated

Received: June 9, 2012 Revised: August 24, 2012 Published: August 25, 2012

Department of Chemistry, Faculty of Science, Chulalongkorn University, Phayathai Road, Patumwan, Bangkok 10330, Thailand

Department of Chemistry, Faculty of Science, King Mongkut's University of Technology Thonburi, Bangkok 10140, Thailand

[§]School of Chemistry, Institute of Science, Suranaree University of Technology, Nakhon Ratchasima 30000, Thailand

¹Theoretical Chemistry Division, Institute of General, Inorganic and Theoretical Chemistry, University of Innsbruck, Innrain 52a, A-6020 Innsbruck, Austria

that the sulfonate ion is more stable than the bisulfite ion by approximately 4 and 5 kcal mol^{-1} in the gas and aqueous phase, respectively. Otto et al. also concluded a more stable sulfonate ion in the gas phase. The bisulfite with the C_s symmetry has two conformations, namely cis- and trans- SO_3H^- , in which the O–H bond is located bisecting and opposite the \angle OSO angle, respectively. Both C_s conformations are the transition state in the gas phase according to the negative eigenvalue in their calculated Hessian matrices; however, the trans- SO_3H^- has a higher energy than the cis-conformer by about 5 kcal mol^{-1} . Voegele et al. proposed a mechanism of tautomerization from the bisulfite into the sulfonate ions through the trans- SO_3H^- .

According to the coexistence of bisulfate and sulfonate ions in equilibrium solutions and other variety of sulfite(IV) species, ^{1,8,10} their hydration structure has never been characterized in any experiments. Within a computer simulation, we set up aqueous solutions of bisulfite and sulfonate ions to acquire the structural and dynamical of these solutes and their respective hydration shells by means of an ab initio quantum mechanical charge field molecular dynamics (QMCF MD) formalism^{18,19} to compare the stability for both ions in the environment of explicit water molecules. We evaluated the vibrational frequencies for all normal modes of both ions based on a precise vector analysis, and also investigated the role of water molecules within the hydration shell on the strength of chemical bonds.

METHODS

In order to investigate the structural and dynamical properties of solutes and their hydration shell, we have applied the ab initio quantum mechanical charge field molecular dynamics (QMCF MD) formalism. This method avoids the construction of potential functions between the solute and water molecules in bulk by extending the quantum mechanically treated solvent layer beyond the first hydration shell of the solute species, resulting in negligible non-Coulombic interactions between the solute and bulk water. The involvement of the point charges of the atoms in the molecular mechanical (MM) region with their changing positions in the core Hamiltonian for the quantum mechanical (QM) calculations is a valuable feature of this method with a perturbation term as

$$V' = \sum_{i=1}^{n} \sum_{j=1}^{m} \frac{q_{j}^{\text{MM}}}{r_{ij}}$$
 (1)

where n is the number of atoms in the QM region, m is the number of atoms in the MM region, q_i^{MM} is the partial charges of these atoms according to the selected water model, and r_{ij} refers to the distance between a pair of particles in the QM (i) and MM (j) regions. On the other hand, the dynamically changing charges of QM particles, q_i^{QM} , determined by population analysis contribute to the force on each atom j in the MM region as Coulombic forces,

$$F_j^{\text{QM}\to\text{MM}} = \sum_{i=1}^n \frac{q_i^{\text{QM}} \cdot q_j^{\text{MM}}}{r_{ij}}$$
 (2)

The QMCF MD method permits the migration of water molecules between the QM and MM region by including a smoothing function, ²⁴

$$S(r) = \begin{cases} 1 & \text{for } r < r_{\text{on}}, \\ \frac{(r_{\text{off}}^2 - r^2)^2 (r_{\text{off}}^2 + 2r^2 - 3r_{\text{on}}^2)}{(r_{\text{off}}^2 - r_{\text{on}}^2)^3} & \text{for } r_{\text{on}} \le r \le r_{\text{off}}, \\ 0 & \text{for } r > r_{\text{off}} \end{cases}$$
(3)

where r is the distance of a given solvent molecule from the center of the simulation box, $r_{\rm off}$ is the radius of the QM region and $r_{\rm on}$ is the inner border of the smoothing region. In this way, one applies this function to all atoms of molecules located in the smoothing region to ensure a continuous transition and change of forces for these molecules according to

$$F_i^{\text{smooth}} = F_i^{\text{MM}} + (F_i^{\text{layer}} - F_i^{\text{MM}}) \times S(r)$$
(4)

where F_j^{layer} is the force acting on a particle j located in the (outer QM) smoothing zone and F_j^{MM} is the force acting on a particle j in the MM region. In this context, it has to be mentioned that energy is not rigorously conserved, but the related error due to the short simulation time and the large size of the QM region can be considered extremely minor.

The systems consisted of 495 water molecules with one bisulfite and one sulfonate anion in the bisulfite and sulfonate solution, respectively, in a cubic box of 24.66 Å with periodic boundary condition. The simulations performed in the canonical ensemble using a general predictor-corrector algorithm with a time step of 0.2 fs. We applied the Berendsen temperature-scaling algorithm²⁵ to maintain the temperature of systems at 298.16 K with a relaxation time of 100 fs. Although this temperature-scaling algorithm requires, in principle, a long simulation period to describe the phase space sufficiently, a large number of successful publications of QMCF MD simulations²⁶⁻³³ indicate that the simulation period of 10 ps is adequate to reproduce the properties of hydrated ions well. The density of the simulation boxes was 0.997 g cm⁻³, as the experimental value of pure water at 298 K. The QM subregions, namely the core and layer zones, extended for both bisulfite and sulfonate anions to 3.5 and 6.0 Å, respectively. The structural and dynamical results obtained from previous QMCF MD studies 26-33 have also indicated the Hartree-Fock (HF) method to be a decent compromise between accuracy and affordable computational effort; thus, we also utilized the quantum mechanical calculation at the HF level with the Dunning double- ζ plus polarization (DZP)^{34,35} basis sets for hydrogen and oxygen atoms of water molecules and the Dunning double- ζ plus polarization and diffuse functions (DZP +)^{34,35} basis sets for hydrogen, oxygen, and sulfur atoms of both bisulfite and sulfonate anions. Although HF and the methodical problems associated with the thermostat probably led to slightly underestimated values of H-bond energies, the associated errors are probably within a 10% range.³³ The thickness of the smoothing region was 0.2 Å with the values of $r_{\rm on}$ and $r_{\rm off}$ respectively as 5.8 and 6.0 Å, according to the radial distribution functions (RDFs) obtained from the equilibrated simulations. In QMCF MD formalism, we utilized the flexible BJH-CF2 water model^{36,37} to calculate the interactions between pairs of water in the MM region, with the cutoff distances of 3.0 and 5.0 Å for non-Coulombic interactions between H atoms and between O and H atoms, respectively. This water model supports the fully flexible geometries of water molecules transiting between the QM and MM region and uses the partial charges for oxygen and hydrogen atoms of -0.65966 and +0.32983, respectively. The Coulombic interactions between the Mulliken charges on the atoms within the QM region and the point charges of water molecules according to the BJH-CF2 model provide electrostatic forces described by a dynamical field of point charges, which vary according to the movements of atoms inside the QM region and water molecules in the MM region during the simulation. This ensures the continuous adaptation of the Coulombic interactions to all polarization and charge-transfer effects within the solute and surrounding solvent layers. 18,19 In addition, the reaction field method combined with the shifted-force potential technique accounted for the long-range electrostatic potentials and forces within the systems, with a spherical cutoff limit of 12.350 Å. We equilibrated the systems with the QMCF MD method for 50,000 steps (10 ps), and collected further 50,000 steps (10 ps) as data sampling for analyzing the structural and dynamical properties. The average number of water molecules in the QM region was 24.7 and 23.6 for the bisulfite and sulfonate solution, respectively.

In this work, we evaluated the structural and dynamical properties for the hydration shell of bisulfite and sulfonate anions in both individual and molecular manners such as the molecular RDFs, molecular coordination number distributions (CNDs), and molecular ligand mean residence times (MRTs). The definition of the molecular hydration shell is the combination of all atomic hydration spheres for each anion, producing the molecular domain.³⁸ The coordinating site for each water molecule to the anions is the shortest distance between the oxygen atom of a water molecule and each atom within each anion. 31,33 We calculated all MRT values on the basis of direct method,³⁹ counting the water exchange processes between hydration shell and bulk. The most appropriate time span to record a water displacement from its original coordination sphere as an exchange process is 0.5 ps, which corresponds to the average lifetime of a hydrogen bond in the solvent.41

The velocity autocorrelation function (VACF) is one method to evaluate the dynamical properties of a fluid system related to macroscopic transport coefficients, and its Fourier transformation yields the vibrational spectrum via normal-coordinate analysis. The definition of normalized VACF, C(t), is

$$C(t) = \frac{\sum_{i}^{N_{t}} \sum_{j}^{N} \nu_{j}(t_{i}) \nu_{j}(t_{i} + t)}{N_{t} N \sum_{i}^{N_{t}} \sum_{j}^{N} \nu_{j}(t_{i}) \nu_{j}(t_{i})}$$
(5)

where N is the number of particles, N_t is the number of time origins t_v and v_j denotes a certain velocity component of the particle j. A correlation length of 2.0 ps was used to obtain the power spectra with 4000 averaged time origins.

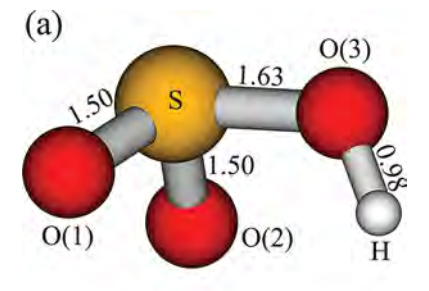
RESULTS AND DISCUSSION

Structural and Dynamical Properties of Solutes.

According to the molecular dynamics protocol, all atoms in the simulation box move along the gradient of forces during the simulation period. Thus, average internal coordinates such as bond distances, angles, and dihedral angles are suitable to represent the geometry of bisulfite and sulfonate ions obtained from the QMCF MD simulations. Nine structural parameters with their statistical deviation used to construct each average geometry of ions are listed in Table 1 and their geometries shown in Figure 1. All S–O distances are shorter than those within SO_3^{2-} of 1.53 Å obtained from QMCF MD and LAXS.⁴³

Table 1. Nine Structural Parameters for the Geometry of SO₃H⁻ and HSO₃⁻ Ions Obtained from the Averaging of Their Distributions with Their Variations

SO ₃ H	-	HSO ₃			
structural pa	rameter	structural parameter			
S-O(1) (Å)	1.50 ± 0.03	S-O(1) (Å)	1.47 ± 0.03		
S-O(2) (Å)	1.50 ± 0.03	S-O(2) (Å)	1.47 ± 0.03		
S-O(3) (Å)	1.63 ± 0.04	S-O(3) (Å)	1.46 ± 0.02		
O(3)-H (Å)	0.98 ± 0.03	S-H (Å)	1.33 ± 0.04		
$\angle O(1)SO(3)$ (deg)	102 ± 4	$\angle O(1)SO(2)$ (deg)	112 ± 3		
$\angle O(2)SO(3)$ (deg)	102 ± 4	$\angle O(2)SO(3)$ (deg)	112 ± 3		
∠SO(3)H (deg)	119 ± 7	∠O(1)SH (deg)	106 ± 3		
O(1)SO(3)O(2) dihedral (deg)	-111 ± 3	O(2)SO(1)H dihedral (deg)	116 ± 3		
O(2)SO(3)H dihedral (deg)	52 ± 67	O(3)SO(2)O(1) dihedral (deg)	-128 ± 4		



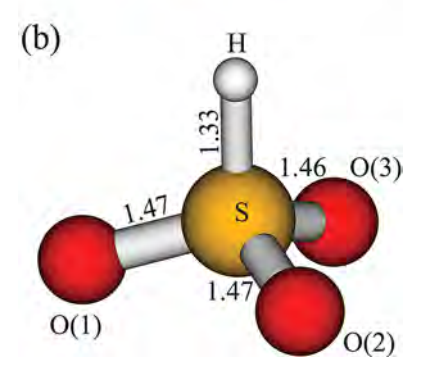


Figure 1. Average geometries of (a) bisulfite (SO_3H^-) and (b) sulfonate (HSO_3^-) ions obtained from the QMCF MD simulations.

Remarkableness is the large variation of the O(2)SO(3)H dihedral angle of 67° within the bisulfite ion, while other angles vary within 7°. However, the interpretation of the data only from the statistical distribution has some limitation. The visualization of the solutes in the simulations period provides more details, but the large number of configurations realized in the dynamics require a specific analysis. Thus, we utilized the superimposed configurations with the three-dimensional (3D) alignment by using the contravariant transformation, representing the dynamical motions of bisulfite and sulfonate ions shown in Figure 2. We defined new basis vectors via the facet constructed from three oxygen atoms for each trajectory configuration. The z-axis is the unit normal vector of the facet, while the unit vector of the vector sum between two vectors of vertices defines the x-axis. The y-axis is the unit normal vector of the cross product between the z- and x-axes. Figure 2a shows the ease of rotations for the hydrogen atom around the S-O(3) bond in bisulfite ion, while Figure 2b presents small motions for all atoms in the sulfonate ion. The small diffusion

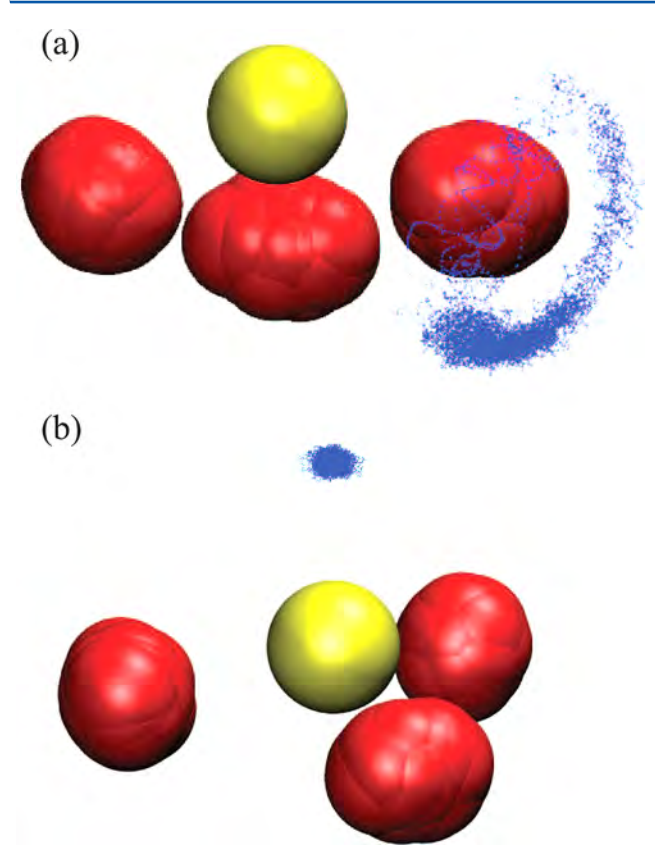


Figure 2. All superimposed trajectories for the coordinates of (a) bisulfite (SO₃H⁻) and (b) sulfonate (HSO₃⁻) ions with 3D alignment obtained from the QMCF MD simulations. The yellow sphere is the sulfur, red spheres are the oxygen, and blue points are the hydrogens.

of motions for the sulfonate ion indicates a higher kinetic stability of the interaction with its hydration shell than the bisulfite ion, consisting of the active hydrogen atom, rotating around the O(3) atom. These data agree with the XANES results that the number of sulfonate ions increased with increasing temperature.8 According to the proposed mechanism of tautomerization by Voegele et al., 17 the hydrogen atom of SO₂H⁻ aligned in the *trans*-conformer yields the sulfonate ion. This conformer is the transition state in the gas phase, according to its single negative eigenvalue in its calculated Hessian matrix. We also performed G3(MP2) calculations⁴⁴ in the polarizable continuum model (PCM) on the transconformer by using the Gaussian03 package, 45 obtaining all positive eigenvalues of the calculated Hessian matrix. This reveals the role of solvent to stabilize the energy of trans-SO₃H⁻, providing the suitable arrangement of water cluster for the tautomerization process.¹⁷ However, the local minimum for the rotamer of SO₃H⁻ ion is located in between the cis- and trans-conformers. Its low probability apparently is not sufficient to observe on isomerization reaction within the short time-span of the simulation. In order to investigate the probability of the rotation for the hydrogen atom of bisulfite ion, we defined a new dihedral angle, namely H-O(3)- α -S, where α is the center of the facet constructed from three oxygen atoms, presenting the cis- and trans-SO₃H⁻ by ±180° and 0°, respectively. This angle distribution clarified the ratio of conformers by the rotational ability of the hydrogen atom around the S-O(3) bond throughout the simulation period shown in Figure 3. The active forms of bisulfite tend to be the

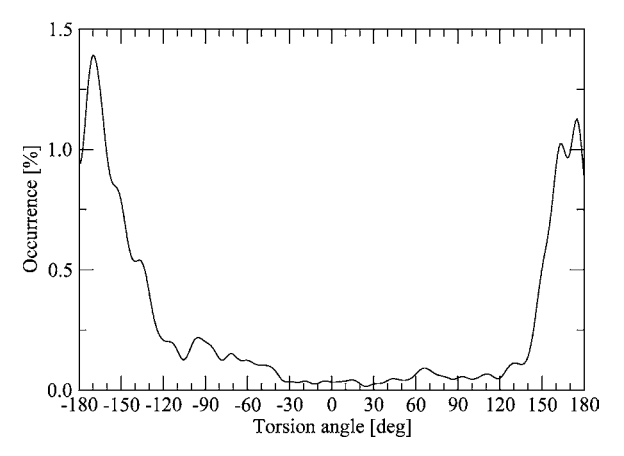


Figure 3. Angle distribution of the O(2)SO(3)H dihedral angle in SO_3H^- ion.

trans-conformer having the $H-O(3)-\alpha-S$ angle in the range from -90° to 90° to be only 12.23%, indicating a reduced probability of conversion to the sulfonate ion based on the proposed mechanism by Voegele et al.¹⁷ This agrees with the equilibrium quotient obtained from the experiments, specifying an excess of bisulfite ion over the sulfonate ion.^{8,10}

One dynamical property of the solutes obtained from the QMCF MD simulations comparable to the infrared (IR) and Raman (R) data is the vibrational spectrum. According to the dynamical motions of all atoms within the bisulfite ion, its symmetry is the C_1 consisting of nine vibration modes. We analyzed the normal modes by separating the ion into three bases such as (SO_2) , $(SO_2)-(O^*)$, and $(SO_2O)-(H)$ models. The (SO₂) part comprises two equivalent S-O bonds assigned with the $C_{2\nu}$ symmetry consisting of three modes, namely symmetric SO_2 stretching ($\nu_s(SO_2)$), asymmetric SO_2 stretching ($\nu_{as}(SO_2)$), and SO_2 bending ($\delta(SO_2)$). The addition of an oxygen atom to the first part produced the (SO_2) - (O^*) model having three additional vibrational modes, defined as S-OH stretching (ν (S-OH)), S-OH bending, and S-OH out-ofplane bending. These two bending modes equal the SO₂ wagging $(\omega(SO_2))$ and SO_2 twisting $(\tau(SO_2))$ modes, respectively, assigned in other works. 8,46 The last three modes, namely O*-H stretching (ν (O*H)), S-O*-H bending ($\delta(SO^*H)$), and $S-O^*-H$ wagging ($\omega(SO^*H)$), occur when attaching the hydrogen atom producing the (SO₂O)-(H) model. Figure 4 displays the defined vectors for all normal modes of the bisulfite ion, and all power spectra are displayed in Figure 5. On the other hand, the sulfonate ion in $C_{3\nu}$ symmetry, also having nine modes, will span into two types of symmetry species as the following representation:

$$\Gamma(C_{3\nu}) = 3a_1(R, IR) + 3e(R, IR)$$
 (6)

predicting only six bands with three of them becoming doubly degenerate modes. Figure 6 presents all power spectra of the sulfonate ion. All frequencies evaluated from the QMCF MD simulations for both ions are shown in Table 2, also presenting the scaled values in parentheses with the factor of 0.902 obtained from the correction with the coupled-cluster singles and doubles (CCSD) level. Three calculated frequencies (without scaling) of the (SO₂) model for the bisulfite ion are higher than the data from the Raman and FTIR experiments within 80 cm⁻¹, while the scaled values around 50 cm⁻¹ are too low. The ν (S–OH) is a simple mode as shown in Figure 4, obtained from the projection of velocity for the O(3) atom

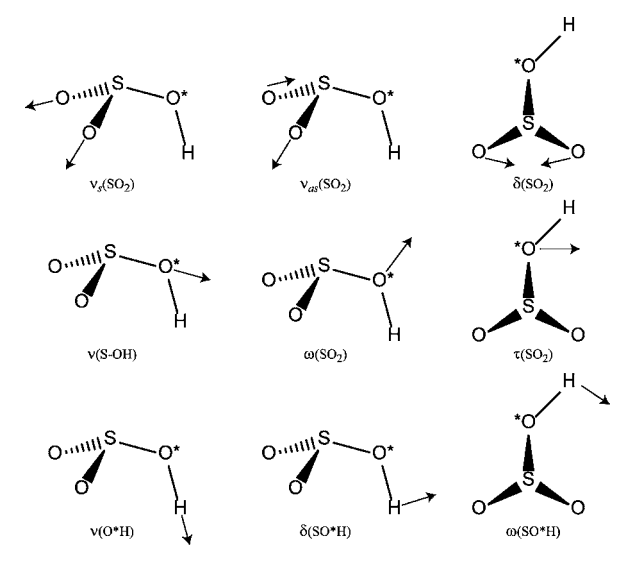


Figure 4. Defined vectors of the normal modes for the SO_3H^- ion in the C_1 symmetry.

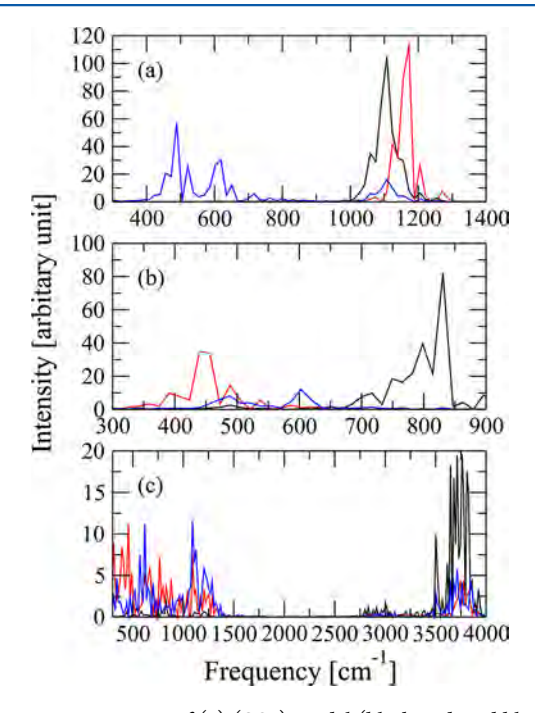


Figure 5. Power spectra of (a) (SO₂) model (black, red, and blue solid lines refer to $\nu_s(SO_2)$, $\nu_{as}(SO_2)$, and $\delta(SO_2)$, respectively), (b) (SO₂)–(O*) model (black, red, and blue solid lines refer to $\nu(S-OH)$, $\omega(SO_2)$, and $\tau(SO_2)$, respectively), and (c) (SO₂O)–(H) model (black, red, and blue solid lines refer to $\nu(O*H)$, $\delta(SO*H)$, and $\omega(SO*H)$, respectively).

onto the S–O(3) vector. The calculated frequency for this mode supports the assignment by Connick et al. at 730 cm⁻¹. The values of more sophisticated modes, $\omega(SO_2)$ and $\tau(SO_2)$, agree with the Raman data reported by Risberg et al., again indicating a good quality of vector analysis for the normal modes. The spectra of the OH group present very broad bands, due to the different orientation of the O(3)–H bond for each time origin producing the mixed modes as the previous results of HSO₃ ion. We subtracted one spectrum of O(3)–H from five other spectra, the rest being two modes of (SO_2O) –(H) including three modes from the (SO_2) – (O^*) model, to clarify

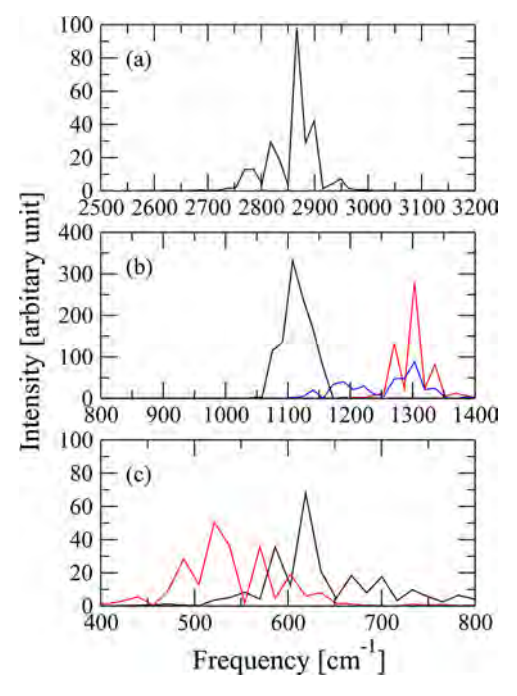


Figure 6. Power spectra of (a) $\nu(SH)$ mode, (b) $\nu_s(SO_3)$, $\nu_{as}(SO_3)$, and $\delta(SH)$ modes (represented via a black, red, and blue solid line, respectively), and (c) $\delta_s(SO_3)$ (black solid line) and $\delta_{as}(SO_3)$ (red solid line) modes.

the location of the peak for each mode. Figure 7 shows three isolated spectra, obtained from the procedure. The characteristic of the isolated spectrum for $\nu(O^*H)$ has still the broad band, found in the region of 3486-3974 cm⁻¹, while the remaining two spectra display the same pattern with two main peaks. There are two main peaks of the $\delta(SO^*H)$ spectrum located at 309 and 880 cm⁻¹ and of ω (SO*H) at 570 and 1091 cm⁻¹. To our knowledge, these two modes have never been assigned in the spectra obtained from the experiments. 5,7-According to an ambiguous assignment of $\nu(\hat{O^*H})$ mode, $^{7-9}$ we again clarified the characteristic frequency of this mode by investigating the influence of water molecules in the hydration shell of the hydrogen atom with a method similar to that used for the bicarbonate ion. 32 We evaluated the number of H-bonds between the hydrogen atom of bisulfite ion and water molecules within its hydration shell during the simulation period shown in Figure 8a, according to the geometric criteria. 32,47 Two short time periods, 1.9–4.4 ps and 4.5–7.0 ps, were selected to evaluate the power spectra of the $\nu(O^*H)$ mode without and with the effect of H-bonds, respectively. The spectrum without the effect of H-bonds has a strong peak located at 3828 (3453) cm⁻¹ and a weak peak at 3762 (3393) cm⁻¹, while the main peaks of the spectrum with the H-bonds are red-shifted to 3746 (3379) and 3648 (3290) cm⁻¹. The weak peak located at 3518 (3173) cm⁻¹ also occurs in the latter spectrum, revealing the interaction between the hydrogen atom and water molecules.

The power spectrum of the $\nu(SH)$ mode in the sulfonate ion displays a split peak, and we again analyzed the influence of hydration shell with the geometric criteria of H-bonds between S-H and oxygen of water shown in Figure 8b. A stronger interaction with solvent molecules is found in the time period of 0.5-2.5 ps, while between 4.6 to 6.6 ps fewer interactions are registered. The spectrum of the $\nu(SH)$ mode in each period presents the single strong peak at 2915 and 2867

Table 2. Vibration Frequencies (cm⁻¹) of Peaks for Each Normal Mode of SO₃H⁻ and HSO₃⁻ Ions Evaluated by the VACFs of QMCF MD Simulations, Given As Values Scaled by the Factor 0.902²⁷ in Parentheses

	SO ₃ H ⁻			HSO ₃	
vibration mode ^a	QMCF MD	Raman and IR	vibration mode ^a	QMCF MD	Raman and IR
$\nu_{\rm s}({\rm SO}_2)$	1108 (999)	1053 ^b , 1050 ^c	$\nu(\mathrm{SH})$	2867, 2932 (2586, 2645)	2535 ^b , 2573 ^f
$\nu_{\rm as}({ m SO}_2)$	1173 (1058)	1095 ^b	$\nu_{\rm s}({ m SO_3})$	1124 (1014)	1025^b , 1030^c , 1038^f
$\delta(\mathrm{SO}_2)$	619 (558)	582 ^b	$\delta_{\rm s}({\rm SO_3})$	651 (587)	496 ^b , 626 ^f
ν (S-OH)	831 (750)	1082 ^b , 1090 ^c , 730 ^d	$\nu_{\rm as}({ m SO_3})$	1303 (1175)	1210 ^b , 1180 ^c , 1250 ^f
$\omega(SO_2)$	440 (397)	378^{b}	$\delta(\mathrm{SH})$	1238 (1117)	1126 ^b , 1120 ^c , 1122 ^f
$\tau(SO_2)$	603 (544)	432 ^b	$\delta_{\rm as}({ m SO_3})$	521 (470)	648 ^b , 509 ^f
$\nu(O*H)$	3648, 3762 (3290, 3393)	3145 ^b , 3247 ^c , 3622 ^e			
δ (SO*H)	309 (279)				
$\omega(SO*H)$	570 (514)				

"Notation of vibration modes: stretching (v); bending (δ) ; twisting (τ) ; wagging (ω) ; symmetric (subscript s); asymmetric (subscript as). Baman data of 1 M NaHSO₃ at pH 3.9. FTIR data of 1 wt SO_2 H₂O. Attenuated total internal reflection (ATR) data of aqueous SO_2 solution at SO_2 solution at SO

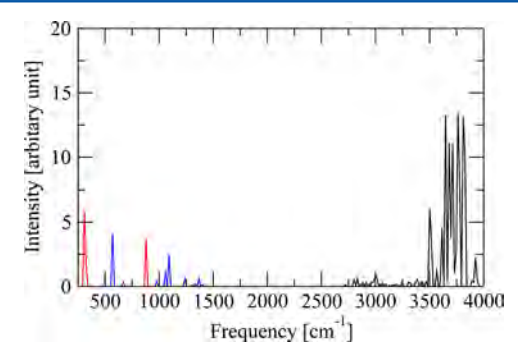


Figure 7. The isolated spectra of $\nu(S-OH)$ (black solid line), $\omega(SO_2)$ (red solid line), and $\tau(SO_2)$ (blue solid line) modes for the $(SO_2)-(O^*)$ model.

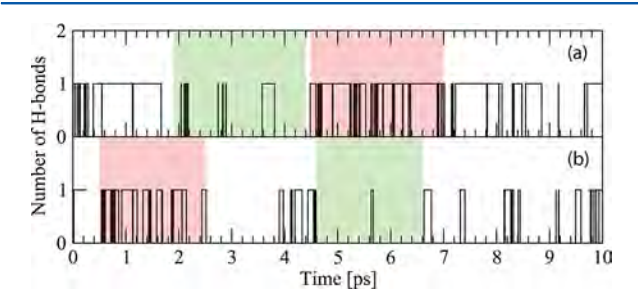


Figure 8. Number of hydrogen bonds between the hydrogen of (a) bisulfite and (b) sulfonate ion and water molecules evaluated by the geometric criteria 32,47 during the simulation period, utilizing short time periods to investigate the effect of H-bonds on the $\nu(O^*H)$ and $\nu(SH)$ frequencies. The selected short time periods with and without the effect of H-bonds are represented by red and green boxes, respectively.

cm⁻¹ with and without the effect of water molecules, respectively, specifying a peculiar property of the S–H bond induced by the hydration shell. Steudel et al. reported the blue-shifted peak of $\nu(SH)$ by increasing water molecules in a small cluster. Thus, we also investigated the influence of water on the S–H bond with a small model, containing one water molecule interacting on the hydrogen atom of sulfonate ion. HF, MP2, and QCISD calculations with the same basis sets of the QMCF MD simulations were performed on the system with a constrained distance of $S_{sulfonate}$ ····O_{water} from 3.50 to 4.50 Å by a step of 0.1 Å solvated in the PCM, by using the *Gaussian 03* package. Figure 9 shows the changing distances of the S–

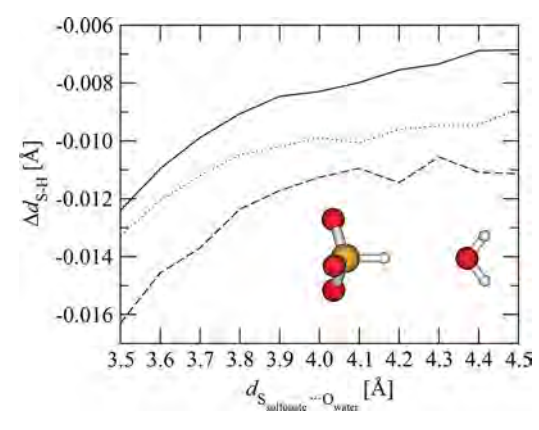


Figure 9. The function between the relative S–H distance with its optimized distance in a single ion calculation at the same theoretical level $(\Delta d_{\rm S-H})$ and the distance of $\rm S_{sulfonate}\cdots O_{water}$ ($d_{\rm S_{sulfonate}\cdots O_{water}}$) calculated at the HF (solid line), MP2 (dotted line), and QCISD (dashed line) levels.

H bond affected by the distance of the water molecule. The shorter S–H distance represents a stronger bond and reflects a blue-shifted peak in the spectra, denoting an increased stability of the sulfonate ion in aqueous solution compared to that of the bisulfite ion. The calculated frequencies of $\nu_s(SO_3)$, $\nu_{as}(SO_3)$, and $\delta(SH)$ modes agree with the recent assignment of corresponding modes in the experimental spectra, ^{6,8,9} again confirming the validity of normal-mode analysis. Our SO_3 deformation frequencies, $\delta_s(SO_3)$ and $\delta_{as}(SO_3)$ modes, support the assignment of Meyer et al., who utilized an accurate investigation with the isotope effect, and assigned the lower frequency to $\delta_{as}(SO_3)$ not the $\delta_s(SO_3)$ mode.

Structural and Dynamical Properties of the Hydration Shell. As for other polyatomic solutes, the fundamental information for a further analysis is the atomic RDFs. 31,33,49 We summarized the position of the first peak and its boundary for (site)···O_{water} and (site)···H_{water} RDFs in Table 3 for both ions. The evaluation of the atomic coordination numbers (CNs) utilizes the position of the atomic hydration boundary obtained from its (site)···O_{water} RDF, also listed in Table 3. According to the coincidence between the hydration shell of sulfur and three oxygen atoms in both ions within the radius of ~4.6 Å, we investigated all hydration properties without the inclusion of the sulfur atom to reduce the complexity of solutes. The smaller effect of the sulfur atom is reflected in a similar

Table 3. Characteristic Values of the Radial Distribution Function $g_{\alpha\beta}$ (r) for Each Site of Bisulfite and Sulfonate Anions in the Hydration Shell Determined by the QMCF MD Simulations

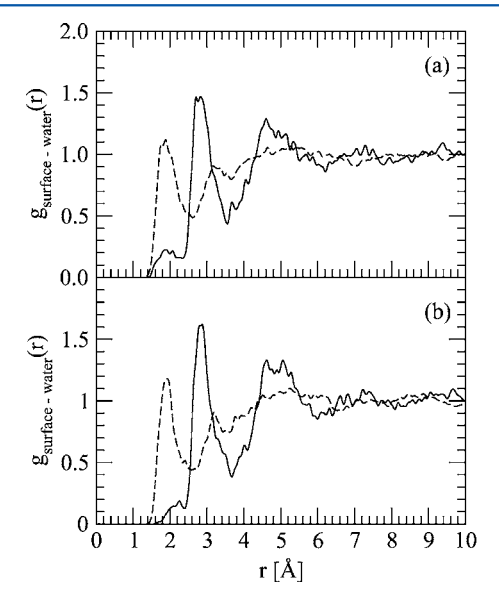
coordinating site	$r_{\max}(O_{\mathrm{w}})^a$	$r_{\min}(O_{\mathrm{w}})^a$	$r_{\rm max}(H_{\rm w})^a$	$r_{\min}(H_{\mathrm{w}})^a$	na
		SO ₃ H ⁻			
S	3.96	4.62	3.04	3.70	
O(1)	2.70	3.48	1.76	2.40	2.6
O(2)	2.72	3.54	1.78	2.50	2.9
O(3)	2.90	3.32	1.92	2.40	1.6
Н	1.88, 2.08	2.68	2.50	2.66	0.7
molecular surface	2.72, 2.84	3.56	1.76, 1.88	2.64	6.5
		HSO_3^-			
S	3.94	4.58	3.04	3.86	
O(1)	2.84	3.68	1.92	2.58	2.7
O(2)	2.68, 2.90	3.58	1.80	2.64	2.4
O(3)	2.78, 2.94	3.38	1.86, 2.00	2.74	1.9
Н	2.26	2.48	2.92	2.98	0.4
molecular surface	2.80, 2.88	3.68	1.88	2.74	6.6

 ${}^{a}r_{\max}$ and r_{\min} are the distances of the maximum and minimum of $g_{\alpha\beta}$ (r) for the hydration shell in Å, and n is the averaged coordination numbers of the shell, respectively.

hydration shell in both ions, showing in the atomic S···O_{water} and S···H_{water} RDFs. The atomic RDFs of oxygen atoms in both ions represent a similar interaction with the water molecules, whereas the hydration shell of hydrogen atom in the bisulfite is stronger than that in the sulfonate ion. This agrees with the vibration analysis in the previous section. A difference of atomic hydrogen CNs reveals a slightly stronger interaction with the hydration shell of the bisulfite ion, which is in good agreement with the experimental^{8,10} and theoretical^{15–17} findings. However, only atomic properties are unsuitable to compare with experimental data, and hence, we also evaluated the molecular RDFs and CNDs of the hydration shells based on the molecular domain.³⁸ The molecular RDFs provide the possibility to find water molecules in the isotropic molecular domain constructed from the union of spheres having identical

radii, by assigning the coordinating site with the shortest distance among the values obtained from the oxygen of water and each site within the solute. Parts a and b of Figure 10 present the molecular RDFs of bisulfite and sulfonate ions, respectively, showing a well-defined and similar hydration structure. The (molecular)···O_{water} RDF of bisulfite ion again reveals a slightly stronger interaction with water at the hydrogen site (a weak band at 1.36-2.34 Å) than that of the sulfonate ion (a weak band at 1.56-2.40 Å). Parts c and d of Figure 10 show the molecular CNDs of bisulfite and sulfonate ion, respectively, evaluated with the molecular domain, constructed by applying the boundary obtained from the atomic RDFs for each site of the solute.³⁸ The possible CNs of bisulfite are in a range of 4-9 with a dominant value of 7, while the molecular CND of sulfonate prefers 6 as the main CN with a higher flexibility of the hydration shell ranging from 4 to 11. The characteristic values of molecular hydration shells and their average CNs from the molecular RDFs and CNDs are also listed in Table 3. The higher CNs of bisulfite (7.8) and sulfonate (7.4) ions from the direct sum of atomic CNs than in the corresponding molecular CN, differing by 1.3 and 0.8 molecules, indicate the location of waters in the intersection volumes of the atomic hydration spheres. The visualization of the hydration shell during the simulation period provides an insight to understand the motion of water molecules around the solute. We again applied the contravariant transformation for the 3D alignment on the coordinates of solute and one selected water molecule within its molecular hydration shell, illustrating a motion of the solvent shown in Figure 11. The water molecule within the molecular hydration shell rapidly changes the coordinating site around the solutes during the simulation period, obviously supporting the statement in previous studies. ^{26,31,33,49} This is the evidence that the total atomic CNs include an overcounting of some water molecules, migrating around many coordinating sites during the simulation period.

According to the dynamical change of the water molecules across the coordinating sites, the number of actual contacts



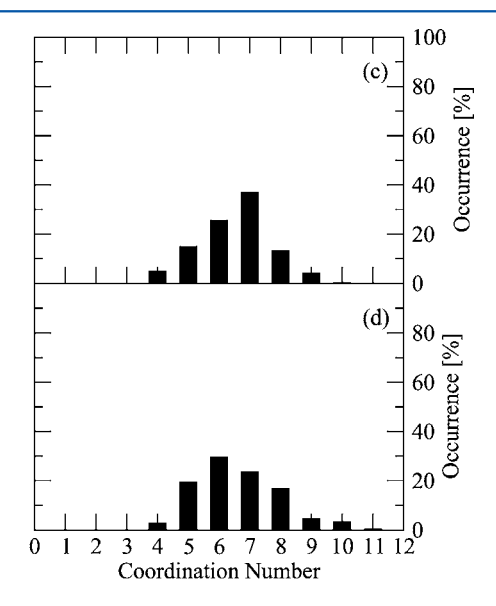


Figure 10. Molecular RDF plots of (a) SO_3H^- and (b) HSO_3^- anions obtained from the QMCF MD simulations evaluated by means of the molecular domain; solid and dashed lines refer to the RDFs for the O and H atoms of water, respectively. The molecular hydration shell coordination number distribution of (c) SO_3H^- and (d) HSO_3^- anions.

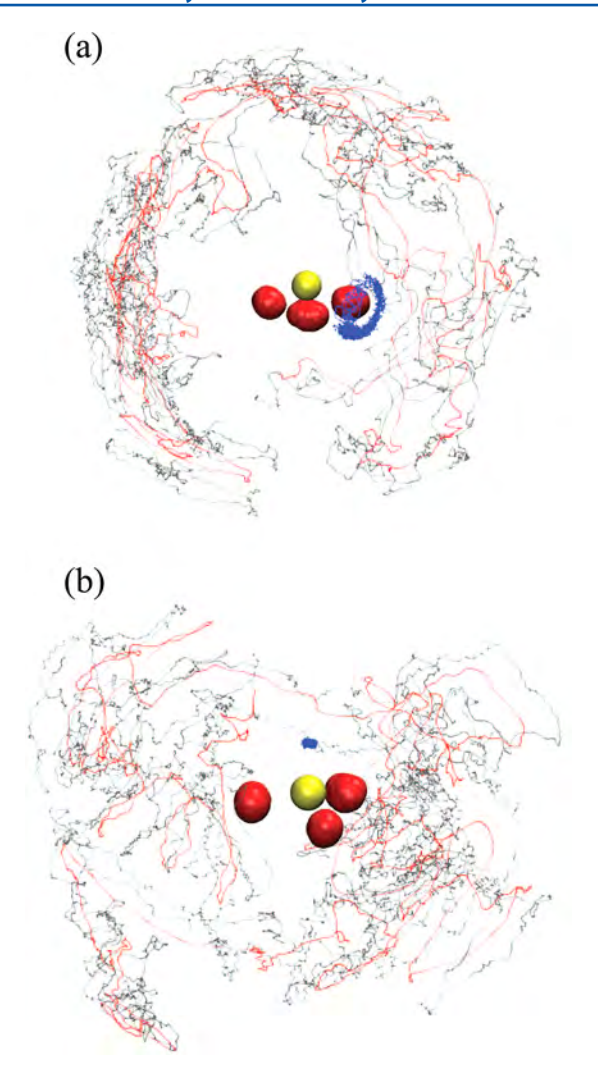


Figure 11. All superimposed trajectories for the coordinates of one selected water molecule in the molecular hydration shell for (a) bisulfite (SO_3H^-) and (b) sulfonate (HSO_3^-) ions with 3D alignment obtained from the QMCF MD simulations. The yellow sphere is sulfur, red spheres are oxygen of solutes, blue points are hydrogens of solutes, red dots are oxygens of the selected water molecules, and gray dots are the hydrogen atoms of the water.

based on the H-bonds determines the CNs and some extra waters in the H-bonds network between the hydration shell and bulk. 33,49 We utilized the structural criterion depending on the cutoff parameters in analogy to water—dimethyl sulfoxide 47 and our previous studies. 33,49 The cutoff distances $R_{\rm OO}^{\rm (c)}$ and $R_{\rm HO}^{\rm (c)}$ for each coordinating site correspond to the boundary of atomic hydration shells obtained from (site)…O $_{\rm water}$ and (site)…H $_{\rm water}$ RDFs, respectively. The angle $\varphi^{\rm (c)}$ was set to 30°. 47 Table 4 lists the average number of H-bonds for each site and the molecular hydration (surface) of the SO $_{\rm 3}$ H $^{-}$ and HSO $_{\rm 3}^{-}$ ions. The average H-bonds of the surface were evaluated by averaging the summation of all H-bonds in each time step over the simulation

period. The equivalence between the total of each site and the surface values presents the ratio 1:1 for the formation of an H-bond between the water molecule and the coordinating site, resulting in the actual CN for bisulfite (5.3) and sulfonate (5.0) ions. The comparison for these H-bond data with the molecular CNDs (6.5 and 6.6 for the bisulfite and sulfonate ion, respectively) specifies some extra water molecules located in the molecular hydration shell of bisulfite (1.2) and sulfonate (1.6) ion without forming the direct interaction to the solutes, readily changing the coordinating sites and connecting with bulk. The smaller number of extra water for bisulfite also indicates a stronger hydration structure than that of the sulfonate ion, in good agreement with previous experimental and theoretical 15-17 conclusions.

A further dynamical property of water molecules within the hydration shell was investigated by the ligand MRT calculated by the direct method,³⁹ dividing the average number of water molecules within the hydration shell throughout the simulation period by the number of exchange events with two time parameters ($t^* = 0.0$ and 0.5 ps) corresponding to all displacements and to sustainable exchange events.⁴¹ MRT values for all coordinating sites and molecular hydration shell for both ions are summarized in Table 5, compared with the data of pure water simulations. 39,40 The number of involved ligands (N_{inv}) represents the coordination of water molecules with the evaluated site in the criterion of t^* , while the number of accounted exchange events $(N_{\rm ex})$ accumulates the exchange process of $N_{\rm inv}$ throughout the simulation period. The standard relaxation time utilized in the direct method with $t^* = 0.5$ ps leads to the MRT of water ligands at the coordinating sites, while the hydrogen bond liftimes can be estimated with $t^* = 0.0$ ps. ^{31,39} The total number of individual $N_{\rm inv}$ of sulfonate evaluated by $t^* = 0.5$ ps is larger than that of bisulfite ion, whereas the molecular values present the reverse order. This again indicates a higher degree of overcounting for each coordinating site of sulfonate than of bisulfite ion. The difference value between the total atomic $N_{\rm ex}^{0.5}$ and the molecular $N_{\rm ex}^{0.5}$ suggests that the migrations of water molecules between the coordinating sites were 14 and 24 processes for bisulfite and sulfonate ion, respectively. The number of migrations for the water among the coordinating sites within the sulfonate ion is larger than its molecular $N_{\rm ex}^{0.5}$ (18), representing the confined waters within the molecular hydration shell and reflecting a longer MRT of the molecular hydration shell of the sulfonate than of the bisulfite ion. Our MRT results compared with the simulations data of pure water^{39,40} classify the bisulfite as a structure-making ion, while the sulfonate ion shows more complex properties due to the zero of $N_{inv}^{0.5}$ and $N_{ex}^{0.5}$ values of the hydrogen atom. The atomic MRTs of oxygen atoms within the sulfonate ion show a similar property with the pure water, whereas the value of hydrogen atom indicates that it is not involved in any H-bond agreeing with the data reported by Steudel et al. 48 However, the molecular MRT of sulfonate ion reveals a stronger hydration structure than the pure water, thus we also classify it as a

Table 4. Average Number of Hydrogen Bonds for Each Coordinating Site and Molecular Surface of SO₃H⁻ and HSO₃⁻ Anions in the Simulation Period

	O(1)	O(2)	O(3)	Н	surface
SO ₃ H ⁻	2.0 ± 0.7	2.1 ± 0.7	0.7 ± 0.6	0.5 ± 0.5	5.3 ± 1.1
HSO_3^-	1.7 ± 0.6	1.6 ± 0.6	1.5 ± 0.6	0.2 ± 0.4	5.0 ± 1.1

Table 5. Mean Ligand Residence Time t (ps), Number of Accounted Ligand Exchange Events N and Total Number of Processes Needed for One Successful Water Exchange $R_{\rm ex}$ Obtained from the QMCF MD Simulations

		$t^* = 0.0 \text{ ps}$			$t^* = 0.5 \text{ ps}$			
	$N_{ m inv}{}^a$	$N_{\rm ex}^{0.0}/10~{\rm ps}^b$	$ au_D^{0.0c}$	$N_{\mathrm{inv}}{}^{a}$	$N_{\rm ex}^{0.5}/10~{\rm ps}^b$	$ au_D^{0.5c}$	$R_{\rm ex}^{d}$	
SO ₃ H ⁻								
O(1)	18	95	0.28	8	14	1.88	6.8	
O(2)	22	136	0.22	8	13	2.28	10.5	
O(3)	20	141	0.12	5	10	1.67	14.1	
H	11	99	0.07	1	3	2.37	33.0	
surface	34	417	0.15	15	26	2.46	16.0	
			HS	5O ₃				
O(1)	21	118	0.23	10	18	1.52	6.6	
O(2)	20	120	0.20	8	14	1.72	8.6	
O(3)	15	84	0.23	7	10	1.93	8.4	
H	6	57	0.06	0	0	0.00	_	
surface	29	258	0.25	13	18	3.38	14.3	
			Pure	Water				
H_2O^e		269 ³⁹	$0.2^{39}_{,} 0.33^{40}_{,}$		24 ³⁹	1.7, ³⁹ 1.51 ⁴⁰	11.2^{39}	
H_2O		131^f	$0.2^{f}_{,} 0.55^{41}_{,}$		20 ^f	1.3 ^f	6.5^{f}	

^aNumber of ligands involved in the MRT evaluation according to the value of t^* . ^bNumber of accounted exchange events per 10 ps lasting at least 0.0 and 0.5 ps, respectively. ^cMean residence time determined by the direct method³⁹ in picoseconds. ^dAverage number of processes needed for one successful ligand exchange. ^eValues obtained from a QM/MM-MD simulation of pure water^{39,40} in picoseconds. ^fUnpublished results: values obtained from a QMCF MD simulation of pure water in picoseconds.

structure-maker consisting of three hydrophilic S–O and one hydrophobic S–H bonds. The number of processes needed for one successful water exchange, $R_{\rm ex}$, being the ratio of $N_{\rm ex}^{0.0}$ to $N_{\rm ex}^{0.0}$ also shows a complexity of the exchange process. The $R_{\rm ex}$ for the interchanging of coordinating site within the molecular hydration shell was 3.8 and 5.0 for bisulfite and sulfonate ion, respectively, indicating a higher reactivity of the coordinating sites within the former than those of the latter.

CONCLUSION

Vibrational investigations based on the precise assignment of normal modes for the aqueous bisulfite and sulfonate ions were performed on the basis of the data obtained from the OMCF MD simulations. The complexity of C_1 symmetry for the bisulfite ion was simplified with (SO_2) , $(SO_2)-(O^*)$, and (SO₂O)-(H) models, providing the data for all nine modes. All six normal modes of sulfonate ion were also evaluated to compare with the experimental data. Here, the vector analysis gave the frequency of $\delta_s(SO_3)$ lower than that of the $\delta_{as}(SO_3)$ mode, which is in a good agreement with the assignment in accurate experimental data. The S-H bond in the sulfonate ion displays a hydrophobic property as it presents a stronger bond and shorter distance when a water molecule comes close to the hydrogen atom, reflected in a blue-shifted peak of the $\nu(SH)$ mode. The superimposed trajectories of the atomic coordinates for the solutes with 3D alignment, presenting the possibility of bisulfite ion to arrange a suitable orientation of the active hydrogen atom to form the trans-SO₃H⁻ conformer, support the proposed mechanism for the tautomerization from the bisulfite to sulfonate ion. 17 Unfortunately, the isomerization was not observed in this work, due to the short time-span of simulation. We illustrated the migration of water molecules within the molecular hydration shell among coordinating sites of the solutes, confirming related statements in previous studies of hydrated anions. 26,31,33,49 The investigated properties of vibrations and hydration shells in this study indicate more stability of the sulfonate than the bisulfite ion in aqueous solution, while the former has a weaker hydration structure

than the latter ion. Our results provided the characteristics of the specified ions in a separated system that is difficult to realize in experiment, due to the coexistance of bisulfite and sulfonate ions in equilibrium in the prepared solutions.^{8,10}

AUTHOR INFORMATION

Corresponding Author

*Viwat.V@Chula.ac.th

Notes

The authors declare no competing financial interest.

ACKNOWLEDGMENTS

Financial support by ASEA-UNINET, the National Research University (NRU) Project of Thailand's Office of the Higher Education Commission, and Centre for Petroleum, Petrochemicals and Advanced Materials, Chulalongkorn University are gratefully acknowledged. A.T. acknowledges support by the Thailand Research Fund (TRF) and Suranaree University of Technology (SUT). This work was also supported by the National Research Council of Thailand (NRCT) and the commission of Higher Education (CHE) of Thailand.

REFERENCES

- (1) Brandt, C.; van Eldik, R. Chem. Rev. 1995, 95, 119-190.
- (2) Bakker, J.; Clarke, R. J. Wine Flavour Chemistry, 2nd ed.; Blackwell Publishing: West Sussex, UK, 2012.
- (3) Golding, R. M. J. Chem. Soc. 1960, 3711-3716.
- (4) Herlinger, A. W.; Long, T. V. Inorg. Chem. 1969, 8, 2661-2665.
- (5) Connick, R. E.; Tam, T. M.; Von Deuster, E. Inorg. Chem. 1982, 21, 103-107.
- (6) Meyer, B.; Peter, L.; Shaskey-Rosenlund, C. Spectrochim. Acta, Part A 1979, 35, 345-354.
- (7) Zhang, Z.; Ewing, G. E. Spectrochim. Acta, Part A 2002, 58, 2105-2113.
- (8) Risberg, E. D.; Eriksson, L.; Mink, J.; Pettersson, L. G. M.; Skripkin, M. Y.; Sandström, M. Inorg. Chem. 2007, 46, 8332–8348.
- (9) Townsend, T. M.; Allanic, A.; Noonan, C.; Sodeau, J. R. J. Phys. Chem. A **2012**, 116, 4035–4046.

- (10) Horner, D. A.; Connick, R. E. Inorg. Chem. 1986, 25, 2414–2417.
- (11) Baird, N. C.; Taylor, K. F. J. Comput. Chem. 1981, 2, 225-230.
- (12) Strömberg, A.; Gropen, O.; Wahlgren, U.; Lindqvist, O. *Inorg. Chem.* 1983, 22, 1129–1133.
- (13) Squires, R. R. Int. J. Mass Spectrom. Ion Processes 1992, 117, 565-600.
- (14) Smith, A.; Vincent, M. A.; Hillier, I. H. J. Phys. Chem. A 1999, 103, 1132–1139.
- (15) Brown, R. E.; Barber, F. J. Phys. Chem. 1995, 99, 8071-8075.
- (16) Otto, A.; Steudel, R. Eur. J. Inorg. Chem. 2000, 617-624.
- (17) Voegele, A. F.; Tautermann, C. S.; Rauch, C.; Loerting, T.; Liedl, K. R. J. Phys. Chem. A **2004**, 108, 3859–3864.
- (18) Rode, B. M.; Hofer, T. S.; Randolf, B. R.; Schwenk, C. F.; Xenides, D.; Vchirawongkwin, V. Theor. Chem. Acc. 2006, 115, 77–85.
- (19) Hofer, T. S.; Pribil, A. B.; Randolf, B. R.; Rode, B. M. Ab Initio Quantum Mechanical Charge Field Molecular Dynamics: A Non-parametrized First-Principle Approach to Liquids and Solutions. In Combining Quantum Mechanics and Molecular Mechanics. Some Recent Progresses in QM/MM Methods; Sabin, J. R., Brändas, E., Eds.; Academic Press: New York, 2010; Vol. 59, pp 213–246.
- (20) Warshel, A.; Levitt, M. J. Mol. Biol. 1976, 103, 227-249.
- (21) Field, M. J.; Bash, P. A.; Karplus, M. J. Comput. Chem. 1990, 11, 700-733.
- (22) Gao, J. J. Am. Chem. Soc. 1993, 115, 2930-2935.
- (23) Bakowise, D.; Thiel, W. J. Phys. Chem. 1996, 100, 10580-10594.
- (24) Brooks, B. R.; Bruccoleri, R. E.; Olafson, B. D.; States, B. D.; Swaminathan, S.; Karplus, M. J. Comput. Chem. 1983, 4, 187–217.
- (25) Berendsen, H. J. C.; Postma, J. P. M.; van Gunsteren, W. F.; DiNola, A.; Haak, J. R. *J. Chem. Phys.* **1984**, *81*, 3684–3690.
- (26) Vchirawongkwin, V.; Rode, B. M.; Persson, I. J. Phys. Chem. B **2007**, 111, 4150–4155.
- (27) Vchirawongkwin, V.; Rode, B. M. Chem. Phys. Lett. 2007, 443, 4152–157.
- (28) Pribil, A. B.; Vchirawongkwin, V.; Hofer, T. S.; Randolf, B. R. Structure and Dynamics of Composite Anions in Aqueous Solution. Computation in Modern Science and Engineering, Proceedings of the International Conference on Computational Methods in Science and Engineering 2007, 921–923.
- (29) Pribil, A. B.; Hofer, T. S.; Randolf, B. R.; Rode, B. M. J. Comput. Chem. 2008, 29, 2330–2334.
- (30) Pribil, A. B.; Hofer, T. S.; Vchirawongkwin, V.; Randolf, B. R.; Rode, B. M. Chem. Phys. **2008**, 346, 182–185.
- (31) Vchirawongkwin, V.; Pribil, A. B.; Rode, B. M. J. Comput. Chem. **2010**, *31*, 249–257.
- (32) Vchirawongkwin, V.; Kritayakornupong, C.; Ruangpornvisuti, V.; Rode, B. M. J. Mol. Struct. (THEOCHEM) 2009, 913, 236–239.
- (33) Vchirawongkwin, V.; Kritayakornupong, C.; Rode, B. M. J. Phys. Chem. B **2010**, 114, 11561–11569.
- (34) Dunning, Jr., T. H.; Hay, P. J. In Gaussian Basis Sets for Molecular Calculations; Schaefer, H. F., III, Ed.; Plenum Press: New York, 1977; Vol. 3, Chapter 1, pp 1–27.
- (35) Dunning, T. H., Jr. J. Chem. Phys. 1970, 53, 2823-2833.
- (36) Stillinger, F. H.; Rahman, A. J. Chem. Phys. 1978, 68, 666-670.
- (37) Bopp, P.; Janscó, G.; Heinzinger, K. Chem. Phys. Lett. 1983, 98, 129-133
- (38) Vchirawongkwin, S.; Vchirawongkwin, V. Comput. Theor. Chem. 2011, 974, 26–30.
- (39) Hofer, T. S.; Tran, H. T.; Schwenk, C. F.; Rode, B. M. J. Comput. Chem. **2004**, 25, 211–217.
- (40) Xenides, D.; Randolf, B. R.; Rode, B. M. J. Chem. Phys. 2005, 122, 174–506.
- (41) Lock, A. J.; Woutersen, S.; Bakker, H. J. J. Phys. Chem. A 2001, 105, 1238–1243.
- (42) Bopp, P. Chem. Phys. 1986, 106, 205-212.
- (43) Eklund, L.; Hofer, T. S.; Pribil, A. B.; Rode, B. M.; Persson, I. *Dalton Trans.* **2012**, *41*, 5209–5216.
- (44) Curtiss, L. A.; Redfern, P. C.; Raghavachari, K.; Rassolov, V.; Pople, J. A. J. Chem. Phys. 1999, 110, 4703–4709.

- (45) Frisch, M. J.; et al. *Gaussian03*, Revision D.02; Gaussian, Inc., Wallingford, CT, 2004.
- (46) Noblet, J. A.; Schugart, K. A. J. Mol. Struct. (THEOCHEM) 1994, 304, 1-11.
- (47) Luzar, A.; Chandler, D. J. Chem. Phys. 1993, 98, 8160-8173.
- (48) Steudel, R.; Steudel, Y. Eur. J. Inorg. Chem. 2009, 2009, 1393-1405.
- (49) Vchirawongkwin, V.; Kritayakornupong, C.; Tongraar, A.; Rode, B. M. J. Phys. Chem. B 2011, 115, 12527–12536.